

**On the composition, properties and physiological roles of
K⁺ currents found at a central auditory synapse**

A thesis submitted for the degree of
Doctor of Philosophy
At the University of Leicester

By

Jamie Johnston B.Sc.

Department of Cell Physiology & Pharmacology
University of Leicester

December 2006

UMI Number: U227325

All rights reserved

INFORMATION TO ALL USERS

The quality of this reproduction is dependent upon the quality of the copy submitted.

In the unlikely event that the author did not send a complete manuscript and there are missing pages, these will be noted. Also, if material had to be removed, a note will indicate the deletion.



UMI U227325

Published by ProQuest LLC 2013. Copyright in the Dissertation held by the Author.
Microform Edition © ProQuest LLC.

All rights reserved. This work is protected against
unauthorized copying under Title 17, United States Code.



ProQuest LLC
789 East Eisenhower Parkway
P.O. Box 1346
Ann Arbor, MI 48106-1346

We must not forget that when radium was discovered no one knew that it would prove useful in hospitals. The work was one of pure science. And this is a proof that scientific work must not be considered from the point of view of the direct usefulness of it. It must be done for itself, for the beauty of science, and then there is always the chance that a scientific discovery may become like the radium a benefit for humanity.

Marie Curie (1867 - 1934), *Lecture at Vassar College, May 14, 1921*

Nothing occurs at random, but everything for a reason and by necessity.

Leucippus (5th century B.C.)

On the composition, properties and physiological roles of K⁺ currents found at a central auditory synapse

Jamie Johnston

The medial nucleus of the trapezoid body forms part of the circuits involved in sound source localisation. It receives the synapse called the calyx of Held and rapidly transmits this information to other neurons in the circuit. This thesis characterises the composition and properties of the K⁺ channels found in the medial nucleus of the trapezoid body neuron and shows how they regulate action potential firing.

I have shown that a large K⁺ leak current (0.8nA at +10mV) contributes to the resting membrane potential and action potential repolarisation. Kv1 channels open with small depolarisations and prevent the medial nucleus of the trapezoid body from firing multiple action potentials in response to its giant synaptic input. Kv3 channels make a large contribution to the outward current and promote brief action potentials by rapid repolarisation. A smaller A-type current is also present, mediated by a Kv4 subunit. However this current is largely inactivated at rest.

I show that the major conductance contributing to the outward K⁺ current in the medial nucleus of the trapezoid body is mediated by Kv2.2 containing channels. These channels are localised to the initial segment of the axon. Due to their slow kinetics, they contribute little to a single action potential. Rather their activity accumulates through high frequency trains, providing a hyperpolarisation of the inter-spike potential, necessary to promote recovery of Nav channels from inactivation. Thus the Kv2.2 channels facilitate sustained high frequency firing.

Major findings of this thesis

- Kv3 channels in the mouse MNTB have a more negative $V_{1/2}$ than previous reports.
- Kv1 channels in the mouse MNTB are entirely composed of Kv1.1/Kv1.2 heteromers.
- The mouse MNTB neurons possess an A-type current (in contrast to the rat).
- The A-current is mediated by a Kv4 subunit and may be involved in integration of inhibitory inputs.
- Kv2.2 containing channels mediate the predominant outward current in MNTB neurons.
- Kv2.2 channels are located in the initial segment of the axon.
- The slow kinetics of Kv2.2 mean that it only activates through high frequency trains, resulting in a hyperpolarisation of the inter-spike potential.
- The hyperpolarisation by the Kv2.2 containing channels promotes prolonged high frequency firing by preventing accumulation of inactivation of the Nav channels
- The Kv2.2 current is tonotopically distributed with higher magnitude current in lateral neurons.
- The Kv2.2 current increases with development.
- A K2p current makes a significant contribution to outward K^+ current and sets the resting membrane potential.
- The K2p current is likely mediated by TWIK and/or TREK channels.

Acknowledgements

Firstly I would like to thank my supervisor Prof. I. D. Forsythe, for "hiring" me in the first place; I have learnt a lot and enjoyed my time in his lab.

I thank A. Skrzypiec for her hard work on the PCR and immunohistochemistry of the Kv2 subunits, along with M. Barker for the Kv1 and Kv3 immunohistochemistry. Also thanks to Drs M. Postlethwaite, S.J. Griffin and Clare Baker for their contributions.

I would also like to thank all the staff and students of the department of Cell Physiology and Pharmacology, for useful discussions, loan of a substance, and for making my time at Leicester enjoyable, especially Dr. B. Billups and Dr. N. Davies for useful discussions.

Special thanks to everyone who provided non-academic support (i.e. accompanying me to the pub) especially Matt Hardy, Mike Postlethwaite, Becky Read and Jude Gittins. I would also like to thank my family for all their help and support.

Special thanks to Jude for all her love and support throughout my PhD and during the write up.

Declaration

The material in this thesis is all my own work. For the immunohistochemistry, PCR and western blot I received assistance from Matt Barker (Kv1 and Kv3), Anna Skrzypiec (Kv2, immunohistochemistry, western and PCR) and Clare Baker (Kv1 and Kv4 immunohistochemistry). I have included data from 5 recordings from P18-19 animals, which were performed by Dr. S. J. Griffin and the data collected for the orthodromic synaptic recordings were made with the assistance of Dr. M. Postlethwaite.

Table of contents

MAJOR FINDINGS OF THIS THESIS	4
ACKNOWLEDGEMENTS	5
TABLE OF FIGURES	12
LIST OF ABBREVIATIONS	14
CHAPTER 1 – INTRODUCTION	15
THE AUDITORY SYSTEM	16
SOUND TRANSDUCTION IN THE EAR	16
THE BINAURAL AUDITORY BRAINSTEM	17
The Cochlear Nucleus	17
The superior olivary complex (SOC)	17
The Medial Nucleus of the Trapezoid Body (MNTB).....	18
The Lateral Superior Olive (LSO).....	19
The Medial Superior Olive (MSO).....	19
SOUND SOURCE LOCALISATION	20
PROCESSING OF INTERAURAL LEVEL DIFFERENCES (ILDs) IN THE LSO.....	21
PROCESSING OF INTERAURAL TIMING DIFFERENCES (ITDs) IN THE MSO	22
Delay lines and coincidence detectors	22
The role of inhibition in mammalian ITDs.....	23
ION CHANNELS	26
EXCITABLE MEMBRANES.....	26
LIGAND-GATED ION CHANNELS.....	27
VOLTAGE-GATED CHANNELS	27
Voltage-gated sodium (Nav) channels.....	28
Voltage-gated calcium (Cav) channels.....	28
Hyperpolarisation activated (HCN/Ih) channels.....	29
THE SUPER-FAMILY OF POTASSIUM CHANNELS	31
STRUCTURAL DIVISIONS	31
K ⁺ CHANNEL PROPERTIES.....	32
Ion permeation and selectivity.....	32
VOLTAGE SENSING AND ACTIVATION.....	34
INACTIVATION.....	36
N-Type inactivation.....	36
C-Type inactivation	37
2TM DOMAINS / INWARD RECTIFIERS	38
4TM DOMAINS / TWIN-PORE CHANNELS.....	38
6TM DOMAINS / VOLTAGE-GATED AND CA ²⁺ -ACTIVATED CHANNELS.....	41
Calcium-activated K ⁺ channels (K _{Ca}).....	42

KCNQ / Kv7 / M-channels	43
Ether-à-go-go (EAG) channels	43
THE VOLTAGE-ACTIVATED K ⁺ (KV) CHANNELS	44
Delayed rectifiers and A-Currents	44
Kv1 sub-family	44
Kv2 subfamily	45
Kv3 subfamily	45
Kv4 subfamily	46
The silent subunits (Kv5, 6, 8 &9)	46
Accessory subunits	46
CHAPTER 2 – METHODS	47
TISSUE PREPARATION, MAINTENANCE AND VISUALISATION.....	47
SOLUTIONS	47
DISSECTION.....	48
TISSUE BLOCK PREPARATION	49
SLICE COLLECTION	50
EXPERIMENTAL SETUP.....	51
EXPERIMENTAL MICROSCOPE.....	51
DIFFERENTIAL INTERFERENCE CONTRAST OPTICS	53
FLUORESCENCE MICROSCOPY.....	55
PERFUSION AND DRUG APPLICATION.....	55
ELECTROPHYSIOLOGY AND PATCH-CLAMP RECORDING	58
PRINCIPLES OF ELECTROPHYSIOLOGY	58
Electrical Properties of Cells	58
Membrane Resistance.....	58
Membrane Capacitance.....	59
Membrane Time Constant	59
Ionic Equilibrium Potentials	60
VOLTAGE CLAMP	61
THE PATCH CLAMP TECHNIQUE.....	62
Measurement of ionic currents in whole cell patch-clamp	64
Liquid junction potentials	65
Electrode preparation.....	66
PATCH CLAMP RECORDING EQUIPMENT	66
Amplifier headstage design	68
Stimulation	70
DATA ANALYSIS.....	71
DETERMINING VOLTAGE DEPENDENCE OF INACTIVATION	71
DETERMINING VOLTAGE DEPENDENCE OF ACTIVATION.....	72
EXPONENTIAL FITS	73
IMMUNOHISTOCHEMISTRY ANALYSIS	73
STATISTICAL TESTS	74

IMMUNOHISTOCHEMISTRY	74
IMMUNOHISTOCHEMISTRY METHODS.....	75
CONFOCAL MICROSCOPY.....	77
WESTERN BLOT FOR ANTI-KV2.2.....	77
REVERSE TRANSCRIPTION PCR	78
QUANTITATIVE REAL-TIME RTPCR.....	80
Relative quantification.....	81
QrtRTPCR procedure	83
CHAPTER 3 – RESULTS 1	84
PROPERTIES CONCERNED WITH SHORT LATENCY RESPONSES	84
DEVELOPING A METHOD TO STUDY ISOLATED SYNAPTIC ACTION POTENTIALS.....	86
PROPERTIES CONCERNED WITH HIGH FREQUENCY FIRING	88
SODIUM CURRENT	88
HIGH VOLTAGE-ACTIVATED K ⁺ CURRENT.....	90
Kv3 subunit composition.....	93
The physiological role of Kv3 channels	95
PROPERTIES CONCERNED WITH FIDELITY OF TRANSMISSION	96
DTX-I SENSITIVE LOW-VOLTAGE CURRENTS	98
The physiological role of Kv1 channels.....	101
Kv1 channel subunit composition.....	102
DISCUSSION.....	108
SHORT LATENCY RESPONSE TO THE PRESYNAPTIC INPUT.....	108
HIGH FREQUENCY FIRING.....	109
High-threshold Kv3 channels	109
High-threshold Kv3 channels in the MNTB.....	109
Origins and further misconceptions of Kv3.1 in the MNTB	112
Subcellular localisation of Kv3	112
Tonotopic distribution of Kv3	113
Functional consequences of Kv3.....	113
HIGH FIDELITY TRANSMISSION.....	114
Low voltage-activated Kv1 channels.....	114
Kv1 channels in the MNTB.....	115
Kv1 subunit composition.....	116
Subcellular localisation of Kv1	117
Activation of Kv1 channels in the MNTB.....	118
Functional consequences of Kv1 channels	119
Tonotopic distribution	120
CHAPTER 4 – RESULTS 2	121
METHODS.....	122

TWO ADDITIONAL K⁺ CURRENTS TO Kv3 AND Kv1 IN THE MNTB	123
THE A-CURRENT	125
BIOPHYSICAL PROPERTIES OF THE A-CURRENT	125
PHARMACOLOGY OF THE A-CURRENT.....	129
Kv4.3 SUBUNITS ARE EXPRESSED IN THE MNTB.....	132
A PHYSIOLOGICAL ROLE FOR THE A-CURRENT	133
THE SLOW ACTIVATING CURRENT.....	135
BIOPHYSICAL PROPERTIES OF THE SLOW CONDUCTANCE.....	135
Kv2.2 CONTRIBUTES TO THE SLOW CONDUCTANCE.....	142
PHARMACOLOGY OF THE SLOW CONDUCTANCE.....	147
A PHYSIOLOGICAL ROLE FOR Kv2.2 CONTAINING CHANNELS	151
THE SODIUM CURRENT IS EXQUISITELY SENSITIVE TO INTER-SPIKE VOLTAGES	155
DEVELOPMENTAL AND TONOTOPIC GRADIENTS.....	159
Kv2.2 CURRENT MAGNITUDE INCREASE WITH DEVELOPMENT	159
Kv2.2 IS TONOTOPICALLY DISTRIBUTED.....	161
DISCUSSION.....	164
THE A-CURRENT.....	164
Molecular identity of the A-current	164
The Physiological role of the A-current	166
THE SLOWLY-GATING HIGH THRESHOLD Kv2.2 CURRENT.....	168
Kv2.2 containing channels mediate the slowly gating sustained current	168
Kv2 channels	171
Subunit composition	171
Subcellular location	172
A physiological role of Kv2.2 channels in the MNTB	174
The affect of the Kv2.2 mediated cumulative hyperpolarisation	175
DEVELOPMENTAL CHANGES.....	176
TONOTOPIC GRADIENT	176
CHAPTER 5 – RESULTS 3	178
METHODS.....	179
HOW TO STUDY LEAK.....	180
THE K⁺ LEAK IN THE MNTB.....	185
K2P CHANNELS SET THE RESTING MEMBRANE POTENTIAL	188
WHICH K2P CHANNELS MEDIATE THE K⁺ LEAK IN THE MNTB	190
DISCUSSION.....	193
K2P CHANNELS.....	193

THE K ₂ P CURRENT IN THE MNTB.....	193
SUBUNIT COMPOSITION	194
CHAPTER 6 – DISCUSSION.....	196
THE K⁺ CHANNELS OF THE MNTB	196
KV CHANNELS OF THE MNTB.....	196
OTHER CHANNELS OF THE MNTB	198
THE VOLTAGE-GATED SODIUM CURRENT IN THE MNTB	198
A ROLE FOR K _{NA} SUBUNITS?	199
SUMMARY OF HOW THE MNTB ACTS AS A FAST RELAY	200
FUTURE DIRECTIONS	202
REFERENCES.....	203

Table of figures

Figure 1-1. The Binaural Brainstem:	18
Figure 1-2. The Duplex theory of sound localisation	21
Figure 1-3 Delay lines and coincidence detectors	23
Figure 1-4 Role of inhibition in mammalian ITD discrimination	25
Figure 1-5. Structural divisions of the K ⁺ channel family	31
Figure 1-6. The crystal structure of KcsA reveals the basis of ion permeation and selectivity	33
Figure 1-7. The Kv1.2 channel is a tetramer of subunits.....	35
Figure 1-8. Inactivation of Kv channels.....	37
Figure 1-9 Family tree of the K2p members	40
Figure 1-10. The subfamilies of the 6 transmembrane domain K ⁺ channels	42
Figure 1-11. Delayed rectifier and A-current Phenotypes	45
Figure 2-1 Slicing equipment	50
Figure 2-2 Experimental setup	52
Figure 2-3 Differential Interference Contrast (DIC) optics	54
Figure 2-4 The perfusion system.....	56
Figure 2-5 The suction needle	57
Figure 2-6 Patch-clamp configurations	63
Figure 2-7 Patch-clamp recording equipment.....	67
Figure 2-8 Conventional resistive headstage	68
Figure 2-9 The Optopatch head stage.....	69
Figure 2-10 Stimulating electrode	70
Figure 2-11 Method of normalisation for driving force affects $V_{1/2}$	73
Figure 2-12 Principles of immunohistochemistry	75
Figure 2-13 Principles of reverse transcriptase PCR	79
Figure 2-14 Real time PCR methods.....	82
Figure 3-1 Somatic supra-threshold synaptic currents generate a single action potential	85
Figure 3-2 Generating a synaptic current waveform	87
Figure 3-3 Estimating parameters of the Nav current in MNTB neurons	89
Figure 3-4 A high voltage-activated K ⁺ current is blocked by TEA.....	91
Figure 3-5 The voltage dependence of activation for the Kv3 current	92
Figure 3-6 Immunoreactivity for the Kv3 family	94
Figure 3-7 Block of Kv3 channels results in action potential broadening.....	95
Figure 3-8 Sequential pharmacology of the low voltage-activated current	96
Figure 3-9 The Kv1.3 and 1.4 antagonist CP 339,818 has no effect on the TEA and DTx-I insensitive current.....	98
Figure 3-10 DTx-I blocks a low voltage-activated current.....	99
Figure 3-11 The DTx-I sensitive current activation.....	100
Figure 3-12 Kv1 channels set threshold and prevent aberrant firing	101
Figure 3-13 Immunoreactivity of the neuronal Kv1 subunits	103
Figure 3-14 DTx-K inhibits a low voltage-activated current.....	104
Figure 3-15 The absence of Kv1.1 homomers	105
Figure 3-16 TsTx blocks a low voltage-activated current	116
Figure 4-1 K ⁺ current not mediated by Kv1 or Kv3 channels	123
Figure 4-2 The antagonist-insensitive current is comprised of two components	124
Figure 4-3 Voltage dependence of inactivation of the A-current	126
Figure 4-4 Determining the voltage-dependence of activation for the A-current	128
Figure 4-5 Recovery of inactivation of the A-current	129
Figure 4-6 The A-current is sensitive to Ba ²⁺ and 4-AP	131
Figure 4-7 Kv4.3 is present in the MNTB principal neurons.....	132
Figure 4-8 Physiological consequences of the A-current?	133
Figure 4-9 Assessing the voltage dependence of activation for the slow conductance..	135
Figure 4-10 Assessing the voltage-dependence of inactivation for the slow conductance	137

Figure 4-11 Voltage-dependence of activation rate for the slow conductance	138
Figure 4-12 Deactivation rate of the slow conductance.....	139
Figure 4-13 Inactivation rate of the slow conductance	140
Figure 4-14 Long duration pulses results in a shift of the K^+ reversal potential.....	141
Figure 4-15 Kv2.2 mRNA is present whereas Kv2.1 is absent	142
Figure 4-16 Anti-Kv2.2 stains a single band at the predicted molecular weight of Kv2.2.....	144
Figure 4-17 Kv2.2 is present in principal neurons of the MNTB.....	145
Figure 4-18 Kv2.2 is located in the initial segment of the axon.....	146
Figure 4-19 The slow conductance is blocked by quinine and partially blocked by Ba^{2+}	148
Figure 4-20 The slow conductance is partially blocked by 4-AP and unaffected by rScTx	150
Figure 4-21 Action potential frequency determines amount of inter-spike hyperpolarisation, consistent with accumulation of Kv2.2	153
Figure 4-22 Voltage-dependence of inactivation of the sodium current.....	155
Figure 4-23 Protocol to assess the affect of V_{is} on I_{Na}	157
Figure 4-24 I_{Na} is exquisitely sensitive to the inter-spike voltage	158
Figure 4-25 The Kv2.2 conductance increases with development.....	160
Figure 4-26 Tonotopic distribution of Kv2.2 current in the MNTB at P12.....	162
Figure 4-27 The subcellular location of Kv2.2 influences the apparent activation of Kv1	173
Figure 5-1 The problem with seal leak.....	180
Figure 5-2 Leak subtraction methods	182
Figure 5-3 The MNTB lacks a Cl^- current	184
Figure 5-4 K^+ mediated leak in the MNTB	185
Figure 5-5 The K^+ leak is non voltage-gated.	187
Figure 5-6 Ba^{2+} blocks a substantial portion of the K^+ leak	188
Figure 5-7 Block of the K^+ leak depletes the membrane potential	189
Figure 5-8 Volatile anaesthetics potentiate the quinine insensitive K^+ leak.....	191
Figure 6-1 The activation ranges of the Kv channels in the MNTB.....	197
Figure 6-2 Summary of the composition, locations and roles of the MNTB's voltage gated channels.	201

List of abbreviations

AVCN: Anteroventral cochlear nucleus

Cav: Voltage gated Ca^{2+} channel

CNQX: 6-cyano-7-nitroquinoxaline-2,3-dione

DNQX: 6,7-Dinitroquinoxaline-2,3-dione

DTx-I: Dendrotoxin-I

EPSC: Excitatory post synaptic current

EPSP: Excitatory postsynaptic potential

ERG: ether-a-go-go related gene

GBC: Globular bushy cell

I_h : Hyperpolarisation activated cation current (HCN)

ILD: Interaural level difference

I_{Na} : Sodium current

IPSP: Inhibitory post synaptic potential

ITD: Interaural timing difference

K_{ac} : Slope constant for activation

K_{in} : Slope constant for inactivation

K2p: Twin pore K^+ channel

Kv: Voltage gated K^+ channel

LSO: Lateral superior olive

MNTB: Medial nucleus of the trapezoid body

MSO: Medial superior olive

Nav: Voltage gated Na^+ channel

PSP: Post synaptic potential

RMP: Resting membrane potential

SBC: Spherical bushy cell

SOC: Superior olivary complex

TEA: Tetraethyl ammonium

TsTx: Tityustoxin

TTx: Tetrodotoxin

$V_{1/2ac}$: Voltage of half-activation

$V_{1/2in}$: Voltage of half-inactivation

Chapter 1 – Introduction

This chapter aims to provide a background to the relevant topics of this thesis. In this study I have examined the K^+ channels that contribute to excitability of principal neurons of the medial nucleus of the trapezoid body (MNTB) in mice. This synapse is part of the auditory brainstem; it functions as a high fidelity inverting relay in circuits involved with sound source localisation. MNTB neurons are amenable to voltage-clamp as they have few processes (Kuwabara & Zook, 1991) allowing good voltage control (i.e. few problems with space clamp) and the calyx of Held is also accessible to whole cell recordings (Forsythe, 1994). Together these factors make an attractive model for studying the function of native ion channels. Previous work in this laboratory has examined the role of two voltage-gated K^+ currents in the rat MNTB, one a high voltage-activated and one a low voltage-activated current (Brew & Forsythe, 1995). The low voltage-activated currents, found to be mediated by Kv1 channels have been studied in more depth both pre (Dodson *et al.*, 2003) and post-synaptically (Dodson *et al.*, 2002). Here I have used the mouse as a model, originally with the aim to study Kv1.1 and Kv1.2 knockouts. However, I noticed that there was a slight species difference and that a considerable proportion of the current was not mediated by the previously characterised currents in the rat.

I will begin by introducing the auditory system, focusing on the central auditory brainstem and the MNTB. I will then go on to describe the ion channel families relevant for understanding the physiology of this region i.e. the voltage-gated K^+ (Kv) and Twin-pore K^+ (K2p) channels.

The Auditory system

Sound transduction in the ear

Sound waves arrive at the outer ear, pass along the auditory canal and cause vibration of the tympanic membrane. This vibration is amplified in the middle ear by the ossicles (*malleus*, *incus* and *stapes*), then passes across the oval window to the cochlea. The vibration in the fluid-filled cochlea causes movement of the basilar membrane, which in turn moves the hair bundles (stereocilia) of hair cells. Hair cells encode two properties of sound, frequency and intensity. There are two types of hair cells: outer hair cells, which are concerned with frequency tuning and amplification of sound through their interaction with the tectorial membrane and efferent systems, and inner hair cells, which are concerned with sound transduction. Hair cells are arranged in linear arrays along the basilar membrane (Kandel *et al.*, 2000).

Deflection of the hair bundle of an inner hair cell towards the tallest stereocilia opens ion channels, which allows influx of potassium from the potassium rich endolymph, depolarising the cell body. Depolarisation induces calcium influx which triggers release of neurotransmitter onto type 1 spiral ganglion cells. These spiral ganglion cells fire action potentials along axons (the VIII nerve) projecting to the cochlear nucleus (it is inner hair cells that transduce sound waves into electrical activity, i.e. APs). Since the basilar membrane becomes less stiff along the cochlea moving away from the oval window, high frequency sounds will resonate at the base of the basilar membrane and low frequency at the apex (Lieberman & Oliver, 1984; Fettiplace & Hackney, 2006). Therefore hair cells which are arranged all along the spiralling cochlea will sense different frequencies of sound depending on their location. This transformation of sound frequency to special location is known as tonotopy and is preserved along most of the auditory pathway (Kandel *et al.*, 2000). Intensity is coded as the rate of action potential firing of the VIII nerve as a result of the transmitter released from the inner hair cells.

The Binaural Auditory Brainstem

The Cochlear Nucleus

Each axon of the VIII nerve branches as it enters the cochlear nucleus. The ascending branch terminates in the ventral cochlear nucleus (VCN) while the descending branch innervates the dorsal cochlear nucleus (DCN). It is the VCN that projects to the binaural auditory brainstem so I shall focus on this rather than the DCN, which is concerned with spectral features of sound and compensating for movements of the head and pinna (Forsythe, 2002).

The VCN contains four cell types classified by their morphology, firing pattern and projections (Oertel, 1983). Of these, it is the spherical and globular bushy cells that project to the binaural brainstem. They are termed 'bushy cells' due to the sparse dendrites that form numerous fine branches at their ends. Spherical bushy cells (SBC) receive up to four giant glutamatergic synapses (end bulbs of Held) and project excitatory synapses bilaterally to the medial superior olives (MSO) and ipsilaterally to the lateral superior olive (LSO). Globular bushy cells (GBCs) receive afferent synaptic input from 20-40 fibres. This larger number of inputs helps to eliminate jitter in the timing signal (Joris *et al.*, 1994). They have a primary-like firing pattern (i.e. follow the auditory nerve, Forsythe, 2002). GBCs are of particular interest as they send a single large excitatory synapse (calyx of Held, Held, 1893) to the ipsilateral MNTB.

The superior olivary complex (SOC)

The SOC appears at the level of the 7th nerve and in the mouse extends rostrally around 500µm bilaterally. It is the first level of binaural sound-source localisation in the brain and consists of several nuclei specialised for this role: the MSO, LSO and a fast inverting relay synapse, the MNTB (Figure 1-1).

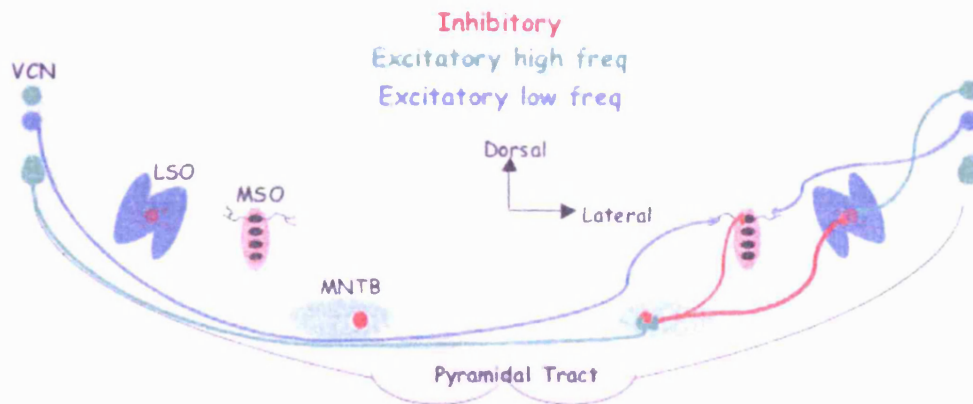


Figure 1-1. The Binaural Brainstem: A schematic diagram in the transverse plane illustrating the pathways and nuclei involved in sound localisation in the brainstem. SBCs project bilaterally to the MSO and ipsilaterally to the LSO. Axons from the GBCs project contralaterally to the MNTB which innervates its neighbouring MSO and LSO, which is crucial for sound localisation.

The Medial Nucleus of the Trapezoid Body (MNTB)

The MNTB is so named because of its position among trapezoid body axons. It primarily contains principal neurons (Kuwabara & Zook, 1991), which are easily identified by their spherical or elliptical cell bodies (~20µm in diameter) and their eccentric nucleus (Banks & Smith, 1992; Forsythe & Barnes-Davies, 1993). MNTB neurons usually have one or two small dendrites that extend only a short distance (20-40 µm). Together these properties make the MNTB ideal for voltage-clamp, as there will be little space clamp error. The MNTB is tonotopically organised with medial neurons receiving the lowest frequencies and lateral neurons receiving higher frequencies (Smith *et al.*, 1998).

As previously mentioned the MNTB receives one huge secure glutamatergic synaptic input (the calyx of Held) from the globular bushy cells of the VCN (Forsythe, 1994). The synaptic terminal and postsynaptic cell are specialised to faithfully preserve the temporal pattern of action potentials from the GBCs of the VCN (Forsythe & Barnes-Davies, 1993; Brew & Forsythe, 1995), which in turn preserve that of the auditory nerve. The output from the MNTB forms inhibitory synapses on the adjacent LSO and MSO, this output matures from GABAergic to glycinergic between postnatal day 3 and day 12

(Kotak *et al.*, 1998; Smith *et al.*, 2000). Therefore the MNTB acts as high fidelity, fast inverting relay from one cochlear nucleus to the contralateral MSO and LSO (Figure 1-1). Since the MNTB participates in a specific function (sound localisation) and there is accessibility to good voltage clamp and patch-clamp access to its presynaptic terminal (Forsythe, 1994), the MNTB is an attractive model to study the expression and function of ion channels in the central nervous system.

The Lateral Superior Olive (LSO)

In a transverse slice the LSO appears as a distinct S or U shape (depending on the species, S in rats, U in mice) and is easily seen in brain slices under low magnification (Figure 1-1). The folds in the nucleus are the major sites of afferent axons entering the LSO. The LSO is comprised of numerous cell types, but the most abundant (~70%, Wu & Kelly, 1991) are the principal neurons, which are arranged in transverse sheets perpendicular to the transverse axis of the LSO. The dendrites of the principal neurons are multipolar with discoid organisation.

The LSO is biased toward higher frequency sounds (>2kHz Guinan *et al.*, 1972) and is tonotopically arranged with frequencies increasing from medial to lateral. The primary role of the LSO is to discriminate the interaural level difference (ILD) of sound between the two ears (i.e. volume differences). As previously mentioned the LSO receives excitatory inputs from the spherical bushy cells in the ipsilateral VCN and inhibitory inputs via the MNTB from the contralateral VCN. It acts as an ILD detector by integrating the contralateral inhibition and ipsilateral excitation (Tollin, 2003).

The Medial Superior Olive (MSO)

Similar to the other SOC nuclei, the MSO is tonotopically organised with low frequencies located dorsally and higher frequencies ventrally. However in contrast to the LSO, the

MSO is biased to lower frequency sounds (<3 kHz, Smith, 1995), a consequence of its functional role as will be discussed later.

The MSO appears as a ladder-like structure in transverse slices as the cell bodies are arranged in a vertical band each with bipolar dendrites extending medially and laterally (Figure 1-1). The lateral dendrite receives excitatory synapses from the SBCs of the ipsilateral VCN, and the medial dendrites receive excitatory input from the SBCs of the contralateral VCN (Lindsey, 1975). MSO neurons also receive an inhibitory input from the ipsilateral MNTB (Kuwabara & Zook, 1991). The primary role of the MSO is in discriminating interaural timing differences (ITDs, Joris *et al.*, 1998). Note the MSO in the mouse is hard to detect due to its small size, which is likely due to the small size of its head, which results in little phase differences between the ears of a mouse.

Sound Source Localisation

Our ability to discriminate the location of a sound source has been crucial to our evolution and that of many other species. The first clue to how we may do this was the observation that a sound originating to the left will be louder in the left ear than in the right, due to shadowing by the head (ILDs, Strutt, 1877). Later the idea was put forward that we also use timing differences (ITDs, Strutt, 1907). These two different mechanisms are known as the Duplex Theory of sound localisation. The superior olivary complex is, at least in part, responsible for these functions, each of which will be discussed in turn.

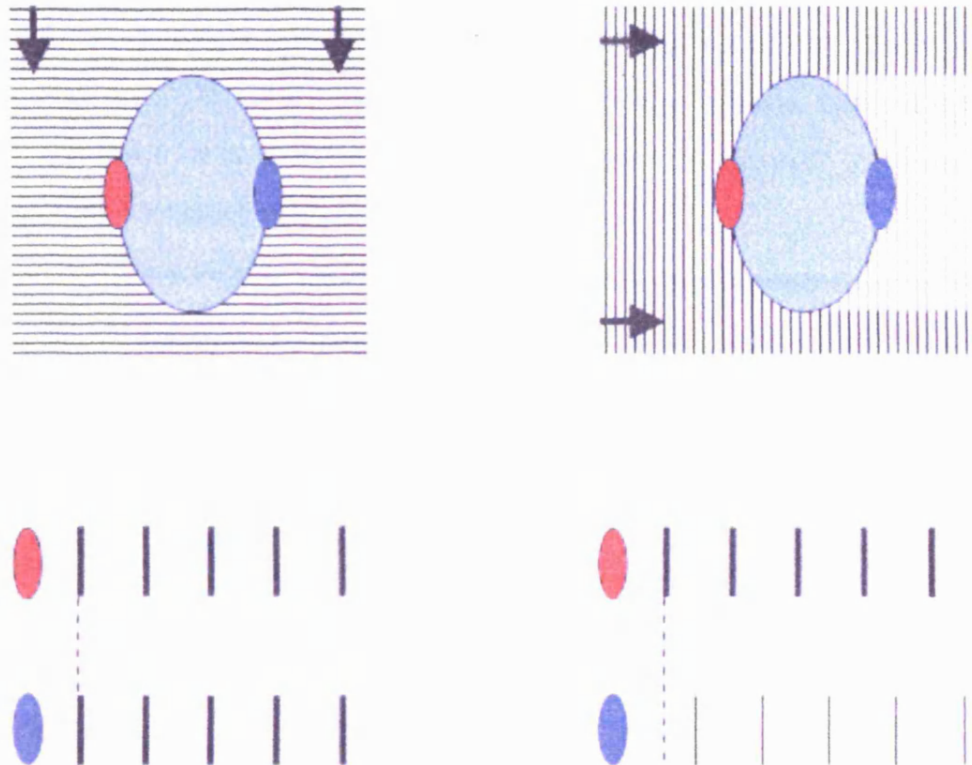


Figure 1-2. The Duplex theory of sound localisation *Left* sound arriving perpendicular to the axis of the ears will have the same intensity and timing. *Right* sound arriving off centre will be louder in the closest ear due to shadowing of the head, and there will be a phase difference between the ears.

Processing of Interaural Level Differences (ILDs) in the LSO

LSO principal neurons receive contralateral inhibition and ipsilateral excitation, therefore firing is determined by summation of excitatory and inhibitory post synaptic potentials (EPSP and IPSP respectively). A sound arriving at the ipsilateral ear will cause a large short latency EPSP and a smaller longer latency IPSP, which will result in the neuron firing (Tollin, 2003). However in the opposite LSO the IPSP will be larger, causing a shunt of the EPSP, resulting in no firing.

In comparing the relative weights of excitation versus inhibition, the refractoriness of the input needs to be minimal to aid the coding of intensity. The MNTB (being the

inhibitory input) is specialised for high frequency firing in a number of ways (e.g. rapid AMPA receptors, fast Kv3 channels, for review see Forsythe, 2002) and has been reported to fire up to 800Hz *in vitro* (Taschenberger & von Gersdorff, 2000) and in *in vivo* (Kopp-Scheinflug *et al.*, 2003).

As previously mentioned the LSO is skewed to higher frequencies (>2kHz). This fits well with a role in detecting intensity differences as it is not possible to detect level differences with low frequency sounds (Strutt, 1907).

Processing of Interaural Timing Differences (ITDs) in the MSO

The arrival of a sound at one ear (versus the other) may only vary by a few microseconds as the speed of sound at sea level is 343m s^{-1} , yet mammals and birds use this information to discriminate the origin of lower frequency sounds (<3kHz). A model to describe how this may be achieved was published in 1948 (Jeffress, 1948) and was based on the presence of delay lines and coincidence detectors. However recent evidence from mammals suggests a slightly different mechanism.

Delay lines and coincidence detectors

The Jeffress model is based on the presence of coincidence detectors and delay lines. Figure 1-3 is a schematised representation of the model. The delay lines in the model are created by the path length of the axons, and the coincidence detectors are the cells 1-5 which fire maximally in response to simultaneous bilateral excitation. This will occur when interaural time difference is exactly compensated by the delay line introduced by the pattern of innervation. For example, neuron 1 (Figure 1-3) will fire maximally when the sound originates far to the left ear, as the path length from the left ear is longer than that of the right, whereas neuron 3 will fire maximally when the sound is equidistant from the ears as the path lengths are equal. Therefore these cells will act as place cells for auditory space (Joris *et al.*, 1998).

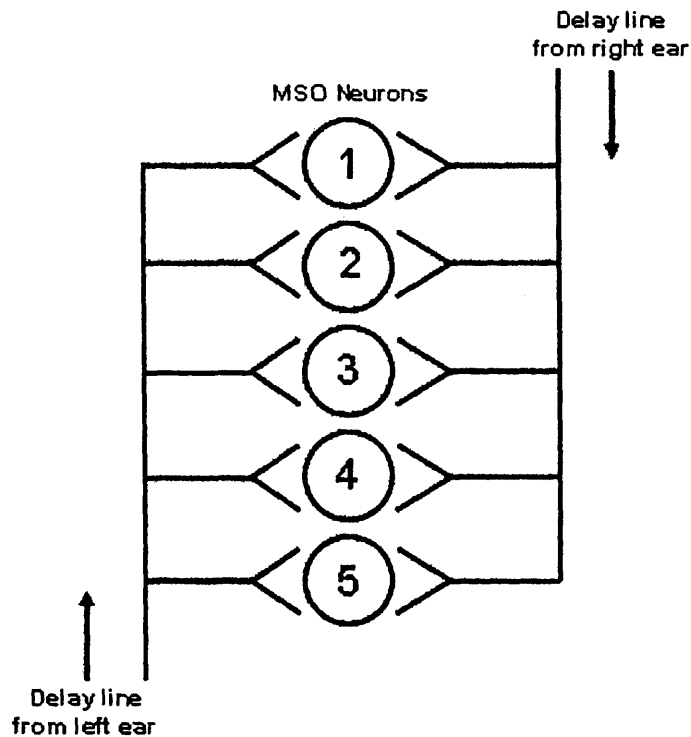


Figure 1-3 Delay lines and coincidence detectors: Representation of the Jeffress model. MSO neurons act as coincidence detectors only firing when they receive concurrent excitation. MSO neuron 1 will fire in response to a sound originating far to the left of the head, although sound reaches the left ear first, the path length introduces a delay, whereas the right only introduces a small delay, resulting in simultaneous excitation of neuron 1.

The barn owl has been shown to possess delay lines mediated by the axons of the nucleus magnocellularis and coincidence detectors mediated by cells of the nucleus laminaris (Sullivan & Konishi, 1986; Carr & Konishi, 1988, , 1990). In mammals the equivalent of the nucleus magnocellularis and nucleus laminaris are the VCN and the MSO respectively. However recent evidence does not support a delay line in mammals (Brand *et al.*, 2002).

The role of inhibition in mammalian ITDs

Recent work (McAlpine *et al.*, 2001; Brand *et al.*, 2002) has led to a new model being postulated, where instead of single neurons encoding auditory space, the brain uses the

relative firing rate across the whole MSO from each side to determine the lateral position of a sound (McAlpine & Grothe, 2003; McAlpine, 2005).

An interesting fact raised by these data is the vital role of inhibition, in coding ITDs. It has been known for some time that the MSO receives inhibition from the contralateral ear (Figure 1-4 A, Kuwabara & Zook, 1991), but its role has only just been realised. When strychnine (a glycine receptor antagonist) is applied to the MSO it abolishes ITD discrimination (Figure 1-4 C) causing all the neurons to fire maximally when a sound is equidistant from the ears. However, in control conditions the maximum firing rate is shifted to the right (i.e. contralaterally). The timing of the inhibition is crucial for this, as illustrated in Figure 1-4 B. Sound originating at the ipsilateral ear causes a short latency EPSP and a longer latency IPSP which minimises the depolarisation, whereas, contralateral sound causes a short latency IPSP followed by a lagging EPSP which results in more depolarisation.

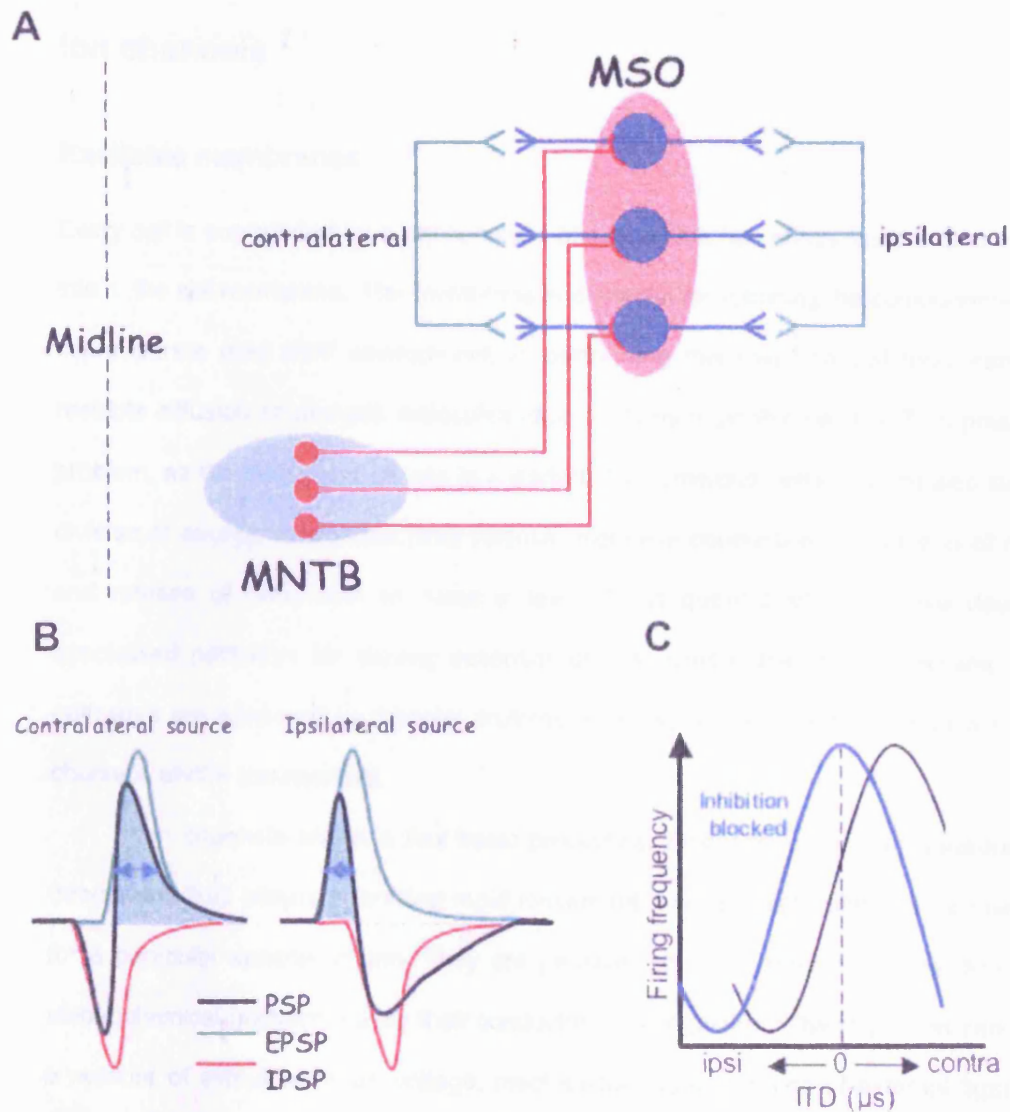


Figure 1-4 Role of inhibition in mammalian ITD discrimination: A) The pathways involved in ITD discrimination. **B)** The effect of contralateral versus ipsilateral sounds on the post synaptic potential of the MSO, highlighting the importance of the timing of the inputs. **C)** The effect of blocking the inhibitory input on the ability of neurons to code for ITD.

Obviously the timing and accuracy of the inhibition is crucial in this pathway. It is achieved at multiple stages along the pathway, which include the large diameter axons of the GBCs that terminate in a calyceal synapse, triggering the MNTB with high fidelity and short latency. The MNTB then rapidly and faithfully couples to the MSO cell bodies.

Ion channels

Excitable membranes

Every cell is surrounded by a phospholipid bilayer which has numerous proteins inserted into it, the cell membrane. The membrane is essential for retaining the components of the cell separate from their environment. In performing this role, the cell membrane also restricts diffusion of charged molecules (due to its hydrophobic centre). This presents a problem, as the movement of ions is important for numerous cellular processes such as: division of energy, neurotransmitter release, electrical conduction, contraction of muscle and release of hormones to name a few. Consequently all cells have developed specialised pathways for moving essential ionic species across the membrane. These pathways are mediated by integral proteins which span the membrane and act as ion channels and/or transporters.

Ion channels share a few basic properties: Firstly they form an aqueous pore through the lipid bilayer permitting rapid movement, and generally show some selectivity for a particular species of ion. They are passive, so once open, ions flow down their electrochemical gradient. Lastly their conductance is regulated. The regulation can be via a number of stimuli such as voltage, mechanical stress, binding of external ligands or internal regulators. In all cases the channel undergoes a conformation change which shifts the probability that it will open, and hence conduct.

Transporters differ from ion channels in that they do not possess an aqueous pore, rather they undergo a conformational change to physically shift molecules, and therefore movement is not as rapid. However they can move large molecules (e.g. neurotransmitters), and can also actively move ions up their concentration gradient, requiring energy, either from ATP (e.g. Na/K ATPase) or from the electrochemical gradient of another ionic species (e.g. Na/Ca exchanger).

Ion channels can be loosely divided into two categories, those that are activated by ligands and those that have another means of gating (which are mainly comprised of

voltage-sensitive channels). I will briefly discuss the latter and then go into greater detail on potassium channels.

Ligand-gated ion channels

Ligand-gated ion channels are specialised for mediating fast chemical synaptic transmission. They generate electrical signals (flux of ions) in response to a number of specific neurotransmitters: glutamate, glycine, acetylcholine, γ -aminobutyric acid (GABA), purines (i.e. ATP, ADP & adenosine) and 5-hydroxytryptamine. A functional ligand-gated ion channel is the combination of 3-5 separate proteins depending on the type (e.g. P_{2X} = 3, glutamate = 4, nicotinic acetylcholine receptor = 5). Interestingly non NMDA glutamate receptors have the same stoichiometry as K⁺ channels and resemble an inverted K⁺ channel (Kuner *et al.*, 2003).

The major excitatory neurotransmitter in vertebrates is glutamate and every cell in the central nervous system is likely to receive glutamatergic excitation (Hille, 2001). Indeed the calyx of Held / MNTB is a glutamatergic synapse, which has a specialised glutamate gated ion channel of the α -amino-3hydroxy-5methyl-D-aspartate (AMPA) family, GluR_D (Geiger *et al.*, 1995). This particular variant of AMPA receptor has extremely fast kinetics, 2-3 times faster than other GluR subunits and displays rapid recovery from desensitisation (Raman *et al.*, 1994), properties which facilitate the MNTB's role of high frequency transmission.

Voltage-gated channels

The voltage-gated super family is chiefly composed of Na⁺, K⁺ or Ca²⁺ permeable channels, whose primary role is transmission of electrical signals, either along axons/dendrites or triggering synaptic transmission (Ca²⁺ channels). The main focus of

this thesis is on potassium channels; nevertheless I will briefly discuss the other members.

Voltage-gated sodium (Nav) channels

The Nav family has little diversity with only nine genes expressed in mammals. A functional Na⁺ channel is formed by a single α protein with four analogous repeats of six transmembrane domains each, further limiting functional diversity as only one gene can encode a functional channel. Nav channels classically open rapidly (<1ms) and then quickly inactivate.

Opening of a Nav channel causes influx of Na⁺ ions, resulting in depolarisation. In axons Nav channels generate the rapid regenerative upstroke of the action potential. In other membranes they can also contribute to pacemaker activity and sub-threshold potentials (Hille, 2001). Nav1.6 and or Nav1.1 predominate in the MNTB (Leao *et al.*, 2005a; Leao *et al.*, 2006a), whereas only Nav1.6 appears to be predominant at the calyx of Held (Leao *et al.*, 2005a). In the Calyx recovery from inactivation is rapid (τ <2ms), whereas in the MNTB recovery is bi-exponential with a fast component (τ ~2ms) and a smaller much slower component (τ ~80-90ms, Leao *et al.*, 2005a) measured at 25-27^oC. These slight differences in the properties pre and post synaptically may be explained by accessory subunits. Once more the properties of the intrinsic channels of the MNTB aid high frequency firing, in this case the rapid recovery from inactivation.

Voltage-gated calcium (Cav) channels

As with the Nav family, Cav channels are formed from a single α_1 protein with four analogous repeats of six transmembrane domains (Catterall *et al.*, 2003b). Cav channels are usually accompanied by an intracellular β subunit and a transmembrane $\alpha_2\delta$ subunit which modulates channel properties. However, the pharmacology and electrophysiological diversity arises mainly from the α_1 subunit (Catterall *et al.*, 2003b).

There are 10 different α_1 genes encoding 5 functional families: Cav1.1 -1.4 (L-type), Cav2.1 (P/Q-type), Cav2.2 (N-type), Cav2.3 (R-type) & Cav3.1 -3.3 (T-type). L-type channels are the main Ca^{2+} channels in muscle and endocrine glands, where they are associated with contraction and secretion respectively. They are also found in neurons. T-type channels activate at modestly depolarised voltages, are transient (i.e. inactivate) and are found in numerous neuron types where they shape action potentials and control repetitive firing (McCormick, 2003). The remaining high voltage-activated N, P/Q and R type channels are found in dendrites, cell bodies and also at fast central synapses where they initiate transmitter release (Catterall *et al.*, 2003b).

The Cav channels present at the immature (around postnatal day 7, ~P7) calyx of Held are a mixture of N, R and P/Q-type channels but at around P10 there is a marked switch to P/Q type (Iwasaki *et al.*, 2000). Interestingly this developmental shift only happens at the terminal; at the GBC cell body there still remains a mixture of Cav channels (Doughty *et al.*, 1998). The role this switch plays is unknown but similar developmental changes are seen at other fast synapses (e.g. GABA terminals of Purkinje cells onto deep cerebellar nuclei and terminals of the reticular nucleus thalami, Iwasaki *et al.*, 2000).

Hyperpolarisation activated (HCN/h) channels

Four HCN genes are known to encode hyperpolarisation cyclic nucleotide gated channels, which mediate the current I_h . HCN channels are similar to K^+ channels in that they are tetrameric, however they lack the selectivity of the other voltage gated channels. They are permeable to both Na^+ and K^+ ions with a permeability ratio of 0.2:1 (Hille, 2001), which gives them an equilibrium potential of around -30mV. As their name suggests they open with hyperpolarisation and close at depolarised potentials. Their voltage sensitivity is positively shifted by direct action of cyclic nucleotides (Ludwig *et al.*, 1998). Therefore when a cell experiences hyperpolarisation, these channels will open and act to depolarise. It is this property that enables them to act as pacemaker channels

in heart and brain (Santoro *et al.*, 1998). HCN channels also have roles in dendritic integration (Magee, 1999) setting the resting membrane potential (Meuth *et al.*, 2006) and possibly long term potentiation (Mellor *et al.*, 2002). HCN1 is absent from the MNTB but HCN2 is strongly expressed (Koch *et al.*, 2004). Additionally I_h in the MNTB has been shown to be modulated by noradrenalin acting via cAMP (Banks *et al.*, 1993). It has been suggested that I_h may help to prevent temporal summation in the MNTB (Leao *et al.*, 2005b). I_h is also present at the calyx of Held where it is modulated by cAMP (Cuttle *et al.*, 2001), although no effect on synaptic transmission was found.

The Super-family of Potassium channels

Structural Divisions

The super family of K^+ channels contains over 80 different subunits, which are involved in many processes and they vary markedly in structure and function. They can be broadly divided into 3 groups based on structural similarities (Figure 1-5).

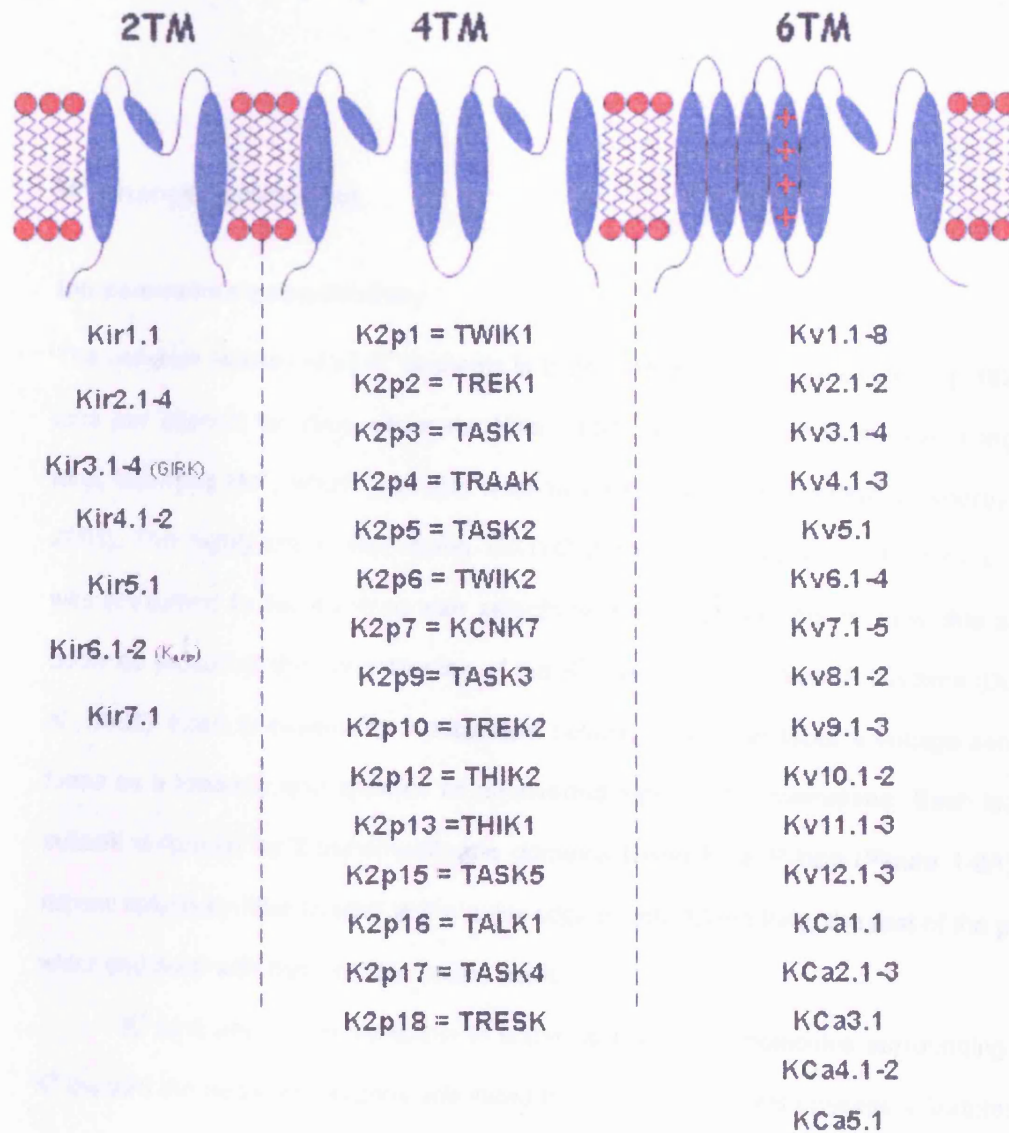


Figure 1-5. Structural divisions of the K^+ channel family

The first group, known as the inward rectifiers are made up of channels that contain only the 2nd TM pore forming domains. The second, termed leak or K₂p channels possess 4th TM domains; each subunit containing two pore regions. The third and largest group have 6th TM domains with the pore region making the 5th and 6th TM domains. They are mainly composed of the voltage-gated channels, the first 4 TM domains being involved in the voltage sensing and gating.

K⁺ channel properties

Ion permeation and selectivity

The common feature of all K⁺ channels is their ability to pass K⁺ ions rapidly (~162million ions per second for BK_{Ca} channels, Hille, 2001) while simultaneously excluding other ions, including Na⁺, which has both a smaller ionic radius and hydration energy (Hille, 2001). The highly conserved region TXGYG (Heginbotham *et al.*, 1994, Figure 1-6 D) was presumed to be involved with selectivity. Much speculation on how this actually occurred preceded the crystallisation of the K⁺ channel, KcsA from *S. lividans* (Doyle *et al.*, 1998). KcsA is essentially a potassium selective pore that lacks a voltage sensor; it forms as a tetramer and appears as an inverted tepee in the membrane. Each identical subunit is formed by 2 transmembrane domains linked by a P-loop (Figure 1-6A). The narrow selectivity filter located at the outer edge is only 1.2nm long, the rest of the pore is wider and lined with hydrophobic amino acids.

K⁺ ions are extremely stable in water, with 8 water molecules surrounding each K⁺ ion with the negative oxygens orientated inwards. K⁺ channels possess 4 features that bestow the exquisite selectivity and near diffusion-limited rates of conduction. First, the pore is initially wide containing a large amount of water (the aqueous vestibule) into which K⁺ ions can diffuse whilst still in their hydrated form (Yellen, 2002). Secondly they achieve some cation selectivity by the dipole moment of the α -helices in the P-loop (Figure 1-6 A) which also help to stabilise cations at the mouth of the selectivity filter

(Doyle *et al.*, 1998). Thirdly, the selectivity filter mimics the coordination state of a K^+ ion in water by presenting a tunnel of oxygens (provided by the carbon backbone of the conserved sequence, Figure 1-6 B, C & D).

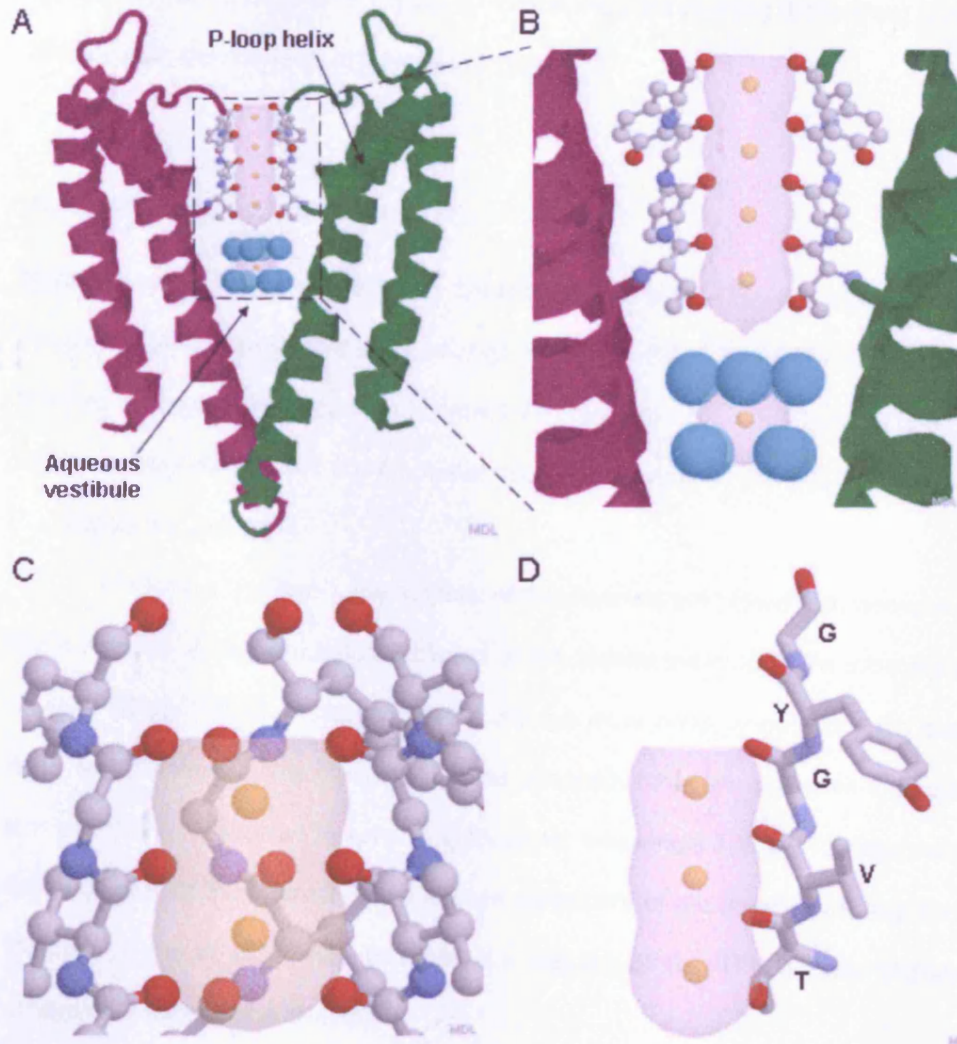


Figure 1-6. The crystal structure of KcsA reveals the basis of ion permeation and selectivity: **A)** Two opposite subunits (green and magenta, cartoon) with 4 K^+ ions (orange) in the selectivity filter (ball & stick). **B)** close up of the box in A, showing the selectivity filter and a K^+ ion still surrounded by water (cyan) in the aqueous vestibule. **C)** The selectivity filter provides a tunnel of oxygens (red) to stabilise the K^+ ions (one subunit removed for clarity). **D)** The conserved sequence (stick) TXGYG is arranged to provide carbonyl oxygens to line the pore. (Pictures produced from the crystal structure of KcsA using protein explorer, PDB 1K4C).

This specific organisation of the oxygens results in dehydration and rehydration energies for K^+ close to zero (Morais-Cabral *et al.*, 2001), whereas for the smaller Na^+ ion greater

energies are required, thus providing the basis of selectivity {confirming the postulation of Armstrong (1974), that selectivity is based upon hydration energies}. Finally, to prevent the K^+ ions from sticking in the pore, the mutual electrostatic repulsion of the K^+ ions spaced $\sim 0.7\text{nm}$ apart destabilise the K^+ ions in the pore pushing them along (Zhou *et al.*, 2001), rather like the balls of a Newton's cradle.

Voltage sensing and activation

Members of the 6TM domain family contain an additional 4TM domains which precede the pore region. The domains are usually named S1-S6, S5 and S6, form the pore and S1-4 the voltage-sensing domain (Figure 1-7A). As with all K^+ channels the pore has four fold symmetry (Figure 1-7 B), the 4 subunits join together at the tetramerization domain (T1, Figure 1-7 A & C).

At rest (i.e. $\sim -70\text{mV}$), the majority of Kv channels are closed (i.e. non-conducting); this is a result of the pore being occluded by the bundle crossing of the intracellular tip of S6 (see Figure 1-6 A). A conformational change must occur in order for the channel to open which removes this occlusion. Some channels have an extensive intracellular C-terminus which is involved in sensing intracellular messengers (e.g. BK_{Ca} channels sense Ca^{2+}). Binding of the internal ligand causes movement of the bundle crossing and opens the pore (Jiang *et al.*, 2002). However the majority of the 6TM domain channels use voltage as a means of activation.

The voltage sensing domain is made up of four TM domains, the fourth (S4) has positive amino acid residues (arginines or lysines) at every third position and is conserved amongst the other voltage sensitive channels (i.e. Nav and Cav). It has been shown that these charges are crucial for voltage sensing (Aggarwal & MacKinnon, 1996; Seoh *et al.*, 1996). This voltage sensing region is coupled to channel opening by the S4-S5 linker and the C-terminus of S6 (Lu *et al.*, 2002). However there still remains some contention over the exact mechanism of voltage-sensing and coupling to activation.

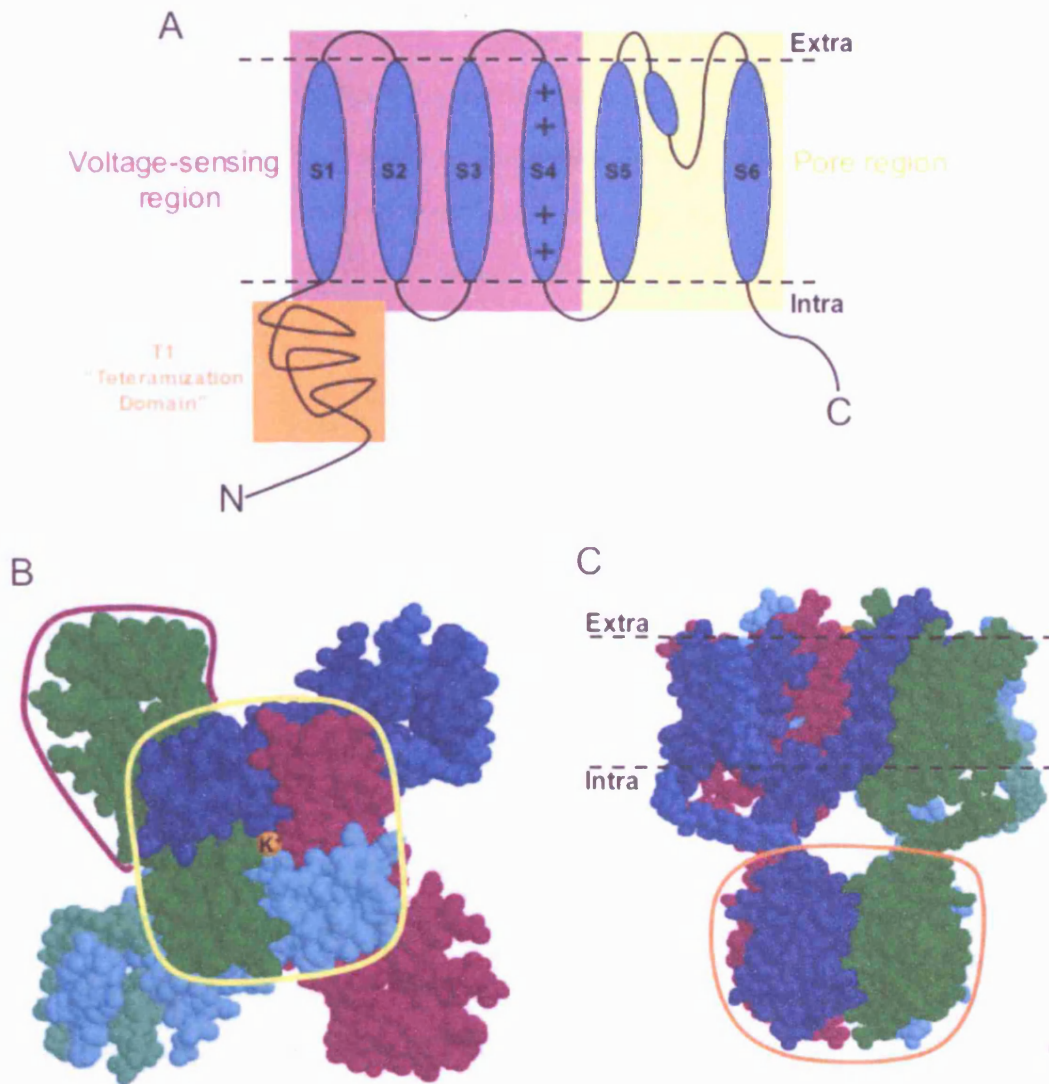


Figure 1-7. The Kv1.2 channel is a tetramer of subunits: **A)** Schematic of the transmembrane domains of a single subunit. **B)** Top down view of the crystal structure of Kv1.2 (PDB 2a79) with the subunits represented in different colours (spacefill), yellow box outlines pore region, purple line defines a single voltage sensor. **C)** Side view of the channel in B, showing the tetramerization domain in orange. (Structural pictures produced in protein explorer).

The voltage sensor has long been known to physically move across the electric field of the membrane, as it is possible to measure the charges moving when conduction is blocked (Armstrong & Bezanilla, 1973; Schneider & Chandler, 1973). It was therefore postulated that this movement causes a conformational change in the channel resulting in opening of the pore. Several different lines of evidence showed that charges are

masked when the channel is at rest and then become exposed to the extracellular environment when the channel is activated (Larsson *et al.*, 1996; Seoh *et al.*, 1996; Yusaf *et al.*, 1996). These movements were thought to be small (<0.5nm), although the crystal structure of KvAP (Jiang *et al.*, 2003) raised some controversy. They postulated a 'flipper' mode of gating where the S1-S4 domain moved considerably through the membrane. At present it is thought that the model put forward by Jiang *et al* is incorrect (possibly due to the method of crystallisation), a more recent structure of mammalian Kv1.2 is in closer agreement with previous functional data (Long *et al.*, 2005a, 2005b). In summary the voltage sensor moves in response to a change in the membrane potential, which results in a new channel conformation where the bundle crossing is more likely to open and thus conduct.

Inactivation

In addition to deactivation (the inverse of activation, i.e. the voltage sensor moving back to the resting position and closure of the channel), Kv channels can inactivate. This process is distinct from activation/deactivation and can be caused by two methods, one generally fast (i.e. N-type) and one generally slower (C-type).

N-Type Inactivation

N-type inactivation is also termed "ball and chain" inactivation because it is caused by the positively charged N-terminal "ball" peptide moving into the mouth of the channel occluding the pore. Binding sites in the internal mouth of the pore and on the T1 domain have been identified (Figure 1-8 A, Long *et al.*, 2005a). The inactivating domain can be supplied by the Kv α subunit or by accessory β subunits (Robertson, 1997). As Kv channels are composed of 4 α subunits and up to 4 β subunits there is potentially up to 8 inactivating peptides present. A greater number of peptides tends to speed the rate of inactivation (Xu *et al.*, 1998) even though only 1 is required for inactivation. Interestingly,

Kv1.6 possesses an N-terminal inactivation prevention (NIP) domain, which tethers the ball peptide “out of the way” (Roeper *et al.*, 1998), and thus prevents N-type inactivation. N-type inactivation is generally rapid and usually occurs within 20ms (Coetzee *et al.*, 1999), however it is not always complete. This may reflect the position of the binding site for the inactivating peptide; in some channels the peptide may not entirely occlude the pore.

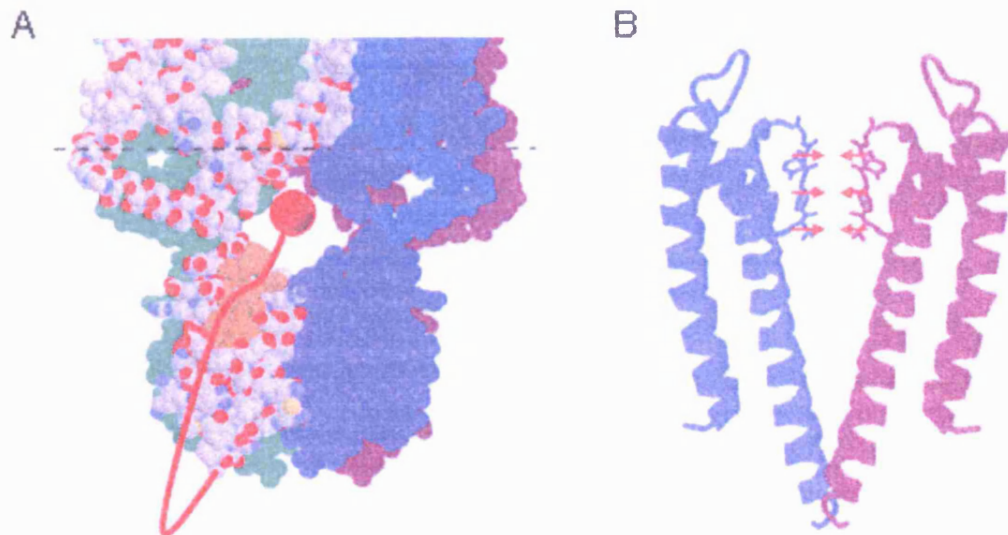


Figure 1-8. Inactivation of Kv channels: **A)** N-type inactivation involves the N terminus (red ball & chain) moving in and plugging the pore, brown region shows putative binding site for N-terminal peptide provided by T1, binding sites are also located at the mouth of the pore. **B)** C-type inactivation involves collapse of the selectivity filter.

C-Type inactivation

C-type inactivation is caused by collapse of the selectivity filter, which results in a no conductance (Figure 1-8 B, Yi & Jan, 2000). It varies with external $[K^+]$ (Baukrowitz & Yellen, 1995). It is thought that K^+ helps to stabilise the selectivity filter. Consistent with this proposal, the partial collapse of the selectivity filter has been observed in the crystal structure of KcsA when the $[K]$ was low (Zhou *et al.*, 2001). C-type inactivation is generally slow, however in some Kv channels (e.g. ERG) C-type inactivation can be rapid (Tristani-Firouzi & Sanguinetti, 2003).

2TM domains / Inward rectifiers

The 2TM domain family, known as the inward rectifiers (Kir, Coetzee *et al.*, 1999) are formed as tetramers. They form a K^+ selective pore in the membrane, however as the name suggests they prefer to pass inward current and do not pass much outward current in voltage-clamp. The basis of this rectification has been known for some time; polyamines and/or intracellular Mg^{2+} occlude the pore when current passes in the outward direction. The actual mechanism was realised with the crystallisation of the Kir3.1 intracellular domain (Nishida & MacKinnon, 2002). The intracellular part of the channel extends 3.2nm (the same length as the transmembrane portion) with a width of ~1.5nm. It holds the pore continually open and is lined with negatively charged amino acids providing binding sites for polyamines and Mg^{2+} . However under normal physiological conditions the membrane potential is rarely more negative than E_K , therefore current is normally outward but only at negative voltages.

Kir channels are involved in stabilising resting membrane potentials (Hille, 2001) but their rectification prevents shunting of any depolarising influences (e.g. EPSP). The Kir6 subfamily is the most extensively studied of the inward rectifiers as, together with the sulphonylurea (SUR) receptor, this forms the K_{ATP} channel. K_{ATP} channels link the membrane potential to the metabolic state of the cell by opening when $[ATP]_i$ is low, therefore hyperpolarising cells that are low on energy. They have received, much interest as they provide a degree of protection against ischemic insult in the heart (Kane *et al.*, 2005), and are involved in type II diabetes mellitus (Proks & Lippiat, 2006). All of the Kir channels are sensitive to low concentrations of extracellular Cs^+ (Coetzee *et al.*, 1999).

4TM domains / Twin-pore channels

Background current or 'leak' has been a part of electrophysiology almost since the beginning of recording; it was used to explain the negative resting potential of neurons

(Hodgkin & Huxley, 1952). Today the term leak is applied to channels that are open at rest and seem to instantaneously reach a new steady-state level with a change of voltage. However, only recently has a molecular correlate been identified, first in yeast (Ketchum *et al.*, 1995) and the following year in *Drosophila melanogaster* (Goldstein *et al.*, 1996). To date there are 15 mammalian “leak” genes (Figure 1-9) encoding channels that are selective for K^+ and are open at rest.

According to the international union of pharmacology (IUPHAR) these channels should be named after their gene names i.e. KCNK1 = K2p1.1. However a more useful nomenclature exists, which is based on the channel's properties and actually divides them into structurally similar families. For example: K2p1.1 is known as TWIK1 (Tandem of P domains in a Weak Inward rectifying K⁺ channel), whereas K2p3.1 is known as TASK1 (Two-pore Acid Sensitive K⁺ channel). Figure 1-9 shows how structurally and functionally related channels are easier to determine with the functional nomenclature.

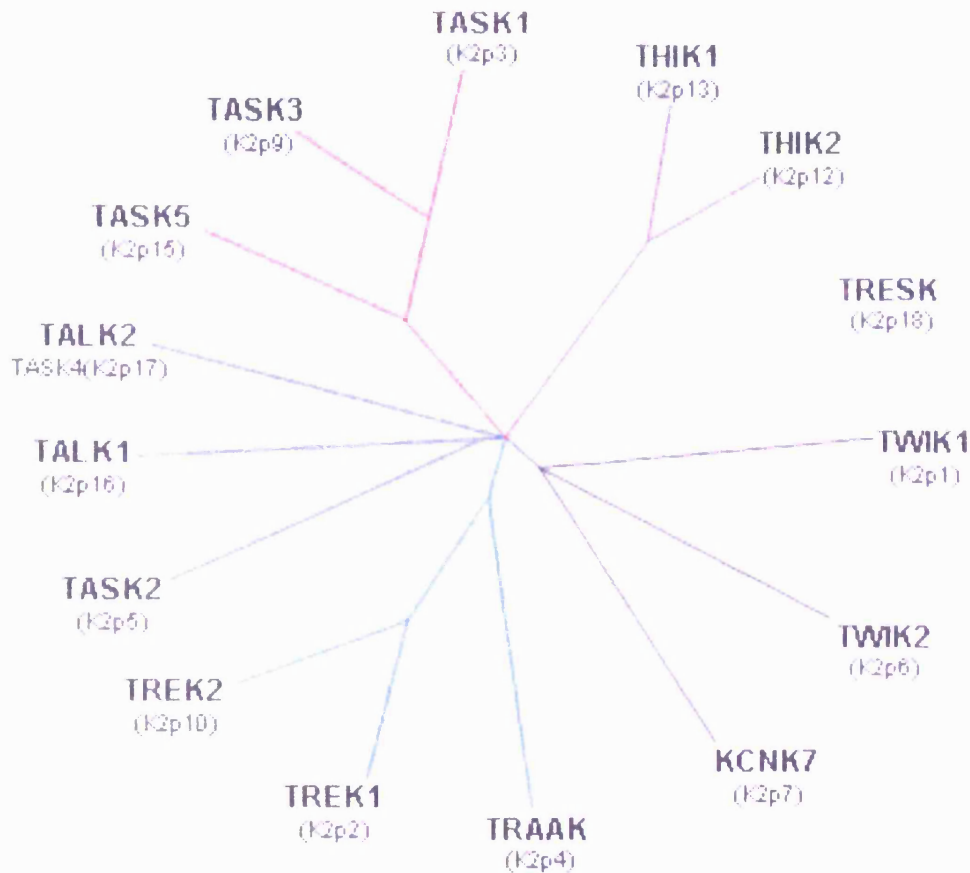


Figure 1-9 Family tree of the K2p members: Dendrogram showing the structural relations among the K2p channels, reproduced from Patel & Lazdunski (2004).

As the name implies these channels have 4TM domains comprised of two pore regions. Uniquely among the K^+ channels, a functional K2p channel is formed as a dimer rather than a tetramer (Goldstein *et al.*, 2001). They are essentially K^+ selective pores that are open at rest, show no voltage-dependence and do not display the strong inward rectification seen in the Kir family. Instead they display some outward rectification in physiological $[K^+]$, explained by the Goldman-Hodgkin-Katz current equation (Equation 2-9), which disappears in symmetrical $[K^+]$. Additionally nearly all members show some form of modulation (Patel & Lazdunski, 2004).

The modulation of these channels is extensive and a complete description is beyond the scope of this thesis (for review see, Goldstein *et al.*, 2001; Patel & Lazdunski, 2004), however some of the salient features are outlined in (Table 1).

Family	Properties
Tandem of 2 pore domains in a Weak Inward rectifying K ⁺ channel	Weak inward rectification, silenced by SUMO (small ubiquitin-like modifier protein)
Twik RElated K ⁺ channel	Potentiated by: intracellular acidosis, halothane, chloroform arachidonate, stretch, cGMP Inhibited by: cAMP, PKC.
Twik related Acid Sensitive K ⁺ channel	Blocked by extracellular acidosis, modulated by metabotropic receptors
Twik related Halothane Inhibited K ⁺ channel	Inhibited by halothane, potentiated by arachidonate
Twik related ALKaline sensitive K ⁺ channel	Absent in the brain. Potentiated by extracellular alkalinization
Twik RElated Spinal cord K ⁺ channel	Exclusive to the spinal cord, inhibited by arachidonate

Table 1: Salient features of the K2p families

The K2p channels are relatively insensitive to classical K⁺ channel blockers (e.g. TEA and 4-AP) but all show some sensitivity to low mM concentrations of Ba²⁺ (Patel & Lazdunski, 2004).

6TM domains / voltage-gated and Ca²⁺-activated channels

The 6TM domain family comprises the largest of the K⁺ channels (the subfamilies are outlined in Figure 1-10); they have an extra 4TM domains per subunit (as discussed earlier), which endows them with the ability to sense voltage; some have additional properties that are bestowed by extensive C-terminal intracellular motifs. I will briefly talk about these members before moving on to the Kv channels.

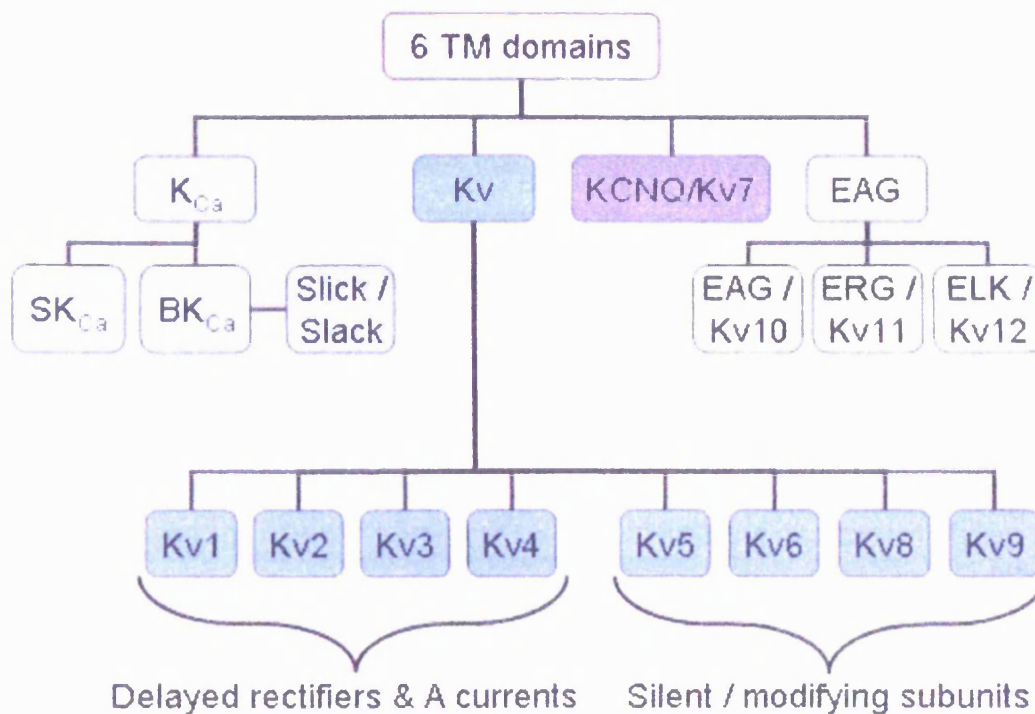


Figure 1-10. The subfamilies of the 6 transmembrane domain K^+ channels

Calcium-activated K^+ channels (K_{Ca})

The K_{Ca} family can be further divided into distinct but distantly related groups. The first group contains the 3 small conductance channels ($K_{Ca2.1}$, 2.2 & 2.3 or SK1-3) and the intermediate conductance channel ($K_{Ca3.1}$ or IK_{Ca}). All of these channels are insensitive to voltage, activated by low concentrations of intracellular Ca^{2+} ($<1\mu M$), and the SKs are sensitive to apamin (100pM-10nM, Stocker M., 2004). These channels do not bind calcium directly rather they have calmodulin constitutively bound to their C-terminus (Xia *et al.*, 1998). IK_{Ca} is mainly expressed in blood and epithelial cells whereas the SK channels are predominantly expressed in the nervous system where they contribute to the medium duration after hyperpolarisation (mAHP, Stocker, 2004).

The second group contains 4 genes that form structurally related channels and unlike the first group are sensitive to voltage. The most extensively studied of these is $K_{Ca1.1}$ also known as BK_{Ca} for its large (Big) conductance, around 260pS. BK_{Ca} channels

bind Ca^{2+} directly which causes a leftward shift in their voltage dependence (Cox *et al.*, 1997). These channels have been extensively studied in numerous brain regions. The other 3 members of this group $\text{K}_{\text{Ca}5.1}$, $\text{K}_{\text{Ca}4.1}$ & 4.2 are rather unfortunately named as they are not in fact Ca^{2+} sensitive; they were grouped in this family before their properties were fully understood. $\text{K}_{\text{Ca}5.1}$ is sensitive to internal alkalization (Schreiber *et al.*, 1998), whereas $\text{K}_{\text{Ca}4.1}$ and 4.2 are sensitive to Na^+ and Cl^- (Bhattacharjee & Kaczmarek, 2005).

KCNQ / Kv7 / M-channels

The KCNQ/Kv7 subfamily has 5 members that form channels structurally similar to the Kv channels. They mediate slowly activating delayed rectifier currents. They are highly modulated and have extended C-termini (the length varies depending on the subunit) where the modulatory sites are located (Jentsch, 2000; Robbins, 2001).

KCNQ1 was first discovered in the heart where it co-assembles with KCNE1 (called IK_{s}), mutations in this channel lead to a form of long QT syndrome (Camm *et al.*, 2000). KCNQ2, 3 and 5 can form channels as homomers and/or heteromers which give rise to the M-current (muscarine inhibited, Wang *et al.*, 1998a). KCNQ4 is expressed highly in the auditory pathway; (including the LSO but apparently absent from the MNTB, Kharkovets *et al.*, 2000) it has a role in K^+ cycling in the cochlea (Jentsch, 2000). Recent work has demonstrated the presence of KCNQ channels at nodes of Ranvier (Schwarz *et al.*, 2006) and in unmyelinated axons (Vervaeke *et al.*, 2006), where they may contribute to excitability at very high frequencies. All of the KCNQ channels are sensitive to low concentrations of linopiridine ($<20\mu\text{M}$, Gutman *et al.*, 2003).

Ether-à-go-go (EAG) channels

Mutations in a K^+ channel of *Drosophila* resulted in leg shaking when anaesthetised with ether, which earned the K^+ channel its unusual name, *ether-à-go-go*. Since their discovery there have been two other related subfamilies ERG and ELK (EAG related gene and EAG like K^+ channel, respectively). In mammals they are widely expressed in

the heart and brain, including the SOC (Saganich *et al.*, 2001). EAG and ELK1 channels mediate an extremely slowly activating delayed rectifier, whereas ERG and ELK2 channels have unusual gating (Bauer & Schwarz, 2001). The most widely studied of these channels is ERG1, as it is involved with repolarisation of the cardiac action potential and is prone to block by many pharmacological agents which can result in fatal arrhythmias. The ERG channels inactivate rapidly, so when the membrane is depolarised little current passes through these channels, however as the membrane starts to repolarise the inactivation is rapidly removed resulting in large transient currents which deactivate slowly (Bauer & Schwarz, 2001).

The voltage-activated K⁺ (Kv) channels

The Kv channels form the largest family of all the K⁺ channels; they are named after their encoding genes: KCNA = Kv1.1-8, KCNB = Kv2.1-2, KCNC = Kv3.1-4, KCND = Kv4.1-3, KCNF = Kv5.1, KCNG = Kv6.1-4, KCNV = 8.1-2 and KCNS = Kv9.1-3. As illustrated in Figure 1-10 they can be divided in to two groups.

Delayed rectifiers and A-Currents

The Kv1s, Kv2s, Kv3s and Kv4s can form homomeric or heteromeric channels but only within their own subfamily (e.g. Kv1.1 and Kv1.2 can form channels but not Kv1.1 and Kv3.1, Coetzee *et al.*, 1999), with the exception of the Kv2s.

Kv1 sub-family

The Kv1 family form low voltage-activated currents, usually of the delayed rectifier phenotype (depending on the subunit, Figure 1-11). Therefore they tend to open at sub action potential thresholds (i.e. more negative than Nav channels, Coetzee *et al.*, 1999), the functional role of these channels will be discussed in detail later.

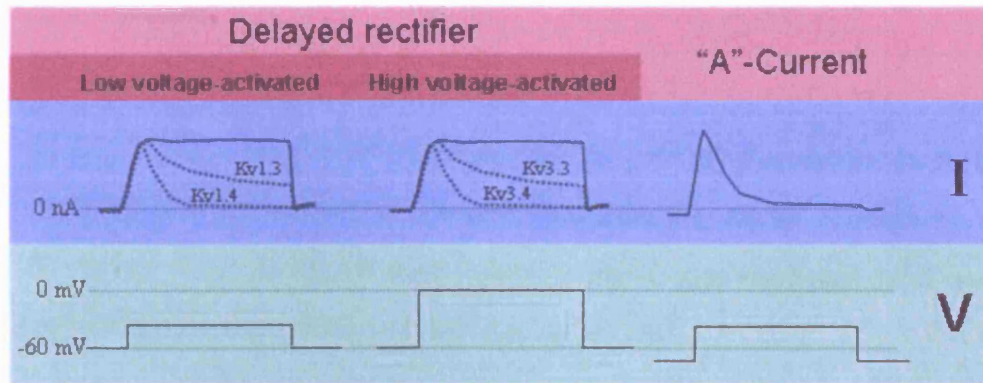


Figure 1-11. Delayed rectifier and A-current Phenotypes: Schematic showing the different 'phenotypes' of K^+ current.

Kv2 subfamily

Although Kv2 subunits have been identified as major components of delayed rectifier current in several neurons (Baranauskas *et al.*, 1999; Murakoshi & Trimmer, 1999), the physiological roles of Kv2 channels in the brain are still poorly understood.

The Kv2 subunits can form heteromeric channels with the electrically silent subunits (see later). Kv2 channels form delayed rectifier currents which have varying ranges and rates of activation and inactivation depending on the composition of the channel but in generally their activation rate is considered slow.

Kv3 subfamily

Kv3 channels form rapidly activating high voltage-activated channels; they only open after considerable depolarisation (~ 30 mV). Due to their high voltage-activated nature, their function is restricted to repolarisation of action potentials since they only open after Nav channels. Depending on their subunit composition they can form inactivating currents or delayed rectifiers (Figure 1-11, Rudy & McBain, 2001) e.g. Kv3.1 is very slowly inactivating delayed rectifier whereas Kv3.4 resembles an A-type conductance.

Kv4 subfamily

Members of the Kv4 subfamily rapidly inactivate (τ 10-100ms), which can be mediated by C-type and / or N-type (Birnbaum *et al.*, 2004). This rapid inactivation results in them mediating transient outward (A-type) currents, they are usually activated by modest depolarisations (\sim -50mV) and display sizeable steady state inactivation ($>1/2$ at resting membrane potentials, Figure 1-11, Birnbaum *et al.*, 2004).

The silent subunits (Kv5, 6, 8 &9)

The remaining four families are termed the “electrically silent” subunits as they are unable to form functional homomeric channels in expression systems (for review see Robertson, 1997). The reason for their non-conducting function appears to be due to retention in intracellular organelles, unless associated with a Kv2 subunit (Salinas *et al.*, 1997b). The silent subunits are also known as “modifier” subunits due to their ability to alter both the biophysical and pharmacological properties of Kv2.1 and Kv2.2 (Post *et al.*, 1996; Salinas *et al.*, 1997b; Kerschensteiner & Stocker, 1999; Sano *et al.*, 2002).

Accessory subunits

In addition to α subunits which by them selves form the functional channels, β -subunits also exist. These are intracellular proteins which bind to the T1 domain (Gulbis *et al.*, 2000). They can act to increase surface expression (Fink *et al.*, 1996), speed inactivation (McCormack *et al.*, 1995) and shift voltage dependence of activation (Heinemann *et al.*, 1996). The physiological roles of these β -subunits are still poorly understood.

Chapter 2 – Methods

This chapter describes the methods and will give more detailed background where necessary. Where particular experiments differ from the methods outlined here, they will be described in the relevant results sections.

Tissue preparation, maintenance and visualisation

Solutions

An artificial cerebrospinal fluid (aCSF) was made to mimic physiological CSF, the composition is summarised in Table 2-1. The aCSF was continuously bubbled with 95%O₂/5%CO₂ (carbogen) to buffer the pH to 7.4. Divalents were added after ~10mins of bubbling to prevent precipitation with the HCO₃ (Forsythe, 1994). For the majority of experiments an artificially low concentration of Ca²⁺ was used (i.e. CaCl₂ 0.5mM which was replaced with MgCl₂ 2.5mM). This was to minimise any contribution from K_{Ca} channels and / or Cav currents (Brew & Forsythe, 1995). This solution is termed Low Ca²⁺ aCSF.

For dissecting and slicing a modified slicing CSF was made, the composition is summarised in Table 2-1. This was also bubbled with carbogen. NaCl was replaced by sucrose to reduce Na⁺ overload that arises during the low temperature slicing conditions. A higher Mg²⁺ and lower Ca²⁺ concentration were used to reduce Ca²⁺ entry through NMDA receptors, among others, which would have a neuroprotective effect. This solution is termed slicing aCSF.

	Slicing aCSF	Low Ca ²⁺ aCSF	Patch solution
KCl (mM)	2.5	2.5	32.5
Kgluconate (mM)	-	-	97.5
KOH (mM)	-	-	13
NaCl (mM)	-	125	-
CaCl ₂ (mM)	0.1	0.5	-
MgCl ₂ (mM)	4	2.5	1
Ascorbic acid (mM)	0.5	0.5	-
NaH ₂ PO ₄ (mM)	1.25	1.25	-
Myo-inositol (mM)	3	3	-
Na pyruvate (mM)	2	2	-
Glucose (mM)	10	10	-
NaHCO ₃ (mM)	26	26	-
HEPES (mM)	-	-	10
EGTA (mM)	-	-	5
Sucrose (mM)	250	-	~ 30
pH	7.4	7.4	7.2
Osmolarity (mOsM)	310-320	310-320	290-300

Table 2-1 The compositions of the most commonly used solutions

The composition of the patch solution used in the majority of experiments is summarised in Table 2-1. The pH was titrated to pH 7.2 with KOH and the osmolarity was adjusted to ~294 mOsM by the addition of sucrose. This results in the final solutions having a different osmolarity, the internal being ~10-20 mOsMoles lower than the external. This aids cell survival by preventing cell swelling.

Dissection

CBA/J P10-19 mice were humanely killed by decapitation in accordance with the Animals (Scientific Procedures) Act 1986. Following decapitation the head was submersed in iced slicing aCSF (~0°C).

The skin was cut using a scalpel (size 26 blade, Swann-Morton, UK) from the forehead, caudally to the spinal cord and folded out of the way. The skull was pierced at the midline and fine scissors were used to cut rostrally to the olfactory bulbs, followed by further cuts perpendicular from the central incision, to just caudal of the eye sockets. A cut was made from the base of the skull rostrally to the initial piercing, which allowed the skull to be carefully folded to either side with a spatula, revealing the brain.

The brain was then removed from the skull by cutting the olfactory bulbs followed by severing of the blood vessels and nerves on the ventral surface with fine scissors.

Tissue Block Preparation

To obtain thin slices, a tissue block is required. This has to be orientated in such a way that when mounted on the stage of the tissue slicer (Integraslice 7550PSDS, Campden Instruments Limited, U.K., Figure 2-1 A & B) horizontal sections result in the appropriate brainstem slices.

To prepare a tissue block of the auditory brainstem, the dissected brain was transferred to fresh iced slicing aCSF, placed dorsal surface down. Fine forceps were used to remove the meninges and blood vessels from the ventral surface of the brainstem. The cerebellum and brainstem were then removed by taking a cut at the base of the brainstem with the scalpel angled 20° from the vertical toward the spinal cord. This tissue block was picked up by skewering the cerebellar hemispheres with a pair of forceps spaced with a 5mm cube of sylgard, dabbed dry and glued to the slicing stage (Figure 2-1 A) with cyanoacrylate glue (Super Grip, Ripmax, U.K.).

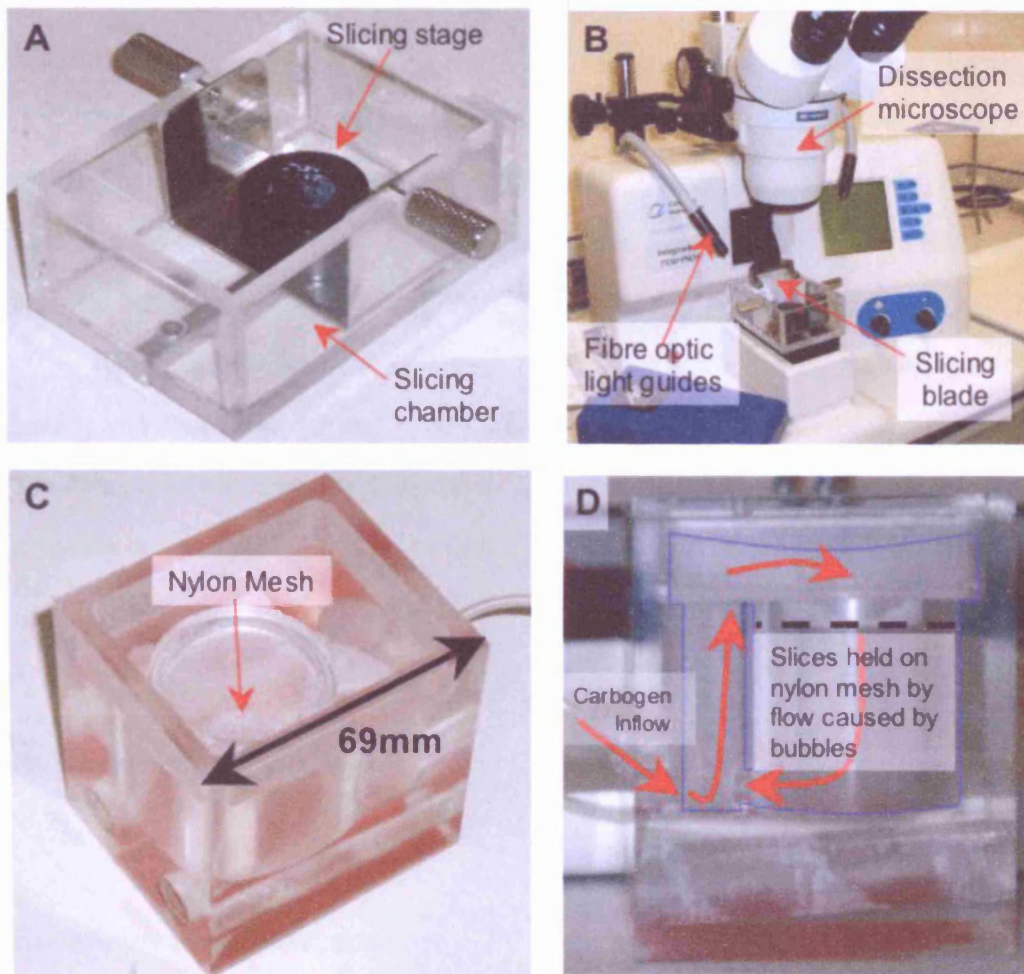


Figure 2-1 Slicing equipment: **A)** The tissue block was glued down to the stage and the chamber was packed with iced slicing aCSF. **B)** The chamber was then attached to the integraslice tissue slicer where slices were collected. **C)** Perspex incubation chamber where slices were maintained until use. **D)** The chamber was bubbled continuously with carbogen; the flow created by the bubbles rising up one side holds the slices in place.

Slice Collection

Around 200mls of slicing aCSF was rapidly frozen into a fine grained slush by briefly stirring it in the bucket of an ice cream maker (Magimix, U.K.). Once the tissue block was glued down to the slicing stage, the iced slicing aCSF was packed around the stage in the slicing chamber (Figure 2-1 A). The slicing chamber was then mounted on the tissue slicer (Figure 2-1 B), where cold slicing aCSF was added to the chamber to cover the

tissue block. The chamber was continuously bubbled with carbogen throughout slice collection.

Slice collection started immediately above the area of interest and between 2-6 slices were cut with a thickness of $\sim 120\mu\text{m}$ using a stainless steel blade (7550/1/SS, Campden Instruments Limited, U.K.) set to vibrate in the horizontal plane at 80Hz and to advance at 0.04mm s^{-1} .

Slices were removed using a large bore blunt fire polished pipette and placed in a holding chamber (preincubated to 37°C) containing low Ca^{2+} aCSF (Figure 2-1 C & D). The slices were incubated for 1 hour at 37°C after which the chamber was allowed to cool to room temperature.

Experimental Setup

Experimental microscope

A Nikon E600FN upright microscope (Nikon, Japan) was used for visualisation. It was fitted with differential interference contrast (DIC) optics and 60x (N.A. 1.00) water immersion objective and a 4x (N.A. 0.1) dry objective. A CCD camera (Cohu, San Diego) and monitor (JVC, Japan) were used for visualisation without needing to look down the eyepieces. The environmental tissue bath was fitted to a wide fixed stage plate to provide greater stability (Figure 2-2), to which the Burleigh PCS-500 micromanipulators (EXFO Burleigh products, NY) were mounted (Figure 2-2). The micromanipulators accommodated the amplifier head stage and allowed the very fine motor control necessary for patch clamping. The microscope was fixed to a remotely controlled x, y translation table, designed and constructed by the biological sciences workshop (University of Leicester, U.K.).

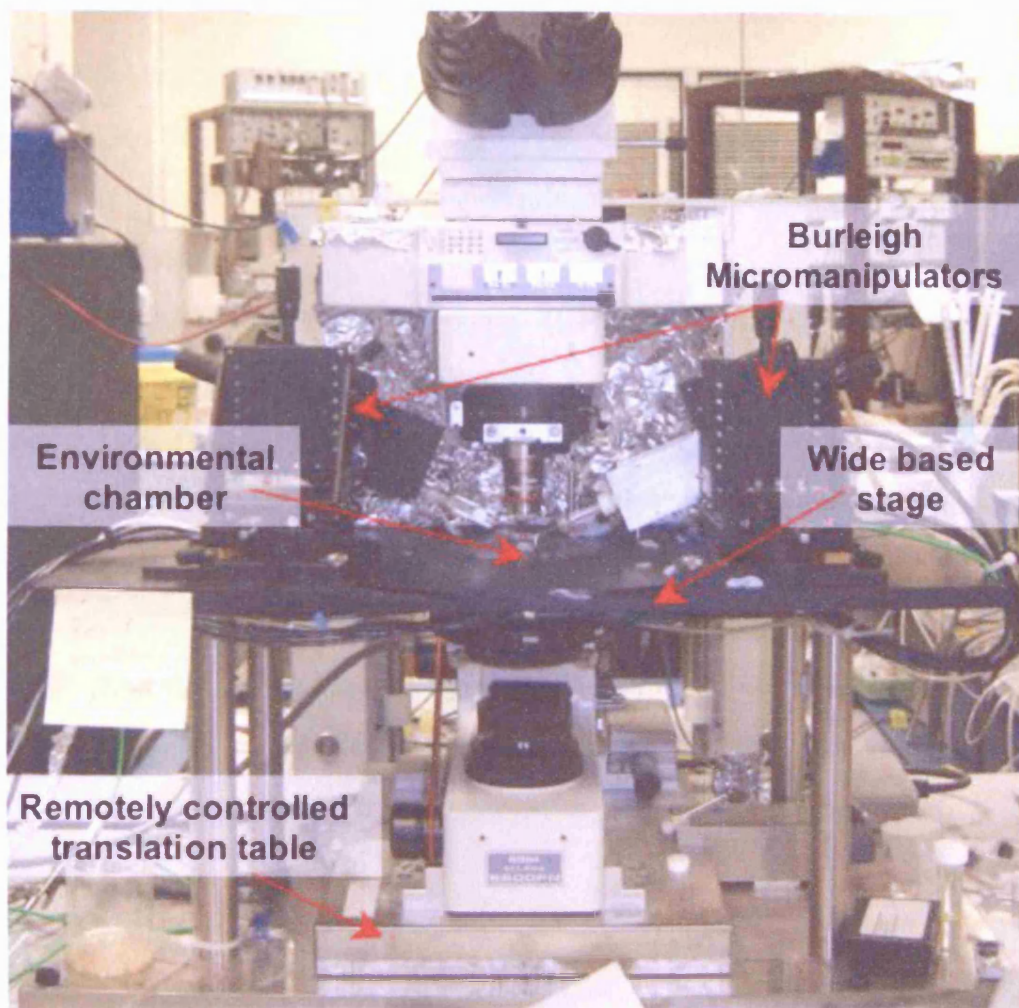


Figure 2-2 Experimental setup: Shows the layout of the setup, the upright microscope is moved independently of the fixed stage. The micromanipulators are fixed to the stage plate to provide maximum stability.

The translation table allowed the microscope to be moved around the slice independently of both the slice and the recording electrode (Figure 2-2). The microscope and stage plate were supported by a vibration isolation table (TMC, UK). This configuration gives the maximum stability for patch recording. A Peltier heat exchange temperature controller, designed and constructed by the biological workshop (University of Leicester, U.K.) was also fixed to the underside of the stage plate (Figure 2-4 C).

Differential Interference Contrast Optics

Visualisation of neurons on the experimental microscope was achieved with differential interference contrast optics (DIC, also known as Nomarski optics). The use of DIC optics affords non-absorbent objects a degree of contrast, allowing visualisation of cells without the use of dyes.

Light is passed through an infrared filter (as red light penetrates further through tissue) and is then linearly polarised before passing through the first Nomarski prism where a single beam is split into two parallel waves; the ordinary and extraordinary, which are very slightly spatially separated (Figure 2-3 A & B). The two parallel waves are then focused on the specimen by the condenser and collected by the objective, before being recombined by passing through the second Nomarski prism (Figure 2-3 C-F).

If on their way through the specimen the two waves experience different optical path differences (i.e. pass through part of the tissue with different refractive indices e.g. the edge of a cell), then on recombination by the second Nomarski prism elliptical polarisation of the wave occurs.

On passing through another linear polarizer (the analyser, Figure 2-3 G) which is orientated 90° from the initial polarizer, light that has not been elliptically polarised will not pass through the analyser. Only a portion of an elliptically polarised ray will pass through the analyser giving a finite amplitude, which allows construction of contrast in the image plane.

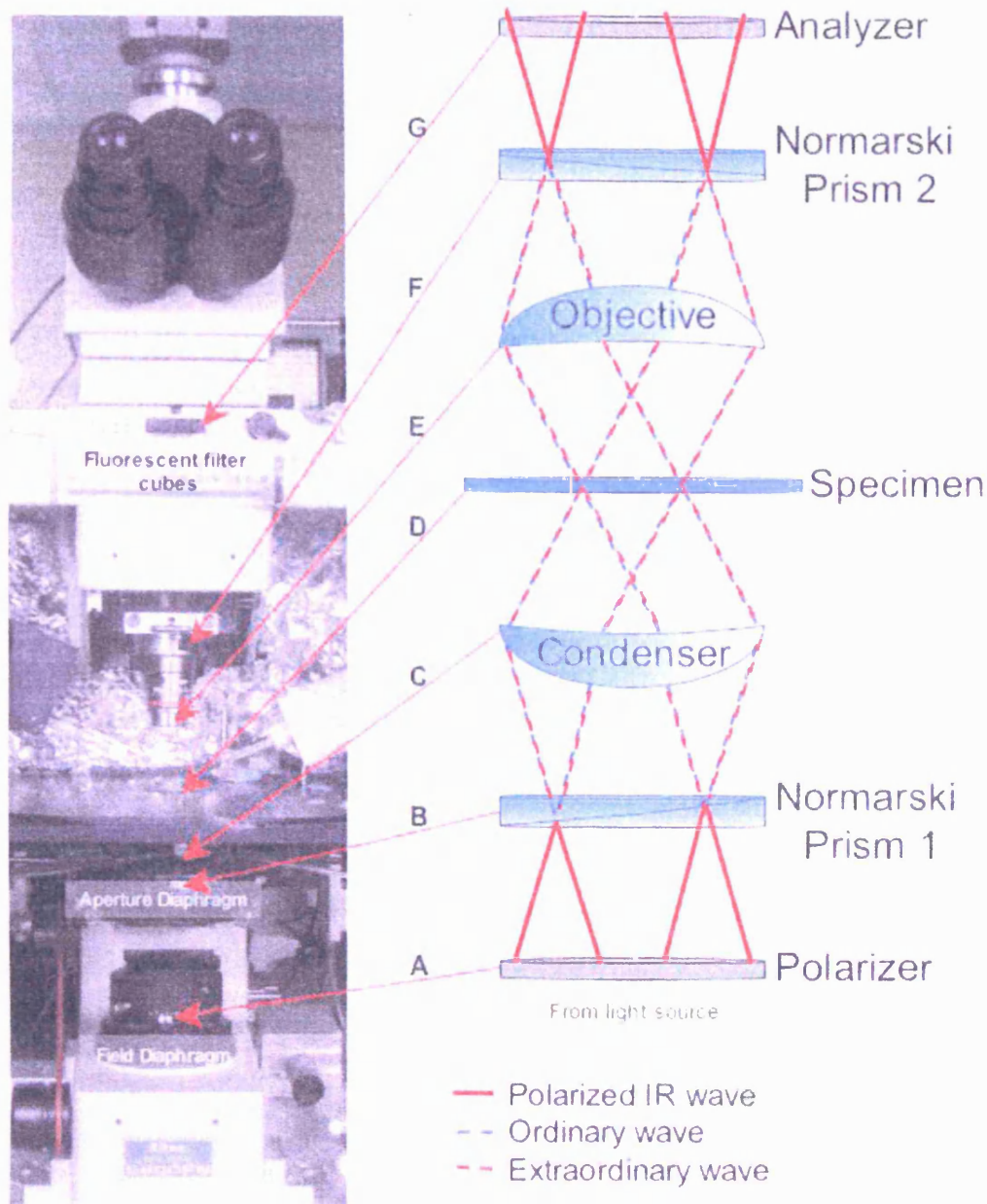


Figure 2-3 Differential Interference Contrast (DIC) optics: **A)** Normal light is passed through a linear polarizer and infrared filter. **B)** The polarised infrared wave is then split by the first Normarski prism in to 2 waves termed ordinary and extraordinary, which are slightly spatially different. **C)** The condenser then focuses the two waves on the specimen. **D)** A phase difference may be introduced by optical path differences of the specimen. **E)** The waves are then collected by the objective and (F) recombined in the 2nd Normarski prism, where elliptical polarisation occurs if the waves are of different phase. **G)** A portion of the elliptical polarised light will pass through the analyser, giving a finite amplitude, ultimately allowing intensity in the image plane.

Fluorescence Microscopy

Fluorescence microscopy was used on the experimental microscope to verify presynaptic recordings, or to estimate axon length in MNTB neurons. The fluorochrome sulforhodamine 101 (~1mg/ml, Molecular probes, OR, USA) was included in the patch pipette. Fluorescence microscopy was achieved without the use of a xenon lamp by removing the infrared filters (Figure 2-3 A & G) and placing an excitation filter (510-560nm, Nikon, UK) over the conventional light source and having an emission filter (590nm, Nikon, UK) in the filter cube unit (Figure 2-3). Maximal light penetration was ensured by removal of the infrared filters and analyser, and ensuring the field and aperture diaphragms were fully opened (Figure 2-3).

Perfusion and drug application

Slices were transferred as required to the environmental chamber and held down by a platinum harp. This consists of a piece of platinum wire bent into a U shape and flattened in a vice, with spaced nylon threads glued across it (thus resembling a harp). The tissue bath was continuously perfused at the rate of ~1ml min⁻¹ with low Ca²⁺ aCSF by way of a peristaltic pump perfusion system (Gilson minipulse III, France, Figure 2-4 A). Drugs were bath applied using individual perfusion lines to avoid contamination. Drug lines were first flushed with carbogen and then primed prior to experimentation to decrease "dead" space (~3mins for an un-primed line) and ensure no change in pH.

In order to prime a line, it was first flushed with carbogen and then low Ca²⁺ aCSF was perfused until it reached the bath. A bubble was allowed into the line followed by the drug containing aCSF. The bubble trap was then monitored for the bubble coming through; once this occurred the line was clamped to prevent any drug from reaching the bath and control solution was sucked back using the attached syringe to maintain a head of solution (Figure 2-4 B).

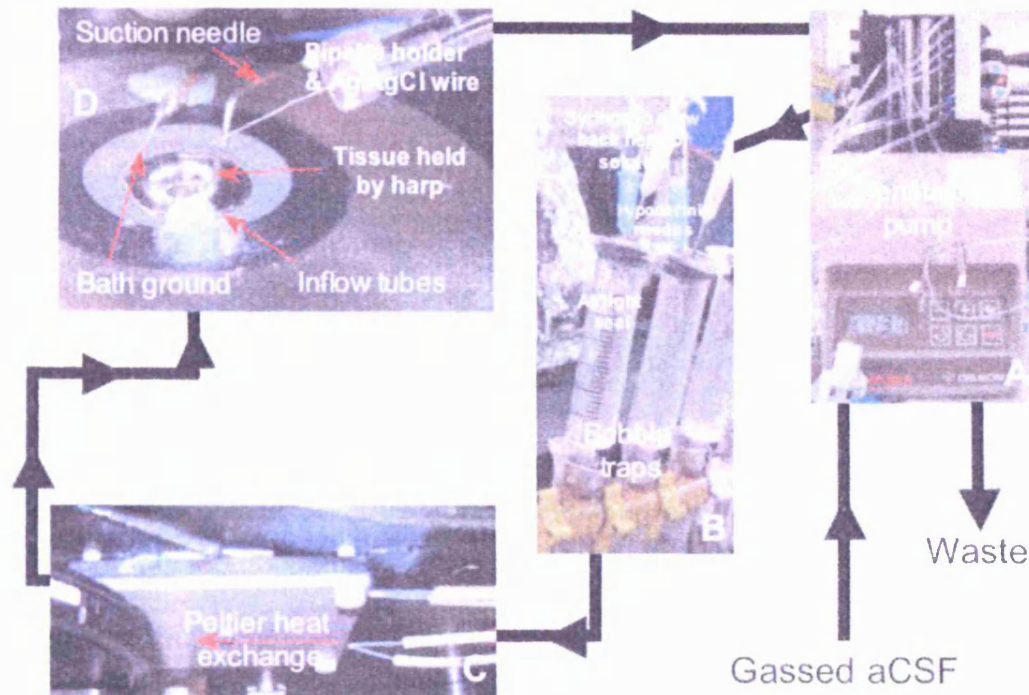


Figure 2-4 The perfusion system: **A)** aCSF bubbled with carbogen is pumped through gas impermeable tubing to bubble traps via a peristaltic pump. **B)** The aCSF drips through the bubble traps (previously flushed with carbogen) and the pressure pushes it through the tubing to the Peltier heat exchanger located on the bottom of the experimental stage. **C)** On reaching the Peltier heat exchanger the aCSF passes through teflon tubing. The teflon tubing is covered in heat-sink compound and winds its way through tracks in a metal plate. The metal plate is in contact with two Peltier devices, which exchange heat with the experimental stage, allowing temperature control of the perfusing solutions. **D)** The aCSF then passes through a hole in the experimental stage and into the tissue bath, where it flows over the tissue and is sucked out through the suction needle via another bubble trap by the pump to a waste container. N.B. Images are not to scale.

The bubble traps were in place for three reasons. Firstly they ensure perfusion is smooth by smoothing peristaltic flow. Secondly they prevent any bubbles from passing into the bath by always maintaining a head of solution in the trap. Finally they reduce electrical noise in recordings by acting as an electrical break in the perfusing salt solution, which would otherwise act as an aerial.

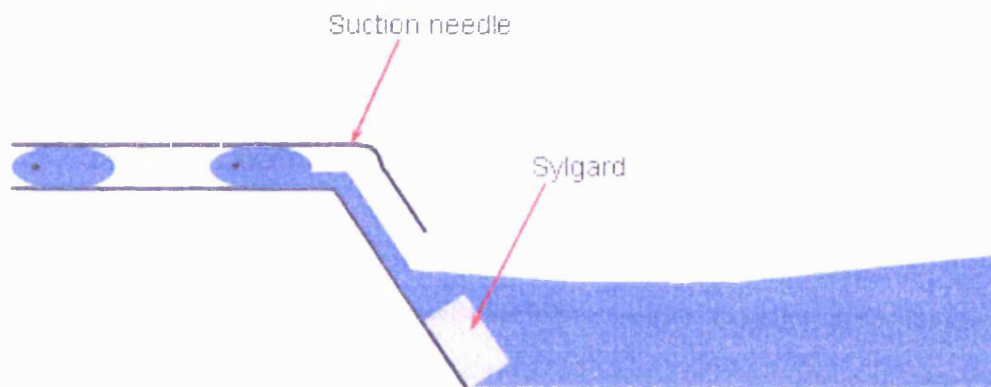


Figure 2-5 The suction needle: The suction needle in cross section, has a slit cut up one edge and the end is blocked with a piece of sylgard to set the level of solution.

The solution then passes through the peltier device (Figure 2-4 C) where it is heated to the required temperature before passing into the environmental tissue bath and across the tissue (Figure 2-4 D). Solution is removed by the suction needle via the peristaltic pump to the waste container. The suction needle has a piece of sylgard blocking its end so that it creates a smooth flow and is used to set the level of the bath solution (Figure 2-5).

Electrophysiology and patch-clamp recording

Principles of electrophysiology

Electrical Properties of Cells

The cell membrane, being composed of a lipid bilayer, insulates the intracellular ionic milieu from the extracellular ionic environment, and also has restricted ionic pathways (ion channels). Accordingly, the cell membrane has two important electrical properties, membrane resistance and membrane capacitance.

Membrane Resistance

Cell membranes possess a resistance that is inversely proportional to membrane conductance (Equation 2-1). Conductance in biological cells occurs through open ion channels. Therefore many open ion channels will reduce membrane resistance.

$$R = \frac{1}{G}$$

Equation 2-1 Where R is resistance in Ohms and G is conductance in siemens

Ohms law (Equation 2-2) relates membrane potential (V) to current (I) flow through the membrane resistance (R). Thus, for a particular voltage, if few ion channels are open i.e. I is small, then membrane resistance will be high.

$$V = IR$$

Equation 2-2 Where V is voltage in Volts, I is current in Amperes and R is resistance in Ohms.

Membrane Capacitance

Capacitance arises when two conductors (intra and extracellular milieu) are separated by a dielectric or insulator (cell membrane). Capacitance, measured in Farads, is proportional to the thickness and the surface area of the dielectric. Since lipid bilayers generally have a constant width, the specific membrane capacitance is $\sim 1\mu\text{Fcm}^{-2}$. Accordingly capacitance can be used to estimate cell size.

Capacitors store charge, and importantly require time to charge and discharge. For a constant voltage no current passes across a capacitor, however for a voltage change (δV) a capacitive current arises, given by Equation 2-3.

$$I_C = C \frac{\delta V}{\delta t}$$

Equation 2-3 Where I_C is the capacitive current, C is the capacitance in Farads, V is the voltage and t is time

The current flowing across the membrane for a rapid change in voltage, such as a voltage step is therefore a result of both capacitive and ionic current (Equation 2-4).

$$I_m = I_i + I_C$$

Equation 2-4 Where I_m is the total membrane current, I_i is the ionic current and I_C is the capacitive current.

Therefore to examine fast ionic currents it is necessary to minimise the capacitive current. This is achieved electronically, as will be discussed later.

Membrane Time Constant

Since the membrane acts as a resistor and capacitor in parallel, applying a given current (e.g. a square pulse or synaptic current) will change the membrane potential

exponentially rather than instantly. The time constant of the exponential is given by Equation 2-5.

$$\tau = RC$$

Equation 2-5 Where τ is the membrane time constant, R is the membrane resistance and C is the membrane capacitance

Since cell membrane capacitance is generally constant, it is apparent from Equation 2-5 that membrane resistance and hence the number of open ion channels, is central for determining synaptic potential decay times.

Ionic Equilibrium Potentials

The cell membrane has an unequal distribution of ions across it. Inside there is a high concentration of proteins (negatively charged) which is balanced by a high concentration of K^+ ions. On the outside the principal cation is Na^+ , which is balanced by a high concentration of Cl^- and a low concentration of K^+ . This ionic gradient arises and is maintained by the Na-K-ATPase.

Therefore there are two opposing gradients across the membrane: a chemical (concentration) gradient and an electrical gradient. The membrane potential at which these gradients balance, known as the reversal potential (E_{rev}), is given by the Nernst equation (Equation 2-6). My solutions contained 143mM internal and 2.5mM external K^+ , giving a Nernstian reversal potential of -103mV for K^+ ions.

$$E_{rev} = \frac{RT}{zF} \ln \frac{[ion]_{out}}{[ion]_{in}}$$

Equation 2-6 Where E is the ionic reversal potential, R is the gas constant, T is temperature in Kelvin, z is the valency of the ion and F is the Faraday constant.

The Nernst equation can be used to calculate the E_{rev} of a channel. However there are limitations, as it assumes that the channel is only permeable to one ion, which is generally not the case. A more useful equation for predicting the E_{rev} of a channel is the Goldman-Hodgkin-Katz (GHK) voltage equation (Equation 2-7), which takes into account the different permeability ratios of permeating ions.

$$E_{rev} = \frac{RT}{F} \ln \frac{P_K [K]_o + P_{Na} [Na]_o + P_{Cl} [Cl]_i}{P_K [K]_i + P_{Na} [Na]_i + P_{Cl} [Cl]_o}$$

Equation 2-7 Where R is the gas constant, T is temperature ($^{\circ}K$), F is the Faraday constant and P_{ion} is the permeability ratio of the ion.

Voltage Clamp

In general this technique allows ion flow across a cell membrane to be measured as electric current, while the membrane voltage is held under experimental control by a feedback amplifier. Voltage clamp was first developed in the study of the squid giant axon (Hodgkin *et al.*, 1952), where two electrodes were used (two-electrode voltage clamp); one to pass current and one to measure the membrane voltage. The technique was later developed for use with a single electrode that alternates between passing current and voltage measurement (discontinuous single-electrode voltage clamp, Wilson & Goldner 1975). An alternative method for voltage clamp was developed in the 1970-80s for use at both the single channel level and for whole cell recording (Neher & Sakmann 1976); this is called the patch clamp. This method uses a single electrode to simultaneously measure voltage and pass current.

The Patch Clamp Technique

The general principle of patch clamp recording is the formation of a high resistance seal (usually 1-10 G Ω) between the tip of the glass pipette and the cell membrane, so that the majority of the current flowing through the membrane flows into the pipette and to the patch clamp amplifier, allowing high signal to noise recording.

To obtain a giga-ohm seal from a cell in a brain slice, positive pressure is applied to the back of the pipette by a 10ml syringe (0.5mls for terminals, 1.5mls for cortical neurons and 2.5mls for MNTB neurons). The pipette is then advanced using the micromanipulators until it forms a dimple on the cell, at which point the pressure is gently released. The positive pressure serves several purposes. It keeps the tip clean from debris that may be in the solution, blows tissue and debris clear that may be on top of the cell of interest and cleans the cell membrane. The holding potential of the pipette is then set to -70mV and gentle suction is applied, aiding seal formation which is assessed by a 5mV square pulse (the seal test). Once a giga-ohm seal is established (cell attached) there are several configurations of the patch clamp technique that can be employed (Figure 2-6). The majority of the experiments performed in this thesis were in the whole cell mode. Whole cell recordings were achieved by applying short pulses of suction by mouth to rupture the membrane under the tip.

The whole cell configuration allows chemical and electrical access to the interior of the cell, and as a result the cell contents are dialysed with the patch solution. Cell dialysis is useful as it allows the control of the intracellular ion concentration and hence the reversal potentials for various ions. With my patch solution the Cl⁻ reversal potential was -35mV, which is beneficial when studying K⁺ currents which reverse at -103mV. A potential disadvantage to cell dialysis is the loss of intracellular messengers (e.g. cAMP) and ATP and GTP, which are required for receptor signalling.

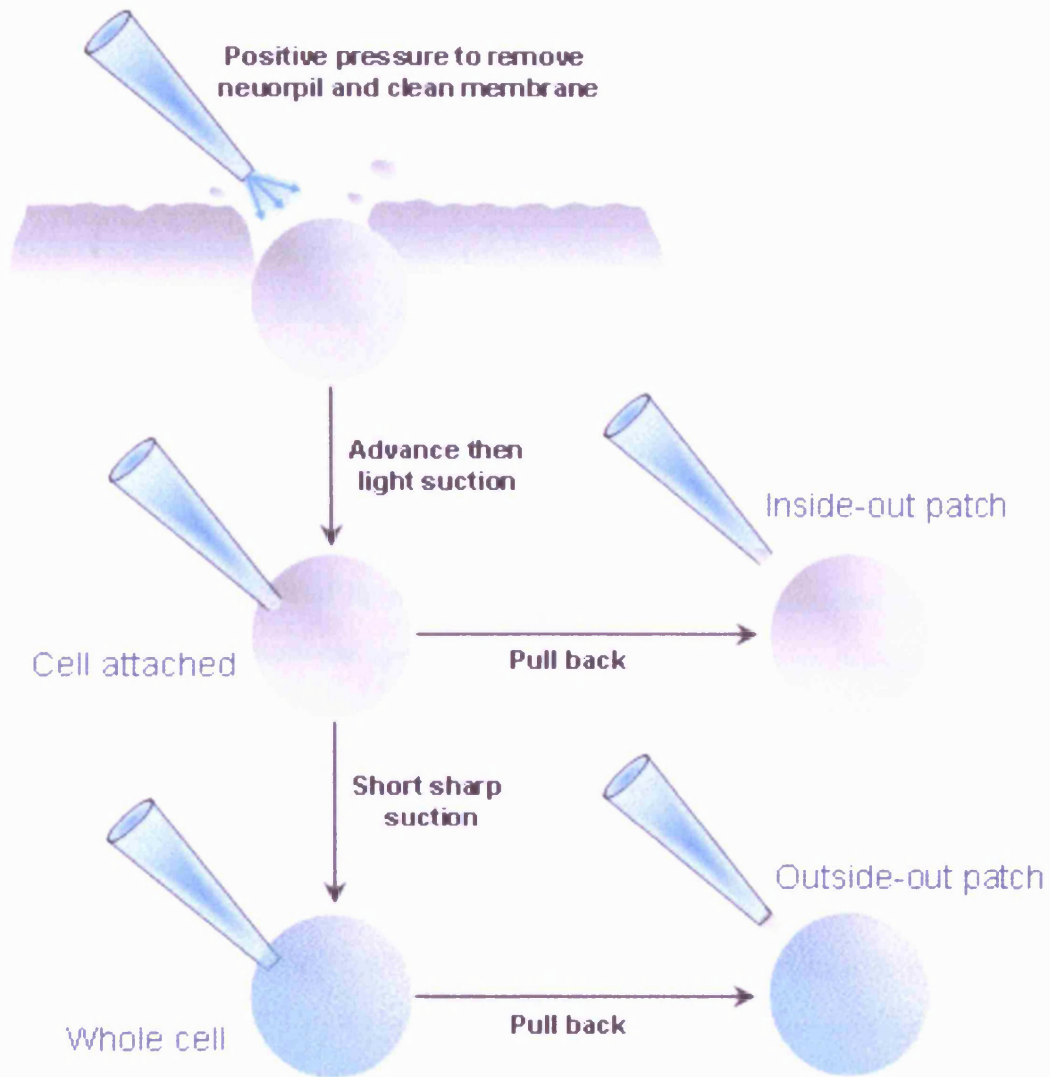


Figure 2-6 Patch-clamp configurations: Once a Giga ohm seal is established by slight suction, the cell attached mode is achieved, further suction leads to rupturing of the membrane under the pipette, giving whole cell access. Membrane patches can be formed by pulling back either in cell attached mode (giving inside-out) or in whole cell mode (giving outside-out).

A way to overcome this disadvantage is to use the perforated patch configuration, which requires including a pore forming antibiotic in the patch solution. On forming a giga-seal the antibiotic slowly inserts itself in the membrane and forms pores allowing electrical access with limited dialysis (e.g. amphotericin B forms pores permeable to monovalent cations and chloride, whereas gramicidin D forms cation only permeable pores).

From the whole cell configuration, pulling the pipette back gently allows formation of an excised outside-out patch. The advantage of an excised patch over whole cell mode is greater voltage control due to less membrane being clamped. It also provides information to the location of ion channels (e.g. the non release face versus the release face of a terminal). A potential disadvantage is that the signal to noise ratio will decrease as less channels are recorded from, but with careful earthing of equipment, noise can be limited.

Measurement of ionic currents in whole cell patch-clamp

Ion channels are studied by measuring the current being conducted through them. However, to study them we can only measure the current through the cell membrane, which as Equation 2-4 points out is composed of both ionic current and capacitive current. Additionally the patch electrode also has a capacitance current associated with it.

In order to record the ionic membrane current in isolation the other capacitive currents need to be electrically cancelled (or "compensated"). To summarise: Once a tight seal has formed between the glass and the cell, the pipette capacitance (which is fast) is cancelled using circuitry in the patch amplifier. After rupture of the membrane under the pipette the capacitance of the cell becomes apparent (this is slower). This is then compensated by circuitry in the amplifier, which basically injects extra current through the pipette (but bypassing the headstage op amp, therefore it does not appear on the output) to charge this capacitance.

Another potential problem with whole cell recordings is the pipette resistance, which is in series with the membrane resistance. Furthermore the access to the cell is usually less than the size of the pipette tip, resulting in an even greater resistance associated with the pipette (together termed R_s , series resistance). The result of R_s is to create a voltage drop across the pipette when current is passed (effectively a voltage divider), resulting in the cell being a different voltage to the pipette. This is a particular problem when passing large currents across a sizeable R_s ; For example, if 4nA of current

is passing across a $5\text{M}\Omega$ R_s when trying to hold the membrane at $+20\text{mV}$, the voltage drop would be 20mV , which is obviously unacceptable. To partially overcome this problem electrical compensation of $\sim 70\text{-}85\%$ of R_s is applied, achieved by scaling the command voltage to compensate for the predicted voltage drop. Therefore with R_s compensation the voltage drop is now only 4mV . The R_s compensation also prevents filtering of the measured current, which would otherwise occur due to the pipette having a capacitance and resistance (i.e. a low pass filter). The average series resistance from 28 recordings was $6.0 \pm 0.4\text{M}\Omega$.

Liquid junction potentials

In patch recording the pipette is first "zeroed" near the cell before sealing. However when the patch solution differs from the bath solution a liquid junction potential (LJP) arises at the tip, which is then absent after the seal is made. LJPs are due to different mobilities of ions at the interface of the liquids, the junction potential is the voltage required to balance the difference in charge arising from the quicker diffusion of some ions versus others (Neher, 1992). Therefore the actual voltage of the pipette is given by Equation 2-8.

$$V_{pip} = V_{com} - (LJP)$$

Equation 2-8 Correction for the liquid junction potential

Junction potentials can be estimated by measurement or by calculation. Using an agar bridge, a pipette is placed in the bath containing the patch solution. The pipette is then zeroed (as there is now no LJP because the solutions are the same) in $I=0$ mode on the amplifier. The low Ca^{2+} aCSF is then washed into the bath, and the LJP is read from the meter once the solutions have fully exchanged. For my standard pipette solution I found the junction potential to be $\sim 6.6\text{mV}$ when measured experimentally and 7mV when calculated (using *JPCalcW*). As calculation is considered more accurate (Barry, 1994) all voltages have been corrected for calculated LJPs post hoc.

Electrode preparation

Patch pipettes were made from filament containing thick walled borosilicate glass capillaries (GC150F 7.5, Clark Electromedical, UK). Pipettes were produced by pulling the capillaries on a vertical two-step puller (PC-10, Narishige, Japan). Pipettes were then filled with patch solution that was filtered by a 0.22 μ M filter (Millipore, UK). Final pipette resistances measured in low Ca²⁺ aCSF in the bath were 2.5-4M Ω for postsynaptic recordings. Occasionally pipettes were fire polished with a microforge (F-830, Narishige, Japan).

Patch clamp recording equipment

All experimental patch-recordings were made using an Optopatch amplifier (Caim Research, UK). Data was digitized by a Digidata 1322A (Molecular Devices, USA) and recorded to a PC (Centreprise, UK) using pClamp 9.2 software (molecular devices, USA) for acquisition and analysis (Figure 2-7). Data were filtered at 2-10 kHz using an 8-pole Bessel filter on the amplifier. Data were digitized at 10-50 kHz (always at least 3 times the filter) for voltage clamp or 50-100 kHz for current clamp. See Figure 2-7 for details.

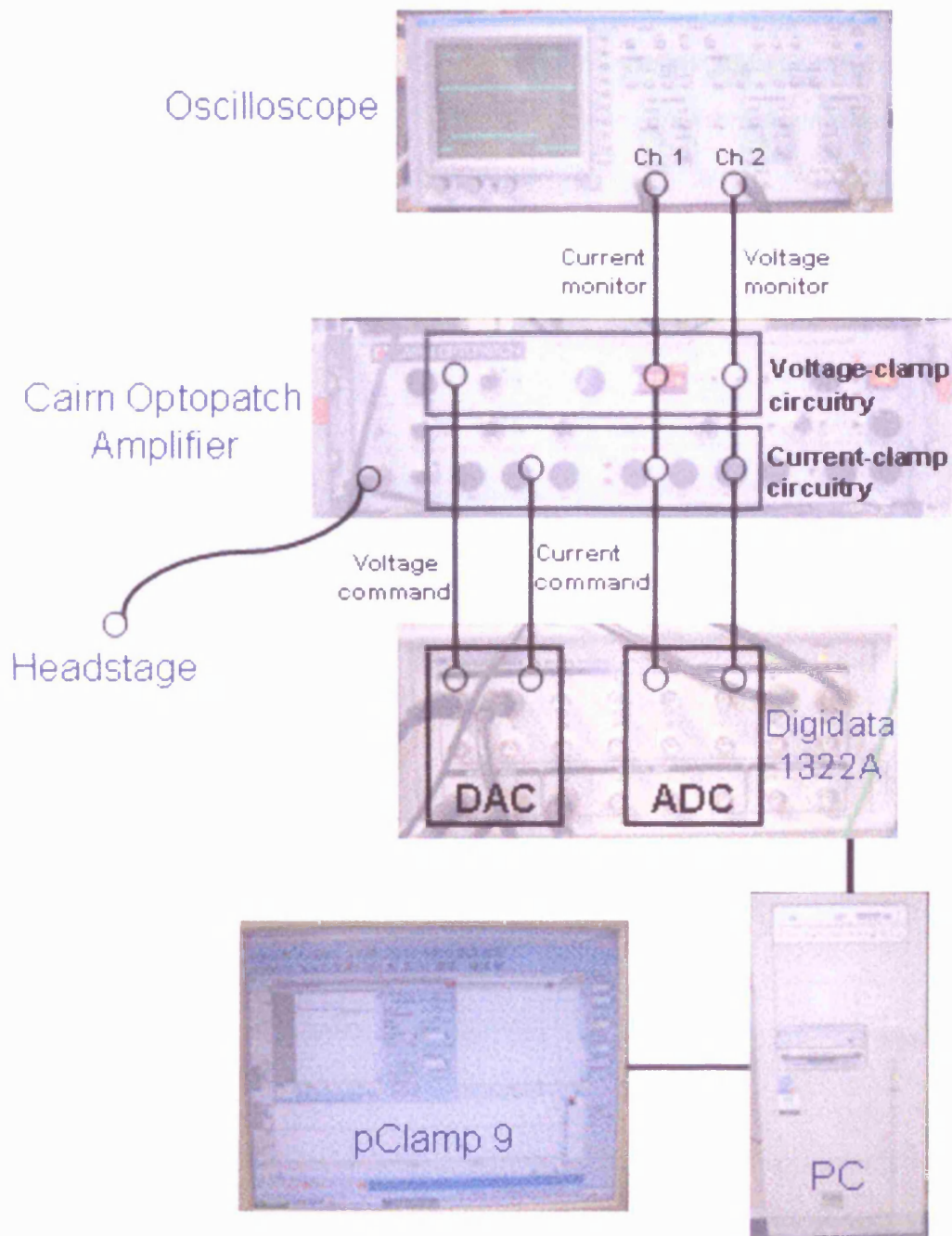


Figure 2-7 Patch-clamp recording equipment: Voltage commands are given by the computer via the digital to analogue converter (DAC) which is then applied to the pipette through the amplifier and its headstage. The response to the voltage commands are simultaneously monitored by the headstage and amplifier which then gets sent to the computer via the ADC where they recorded to the hard drive. An oscilloscope is also connected for continuous monitoring of cell viability and to check series resistance throughout protocols.

Amplifier headstage design

Conventional patch clamp amplifiers use a feed back resistor (R_f) in the headstage to pass current, as arranged in Figure 2-8. Any difference between V command and the pipette causes a current to be passed across R_f in such a way as to oppose the difference.

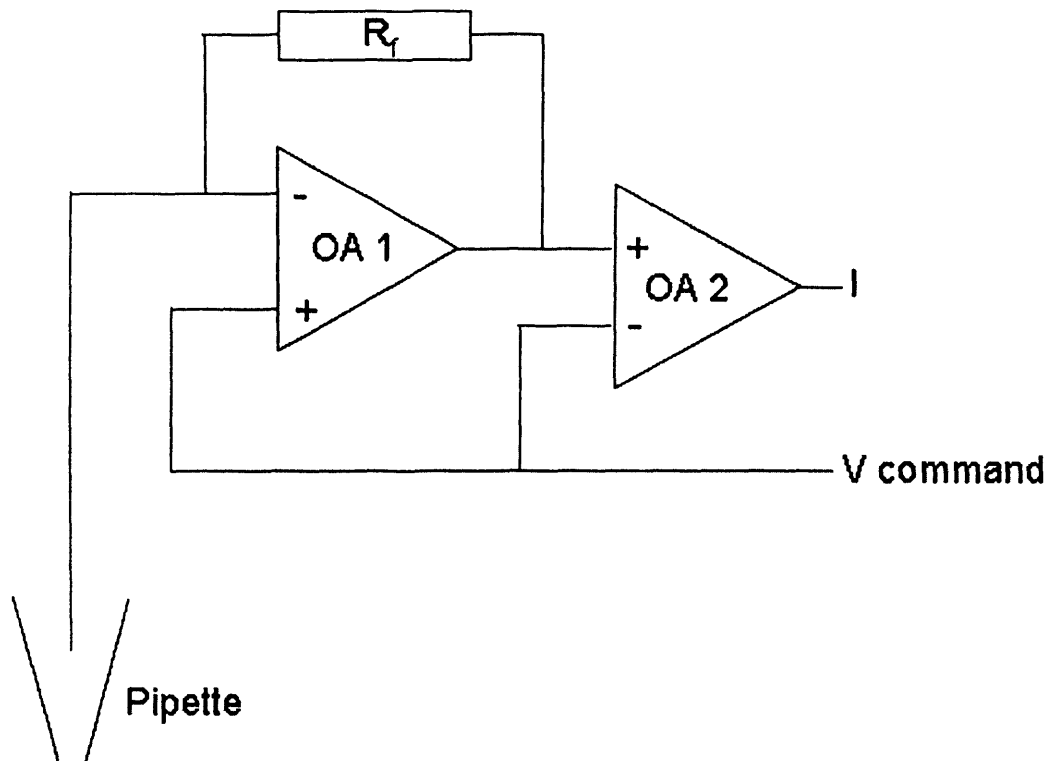


Figure 2-8 Conventional resistive headstage: OA1 is an operation amplifier, R_f is feed back resistor, OA2 is an operational amplifier.

The current passing through R_f causes a potential difference to appear across it, which can be measured by subtracting the command voltage from the output (in OA2 Figure 2-8). To be effective R_f has to be large i.e. $>10G\Omega$ (to improve the signal to noise ratio), but this limits the bandwidth of the headstage and capacitive transients become a problem.

In the Optopatch current is passed by shining light directly onto miniature photo diodes connected between the differential inputs of the operational amplifier (Figure 2-9). In this circuit any difference between the command and the pipette voltage generates a

voltage at the amplifier output (OA Figure 2-9). This provides the input to the optical current passing device, which generates a photodiode current that acts to restore the input voltage (Thomas, 2000). The amplifier output is a direct measure of the current, meaning the command voltage does not appear on the output of the amplifier and thus does not need to be subtracted.

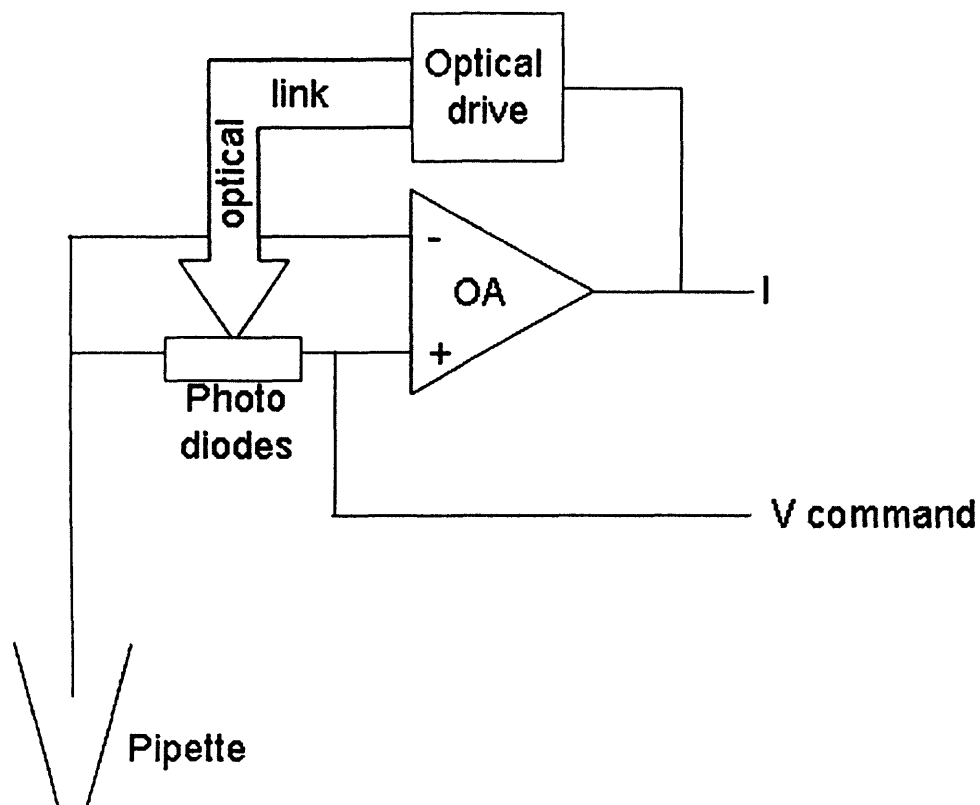


Figure 2-9 The Optopatch head stage: OA is operational amplifier

The advantage of the Optopatch's configuration is that the thermal noise associated with R_f is removed, and there is a greater bandwidth due to lack of restriction from the R_f . Additionally true current clamp can be achieved with the optical head stage by simply inverting the output of the OA in Figure 2-9 and feeding it back into the command input, which effectively switches the polarity of the OA and thus gives a voltage follower circuit (Thomas, 2000). Other patch-clamp amplifiers e.g. axopatch, do not allow accurate current clamp (Magistretti *et al.*, 1996).

Stimulation

For electrical stimulation of axons a bipolar platinum electrode was used (Figure 2-10 A) and adjusted into position using the attached coarse manipulators (Narishige, Japan). The stimulating electrode was connected to a DS2A isolated stimulating pack (Digitimer, UK) and axons were stimulated with a 0.2ms pulses of 3-10V. The stimulating pack was connected to a digital output on the Digidata 1332A, which allowed single stimuli or trains to be triggered through the acquisition software pClamp 9.2 (Molecular devices, USA). The electrode was placed with one prong underneath and one above the slice at the level of the midline (see Figure 2-10 B).

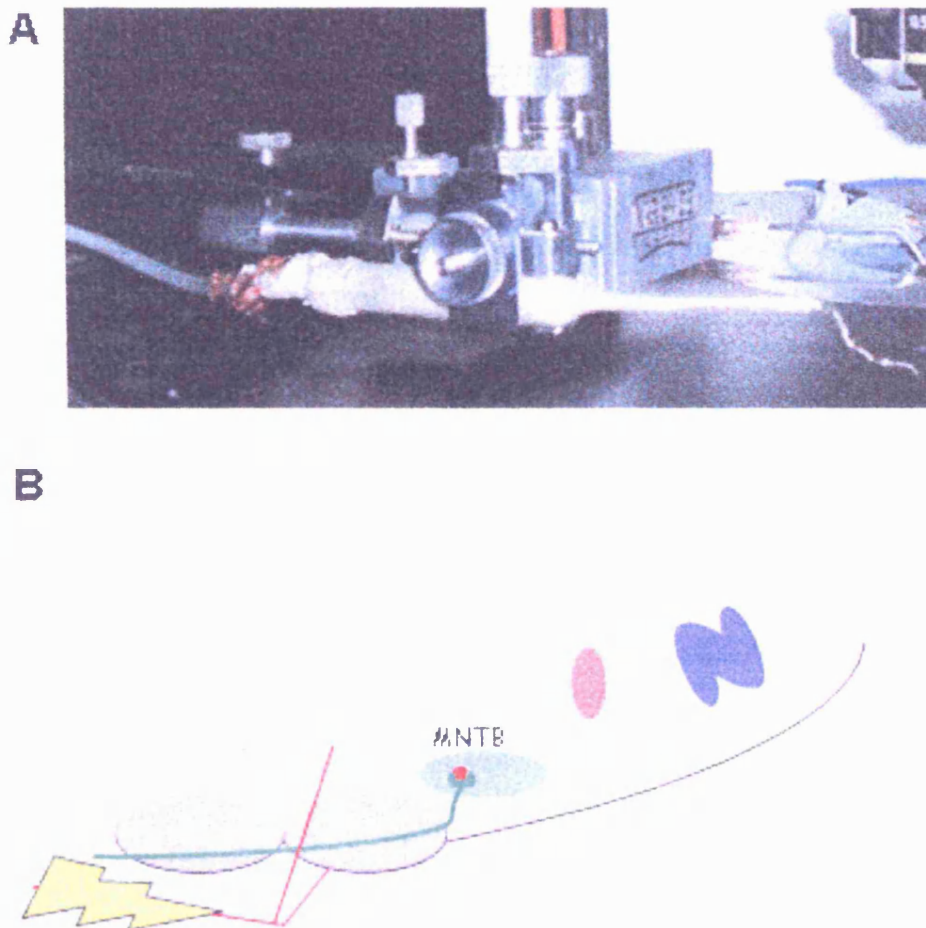


Figure 2-10 Stimulating electrode: A) Bipolar stimulating electrode constructed from Teflon coated platinum wire. Held by Narishige coarse manipulators. **B)** Electrode positioning.

Data Analysis

Current voltage relationships (I/Vs) were analysed in Clampfit 9.2 (Molecular devices USA), and graphs were plotted in Microsoft Excel (Microsoft USA). Current records for figures were produced in Clampfit and exported to Microsoft PowerPoint (Microsoft USA). In general I/Vs were constructed by plotting the current 40ms into each test step against the holding potential. Data are expressed as means \pm SEM. As discussed previously all data was corrected for the liquid junction potentials. Figures are examples from single cells unless otherwise stated. No leak subtraction was performed on K⁺ channel data, as all conventional leak subtraction fails to subtract all the "leak", as K⁺ mediated leak is non linear and described by Equation 2-9, the importance of which becomes apparent in (Figure 4-10).

$$I = Pz^2 \frac{VF^2}{RT} \frac{[K]_{in} - [K]_{out} \exp(-zFV/RT)}{1 - \exp(-zFV/RT)}$$

Equation 2-9 The Goldman-Hodgkin-Katz current equation: Symbols have their usual meaning, and P is a permeability factor.

When I have demonstrated only a K⁺ leak remains (chapter 4) the residual current is fit with the GHK equation (Equation 2-9) using Microsoft Excel and the least squares method of fitting, with P as the only free variable.

Determining voltage dependence of inactivation

To determine voltage dependence of inactivation the current normalised to the maximum is plotted versus voltage and the least squares method was used to fit a Boltzmann distribution (Equation 2-10) giving the $V_{1/2}$ and k.

$$\frac{I}{I_{\max}} = \frac{1}{1 + \exp^{(V-V_{1/2})/k}}$$

Equation 2-10 Inactivation Boltzmann: Where k is the slope factor.

Determining voltage dependence of activation

To determine the voltage dependence of activation from K^+ I/Vs the data has to be normalised to take into account the current's dependence on the driving force. A common method for this normalisation has been to use an "ohmic" normalisation i.e. $I / (V-E_{\text{rev}})$. However this assumes the single channel current has a linear dependence on driving force, which is incorrect (Clay, 2000). The single channel current is better described by the GHK equation (Equation 2-9). Therefore the current was corrected for the driving force using Equation 2-9 where P is an arbitrary normalisation factor (which is irrelevant as it is later re-normalised).

Once the I/V data has been normalised for the driving force a Boltzmann distribution (Equation 2-11) was fit using the least squares method.

$$\frac{G}{G_{\max}} = \frac{1}{1 + \exp^{((V-V_{1/2})/k)}}$$

Equation 2-11 The Boltzmann equation: Where k is the slope factor

Note that when this method of normalisation is used the units are theoretically siemens (G). However since a normalisation factor is applied the units are effectively meaningless, which is not important as they are normalised to the maximum in Equation 2-11.

The effect of using an ohmic normalisation versus the GHK method is demonstrated in Figure 2-11. The ohmic normalisation returns a voltage-dependence with a shallower slope and therefore a more positive $V_{1/2}$ than the GHK method. Also note that this discrepancy between the two methods of normalisation is only observed in physiological solutions (i.e. asymmetric K^+).

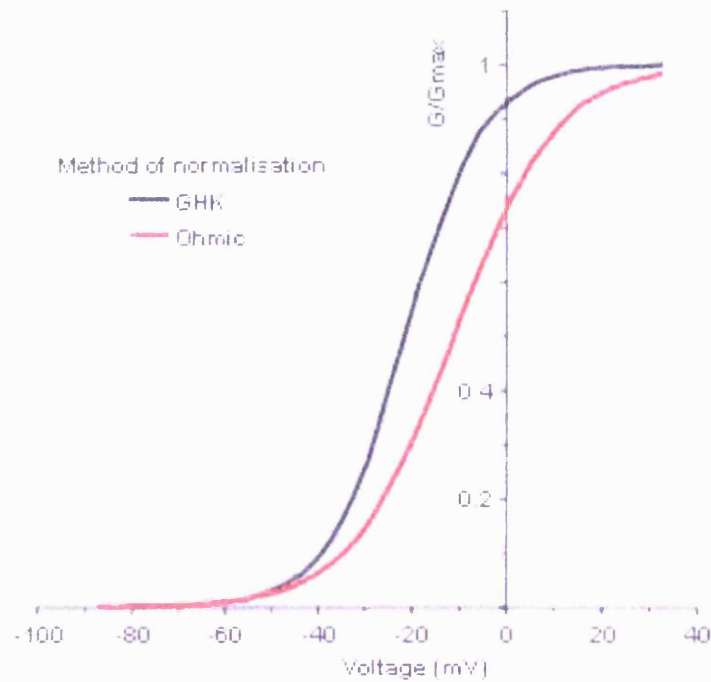


Figure 2-11 Method of normalisation for driving force affects $V_{1/2}$: Data taken from the Kv3 activation from cell in Figure 3-5, demonstrates the error associated with erroneous Ohmic correction (red) vs GHK correction (black).

Exponential fits

When exponential functions were fitted to data they were of the form shown in Equation 2-12, and were fit using the least squares method either in an Excel spreadsheet or in Clampfit.

$$f(t) = Ae^{(-t/\tau)} + C$$

Equation 2-12 Exponential fits: Where t is time, A is the area of the fit and C is a constant

Immunohistochemistry analysis

Image J (NIH) was used for analysis of immunohistochemical data. To assess the pixel intensity an oval was drawn round the MNTB and the gray level was measured. In every

case the control image (blocking peptide or primary antibody omitted) was also analysed. An unpaired t-test was then used to determine if the immunofluorescence was significantly above background.

Statistical tests

In the majority of cases two-tailed t-tests were used to assess significance, paired or unpaired where appropriate. One way ANOVAs were used to assess significance where there were more than two comparisons. All tests were performed using either Microsoft Excel or InStat 3 (Graphpad Software Limited).

Immunohistochemistry

Information on the histological and sub-cellular expression of specific target proteins can be determined using fluorescently labelled antibodies. Specific antibodies are produced by inoculating an animal (e.g. a rabbit) with the desired antigen. The animal then produces antibodies against this foreign antigen.

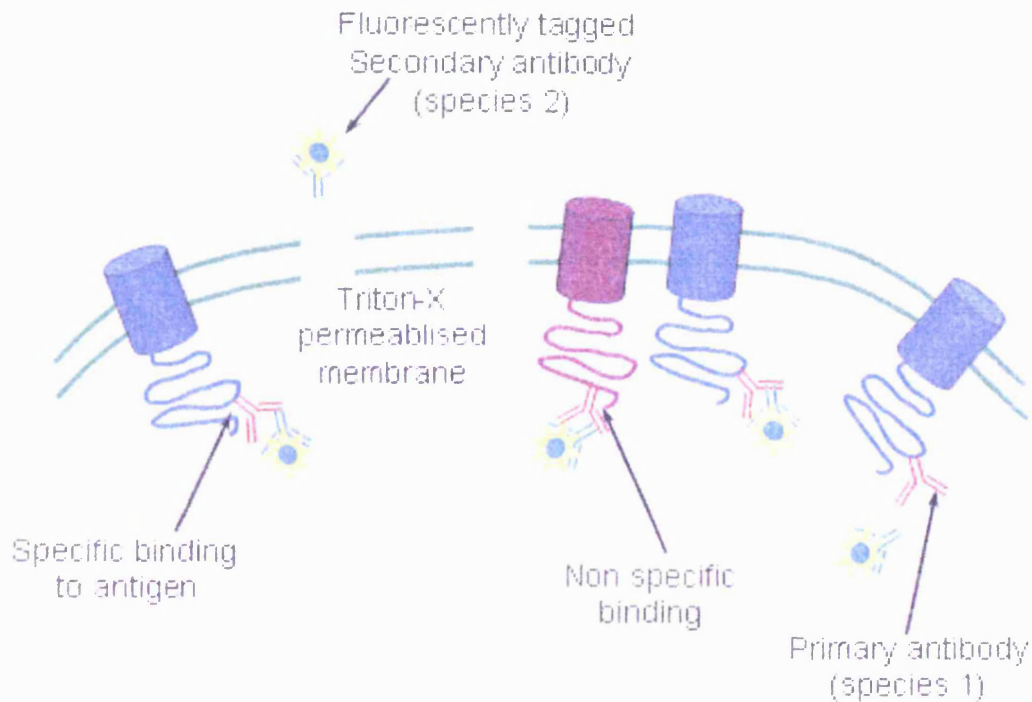


Figure 2-12 Principles of immunohistochemistry: Cell membranes are permeabilised with a detergent. The primary antibody recognises the epitope on the protein of interest and binds with high affinity. However some non-specific binding may occur (which is lower affinity). The fluorescently tagged secondary antibody is applied and binds to the primary.

The most common method of immunohistochemistry is indirect (Figure 2-12) i.e. using a primary antibody raised in one species, and then using a fluorochrome conjugated second antibody from a second species (raised against antibodies from the 1st species). This provides amplification of the signal along with more efficient production of antibodies.

Immunohistochemistry methods

Brainstems were removed as described previously, transferred to Tissue Tec (Sakura) and rapidly frozen in Hexane and dry ice. 12-20 μ m cryostat sections were taken (at -12^oC) and transferred to polylysine-coated slides. The slides were then fixed in 2-4% paraformaldehyde for 10-20mins. Fixed sections were washed in 100mM phosphate buffered saline (PBS) PBS with 0.5% Triton X-100 (PBS-T) for 15mins 3 times.

In some cases antigen retrieval was conducted at this point, which consisted of the slides being treated with citrate buffer (pH6.0) for 20min at 95°C, then rewashed in PBS-T.

Sections were blocked with 1% BSA, 1% serum (from the second species e.g. antigoat) in PBS-T for 1h at 20°C, and incubated with the primary antibody in blocking buffer overnight at 4°C.

Sections were washed with PBS-T and the secondary antibody was applied for 2hr at 20°C, and then mounted with Vectashield (Vector Labs). In some cases DAPI (which binds to DNA) was included to visualize cell nuclei.

Images were obtained using either a Zeiss LSM 510 Meta confocal microscope, a Leica DM2500 or an Olympus fluoview confocal microscope. Control sections underwent identical procedures; either with the primary antibody omitted or were preincubated with the blocking peptide.

Antibody	Epitope
Kv1.1	HRETE GEEQA QLLHV SSPNL ASDSD LSRRS SSTIS KSEYM EIEED MNNSI AHYRQ ANIRT GNCTT ADQNC VNKSK LLTDV
Kv1.2	YHRET EGEEQ AQYLQ VTSCP KIPSS PDLKK SRSAS TISKS DYMEIQEGVNNSNEDFREENLKTANCTLANTNYVNITKMLTDV
Kv1.4	PYLPS NLLKK FRSSST SSSLG DKSEY LEMEE GVKES LCGKE EKCQG KGDDS ETDKN NCSNA KAVET DV
Kv1.5	HRETDHEEQAALKEEQGIQRRESGLDTGGQRKVSCKASFHKTG GPLESTDSIRRGSCPLEKCHLKAQSNVDLRRSLYALCLDTSRETDL
Kv1.6	NYFYH RETEQ EEQQQ YTHVT CGQPT PDLKA TDNGL GKPDF AEASR ERRSS YLPTP HRAYA EKRML TEV
Kv3.1b	CKESPVIKYMPTAVRVT
Kv3.2	DLGGKRLGIEDAAGLGGPDGK
Kv3.3	VTQASPIPGAPPENITNVC
Kv3.4	EAGDDERELALQRLGPHEG
Kv2.2	CRQDIYQAVGEVKKD
Kv4.1	CKRRAIRLANSTAS
K4.2	CSNQLQSSSEDEPAFVSK
Kv4.3	CNEALELTGTPEEEHMGK

Table 2-2 Antibody epitopes. All antibodies were obtained from Alomone labs (Israel), except Kv3.3 which was a kind gift from Dr. T. Perney.

Confocal microscopy

The advantages of confocal microscopy are the elimination of out of focus light and the ability to collect serial optical sections. It can really only be used for fluorescently labelled specimens as the signal has to be very intense. As an intense signal is required a laser is used to excite a point in the plane of focus, the emitted light from the fluorochrome is then visualised. Importantly, only the light at the point of focus is visualised due to confocal apertures (pin holes), which both limit the area being excited and block out of focus light. To build a picture the point of excitation has to be scanned across the specimen (which is time consuming), which then creates an optical section of the specimen.

Western blot for anti-Kv2.2

In chapter 4 a new antibody raised against a peptide corresponding to the C terminus of Kv2.2 is used and we performed a western blot to test the antibody's specificity. Whole brains were dissected as described earlier, homogenized with 100 mM Tris, 0.1% Triton -X 100 and loaded into a 10% Tris-Glycine gel (20µg per lane). After electrophoresis the samples were transferred onto a nitrocellulose membrane and blocked in 5% skimmed milk in TBS-0, 5% Tween 20 (TBS-T) for 1 hour at room temperature. After washing (3 X 10 min in TBS-T) the membranes were probed with a rabbit anti-Kv2.2 primary antibody (1:1000, Sigma) for 2h at room temperature in 5% skimmed milk. The membranes were washed (3 x 10 min in TBS-T) and the HRP conjugated secondary antibody was applied (1:1000, Vector Labs) for 90 min at room temperature. The membrane was washed (5 x 10 min) and the signal detected using an HRP substrate (Pierce).

Reverse transcription PCR

Qrt-PCR is used to asses how much of a gene is transcribed within a given tissue. Firstly RNA is extracted from the tissue and treated with DNAase to remove all the genomic DNA (Figure 2-13 A). The complementary DNA (cDNA) is then produced from all of the RNA using a reverse transcriptase enzyme (Figure 2-13 B). This cDNA is then used for the PCR reaction.

The polymerase chain reaction is a method that allows logarithmic amplification of short DNA (or cDNA) sequences within a longer double stranded DNA molecule. The double stranded DNA is split, and a pair of primers (each ~20 nucleotides), that are complementary to a selected sequence on each of the two strands of the DNA anneal.

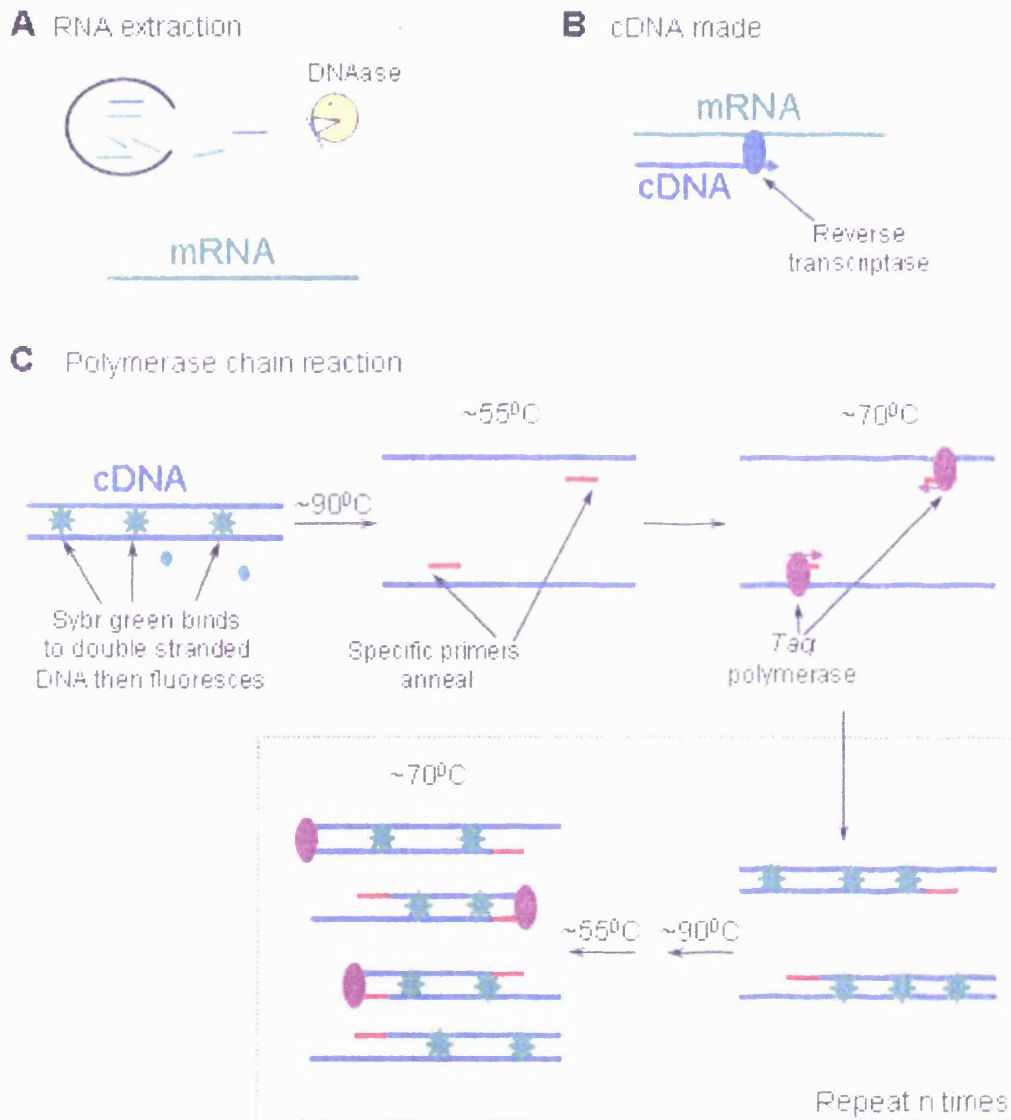


Figure 2-13 Principles of reverse transcriptase PCR: **A)** RNA is extracted from the tissue of interest and genomic DNA is degraded with DNAase. **B)** All the mRNA is converted into cDNA by reverse transcriptase. **C)** The PCR reaction doubles the amount of specific product with every cycle.

The annealed primers are extended by a DNA polymerase so that a copy is made of the intervening sequence of interest. After making this copy, the same primers can be used again, not only to make another copy of the input DNA strand but also of the short copy made in the first round of synthesis (Figure 2-13 C). This leads to a logarithmic amplification.

The whole PCR reaction takes place in one tube with the same substrates (the enzymes, sample, specific primers and oligo dT primers). The reactions are controlled by temperature. Raising the temperature to $\sim 90^{\circ}\text{C}$ separates the two cDNA strands. The temperature is then lowered to the annealing temperature of the primers (usually $\sim 55^{\circ}\text{C}$). The temperature is then raised to $\sim 70^{\circ}\text{C}$ where a thermo-stable DNA polymerase (*Taq*) extends the cDNA strands from the primers. This process is then cycled to produce amplification of a specific product (Figure 2-13 C).

Quantitative real-time rtPCR

In traditional PCR the reaction is stopped at a set point (Figure 2-14 A) and the products are run on a gel. If the cDNA of interest was present it shows up at its corresponding molecular weight. Figure 2-14 shows how the PCR reaction proceeds for two dilutions of the same cDNA (on an arithmetic scale, blue and a logarithmic scale, red. The lighter colours represent a more dilute cDNA). Obviously the reaction cannot go on forever so it eventually tails off to a plateau phase. This highlights that traditional PCR methods are unable to determine the relative amount of starting cDNA.

To combat this, the reaction has to be measured when it is still logarithmic, which can only be achieved with real time measurements (hence the name). Here this was achieved by using a dye (Sybr green) that fluoresces brightly when bound to double stranded DNA but very weakly when bound to single stranded DNA. Therefore as the product increases the fluorescence will increase, allowing real time measurement of the PCR reaction.

An arbitrary threshold level was set on the logarithmic part of the reaction (Figure 2-14 A) called the cT (Threshold cycle). Different concentrations of cDNA will now have different cT values (Figure 2-14 A). If the DNA concentrations differ by a factor of 2 then the difference in cT will be 1 (since each cycle doubles the amount of product), and if the difference were ten times, the difference in cT would be 3.33.

Since Sybr green will bind to all double stranded DNA, how can we check that the fluorescent is due to dsDNA from our specific DNA fragment? For example it may contain dimers of primers and / or non-specific fragments. Luckily the melting temperature of DNA depends on its base composition and length. So the fluorescence is monitored as the temperature is raised (Figure 2-14 C). If the fluorescence is only due to the fragment of interest it will have a single melting point (since it will be homogenous).

Relative quantification

All reactions were performed as triplicates. The efficiency of each primer was assessed by serial 10 fold dilutions of DNA, the cT value was plot against log concentration of RNA and fit with a linear regression which always had a R^2 of >0.99 (e.g. Figure 2-14 B).

If the primers have 100% efficiency the slope of the line would be 3.33 (as 10 fold dilutions were used). Primers were designed to have similar efficiencies (see Table 2-3. β -Actin was used as a reference gene, the ΔcT of each target was found relative to β -actin (Equation 2-13, which normalises for differences in RNA loading). This allows us to compare the relative amounts of different mRNA expression, for example if Kv3.1 had a ΔcT of 2 and Kv2.2 had a ΔcT of 5.33 there would be 10 times as much Kv3.1 mRNA as Kv2.2 mRNA.

$$\Delta cT = cT_{Target} - cT_{actin}$$

Equation 2-13 Normalising for different loading amounts

As the efficiencies are all equal this allows us to compare different genes, for example in chapter four Kv2.1 and Kv2.2 are compared relative to Kv3.1 (see Figure 4-15).

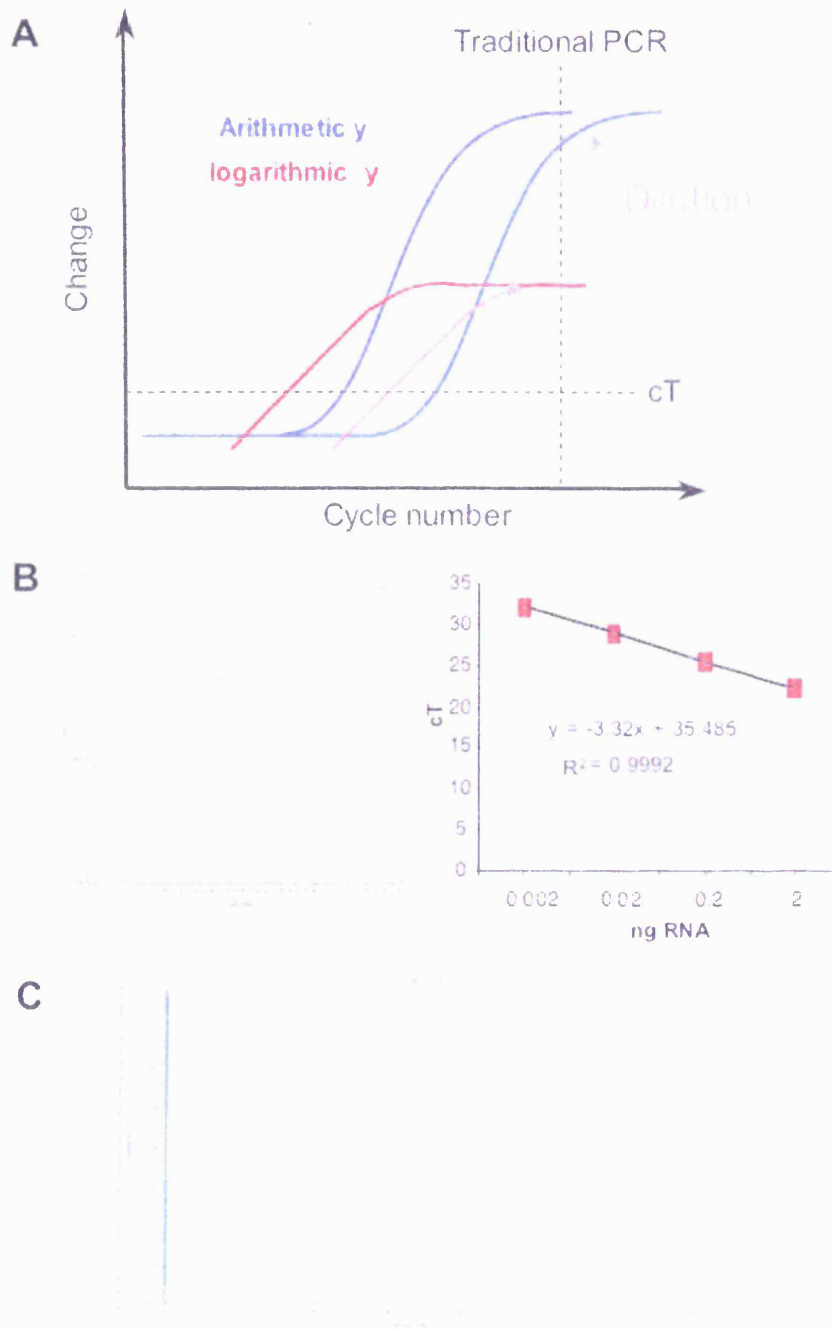


Figure 2-14 Real time PCR methods: **A)** Schematic diagram to illustrating that with real time PCR it is possible to discriminate between different starting concentrations of DNA whereas it is not with traditional PCR. **B)** *Left*, Example of serial dilution to determine the efficiency of the Kv3.1 primers (on a log scale). *Right*, plot of the cT vs RNA concentration gives the efficiency. **C)** Example of a melting curve for Kv3.1 showing a single peak, indicative of specific amplification.

QrtRTPCR procedure

RNA extraction was conducted from a pooled homogenate of MNTBs dissected from 8 mice (P12-P14) using RNeasy lipid tissue mini kit (Qiagen) samples were DNase treated (DNAfree, Ambion).

Reverse transcription was performed on 1–2µg of the RNA sample with SuperScript III first strand synthesis kit (Invitrogen) using oligo-dT primers.

The resultant cDNA was then used for fluorescence real time PCR (Power SYBR Green PCR Master Mix, Applied Biosystems and ABI PRISM 7000 thermal cycler). Amplification occurred under the following conditions: 50°C 2min, 95°C 10min, followed by 95°C 15s and 60°C 60s for 40 cycles.

	Forward	Reverse	Efficiency (%)
Actin	TGCTCCTCCTGAGCGCAAGTACTC	CGGACTCATCGTACTCCTGCTTGC	101.9
Kv2.1	TGGAGAAGCCCAACTCATC	CAATGGTGGAGAGGACAATG	102.1
Kv2.2	CACCTGGCTTGAACAGAAAG	TTGCTTCGGATAATGTCCAC	101.3
Kv3.1	TGAACAAGACCGAAATCGAG	CGAAGGTGAACCAGACCAC	100.1

Table 2-3 Table of primers: All primer were obtained from Sigma.

Chapter 3 – Results 1

Kv3 and Kv1 currents in mouse MNTB

The MNTB is an inverting relay nucleus that codes sound localisation cues. This information is encoded within trains of precisely timed action potentials. A neuron fulfilling the role of transmitting precisely timed action potentials must have several specialisations, which include:

1. A short latency response to its presynaptic input
2. The ability to fire at high frequencies
3. Fidelity of transmission i.e. 1 to 1 firing

This chapter will look at each of these attributes in turn, focusing on the underlying ion channels, which endow the MNTB with these properties.

Properties concerned with short latency responses

The MNTB receives the giant presynaptic terminal, the calyx of Held directly onto its soma (Figure 3-1 A). This morphological specialisation avoids delays associated with cable properties of dendritic processes. Additionally the calyx encapsulates ~40% of the soma (Satzler *et al.*, 2002), which will result in the somatic membrane charging fairly uniformly.

The postsynaptic response to a single unitary synaptic stimulus is the largest known in the brain, with EPSCs of -7 ± 1.2 nA at -60 mV ($n=8$, Figure 3-1 B). The large size of the EPSC serves several purposes; firstly it ensures fidelity of transmission. The postsynaptic MNTB has a threshold for action potentials of between 200-250 pA (measured by current steps of 50 pA increments, cells fired with 224 ± 18.6 pA, $n=23$, Figure 3-1 D). With such a large safety factor the MNTB always fires in response to a presynaptic action potential (Figure 3-1 C).

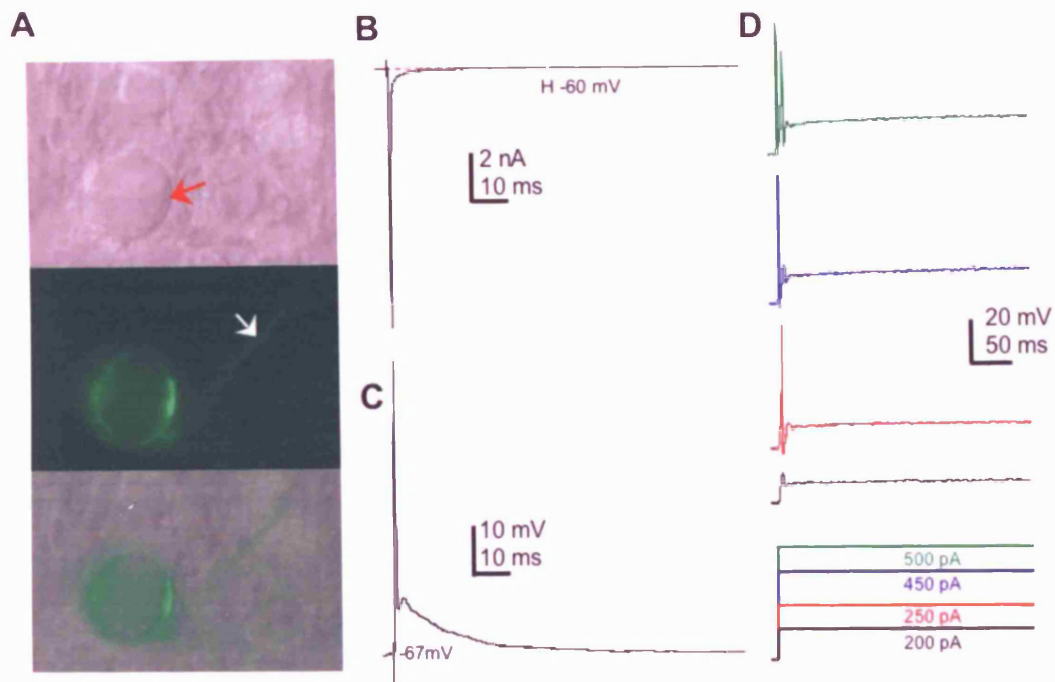


Figure 3-1 Somatic supra-threshold synaptic currents generate a single action potential: **A)** Top, MNTB neuron with presynaptic calyx (red arrow). Middle, the presynaptic terminal from above filled with sulforhodamine 101 and artificially coloured (Note presynaptic axon, white arrow). Bottom, above images merged. **B)** Example EPSC at -60mV. **C)** A single AP generated by orthodromic stimulation of the cell in B. **D)** Step depolarisations of the same neuron in B, showing a typical single AP response except at higher current injections (green) where 2 AP are evoked.

Secondly it ensures minimal latency. The membrane time constant measured at -60mV is $3.0 \pm 0.3\text{ms}$ ($n=10$) meaning that an input just above threshold could take $\sim 15\text{ms}$ ($5 \times \tau$) to generate an action potential. However, the EPSC generated by the calyx is 31 times threshold ($7\text{nA} / 0.224\text{nA}$), which effectively supercharges the membrane, resulting in an extremely short response latency.

The huge EPSC will also help to speed the output from the MNTB as it is likely to depolarise a considerable length of the efferent axon, possibly explaining why the efferent axon remains unmyelinated for considerable distances ($>20\mu\text{m}$, Leao *et al.*, 2005a).

Developing a method to study isolated synaptic action potentials

Current steps are commonly used to study action potential properties; however as can be seen in Figure 3-1 C & D the response to step depolarisation is qualitatively different from orthodromic synaptic stimulation. There is a delay to onset as the membrane charges, the rate of depolarisation is slower, as it is only mediated by the Nav channels. Furthermore the membrane potential does not return to rest after spikes (Figure 3-1 D). To study the roles of K^+ channels in the MNTB we sought to look at more physiological action potential waveforms i.e. those generated by calyceal EPSPs. However, due to the presence of presynaptic K^+ channels (Dodson *et al.*, 2003; Ishikawa *et al.*, 2003), pharmacological studies of orthodromically stimulated action potentials would be contaminated by presynaptic K^+ channel effects, for instance TEA will block Kv3 channels located in the presynaptic terminal resulting in larger EPSCs (Ishikawa *et al.*, 2003), as well as blocking postsynaptic Kv3 currents.

To overcome this problem I decided to use a simulated synaptic current, directly injected through the pipette. This method has two advantages: 1. It avoids quantal fluctuation inherent in orthodromic stimulation. 2. It generates responses similar to physiological stimuli.

The current flowing through the ligand-gated channels at each time point is dependent on the conductance and the driving force for that channel. To generate this simulated waveform, the conductance was obtained by averaging at least 5 EPSCs recorded at -60mV and -70mV (Figure 3-2 A). From these, the average conductance was calculated (Figure 3-2 B). From the same cell the orthodromic action potential waveform was then recorded in true current clamp for the same synaptic stimulation (Figure 3-2C). The average conductance was then multiplied by the action potential waveform resulting in the simulated synaptic waveform in Figure 3-2 D.

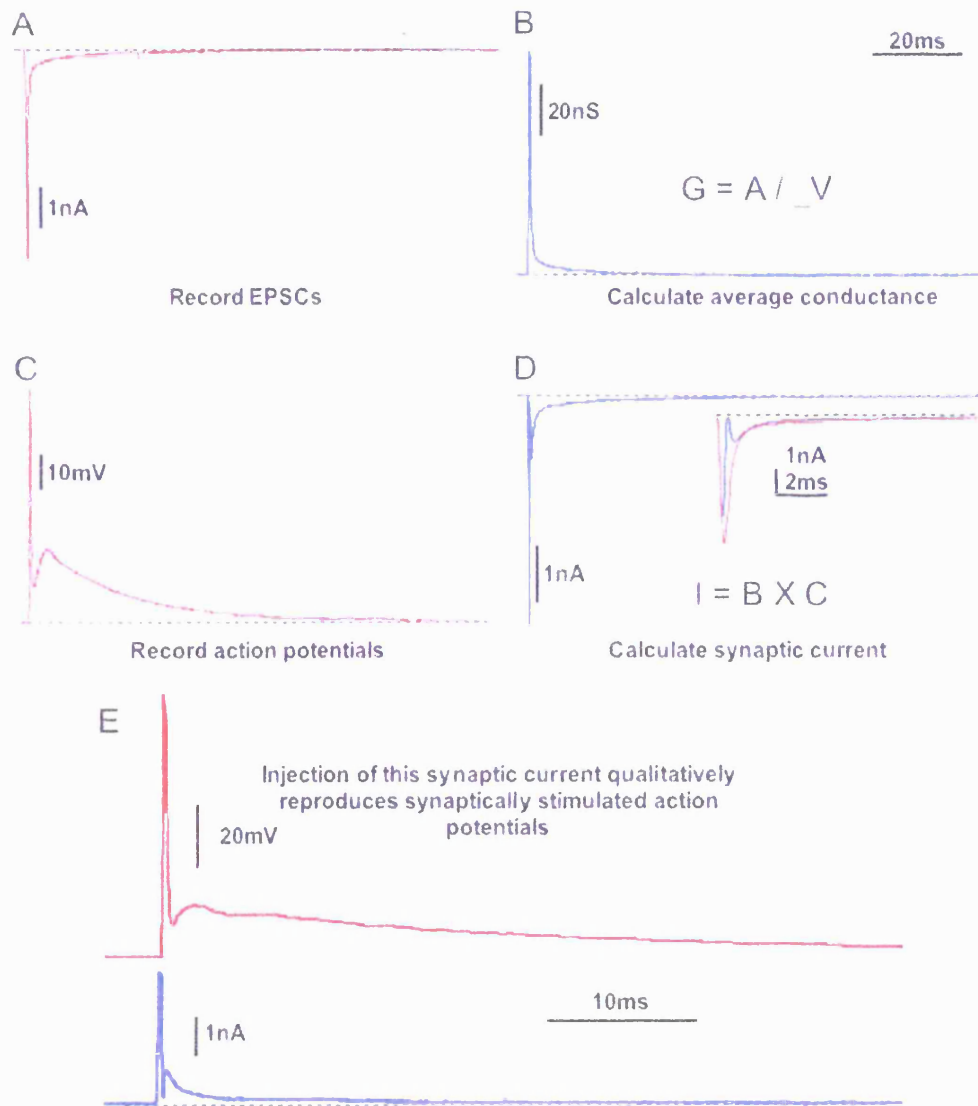


Figure 3-2 Generating a synaptic current waveform: A) EPSCs were recorded at different voltages, example of EPSC at -60mV. **B)** The average conductance was then calculated from the EPSCs in A (current / driving force). **C)** The action potential waveform was recorded from the same cell in A. **D)** The conductance calculated in B was then multiplied by the voltage in C, inset shows expanded scale EPSC in A (red) and calculated synaptic current (blue). N.B. Time base in B applies to A, B, C & D. **E)** Direct injection of the synaptic current (blue) generates an action potential (red) qualitatively similar to one via orthodromic stimulation. Synaptic recordings were carried out with assistance from M. Postlethwaite.

Injection of the simulated synaptic current overcomes synaptic variability as well as avoiding unwanted presynaptic affects. As the MNTB receives its presynaptic input directly onto its cell body (Figure 3-1 A) it is reasonable to directly inject the simulated

synaptic current into the soma and expect it to reproduce an action potential similar to orthodromic stimulation, which is the case as demonstrated in Figure 3-2 E.

Properties concerned with high frequency firing

MNTB neurons have been reported to fire at up to 800Hz *in vivo* (Kopp-Scheinflug *et al.*, 2003), in order to achieve these rates (1 AP every 1.25ms) their action potentials must be extremely brief. I will now examine two ion channels involved with producing brief action potentials.

Sodium current

An inward (depolarising) Na⁺ current is the primary drive of nearly all mammalian action potentials (Hille, 2001). It causes the initial upward deflection of the membrane voltage during an action potential.

Under voltage-clamp, MNTB neurons evoke a rapidly activating inward current when the voltage is stepped to -37mV (Figure 3-3 A). A -97mV pre-pulse was used to remove any steady-state inactivation; under these conditions the inward current had a peak amplitude of 5.8 ± 0.6 nA (n=7, Figure 3-3 A & D). This rapid inward current was blocked by 1 μ M TTX (n=7, single example in Figure 3-3 A&B) indicating that it is mediated by a Nav subunit, but excluding 1.5, 1.8 or 1.9 based on their relative insensitivity to TTx (Catterall *et al.*, 2003a).

The TTx-sensitive current can be fit with an exponential decay (Figure 3-3 A, black – red trace gives the trace in C), which has a tau of 0.26 ± 0.02 ms (n=7). Also note that the Na⁺ current does not completely inactivate (Figure 3-3 C). These values which give an idea of the rapidity of the Na⁺ current are likely to be underestimates, as these recordings were filtered at 2 kHz causing: 1. attenuation of the peak amplitude and 2. rounding of the

signal resulting in a slower measure of the inactivation time constant. These problems may be overcome by filtering at higher frequencies.

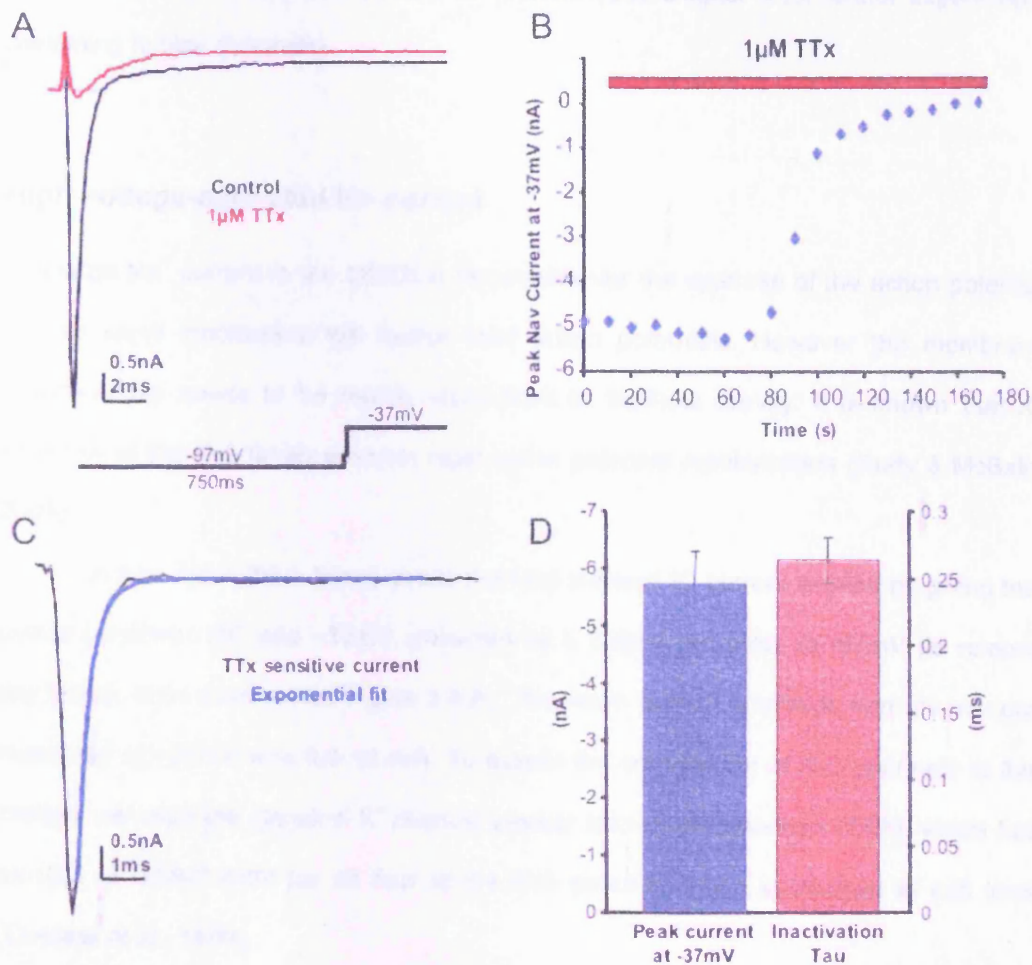


Figure 3-3 Estimating parameters of the Nav current in MNTB neurons: **A)** The inward Na⁺ current (black) evoked at -37mV is blocked by 1µM tetrodotoxin (TTx, red). **B)** Time course of block by TTx for the cell in A. **C)** The subtracted TTx sensitive current from the cell in A is fit with a single exponential decay. **D)** Averaged data (n7) for the peak Nav current measured at -37mV and the inactivation time constant of the TTx sensitive current. N.B. These values are likely to be underestimates, see text for details.

More quantitative studies of Nav channels would require excised patches or reducing the size of the Na current by lowering the Na⁺ concentration or using low concentrations of TTx (e.g.~1nM). The latter may be the best method as pulling a patch may disrupt accessory proteins. Nevertheless, these data gave an indication of the magnitude and rapidity of the Nav current expressed in the MNTB. The rapidity of inactivation is crucial

for brief APs and hence for high frequency firing. In all other voltage-clamp experiments 1 μ M TTx was included to isolate the K⁺ current. (See chapter 4 for further experiments pertaining to Nav channels)

High voltage-activated K⁺ current

The large Na⁺ current in the MNTB is responsible for the upstroke of the action potential and its rapid inactivation will favour brief action potentials. However the membrane potential also needs to be rapidly repolarised to facilitate brevity. It is known that K⁺ channels of the Kv3 family promote rapid action potential repolarisation (Rudy & McBain, 2001).

Figure 3-4 A (blue trace) shows the total outward K⁺ current evoked by giving test pulses between -107 and +18mV, preceded by a 750ms pre-pulse to -97mV (to remove any steady state inactivation, Figure 3-4 B). The mean current amplitude from 21 neurons measured at +28mV was 8.3 \pm 0.4nA. To assess the contribution of Kv3 channels to this current, we used the classical K⁺ channel blocker tetraethylammonium (TEA), which has an IC₅₀ of 0.09-0.2mM for all four of the Kv3 subunits when expressed in cell lines (Coetzee *et al.*, 1999).

Application of 1mM TEA resulted in a 38.5 \pm 7.7% (n=3) reduction in the current measured at +28mV. We also tested 3mM TEA, which reduced the current at +28mV by a similar amount, 36.6 \pm 3.7% (n=3). As the percentage block at 1 and 3mM were not significantly different at all of the measured voltages (p= 0.83 at 28mV), we pooled the data from the two concentrations.

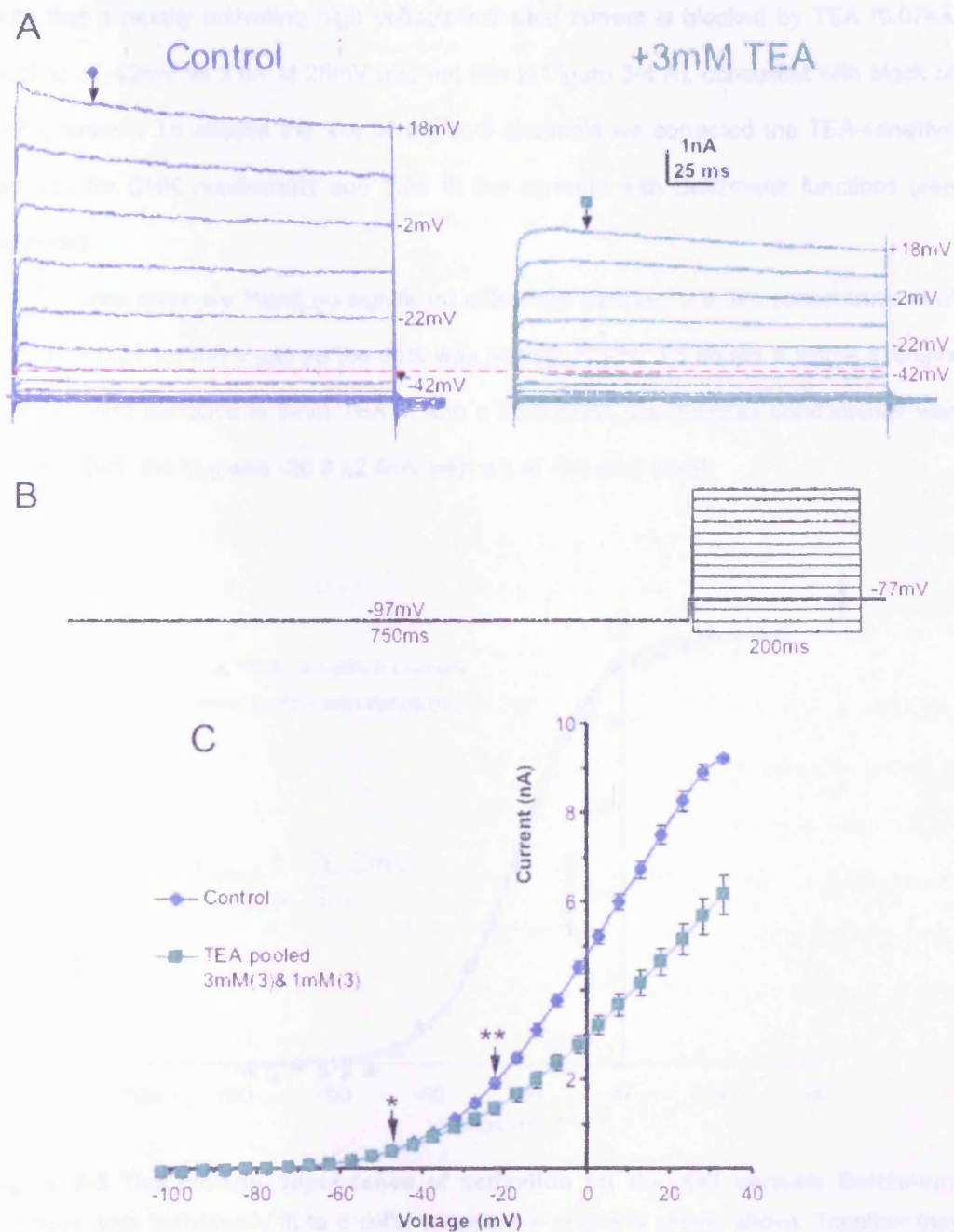


Figure 3-4 A high voltage-activated K^+ current is blocked by TEA: A) The total (blue) and TEA insensitive (green) outward K^+ current in response to the protocol in B, red line indicates current at -42mV. **C)** Average data pooled from 3 cells each at 1 and 3mM, blue=control, green=TEA. * = 95% significance, ** =99% significance.

The I/V relationship of the pooled data is shown in Figure 3-4 C, and a single example from one cell in control and the presence of 3mM TEA is shown above in Figure 3-4 A.

Note that a rapidly activating high voltage-activated current is blocked by TEA (0.07nA blocked at -42mV vs 3.nA at 28mV and red line in Figure 3-4 A), consistent with block of Kv3 channels. To assess the $V_{1/2}$ of the Kv3 channels we corrected the TEA-sensitive currents for GHK nonlinearity and then fit the currents with Boltzmann functions (see methods).

Once more we found no significant difference between the two concentrations of TEA ($P = 0.21$ for the $V_{1/2}$ s) so the data was pooled. Figure 3-5 shows a single example of the current sensitive to 3mM TEA fit with a Boltzmann, the maximal conductance was 31.2 ± 0.3 nS, the $V_{1/2}$ was -20.3 ± 2.4 mV with a k of -9.1 ± 1.0 ($n=6$).

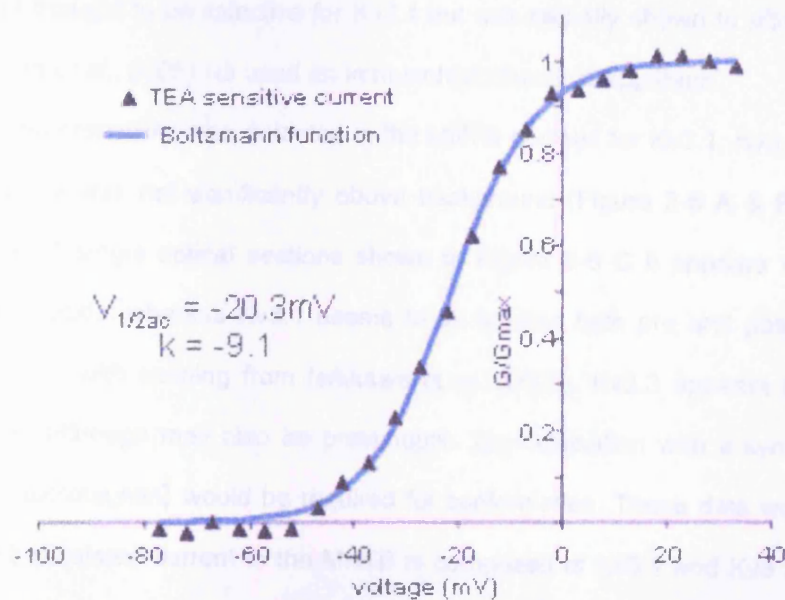


Figure 3-5 The voltage dependence of activation for the Kv3 current: Boltzmann functions were individually fit to 6 cells, an example of one is shown above. Together they gave an average $V_{1/2}$ of -20.3 ± 2.4 mV and k of -9.1 ± 1.0 .

The $V_{1/2}$ obtained for the Kv3 current was more negative than expected (values in expression systems are $\sim +10$ mV). At these concentrations of TEA any Kv1.1 homomeric channels would be partially blocked. However, we are reasonably confident that this difference is not due to a population of Kv1.1 homomers (which have a more negative $V_{1/2}$) as the normalised current exemplified in Figure 3-5 would display a “kink” since it

would be the sum of two activation curves with differing $V_{1/2}$ s, (For further evidence see Figure 3-15). The fact that the $V_{1/2}$ reported here is more negative than that from expression systems may be explained by the erroneous method used by (Rudy & McBain, 2001) for normalising the currents for the driving force; they corrected for an ohmic conductance instead of GHK rectification which returns a more positive $V_{1/2}$ (see methods and, Clay, 2000).

Kv3 subunit composition

As there is no pharmacological means to differentiate between Kv3 channel composition (BDS-I was thought to be selective for Kv3.4 but was recently shown to affect Kv3.1 and Kv3.2, Yeung *et al.*, 2005) we used an immunohistochemical approach.

Immunoreactivity was detected in the MNTB nucleus for Kv3.1, Kv3.3 and Kv3.4. whereas Kv3.2 was not significantly above background (Figure 3-6 A & B). On closer examination of single optical sections shown in Figure 3-6 C it appears that Kv3.4 is mainly presynaptic, whereas Kv3.1 seems to be located both pre and postsynaptically, both consistent with staining from Ishikawa *et al.* (2003). Kv3.3 appears to be mainly postsynaptic, although may also be presynaptic. Co-localisation with a synaptic protein (such as synaptotagmin) would be required for confirmation. These data would suggest that the Kv3 mediated current in the MNTB is composed of Kv3.1 and Kv3.3 homomers and or Kv3.1/Kv3.3 heteromers; however there is no complementary evidence to corroborate these conclusions. More extensive confirmation of the subunit composition will prove difficult as; if one tried co-immunoprecipitation the sample would be contaminated by the presynaptic Kv3 channels.

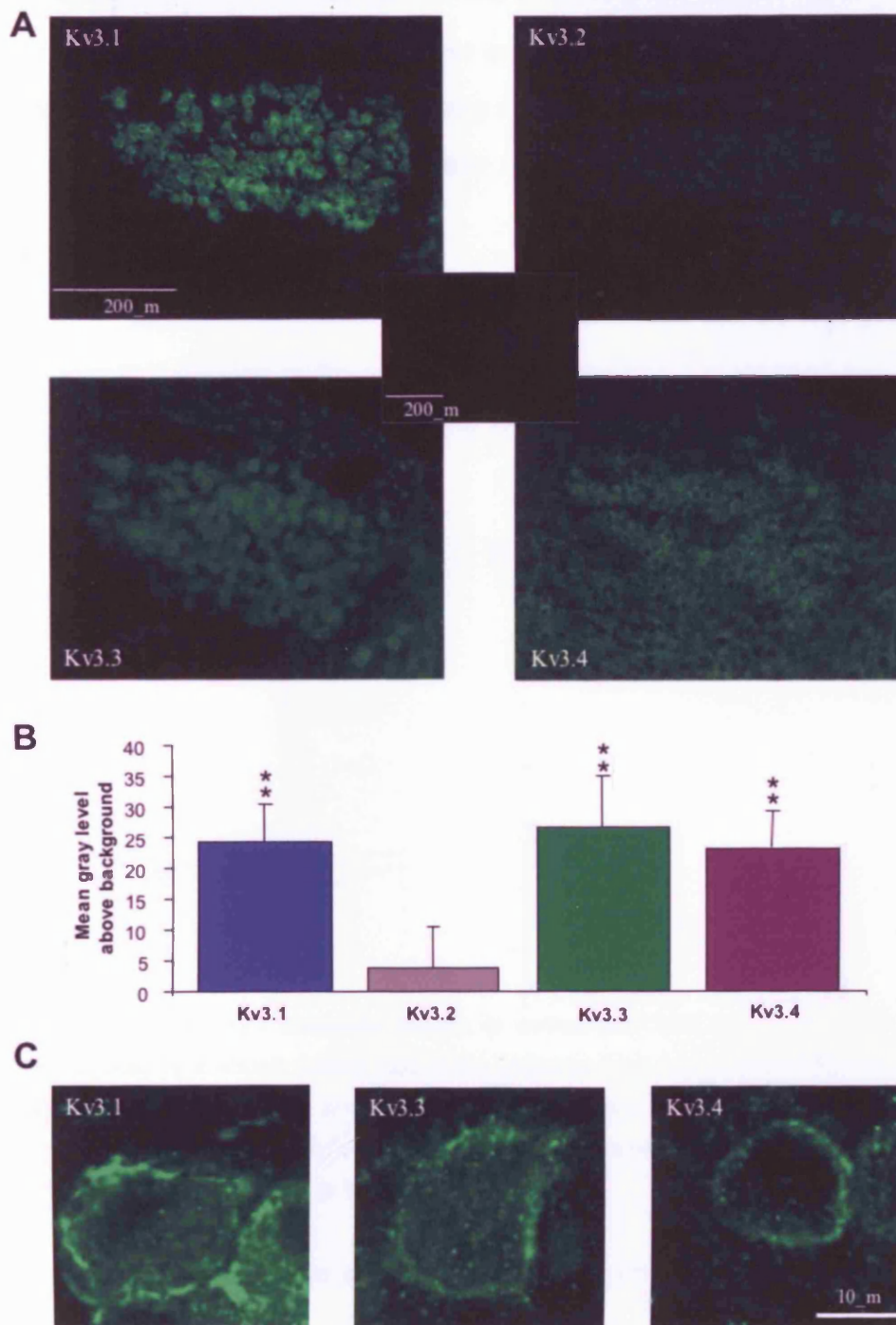


Figure 3-6 Immunoreactivity for the Kv3 family: **A)** 10x pictures showing positive immunostaining for Kv3.1, 3.3 and 3.4 and low Kv3.2. **B)** Plot of the mean gray level above control shows that Kv3.1, 3.3 and 3.4 are all extremely significant whereas Kv3.2 is not (n=3). **C)** Single optical sections show that Kv3.1 is present pre and postsynaptically whereas Kv3.4 appears to be mainly presynaptic, while Kv3.3 is likely only postsynaptic. N.B. control levels of fluorescence = in the absence of primary antibody. Immunohistochemistry performed by M. Barker.

Construction of dominant negative subunits and transfection into cultured MNTB neurons seems the most appealing option; however one would have to assume no change in expression and or subunit composition during culture, a factor which has been reported for other K^+ channels (Watkins & Mathie, 1996; Aller *et al.*, 2005).

The physiological role of Kv3 channels

The role of Kv3 channels in the MNTB has been extensively studied in both rat and mouse MNTB (Brew & Forsythe, 1995; Wang *et al.*, 1998b; Brew & Forsythe, 2005; Song *et al.*, 2005).

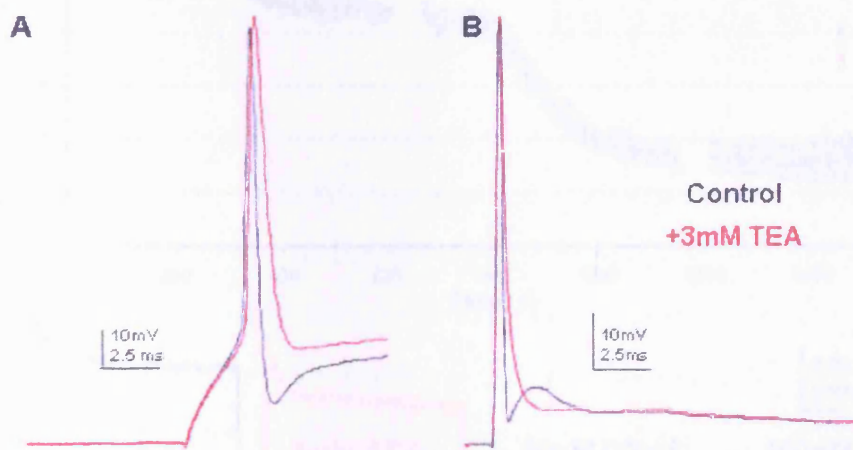


Figure 3-7 Block of Kv3 channels results in action potential broadening. A) Action potential evoked by a 450pA current step in the presence (red) and absence (black) of TEA. **B)** Action potential evoked by a simulated synaptic current in the presence (red) and absence (black) of TEA. Note that in both A & B the action potential broadens in the presence of TEA. Similar results were observed in at least 3 cells.

However to highlight their most obvious role we applied either current steps or synaptic currents under true current clamp. Neurons were held ~ -70 mV (by a DC current injection if required, and if greater than 300pA was required to do this, cells were excluded). Application of 3mM TEA resulted in action potential broadening in all cases along with removal of the fast after hyperpolarisation (Figure 3-7 A & B), which is consistent with block of a fast high threshold K^+ current.

Properties concerned with fidelity of transmission

As shown in Figure 3-1 C & D the MNTB fires just a single action potential in response to supra-threshold current injections. This single action potential phenotype is characteristic of the MNTB and has been shown to be mediated by low-threshold currents belonging to the Kv1 family (Brew & Forsythe, 1995; Dodson *et al.*, 2002).

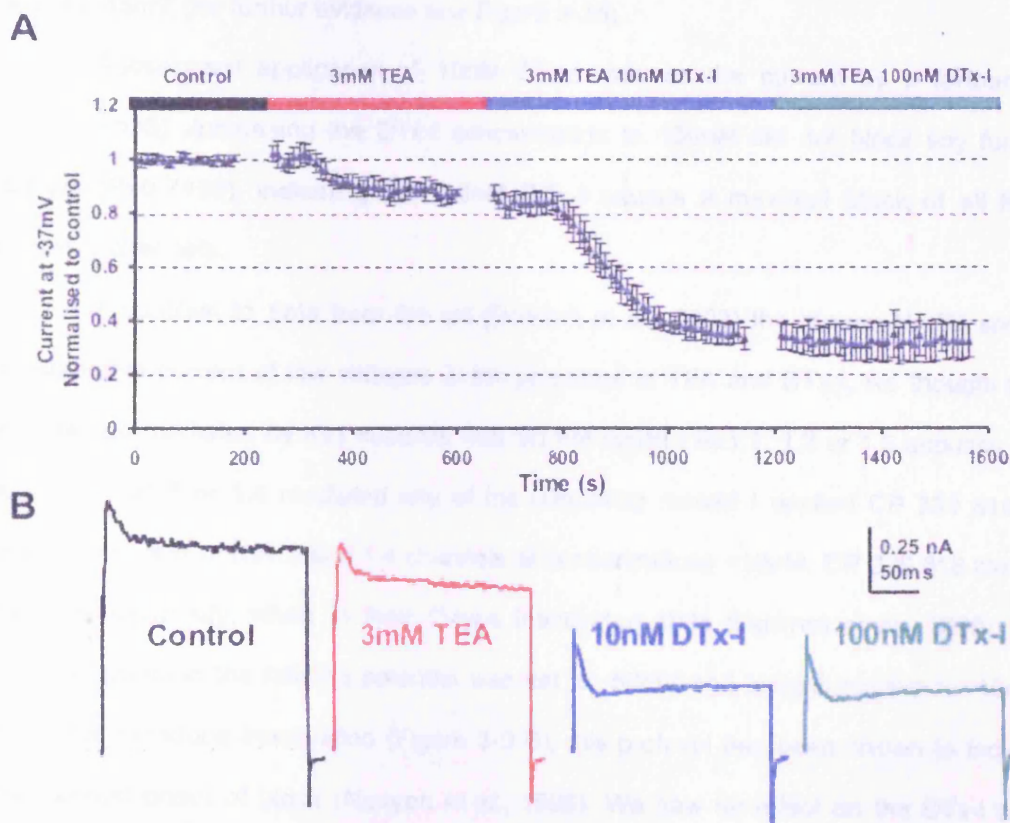


Figure 3-8 Sequential pharmacology of the low voltage-activated current. A) Average time course of drug application. The current measured 40ms into each -37mV pulse was normalised to control. The plot shows the average ($n=3$) normalised amplitude of current evoked 40ms into a -37mV step, during sequential application of TEA and DTx-I. TEA blocked $13 \pm 0.03\%$ of the current, 10nM DTx-I blocked a further $51 \pm 0.04\%$, no further block was seen with 100nM DTx-I. **B)** Example current traces after application of each drug from one cell.

To characterise this current in mice, we examined the outward current active on steps to moderately depolarised levels i.e. -37mV, using dendrotoxin-I (DTx-I). DTx-I blocks Kv1.1

, 1.2 and 1.6 containing channels with IC_{50} s in the low nanomole range (Robertson *et al.*, 1996; Hopkins, 1998; Harvey, 2001) and blocks all the low voltage-activated current in rat (Brew & Forsythe, 1995).

As can be seen in Figure 3-8 application of 3mM TEA blocks $13 \pm 0.03\%$ (n=3) of the current at -37mV, this is likely due to block of Kv3 channels, which begin to activate around -45mV (for further evidence see Figure 3-15).

Subsequent application of 10nM DTx-I reduces the current by a further $51 \pm 0.04\%$ (n=3). Increasing the DTx-I concentration to 100nM did not block any further current (P=0.7495), indicating that 10nM DTx-I causes a maximal block of all Kv1-sensitive channels.

In contrast to data from the rat (Dodson *et al.*, 2002) the mouse MNTB shows considerable current at low voltages in the presence of TEA and DTx-I, we thought that this may be mediated by Kv1 subunits that did not contain Kv1.1, 1.2 or 1.6 subunits. To assess if Kv1.3 or 1.4 mediated any of the remaining current I applied CP 339 818, a selective blocker of Kv1.3 and 1.4 channels at concentrations $<10\mu\text{M}$. CP 339 818 blocks channels externally, when in their C-type inactivated state (Nguyen *et al.*, 1996). So during application the holding potential was set to -50mV and pulsed positive to -10mV every 10s to induce inactivation (Figure 3-9 B), this protocol has been shown to induce the quickest onset of block (Nguyen *et al.*, 1996). We saw no effect on the DTx-I and TEA-insensitive current at any voltage when CP 339,818 was applied at concentrations of 5-10 μM (Figure 3-9, n=3). Indicating that the remaining current is not mediated by the DTx-I insensitive subunits Kv1.3 or 1.4.

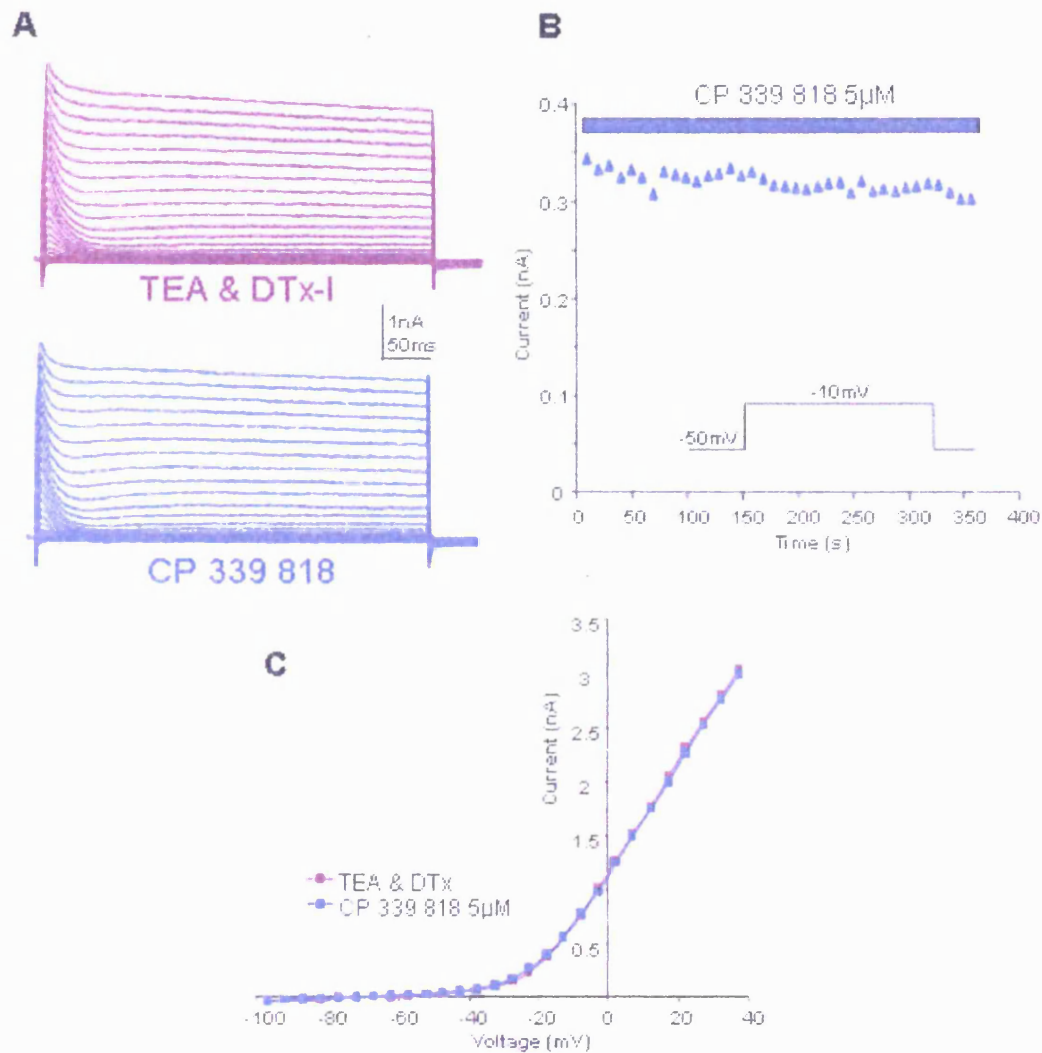


Figure 3-9 The Kv1.3 and 1.4 antagonist CP 339,818 has no effect on the TEA and DTx-I insensitive current. **A)** DTx-I and TEA-insensitive current (purple) and after application of CP 339,818 (blue) from the same neuron. **B)** Time course of CP 339,818 application from cell in A, Note that during application V_{hold} was -50mV (see text for details). **C)** I/V of the cell in A before and after CP 339,818, current measured 40ms into test pulses. Similar results were obtained in 3 cells. N.B. the transient component is also unaffected.

DTx-I sensitive low-voltage currents

Having established that a small amount of Kv3 current is active at -37mV we decided to routinely block it by including 3mM TEA in the aCSF for future experiments. This also helps to reduce voltage errors associated with large current passing across the pipette.

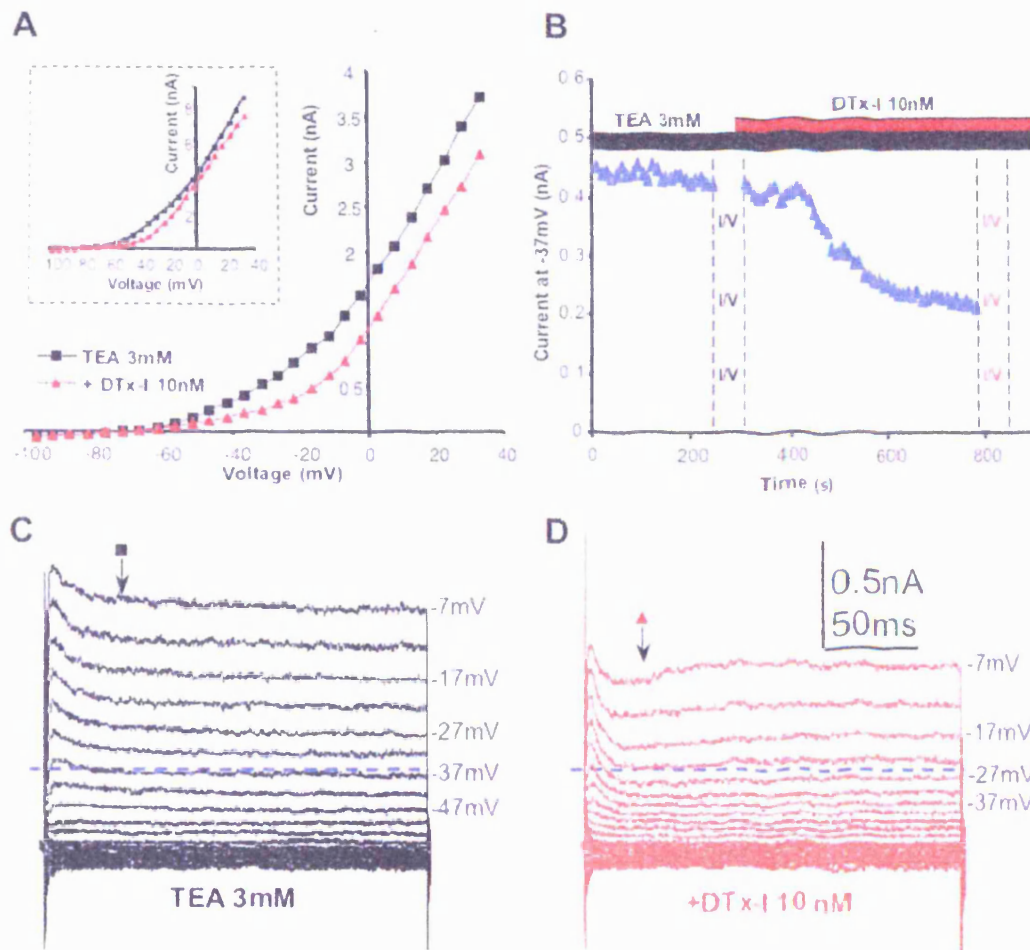


Figure 3-10 DTX-I blocks a low voltage-activated current. **A)** Example I/V before (black) and after application of 10nM DTX-I (red), Inset shows response from a different neuron. **B)** Time course of DTX-I block for the neuron in A. **C)** Current traces for the TEA-insensitive current from the neuron in A. **D)** current traces from the same cell after application of DTX-I (10nM). Blue dashed line indicates the control level of current at -37mV; arrows indicate the current plotted in A. similar results obtained in 6 cells.

A time course was always recorded and analysed online when assessing toxin block to verify maximal block (e.g. Figure 3-10 B) before recording the final I/V. The time to onset of block was dependent on whether the perfusion lines were primed (see Methods). Figure 3-10 A shows the complete I/V for the affect of DTX-I (10nM) on the TEA-insensitive current. Note that the outward current at low voltages i.e. -50 to -20mV is attenuated, consistent with block of low voltage-activated Kv1 channels (n=6). However at more positive voltages i.e. >-10mV the current blocked by DTX-I appears to become

less; this phenomena was seen in all dendrotoxin applications, and in some cases the current in the presence of DTx-I nearly equalled that in control (see Figure 3-10 A inset).

When the dendrotoxin-sensitive current is isolated (by subtracting the current in the presence of DTx-I from the current in its absence) a 'kink' appears in the I/V as shown by the averaged data in Figure 3-11 A (n=6). The interpretation of this 'kink' will be discussed in the conclusion to this chapter. The kink prevents accurate determination of the voltage dependence of activation of the DTx-I sensitive current, which is assessed by converting the current to conductance, then normalising to the maximal conductance (G_{Max}) and fitting this with a Boltzmann function (see methods).

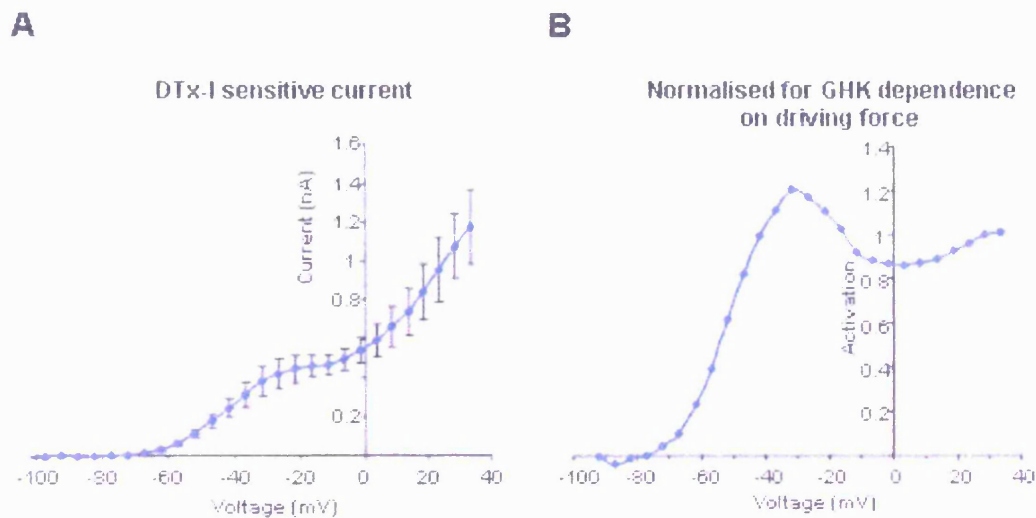


Figure 3-11 The DTx-I sensitive current activation **A)** The average subtracted DTx-I sensitive current (note the kink and the increase in error positive to -40mV). **B)** The data in **A** normalised for the GHK dependence on the driving force, shows that the DTx-I sensitive current activates from around -75mV

Following this procedure, when the current is converted to conductance (taking account for the GHK dependence of the driving force, see methods) the conductance does not reliably plateau rendering determination of G_{Max} impossible (Figure 3-11 B).

Note that the scale in Figure 3-11 B is inconsequential as the GHK current equation (Equation 2-9) used to correct for the driving force requires input of an arbitrary normalisation factor, which is usually rendered irrelevant due to the subsequent

normalisation to G_{Max} . However I included this analysis as it shows that the Kv1 current begins to activate at -75mV.

The physiological role of Kv1 channels

To assess the physiological role of Kv1 channels in mouse MNTB, under true current-clamp I applied current pulses in 50pA increments similar to Figure 3-1 D. Application of DTx-I (10nM) resulted in action potential firing at lower current injections. The first action potential was observed with 116 ± 33.3 pA less current (Figure 3-12 A) than under control conditions. DTx-I lowered the firing threshold from -37.6 ± 1.5 mV to -42 ± 1.5 mV ($n=3$). More positive current injections of 250pA evoked 1 ± 0 action potentials under control conditions and after DTx-I application this increased to 25 ± 11 (Figure 3-12 A, $n=3$).

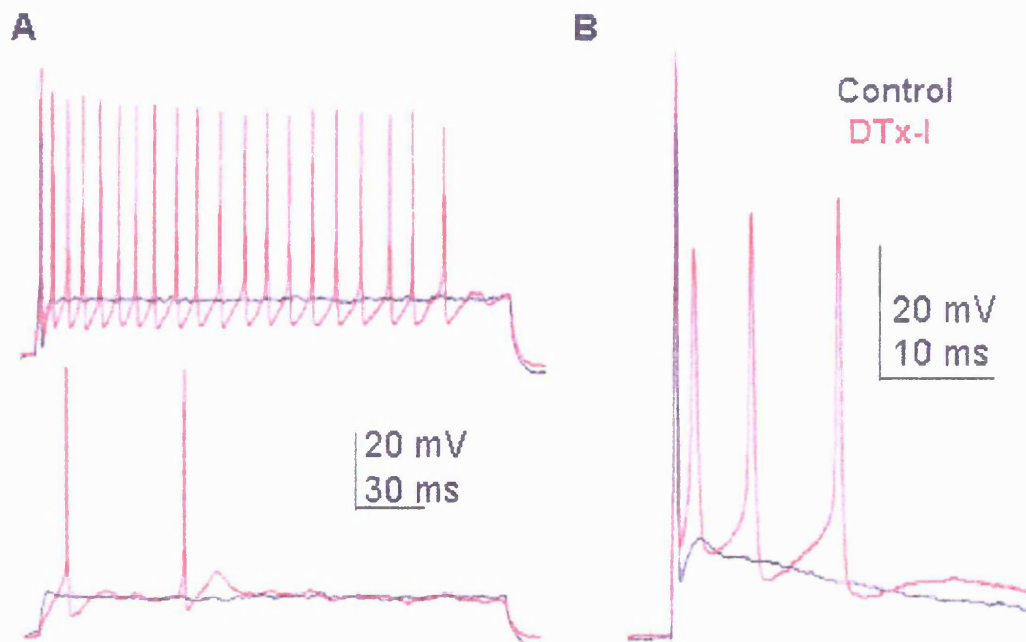


Figure 3-12 Kv1 channels set threshold and prevent aberrant firing. A) Current steps of 100pA (bottom) and 250pA (top) in the presence (red) and absence (black) of DTx-I (10nM) **B)** Simulated synaptic current injection in the same cell as A in the presence and absence of DTx-I.

When the simulated synaptic current was used, again in control conditions only 1 action potential was evoked with the characteristic after depolarisation (ADP). On application of DTx-I multiple action potentials occurred which rode on the ADP (Figure 3-12 B). These data are consistent with findings in the rat (Brew & Forsythe, 1995; Dodson *et al.*, 2002) and the mouse (Brew *et al.*, 2003).

Kv1 channel subunit composition

To probe the possible Kv1 channel subunit composition we used an immunohistochemical combined with a pharmacological approach. Figure 3-13 shows the immunoreactivity for 5 neuronal Kv1 family members (Kv1.7 is absent from brain, Kalman *et al.*, 1998; Kashuba *et al.*, 2001) Kv1.3 was omitted as there was no reliable antibody (the existing Kv1.3 antibody reacts with a Kv1.3 KO animal, Personal communication with L. K. Kaczmarek). We are in the process of obtaining a new Kv1.3 antibody and the Kv1.3 KO out mouse.

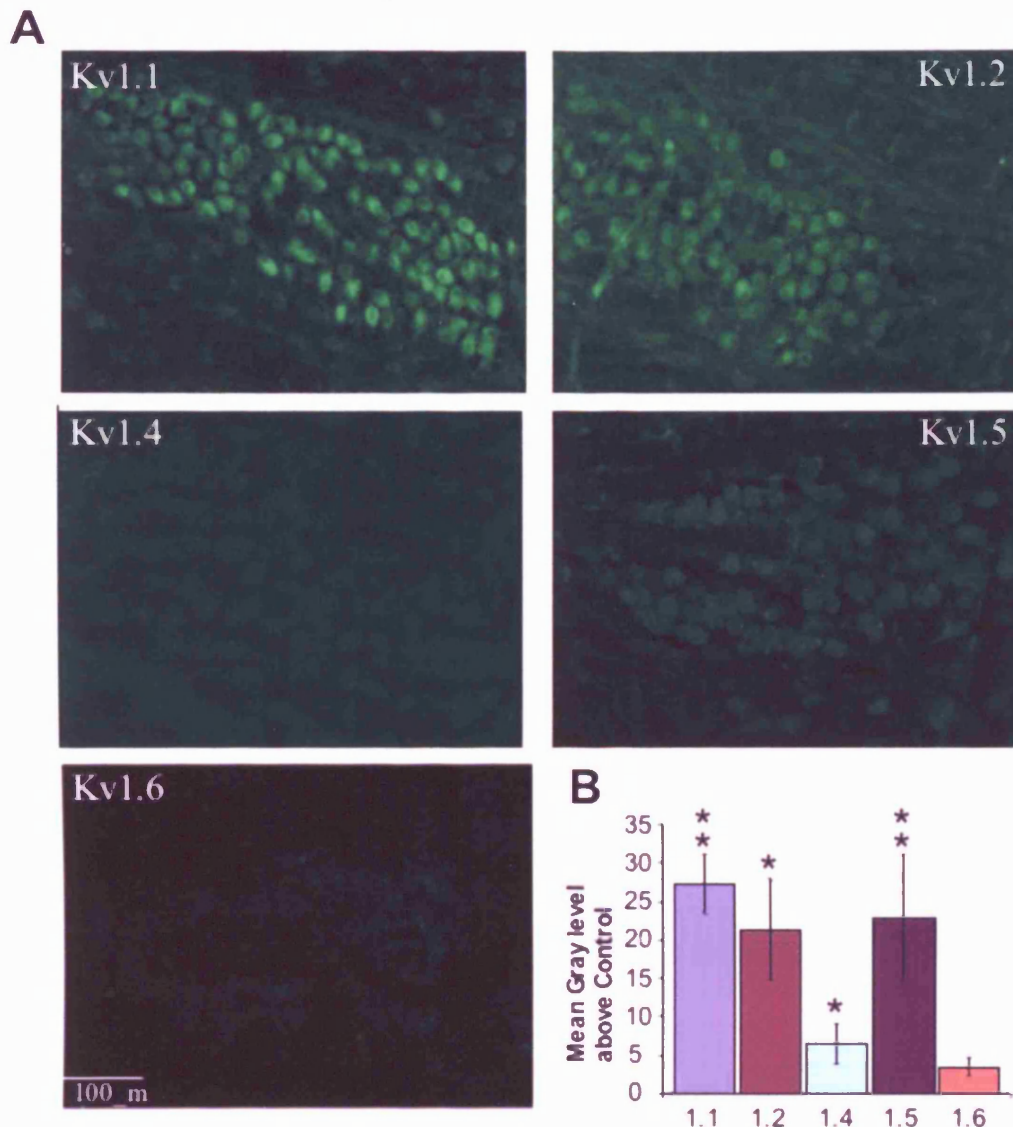


Figure 3-13 Immunoreactivity of the neuronal Kv1 subunits: A) Immunostaining shows the presence of Kv1.1, 1.2 and 1.5 at high levels. **B)** Mean gray level above control (n=3). N.B. control = preincubation with blocking peptide.

The images were analysed with Image J (NIH, USA) by drawing around the MNTB nucleus and analysing the mean gray level. Figure 3-13 B shows the mean gray level above control for each antibody. Kv1.6 was not significantly above control ($P=0.13$, $n=3$), while Kv1.4 was just above control ($P=0.04$, $n=3$) indicating that it may be expressed but if so is at very low levels. Kv1.1 and Kv1.5 showed the most robust staining, although Kv1.5 appeared to be in axons and processes rather than at the soma and may be

located presynaptically. Kv1.2 staining was also high. The higher levels of Kv1.5 than Kv1.6 contrasts with the rat where the opposite is the case (Dodson *et al.*, 2002).

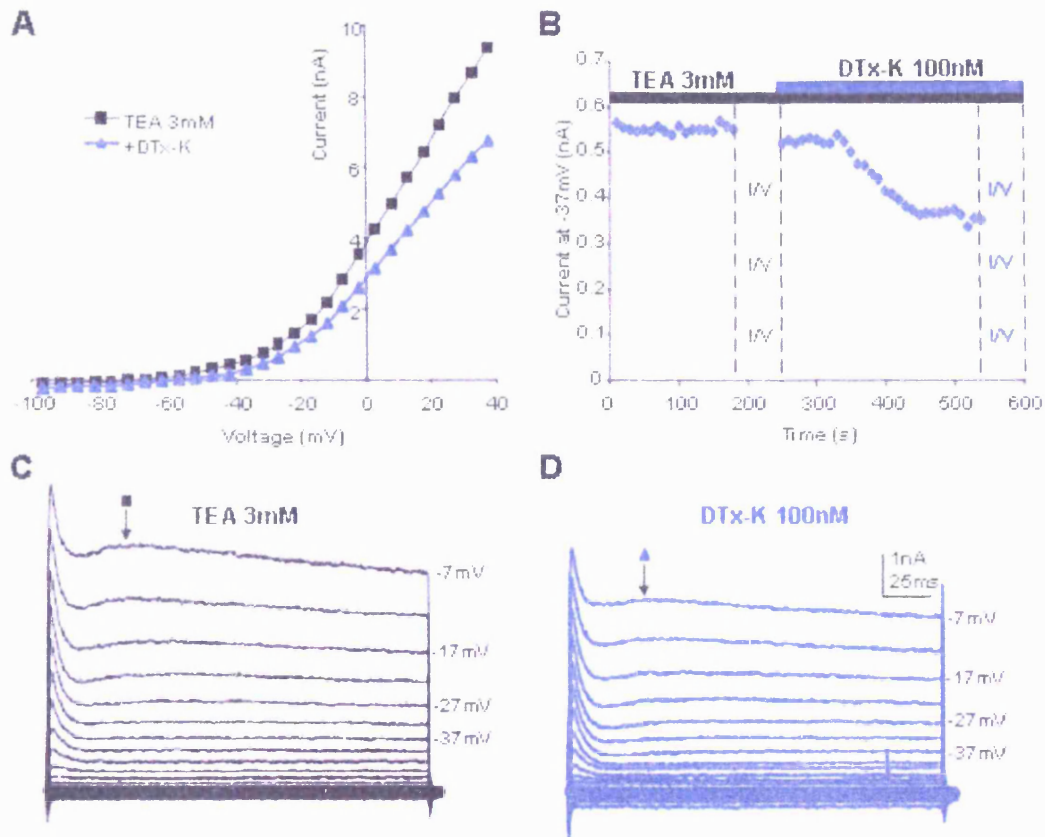


Figure 3-14 DTx-K inhibits a low voltage-activated current: A) Example I/V before (black) and after application of 100nM DTx-K (blue). **B)** Time course of DTx-K block for the neuron in A. **C)** Current traces for the TEA-insensitive current from the neuron in A. **D)** current traces from the same cell after application of DTx-K (100nM); arrows indicate the current plotted in A. Similar example representing an n of 4.

The availability of subunit specific toxins for Kv1 channels allows pharmacological probing of subunit composition. DTx-K is extremely potent for Kv1.1 subunits and blocks in the low nanomole range (Robertson *et al.*, 1996; Dodson *et al.*, 2002). Application of 100nM DTx-K to the TEA-insensitive current reduced the current measured at -37mV by $39 \pm 8.2\%$ (Figure 3-14, $P=0.028$, $n=4$), a similar percentage block as seen with DTx-I.

This indicates that the majority of Kv1 channels in the MNTB contain Kv1.1 subunits. To assess whether these channels are homo- or heteromeric we took advantage of the higher potency of TEA for Kv1.1 subunits (IC_{50} of 0.5mM for Kv1.1 homomers, Coetzee *et al.*, 1999) whereas other Kv1 subunits are blocked at higher concentrations ~ 10 mM (Coetzee *et al.*, 1999). Furthermore the block induced by TEA is described by the energy additive model (Hopkins, 1998), meaning for every insensitive subunit in a Kv1.1 containing channel the IC_{50} increases exponentially and as a result, a Kv1.1 heteromer would be relatively insensitive to TEA.

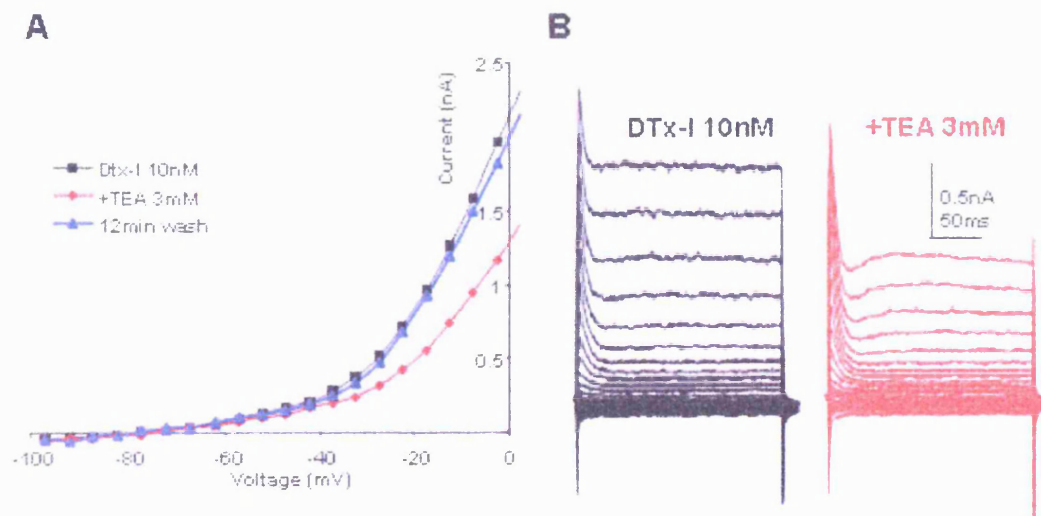


Figure 3-15 The absence of Kv1.1 homomers. A) I/V curves constructed from the current 40ms into the example traces in B, after block of Kv1.1 containing channels, TEA still induces block at negative voltages, which almost completely washes out in 12mins. **B)** Current traces from the cell in A. Similar results seen in 3 cells.

TEA reduced the total outward current at -37mV by $0.15 \pm 0.048\text{nA}$ (Figure 3-4, $n=6$), which in light of the aforementioned pharmacological details may be due to a population of Kv1.1 homomers. To test this hypothesis I first applied DTx-I (10nM), which will block all Kv1.1 homomers (as well as others). Subsequent application of TEA blocked $0.26 \pm 0.13\text{nA}$ block at -37mV (Figure 3-15, $n=3$). Which is not significantly different from the amount blocked in the absence of DTx-I ($P=0.35$). What is important to note is that TEA still causes block, the fact that the block is greater is likely due to recruiting more axonal Kv3 channels once the Kv1 channels are blocked (as block of Kv1 channels will improve the length constant of the axon as mentioned earlier).

Together with the TEA-sensitive activation curve (Figure 3-5) this indicates that a population of Kv1.1 homomers is unlikely and therefore all Kv1.1 subunits are probably constituents of heteromeric channels.

Tityustoxin- $\text{K}\alpha$ (TsTx) blocks channels containing Kv1.2 or Kv1.3 in a similar method to DTx-I, providing Kv1.4 is absent (Hopkins, 1998). Kv1.4 immunoreactivity is detected, although at low levels (Figure 3-13) and it does not contribute to the DTx-I insensitive current (CP-339, 818 Figure 3-9), therefore it is possible that it contributes to the DTx-I sensitive current. To take this into account either 100nM TsTx was bath applied or 500nM was applied by puffer pipette. These concentrations will block Kv1.2/kv1.4 heteromers by around 90% (Hopkins, 1998).

Tityustoxin- $\text{K}\alpha$ applied to the TEA-insensitive current (Figure 3-16) produced a $53.2 \pm 6.5\%$ block (at -37mV , $n=4$, $P<0.05$). In one case a wash off was recorded as shown in Figure 3-16 B.

TsTx produced a similar amount of block to DTx-K and Dtx-I, indicating that all Kv1 subunits in the mouse are composed of Kv1.1/1.2 heteromeric channels. Which differs from the rat where only 50% of the Kv1 channels have this subunit composition (Dodson *et al.*, 2002).

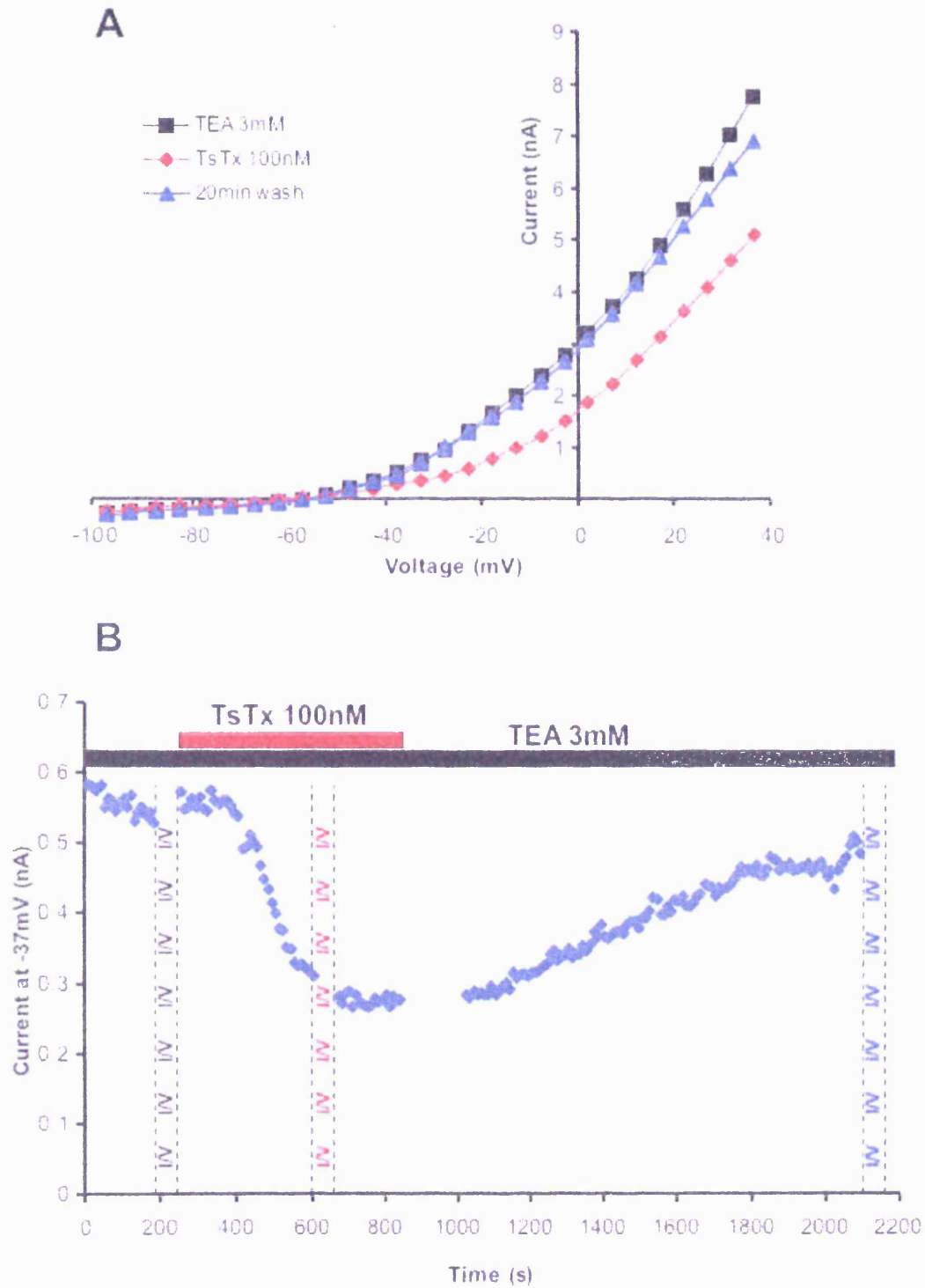


Figure 3-16 TsTx blocks a low voltage-activated current **A)** I/V in the presence of TEA (black), after TsTx (100nM, red) and after 25 of wash (blue). **B)** Time course of antagonist application shown in A.

Discussion

In this chapter I have demonstrated how the calyx of Held/MNTB synapse fulfils some of the roles required of a fast auditory relay synapse: 1. It has a short latency response to its presynaptic input by having a large safety factor in the EPSC. 2. It has extremely brief action potentials due to expression of Kv3 channels. 3. It maintains fidelity of transmission (1 to 1) by expressing Kv1 channels to “manage” the huge EPSC. Each of these points will be discussed in turn below.

Short latency response to the presynaptic input

The large presynaptic calyceal terminal forms directly on to the MNTB cell body (Figure 3-1A) covering ~40% of the soma (Satzler *et al.*, 2002), eliminating conduction delays associated with dendritic cable properties. This specialisation is seen in other fast relay synapses, such as the globular bushy cells in the cochlear nucleus (Neises *et al.*, 1982) and the ciliary ganglion (Stanley, 1992).

The calyx of Held causes a massive postsynaptic response that is ~31 times threshold for action potential generation. This huge safety factor helps minimise response latency by effectively supercharging the membrane, overcoming the postsynaptic membrane time constant, which would normally act to slow the depolarisation rate. Additionally the magnitude of supra-threshold EPSC limits any latency fluctuations, which would result in distortion of the timing information this synapse is relaying.

High frequency firing

In order to relay sound source localisation information the MNTB must be able to follow high frequencies up to 800Hz *in vitro* (Taschenberger & von Gersdorff, 2000) and *in vivo* (Kopp-Scheinflug *et al.*, 2003), therefore the action potentials need to be extremely brief.

The MNTB achieves brief action potentials by having a large Nav conductance which rapidly activates and inactivates with a time constant of ~0.25ms, and a high-threshold K⁺ current which rapidly repolarises. The sodium current will be discussed in the final discussion as in Chapter 4 there are further experiments concerning this conductance.

High-threshold Kv3 channels

There are 4 members of the Kv3 sub family Kv3.1 - 3.4 and each member has at least two splice variants: Kv3.1a-b, Kv3.2a-d, Kv3.3a-d and Kv3.4a-c all of which result in altered C-terminal domains (Rudy & McBain, 2001). Of the Kv3 splice variants that have been studied in expression systems all activate at extremely depolarised potentials i.e. >-10mV and have positive $V_{1/2ac}$ s (Rudy *et al.*, 1999). It is now well accepted that Kv3 channels mediate rapid repolarisation of action potentials; indeed they are expressed in fast spiking neurons of the Globus Pallidus (Baranauskas *et al.*, 1999), sub thalamic nucleus (Wigmore & Lacey, 2000) and hippocampus (Martina *et al.*, 1998).

High-threshold Kv3 channels in the MNTB

The dogma in recent literature is that Kv3.1b mediates the MNTB Kv3 current (Elezgarai *et al.*, 2003; Ishikawa *et al.*, 2003; Macica *et al.*, 2003; Kaczmarek *et al.*, 2005; Song *et al.*, 2005; Song & Kaczmarek, 2006). In large part this opinion has arisen due to positive *in situ* hybridisation (Wang & Kaczmarek, 1998) and the incorrect citation by Macica *et al.* (2003) of previous work apparently showing that the high threshold current in the MNTB is identical to Kv3.1b in CHO cells. However Kv3.1a has not been assessed.

Kv3.1b when expressed in mammalian cells generates a rapid activating and deactivating sustained current with a $V_{1/2ac}$ of +15.5mV in CHO (Macica *et al.*, 2003) or a $V_{1/2ac}$ +7mV in HEK (Baranauskas *et al.*, 2003) cells respectively.

So how does this previous work relate to the findings presented here? Firstly the immunostaining of Figure 3-6 is consistent with Kv3.1b being present, but goes further and rules out any contribution from Kv3.2, both findings being consistent with mRNA expression (Weiser *et al.*, 1994).

Second, Figure 3-6 also shows that Kv3.3 is expressed in the postsynaptic neuron (and possibly also presynaptically) and is at equal levels to Kv3.1b (no significant difference between 3.1 and 3.3, Figure 3-6 B). Surprisingly this is consistent with older work showing the expression of Kv3.3 mRNA in the MNTB and many other auditory neurons e.g. LSO & MSO (Li *et al.*, 2001). Additionally it has been shown that Kv3.3 is as abundant (Grigg *et al.*, 2000) or even higher than Kv3.1 (Li *et al.*, 2001) in the MNTB.

Figure 3-6 A & C also indicate that Kv3.4 is present, although it is likely to be predominantly presynaptic. This conclusion is consistent with the absence of Kv3.4 mRNA in the MNTB (Weiser *et al.*, 1994) but its presence in the ventral cochlear nucleus (the location of the cell body of the calyx of Held, Weiser *et al.*, 1994; Pal *et al.*, 2005) and with previous immunostaining (Ishikawa *et al.*, 2003).

Finally the $V_{1/2ac}$ of the Kv3 current seen in the MNTB is considerably more negative than that reported for Kv3.1b, -20mV vs ~+10mV. This difference will in part be explained by the erroneous method of normalisation for driving force (as discussed in chapter 2), but this will only account for ~10mV of the difference. Additionally I observed no run down in current during recording so dephosphorylation is unlikely to contribute.

Considering the information presented here along with the previous mRNA studies, I think it is unlikely that Kv3.1b homomers mediate the Kv3 current in the MNTB. Rather I would expect that Kv3.1/Kv3.3 heteromers mediate the current. The argument for this being that

Kv3.3 seems to be at least as highly expressed as Kv3.1 (Grigg *et al.*, 2000; Li *et al.*, 2001) and Kv3.3, like Kv3.1b is preferentially found in the soma (Rashid *et al.*, 2001).

Furthermore Kv3.1 and Kv3.2 channels are blocked voltage-dependently by internal Mg^{2+} , resulting in a negative slope conductance (Rudy *et al.*, 1999). As Figure 3-5 shows this is not the case for the Kv3 current in the MNTB even though 1mM Mg^{2+} was included the patch solution for all recordings.

The presence of Kv3.1/3.3 heteromers may explain the more negative $V_{1/2ac}$ found here, as a splice variant of Kv3.3 has been shown to shift its $V_{1/2ac}$ by around -10mV in HEK cells giving a $V_{0.5ac}$ of -2.4mV, as well as altering its inactivation phenotype (i.e. preventing fast inactivation, Fernandez *et al.*, 2003). Kv3.4a has been shown to have a much more negative $V_{1/2ac}$ and when it is incorporated into Kv3.1b results in the heteromeric channels with a negative shifted $V_{1/2ac}$ (Baranauskas *et al.*, 2003). It is likely that one of the Kv3.3 splice variants also has a considerably more negative $V_{1/2ac}$, which may then result in heteromeric channels with $V_{1/2ac}$ s similar to that observed here.

The relatively negative $V_{1/2ac}$ of the Kv3 current in the MNTB makes a lot of sense: The brief ($\leq 0.5ms$) action potentials would activate little Kv3 if it had a $V_{1/2ac}$ of $\sim +10mV$ (that reported for Kv3.1b) and would be inefficient for rapid action potential repolarisation. Indeed in Globus Pallidus (GP) neurons the $V_{1/2ac}$ is more negative ($\sim -15mV$), and it has been shown that this negative $V_{1/2ac}$ is required for activation of the Kv3 current during a GP action potential (Baranauskas *et al.*, 2003) which is considerably slower (half-width of $\sim 1.5ms$) than that of the MNTB.

It may be that the information that fast spiking neurons are encoding cause the neuron to “decide” which splice variant / subunit composition / post-translational modification of Kv3s it requires in order to provide an action potential of the appropriate duration. For example the MNTB, which is transmitting very high frequencies ($\sim 800Hz$), has very brief action potentials and thus has a Kv3 with a more negative $V_{1/2ac}$ than a Globus Pallidus neuron which fires up to 100Hz (Kita & Kitai, 1991) and has longer action potentials (Baranauskas *et al.*, 2003).

Origins and further misconceptions of Kv3.1 in the MNTB

The data that swayed the argument so much in favour of Kv3.1b accounting for all of the Kv3 current in the MNTB was the KO data, from (Macica *et al.*, 2003), who showed that the high-threshold (Kv3) current “disappeared” in the Kv3.1 KO animal along with its ability to fire at high frequencies. However data from a Kv3.1 KO mouse, which examined the reticular thalamic nucleus (where, like the MNTB, Kv3.1 and Kv3.3 dominate), showed that there was very little change in its ability to fire at high rates, probably because the Kv3.1 is compensated by the Kv3.3. Indeed P. Dodson (personal communication) found that there was considerable high voltage activated current in the MNTB of the Kv3.1 KO mouse used by Macica *et al* (2003). Additionally no affect on binaural processing was seen in the Kv3.1 KO mouse (personal communication with A. Palmer).

Kv3.1b is certainly expressed in the MNTB; however Kv3.1a has been overlooked somewhat mainly due, again, to data from Macica *et al* (2003), who showed that Kv3.1b dominated in adult brain homogenate. However mRNA studies show that in the adult Kv3.1b is indeed at higher levels although it is only slightly higher (Liu & Kaczmarek, 1998). More importantly Liu & Kaczmarek (1998) also showed that in P8-15 animals (the age where the vast majority of the work is done in the MNTB) Kv3.1a was higher. The relative levels of Kv3.1 a vs b in the MNTB has never been assessed, therefore it is possible that Kv3.1a is as important as Kv3.1b and Kv3.3.

Subcellular localisation of Kv3

If one assumes that Kv3.1b is only present as heteromers with Kv3.3 it simplifies the conclusions that can be drawn from electron microscopy work by Elezgarai *et al* (2003). As well as Kv3.1 being on the non-release face of the calyx of Held, Elezgarai *et al.* show

that Kv3 is located in the cell soma and in the axon of the MNTB, where it is located extra-synaptically, i.e. between the fingers of the calyx.

The presence of Kv3 on the soma will help limit the duration of the EPSP generated by the huge EPSC, without attenuating the amplitude appreciably.

The exclusion of Kv3 channels from the synaptic cleft is likely to be of functional significance; since the synaptic cleft is a small volume (~28nm), extruded K⁺ would result in local depolarisation of the cleft membrane potential. This in turn would lead to aberrant signalling by NMDA receptors (as the depolarisation would cause less Mg²⁺ block and hence more charge entry via NMDA receptors).

Tonotopic distribution of Kv3

Kv3.1 immunostaining displays a medio-lateral gradient with higher staining seen in the high frequency-receiving medial neurons (Li *et al.*, 2001; Elezgarai *et al.*, 2003). The functional Kv3 current display the same gradient with large amplitude currents in the medial end of the MNTB vs the lateral and correspondingly the action potential half widths tended to be shorter in the medial neurons (Brew & Forsythe, 2005). This tonotopic gradient seems to be activity dependent as in mice which lose their hearing (e.g. C57B1/6) the gradient is absent in older deaf animals yet present in younger hearing animals. Yet the gradient is still present in older animals from a strain resistant to deafness (i.e. CBA, von Hehn *et al.*, 2004).

Functional consequences of Kv3

As already discussed it is well accepted that Kv3 channels promote brief action potentials, and Figure 3-7 shows that this is also the case in the MNTB, consistent with previous findings (Brew & Forsythe, 1995; Wang *et al.*, 1998b).

However it must be noted that this is only due to their negative $V_{1/2ac}$: as demonstrated by Baranauskas *et al* (2003) brief action potentials are unable to sufficiently activate Kv3.1b

($V_{1/2ac} \sim +10\text{mV}$), yet Klug & Trussell, (2006) show that considerable Kv3 current activates (1-3nA) with each action potential in the MNTB.

When Kv3 channels are blocked by TEA, MNTB neurons lose their ability to follow high frequency (>200Hz) trains of stimuli (Macica *et al.*, 2003).

Recently it has been demonstrated that Kv3's level of phosphorylation can control the MNTB's ability to follow trains of stimuli over a range of frequencies (Song *et al.*, 2005).

High fidelity transmission

As discussed earlier the calyx of Held generates a huge EPSC in the postsynaptic MNTB, which ensures the postsynaptic cell fires and provides an extremely short latency. However one detrimental effect of such a large response is that it may result in multiple action potentials for one EPSC (aberrant firing). One mechanism the calyx of Held / MNTB synapse implements to prevent aberrant firing is to ensure the EPSC is extremely brief (Taschenberger & von Gersdorff, 2000). Therefore the EPSC is mostly over with the same time course as the action potential, which will help to prevent a second spike. However having a brief EPSC is not sufficient, the MNTB also uses low-voltage activated (Kv1) channels.

Low voltage-activated Kv1 channels

There are 7 members of the Kv1 sub-family Kv1.1 – 1.7. Kv1.7 is absent in the brain (Kalman *et al.*, 1998; Kashuba *et al.*, 2001). Of the Kv1 channels expressed in the brain (Kv1.1-1.6) none have any splice variants (Coetzee *et al.*, 1999). It is well accepted that Kv1 channels mediate low voltage activated currents (Coetzee *et al.*, 1999; Southan & Robertson, 2000; Dodson *et al.*, 2002; Brew *et al.*, 2003; Dodson *et al.*, 2003; Ishikawa *et al.*, 2003; Shen *et al.*, 2003; Gittelmann & Tempel, 2006). In neurons Kv1 channels tend to be located in the axon hillock (initial segment / action potential initiation zone) and at

presynaptic terminals (Wang *et al.*, 1993; Wang *et al.*, 1994; Dodson *et al.*, 2002; Dodson *et al.*, 2003) and for review see (Dodson & Forsythe, 2004).

Kv1 channels in the MNTB

We find intense staining of Kv1.1 and Kv1.2 in the MNTB principal neurons (Figure 3-13), consistent with previous staining (Dodson *et al.*, 2002; Brew *et al.*, 2003; Ishikawa *et al.*, 2003) and with mRNA expression (Grigg *et al.*, 2000). However we also find that Kv1.6 is absent (Figure 3-13 A & B), this is in contrast to what is found in the rat (Dodson *et al.*, 2002), which represents an interesting species difference. We also find that Kv1.5 is highly expressed, although it appears that the staining is mainly in processes. Kv1.5 is known to be expressed in oligodendrocytes (Attali *et al.*, 1997; Chittajallu *et al.*, 2002), therefore the stained processes may be those of oligodendrocytes, however this would require confirmation at higher magnification, possibly with double staining with myelin basic protein and or labelling of GFP-CNPase mice. Kv1.4 also appears to be present although at relatively low levels. Kv1.3 was not assessed as a satisfactory antibody was unavailable at the time; however there appears to be Kv1.3 staining in the MNTB shown with a new verified antibody (Gazula & Kaczmarek, 2006).

When the Kv3 channels were blocked with 3mM TEA, the current at -37mV was blocked by $44.6 \pm 5.1\%$ with 10nM DTx-I (Figure 3-17), when the concentration of DTx-I was increased to 100nM no further effect was observed (Figure 3-8). DTx-I blocks Kv1.1, 1.2 and 1.6 containing channels (Hopkins, 1998), therefore it is possible that the remaining (antagonist insensitive) current is mediated by a DTx-I insensitive Kv1 channel. However, the Kv1.3 & Kv1.4 antagonist CP-339, 818 had no affect on the insensitive current, ruling out a population of Kv1.3 or Kv1.4 channels (Figure 3-9). Therefore it appears that all the Kv1 current is mediated by DTx-I sensitive subunit containing channels. Additionally the magnitude of the Kv1 current at -47mV ($0.18 \pm 0.003\text{nA}$, $n=7$) is comparable to that observed previously in mouse 0.2nA (Brew *et al.*, 2003) but is considerably smaller when compared to the magnitudes reported from rat $\sim 0.5\text{nA}$

(Dodson *et al.*, 2002) and 0.36nA (Brew & Forsythe, 1995). This difference in the amount of Kv1 current likely explains the fact that mouse MNTB neurons tend to be more excitable than rats (i.e. occasionally more than 1 action potential is observed in mice, data not shown, Brew *et al.*, 2003).

Kv1 subunit composition

As Figure 3-13 shows Kv1.6 is absent, therefore all the Kv1 subunits in the MNTB must contain at least one Kv1.1 or Kv1.2 subunit. The selective Kv1.1 blocker DTx-K was used to probe the contribution from Kv1.1 subunits and as Figure 3-17 shows the % block by DTx-I and DTx-K were similar, suggesting that all the Kv1 channels contain at least one Kv1.1 subunit. A population of Kv1.1 homomers is unlikely as the current blocked at -37mV by 3mM TEA (IC_{50} of 0.5 for Kv1.1 homomers, Coetzee *et al.*, 1999), was insensitive to DTx-I (Figure 3-15, as discussed in the results). Hence all the Kv1 channels in the MNTB must be Kv1.1 containing heteromers, similar to rat (Dodson *et al.*, 2002).

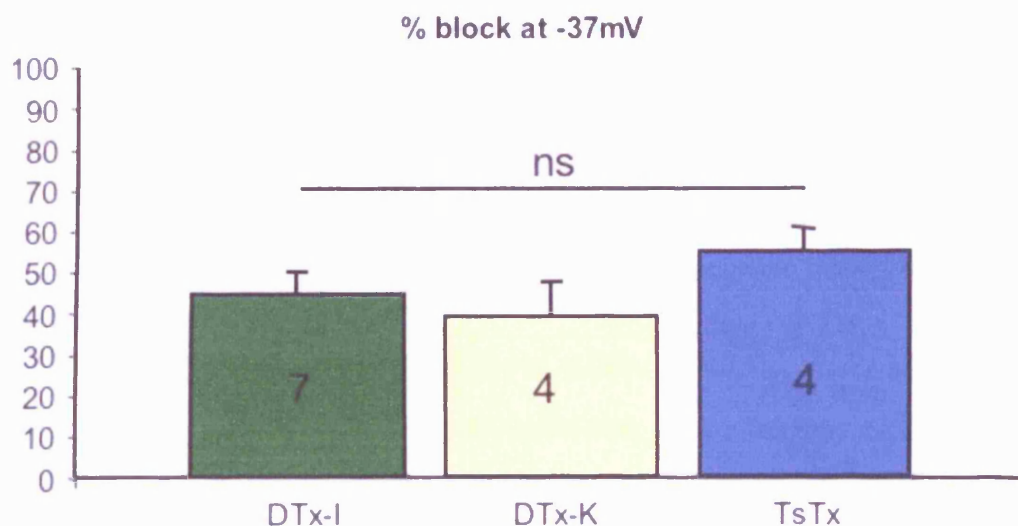


Figure 3-17 Summary of % block by different Kv1 toxins.

Furthermore TsTx-K (a Kv1.2/Kv1.3 blocker) was applied (Figure 3-16) which reduced the current by a similar amount to both DTx-I and DTx-K (Figure 3-17), which implies that all the subunits may be heteromers of Kv1.1/Kv1.2 and/or Kv1.1/Kv1.3 and/or

Kv1.1/Kv1.2/Kv1.3. Additionally the fact that only 10nM DTx-I is required to block all the Kv1 current favours the hypothesis that Kv1.1/Kv1.2 heteromers dominate, as Kv1.1/Kv1.3 heteromers would have less affinity for DTx-I (Hopkins, 1998). However this hypothesis does not take into account the immunohistochemical data which suggests the presence of both Kv1.3 (Gazula & Kaczmarek, 2006) and possibly Kv1.4 (though at low levels). The presynaptic terminals of the globular bushy cells (i.e. calyx of Held) express different ion channels to those at the cell body (Dodson *et al.*, 2003), as do the terminals of basket cells in the cerebellum (Southan & Robertson, 2000). Thus it is possible that the terminals of the MNTB have Kv1 channels that include Kv1.3 and maybe Kv1.4, and that the staining at the cell body observed here is solely cytoplasmic.

This subunit composition (i.e. Kv1.1/Kv1.2) is intriguing as it differs from the rat, where Kv1.1/Kv1.6 heteromers are also present but it is the Kv1.1/Kv1.2 heteromers (which contribute 50% of the total Kv1 current) that make the predominant contribution to physiology (Dodson *et al.*, 2002). Bare in mind that rat has twice the magnitude of Kv1 current. It is likely to be no coincidence that both rat and mouse have similar amounts of Kv1.1/Kv1.2 heteromeric current, which in the rat has been shown to be the dominant contributor to physiology.

Subcellular localisation of Kv1

Although the Kv1 antibodies stain the cell body, the functional Kv1 currents are not on the somatic membrane, as when patches are pulled from the somatic membrane no DTx-I sensitive current is observed (Dodson, 2003). Rather immunostaining shows the Kv1 channels are on the initial segment of the axon (Dodson *et al.*, 2002; Brew *et al.*, 2003). This absence of Kv1 current in patches is also seen presynaptically at the calyx where they are located in the heminode (Dodson *et al.*, 2003; Leao *et al.*, 2005a). This localisation of Kv1 channels to the initial segment is also seen in other neurons e.g. cortical pyramidal neurons (Sheng *et al.*, 1994; Inda *et al.*, 2006).

Activation of Kv1 channels in the MNTB

As noted earlier the $V_{1/2}$ of the Kv1 channels in the MNTB is difficult to estimate, as when the activation curve is plotted there is a noticeable “kink” in it (Figure 3-11). This could be due to three possibilities, being:

1. The Kv1 channels are displaying inward rectification at positive voltages.
2. There are two populations of DTx-I sensitive Kv1 channels, with differing activation parameters.
3. A “space-clamp” phenomena is occurring due to the Kv1s subcellular location.

The inward rectification scenario is unlikely due to the shape of the “kink” (i.e. the “block” does not become more severe with increasing voltage). It is unlikely to be due to two populations of DTx-I sensitive Kv1 channels, based on the earlier subunit composition arguments. Additionally, the two populations would require vastly different $V_{1/2}$ s to produce the observed kink. Therefore the third option seems most likely. But why does it make so much sense?

Firstly we know that Kv1 channels are located in the initial segment and not the cell body. Consequently the input resistance of the soma will be different to that of the initial segment (when Kv1s are open i.e. $>-75\text{mV}$). As it is the soma that is patched, the actual voltage of the initial segment will tend to be lower than the measured somatic voltage when Kv1s are open, but once blocked the axonal voltage will be under better control (as it will now have a similar input resistance) and hence greater currents will be apparent.

The second point to consider is that there is still considerable current remaining once Kv1s and Kv3s are blocked (see Figure 3-10). If only some of this “other” current was in the initial segment of the axon, more of it would be activated once Kv1s are blocked (as the axon would now be clamped better and hence be at higher voltages). This is what is seen at positive voltages, when Kv1s are blocked (see inset of Figure 3-10 A). This would obviously produce a kink, in the DTx-I sensitive I/V . Furthermore the kink develops as the

“other” current starts to activate which is indeed located in the initial segment (see chapter 4).

Functional consequences of Kv1 channels

Because of their low-voltage activated nature the function of Kv1 is more complex than that of the Kv3 channels. Due to Kv1 channels being located in the initial segment and the fact that they open at voltages more negative than the action potential threshold voltage, they will act as a high-pass filter. That is only rapidly rising and incidentally large voltage responses will be able to charge the initial segment to threshold. Kv1s therefore act to favour calyceal responses over the small slower rising inputs to the MNTB that were demonstrated by (Hamann *et al.*, 2003). Additionally the Kv1 channels limit the firing of the MNTB neuron in response to sustained stimulation such that only one or two action potentials can be evoked at the onset of a sustained depolarisation (Figure 3-12 A, and Brew & Forsythe, 1995; Dodson *et al.*, 2002). This has important consequences for synaptic stimulation, as can be seen in Figure 3-12 B, where Kv1 channels ensure that only one action potential is fired at the onset of a synaptic response, consistent with Brew & Forsythe, (1995).

The fact that DTx-I appears to lower the voltage threshold for action potential initiation (Figure 3-12 A, bottom panel), complements the argument for a “space-clamp like” phenomena explaining the difficulty in obtaining the $V_{1/2ac}$. Once Kv1s are blocked a given current injection will cause a greater voltage change in the initial segment, which explains this apparent lowering of threshold.

Klug & Trussell, (2006) demonstrate that Kv1 channels in the MNTB activate rapidly with physiological action potential waveforms and deactivate within 0.25ms after the falling phase. Therefore Kv1 channels should contribute slightly to the action potential waveform, which is indeed what is seen in Figure 3-12 B, the peak of the action potential is slightly greater in DTx-I, as you would expect with increasing the input resistance.

Tonotopic distribution

Like Kv3 channels, Kv1 channels appear to be tonotopically distributed, however they have the opposite gradient. (Brew & Forsythe, 2005) reports greater Kv1 current magnitude in medial vs lateral neurons, however higher optical density of staining for Kv1.1 is seen in the lateral vs the medial end (Leao *et al.*, 2006b). The gradient found by (Leao *et al.*, 2006b) was only of the Kv1.1 subunit whereas that by (Brew & Forsythe, 2005) was of the functional current, a fact that may explain the discrepancies in these gradients.

(Leao *et al.*, 2006b) also try to correlate the $V_{1/2ac}$ of the Kv1 current with location and suggests the medial neurons have a more positive $V_{1/2ac}$ than lateral neurons. However I would consider this with considerable scepticism based on the arguments outlined earlier, since evidence of the same kink is seen in their current traces, but the Boltzmann fits are not shown (see Figure 4A of Leao *et al.*, 2006b).

In conclusion I show that the Kv3 channels have a more negative $V_{0.5ac}$ than previously thought, which is likely to be of importance to their physiological role. Furthermore I have demonstrated that the Kv1 channels in mouse MNTB differ in their subunit composition to those of the rat.

Chapter 4 – Results 2

The MNTB's Lesser Known Kv currents

The previous chapter demonstrated the presence of both Kv1 and Kv3 mediated conductances in mouse MNTB neurons and identified their physiological roles. However, other uncharacterised K⁺ currents are expressed in the MNTB.

The non Kv1/Kv3 currents have been largely ignored in previous work and to my knowledge have only been mentioned twice. First, Brew *et al* 1995 noticed a third slowly inactivating conductance in the rat MNTB, which was insensitive to TEA and 4-AP. Second, Brew *et al* (2003) reported a small inactivating outward current in the mouse MNTB.

In this chapter I have characterised these unknown voltage-dependent conductances in MNTB neurons and report two distinct components: an A-type current and a slowly activating sustained current. Each of these conductances is examined in turn and their physiological roles are assessed.

Methods

The methods used in this chapter are identical to those described in chapter 2, except for the following modifications.

1. The majority of the data in this chapter was recorded in the presence of 3mM TEA and 10nM DTX-I, to eliminate the known Kv1 and Kv3 conductances.
2. The pipette solution used for recording sodium currents was composed of (in mM):120 CsCl, 10 TEA-Cl, 5 4-aminopyridine (4-AP), 5 EGTA, 10 HEPES, 5 NaCl (pH 7.2 with NaOH). These pipettes had series resistances of 3-8 M Ω and junction potentials of 4mV.
3. When the pipette solution in 2 was used, spontaneous synaptic transmission became very evident. Therefore to eliminate mini-post synaptic currents from the current records, 20 μ M 6,7-Dinitroquinoxaline-2,3-dione (DNQX), 10 μ M bicuculline and 1 μ M strychnine were included in the perfusing low Ca²⁺ aCSF to block glutamatergic, GABAergic and glycinergic transmission respectively. 100 μ M CdCl₂, 3mM TEA and 1mM CsCl, was also included in the aCSF to block Cav channels and any Cs⁺ permeable Kvs.
4. P/N leak subtraction was used to eliminate capacitive artefacts from the sodium current recordings. As there was no K⁺ mediated leak in these conditions this was deemed satisfactory.
5. The sodium current data was filtered at 10 kHz and digitised at 50 kHz.
6. All the sodium current and physiological experiments (i.e. current-clamp) were conducted at 37°C.

Two additional K⁺ currents to Kv3 and Kv1 in the MNTB

Figure 4-1 A (black traces) shows the total outward K⁺ current and that remaining in the presence of Kv3 and Kv1 antagonists (TEA, 3mM & DTx-I, 10nM). As can be seen considerable outward current remains in the presence of the antagonists (Figure 4-1 A, red traces).

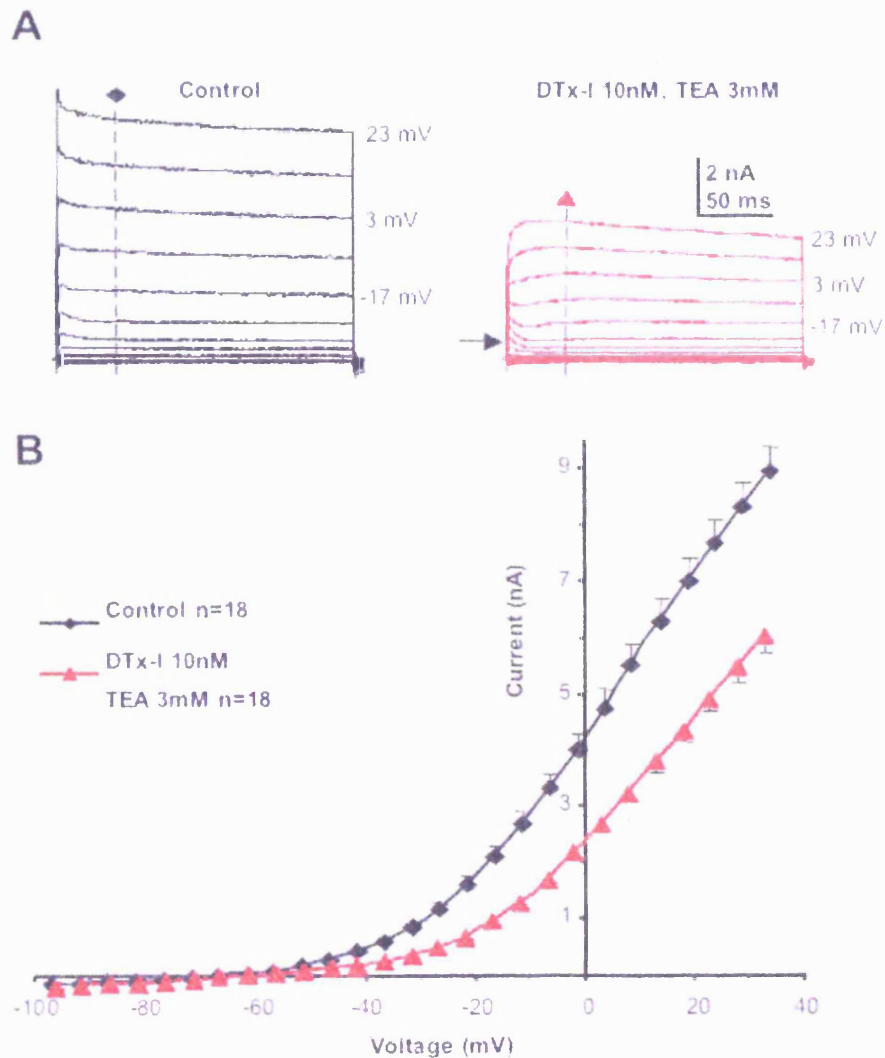


Figure 4-1 K⁺ current not mediated by Kv1 or Kv3 channels: A) Example total outward current (black traces) and that current remaining in the presence of Kv1 and Kv3 antagonists (10nM DTx-I and 3mM TEA, respectively). **B)** Average I/V data recorded 40ms into the pulse (dashed lines in A) for 18 cells in control (black) and 18 different cells in the presence of 10nM DTx-I and 3mM TEA. N.B. Note the “appearance” of an inactivating component in A (black arrow).

There is $4.02 \pm 0.29 \text{ nA}$ ($n=18$) of outward current when the voltage is stepped to -17 mV with no K^+ channel antagonists present. When both Kv1 and Kv3 channels are blocked the current is only reduced by $1.7 \pm 0.07 \text{ nA}$ ($n=18$, measured at the dashed lines in Figure 4-1 A, 40ms into the test step). The averaged I/V in Figure 4-1 B shows the current for 18 cells in control (black) and 18 different cells in the presence of 3 mM TEA and 10 nM DTx-I (red). Note that more than half of the sustained current is insensitive to the antagonists at positive voltages ($>0 \text{ mV}$).

On examination of the antagonist-insensitive current evoked at the more negative voltage steps, a small transient current is seen (Figure 4-1 A, arrow), suggesting that there may be two components to the remaining current.

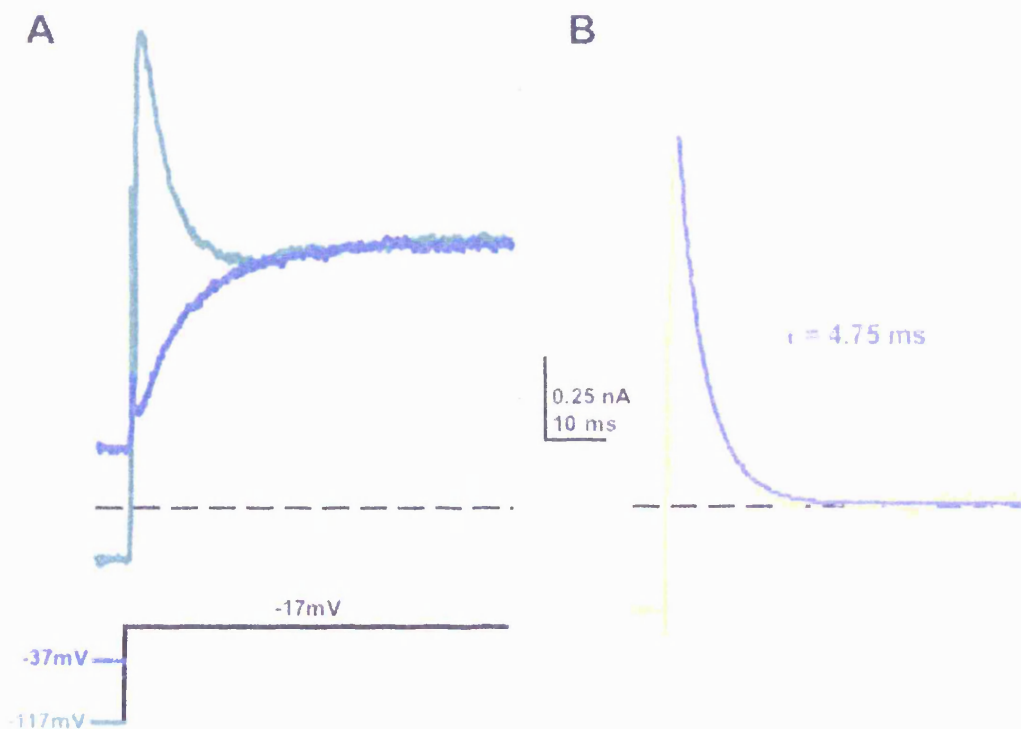


Figure 4-2 The antagonist-insensitive current is comprised of two components: A) A test step to -17 mV from -37 mV evokes only a slowly activating sustained component (blue trace), whereas stepping to -17 mV from -117 mV evokes an additional rapidly activating and inactivating component (green). **B)** Subtracting the blue from the green in A leaves the transient current which completely inactivates with a tau of $4.75 \pm 0.28 \text{ ms}$ ($n=8$). N.B. Dashed lines represent 0 current, all data recorded in the presence of 3 mM TEA and 10 nM DTx-I .

The two current components are distinguished by test steps to -17mV either preceded by a pre-pulse to -37mV or -117mV (Figure 4-2 A, n=8). Stepping to -17mV with a pre-pulse to -117mV results in a rapidly activating and inactivating current with a sustained component, whereas a pre-pulse to -37mV generates only a slowly activating sustained component.

Subtraction of the -37mV pre-pulse test step (Figure 4-2 A, blue) from that with the -117mV pre-pulse (Figure 4-2 A, green) results in the isolated rapidly activating and inactivating A-type current (Figure 4-2 B, yellow). This A-current shows complete inactivation which is fit by a single exponential decay with a time constant of 4.75 ± 0.28 ms (n=8). Therefore the current measured at 40ms and plotted in Figure 4-1 B is the sustained current, because at 40ms (>5 inactivation time constants) the A-current is completely inactivated.

The A-current

Biophysical Properties of the A-current

We examined the A-current in more detail by assessing its level of steady-state inactivation. The steady-state inactivation of the A-current was determined by a test pulse to -17mV, preceded by 200ms pre-pulses to voltages between -117 and -37mV (Figure 4-3 A). The zero current level in the test step was assumed to be where there was no rapidly activating instantaneous current (I am assuming that this current completely inactivates, which is a fair assumption based on Figure 4-2 B).

The peak A-current was then measured at -17mV and normalised to the maximal current, then plotted against the pre-pulse potential (Figure 4-3 B, green squares). A Boltzmann function was fit to the normalised inactivation data (Figure 4-3 B, Blue line) giving a voltage dependence of inactivation ($V_{1/2in}$) of -76.9 ± 0.9 mV and a slope factor (k_{in}) of -7.0 ± 0.3 (n=9). Classical A-currents, mediated by members of the Kv4 family

typically have a large amount of steady-state inactivation (Chen & Johnston, 2004), as seen here. However the inactivation rate here, is somewhat faster than reported values.

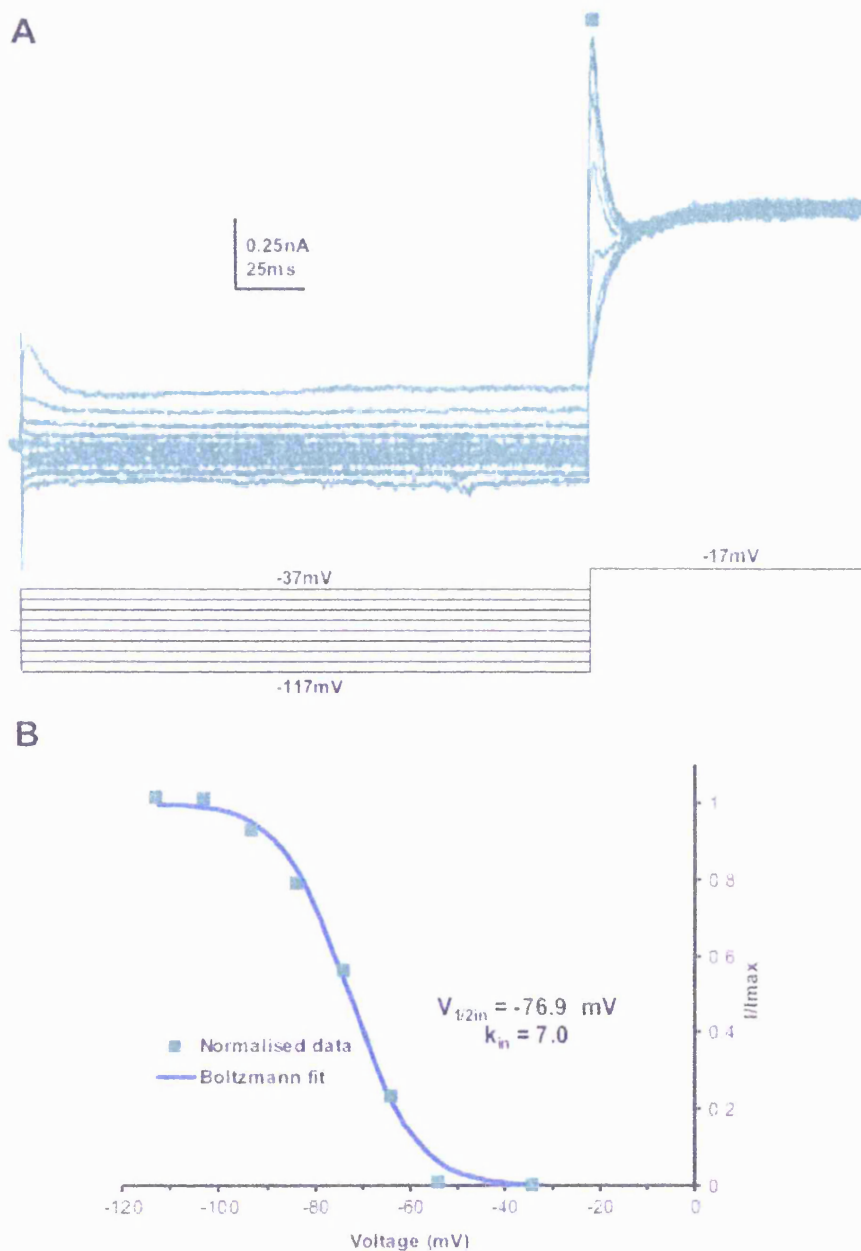


Figure 4-3 Voltage dependence of inactivation of the A-current: A) A test step to -17mV was preceded by pre-pulses between -117 and -37mV, the negative pre-pulses evoked the A-current whereas the more positive pre-pulses inactivated the A-current. **B)** The peak transient current in the test pulse in A was normalised to the maximum and plotted against voltage, which was then fit with a Boltzmann distribution giving a $V_{1/2in}$ of $-76.9 \pm 0.9\text{mV}$ and a k_{in} of -7 ± 0.3 ($n=9$). The A-current was assumed to completely inactivate see text for explanation. N.B. All data recorded in the presence of 3mM TEA and 10nM DTx-I.

I next examined the A-current's voltage-dependence of activation. In order to do this I had to isolate the A-current from the slowly activating component. This was achieved by using a double pulse protocol as shown in Figure 4-4 A. Each test pulse (T) was preceded by a hyperpolarising pre-pulse to -117mV to remove all steady-state inactivation. T1 gives the total A-current along with the sustained current, whereas in T2 only the sustained current is evoked, because the A-current is completely inactivated by an additional 20ms pre-pulse to -37mV (Figure 4-4 A). The dashed line in Figure 4-4 A indicates that the sustained current remains unchanged in the two pulses. The peak transient current was found in T1 and the current at the equivalent time in T2 was subtracted, leaving the isolated A-current I/V (Figure 4-4 B). The latency to the peak decreased with depolarisation.

To obtain the voltage-dependence of activation from this isolated I/V, the current has to be corrected for the driving force. A linear ("ohmic") driving force is commonly used for correction, however this method is erroneous (see methods) therefore Equation 2-9 was used which corrects for the single channel current's dependence on GHK rectification (see methods, Clay, 2000).

As can be seen in Figure 4-4 C (purple squares) at positive voltages the conductance displays inward rectification, which is consistent with block by internal Mg^{2+} of A-type conductances (Forsythe *et al.*, 1992) and some other K^+ channels e.g. Shaker B (Slesinger *et al.*, 1993). Due to this inward rectification the data was normalised to the current at -7mV (i.e. prior the development of the inward rectification) and then fit with a Boltzmann distribution (Figure 4-4 C, blue line), which gave a half-activation voltage ($V_{1/2ac}$) and k_{ac} of $-35.0 \pm 1.3mV$ and -6.7 ± 0.3 , respectively (Figure 4-4, n=9). It should be noted that these values are only estimates, as it is not known whether the channel has reached its maximally activated state by -7mV. If not these values may underestimate the magnitude of k_{ac} , and hence the $V_{1/2ac}$ maybe more positive.

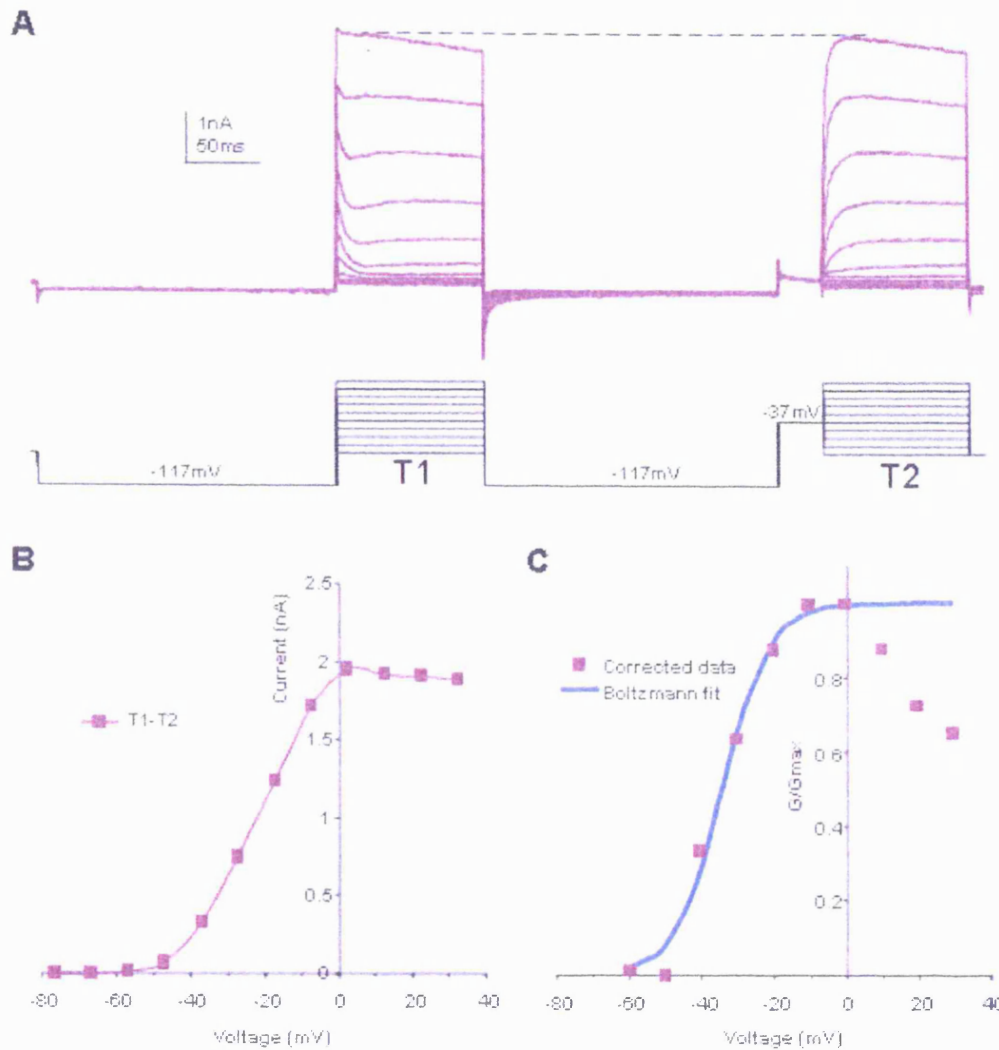


Figure 4-4 Determining the voltage-dependence of activation for the A-current: **A)** In test pulse 1 (T1) the sustained current and A-current are evoked, whereas in T2 only the sustained current is evoked as the A-current is inactivated by a 20ms -37mV pre-pulse. The dashed line shows the sustained current remains unchanged in the two test pulses. **B)** The peak transient current from T1 was measured and the current from the equivalent latency in T2 was subtracted leaving the isolated A-current I/V. **C)** The data in B was corrected for the driving force using Equation 2-9, (see methods) (Purple squares), this was then fit with a Boltzmann distribution (blue line) ignoring the points at positive voltages (see text), which gave a $V_{1/2ac}$ of $-35.0 \pm 1.3\text{mV}$ and a k_{ac} of -6.7 ± 0.3 ($n=9$). N.B. all data recorded in the presence of 3mM TEA and 10nM DTx-I.

It was not possible to determine the A-current's activation parameters from tail current analysis (which would be preferable because the normalisation for driving force isn't

required). The double pulse protocol was required as the A-current rapidly and completely inactivates at potentials that would be required to examine the tails i.e. $\sim -60\text{mV}$.

The A-current begins to activate ~ -60 to -55mV and has a peak outward current at -17mV of $1.25 \pm 0.22\text{nA}$ ($n=5$), however under resting conditions it is greater than half-inactivated. Therefore due to its relatively small size, we postulate that this current will only make a minor contribution to controlling excitability. However one scenario where the A-current may exert a greater affect is directly after inhibition, which would remove some of the steady state inactivation. An important property of the A-current would then be the rate of recovery from inactivation; I assessed this by giving a double pulse protocol as shown in Figure 4-5. The rate of recovery from inactivation at -97mV was fit well by a single exponential function (red line in Figure 4-5) which had a tau of $16.4 \pm 1.6\text{ms}$ ($n=8$).

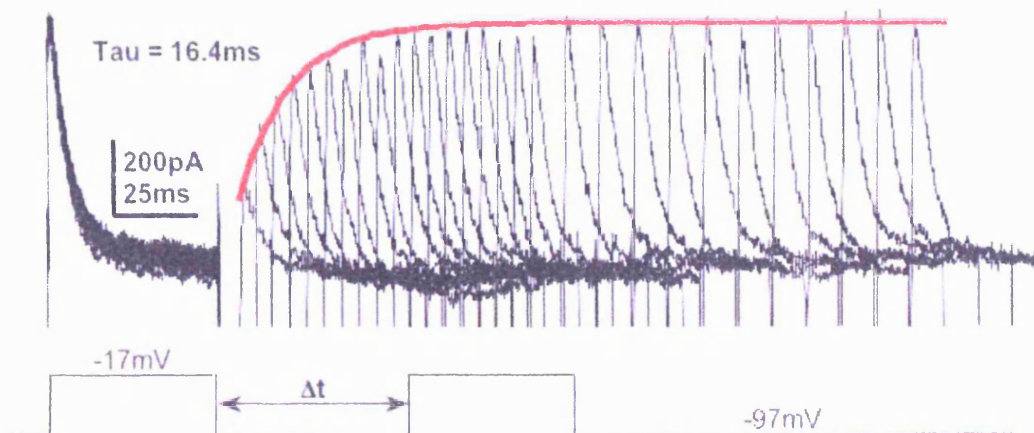


Figure 4-5 Recovery of inactivation of the A-current: The recovery from inactivation was assessed using the voltage protocol shown below. The A-current was maximally inactivated in a 50ms pulse to -17mV and the amount of recovery was assessed after a varying recovery period. A single exponential fit the recovery well (red line) giving a Tau of $16.4 \pm 1.6\text{ms}$ ($n=8$).

Pharmacology of the A-current

Both Ba^{2+} and 4-AP were used in the study of other conductances in the MNTB, though I noticed that they also affect the transient A-current.

Application of 3mM Ba²⁺ in the presence of TEA and DTX-I reduced the peak transient current measured at -2mV from 2.96 ±0.26nA to 1.20 ±0.15nA (Figure 4-6 A&B, n=4, P=0.0007). However, it should be noted that Ba²⁺ also blocks the sustained current (Figure 4-6 A), although it is clear that the A-current is more sensitive to Ba²⁺ at 3mM (Figure 4-6 A arrow).

4-AP (5-10mM) was also applied and block of the A-current was observed in all 4 cases (Figure 4-6 C). In one case a time course for the onset of block by 4-AP was recorded as shown in Figure 4-6 D. 4-AP also affected the sustained current but again it is clear that it also blocks the transient current. This block of the A-current by 4-AP is consistent with previous reports (Brew *et al.*, 2003).

It would have been preferable to have used the same protocol as that used in Figure 4-4 A to obtain more accurate information on the block by pharmacological agents. However we felt it was not worth replicating these experiments, since we have already ascertained that the A-current is sensitive to both 4-AP and Ba²⁺, but neither is selective for the A-current and so are of little use for physiological studies under current clamp.

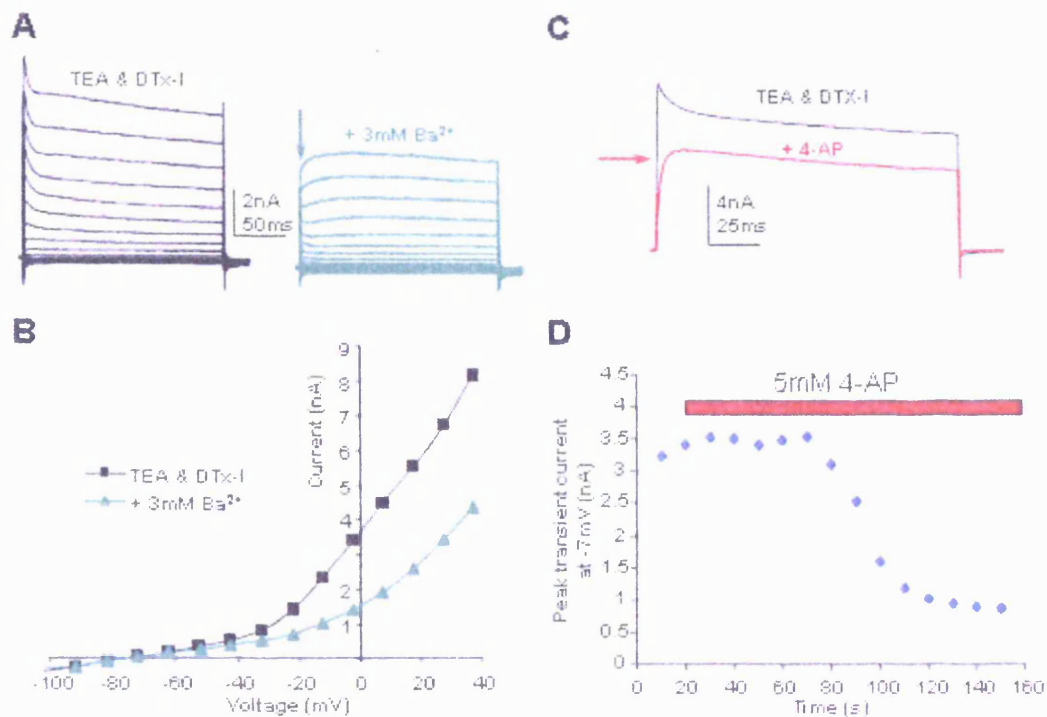


Figure 4-6 The A-current is sensitive to Ba²⁺ and 4-AP: A) Example traces in the presence of 3mM TEA and 10nM DTx-I (black) and with the addition of 3mM Ba²⁺ (green). **B)** Plot of the peak transient current from A shows a reduction in the A-current with the application of Ba²⁺, also note that Ba²⁺ decreases the sustained current (n=4). **C)** Voltage steps to +63mV in the presence of 3mM TEA and 10nM DTx-I (black) and with the application of 5mM 4-AP showed block of the transient current (similar results seen in 4 cells with [4-AP] ranging from 5-10mM). **D)** Time course for the onset of block of the A-current by 4-AP for the cell in C, recorded at -7mV.

The channel's biophysics along with some other pharmacology helps to rule out possible molecular candidates, for example it is not mediated by the inactivating Kv3 members (i.e. Kv3.3 & 3.4) as they are blocked by 3mM TEA (Coetzee *et al.*, 1999). Additionally we can rule out mediation by an inactivating Kv1 (e.g. Kv1.3 or 1.4) as CP 339 818 leaves the current unaffected (Figure 3-9), nor is it mediated by a Kv1.1 with an accessory beta subunit as such a current would be sensitive to DTx-I. Kv4 channels are rapidly activating and inactivating K⁺ channels and are expressed on the cell bodies of the presynaptic globular bushy cells (Fitzakerley *et al.*, 2000; Dodson *et al.*, 2003), therefore it is likely that a member of the Kv4 sub-family mediates this A-current. The insensitivity to TEA and

block by 4-AP is consistent with this conclusion (Coetzee *et al.*, 1999; Birnbaum *et al.*, 2004).

Kv4.3 subunits are expressed in the MNTB

To support the pharmacological data we performed immunohistochemistry for the Kv4 subunits. Figure 4-7 shows that anti-Kv4.3 showed robust staining while anti-Kv4.2 showed minimal staining. Anti-Kv4.1 showed no staining, consistent with its expression being limited to the olfactory bulb and CA1 of the hippocampus (Serodio & Rudy, 1998; Fitzakerley *et al.*, 2000).

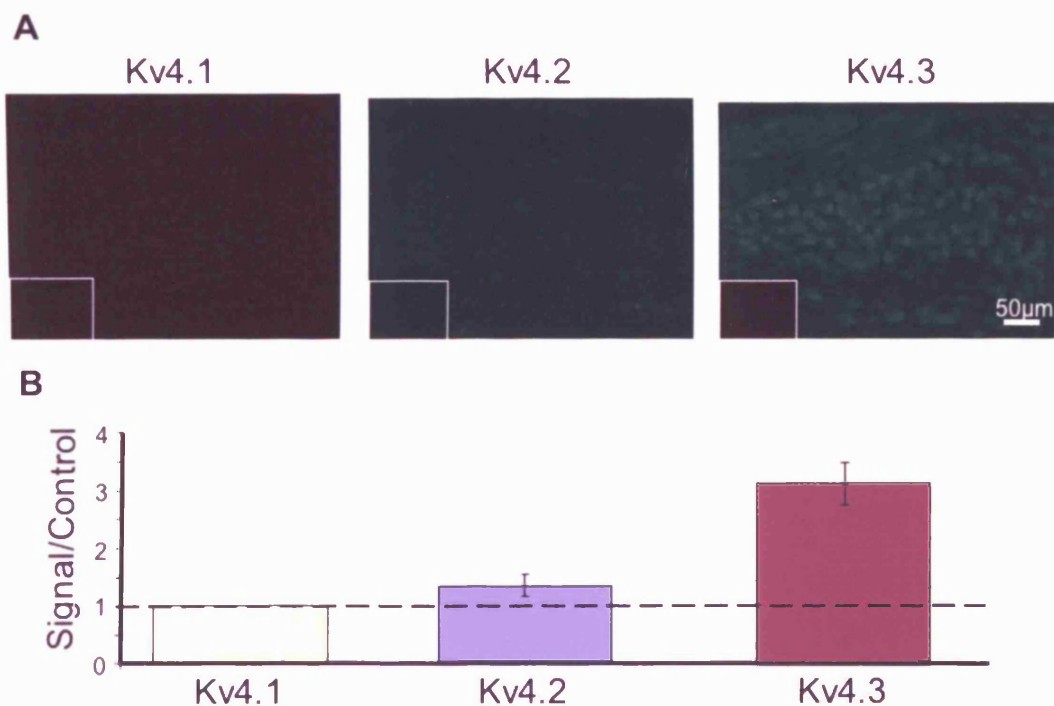


Figure 4-7 Kv4.3 is present in the MNTB principal neurons: A) Immunostaining of the Kv4 subunits, insets show blocking peptide control. Scale bar for Kv4.3 applies to all. **B)** Plot of the signal above blocking peptide control, expressed as a ratio, showing that Kv4.1 is absent while Kv4.3 shows the most staining, the dashed line represents blocking peptide control (n=3).

A physiological role for the A-current

As this current rapidly inactivates it is likely only to contribute to the 1st action potential in a train. Indeed when the MNTB was stimulated at 200Hz with simulated synaptic currents, I found that the 1st action potential had a 1/2 width that was 0.03ms faster than the 2nd (Figure 4-8A, n=4, P=0.01), whereas the 1/2 width of the 2nd action potential was not significantly different from the 60th. Additionally the after hyperpolarisation (AHP) of the second action potential was 1.32 mV more depolarised than the first (n=4, P=0.046). This is consistent with the presence of an inactivating K⁺ conductance which participates only with repolarisation of the first action potential.

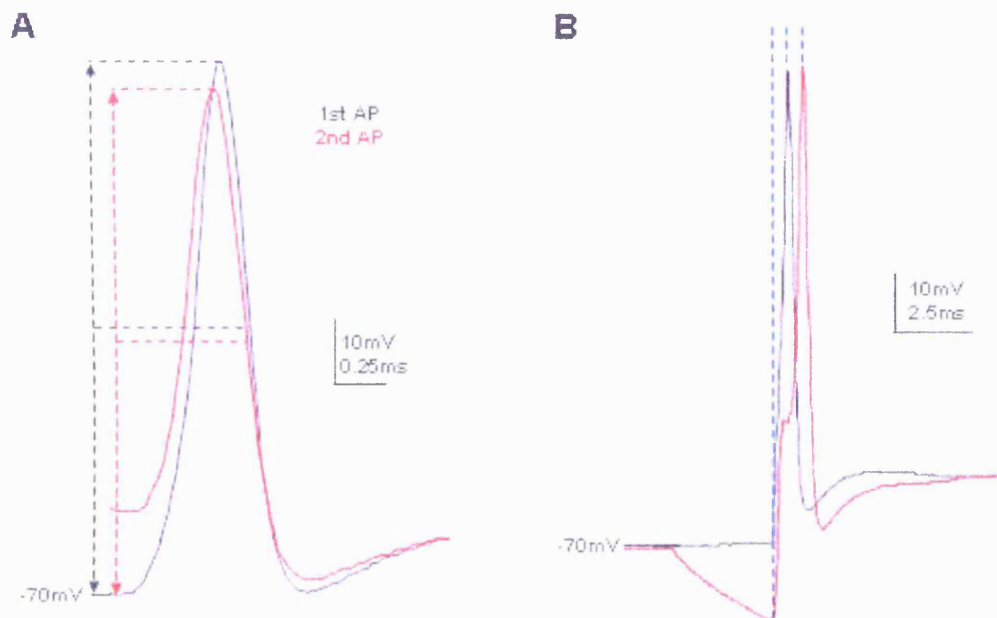


Figure 4-8 Physiological consequences of the A-current? : A) 1st (black) and 2nd (red) action potentials from a 200Hz train overlaid, showing that the width of the action potential is different **B)** Single action potential evoked with a simulated synaptic current (black) and with a 3ms -150pA step preceding the stimulus (red) to simulate an inhibitory input.

The sodium current is likely to be smaller for the second action potential (see Figure 4-24), which will account for the smaller action potential peak observed in Figure 4-8 A. (also see Figure 4-24)

Under resting conditions at ~-70mV, this A-current is more than half-inactivated (Figure 4-3 B). With development, the MNTB receives a large inhibitory glycinergic input

(Awatramani *et al.*, 2004). Therefore I reasoned that synaptic inhibition could remove some of the steady-state inactivation of the A-current possibly allowing it to contribute a larger conductance (assuming the resting Cl^- was low enough, thus giving an E_{Cl} more negative than rest, which is reasonable (Price & Trussell, 2006). To simulate an inhibitory input a 3ms -150pA current injection was given directly before the simulated excitatory synaptic current, resulting in a 0.16 ± 0.06 ms delay in the time to peak as can be seen in Figure 4-8 B (n=3). Unfortunately this was not significant with the 3 cells tested and requires further investigation.

Further work to prove physiological significance should include the use of the selective toxins of the Kv4 family (i.e. Phrixotoxin-2 and or Heteropodatoxin-2). However these toxins shift the voltage-dependence of activation rather than completely block the channels, and they have not been used extensively so may affect other currents.

The slow activating current

Biophysical properties of the slow conductance

To establish the voltage-dependence of activation for the slow conductance I used 100ms pre-pulses to voltages between -57 and +53mV followed by a test step to -37mV to generate a tail current (Figure 4-9 A). The peak current (measured after the capacitance artefact, since no leak subtraction was performed) was plotted against the pre-pulse potential normalised to the peak current (Figure 4-9 B, blue diamonds).

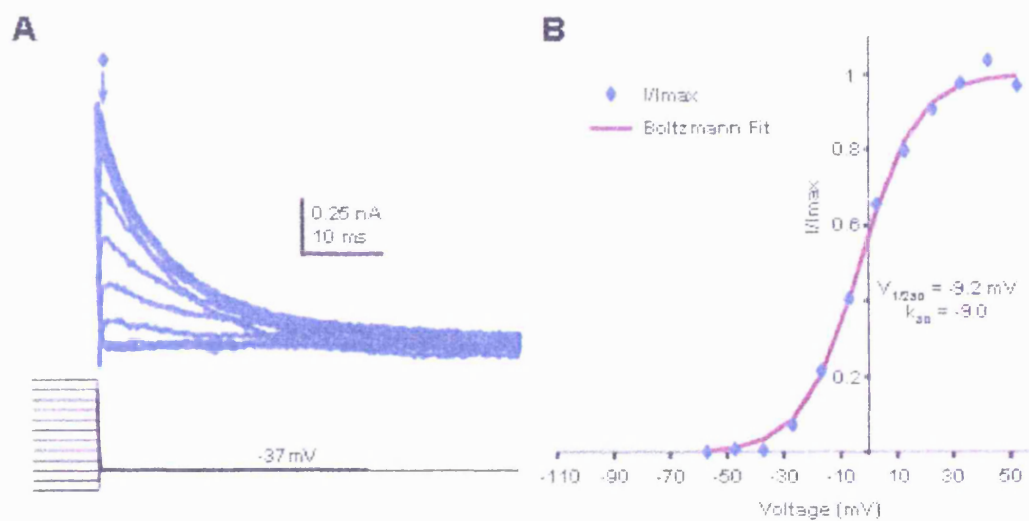


Figure 4-9 Assessing the voltage dependence of activation for the slow conductance:

A) Tail currents were evoked by first stepping to voltages between -55 and +53mV (after inactivation of the A-current) and then stepping back to -37mV. **B)** The peak current measured in A was normalised to the maximum and plotted against voltage (blue diamonds), this was then fit with a Boltzmann distribution (purple line) giving a $V_{1/2ac}$ of -9.2 ± 2.1 mV and a k_{ac} of -9.0 ± 0.4 (n=6).

The normalised current was then fit by a Boltzmann distribution which gave a $V_{1/2ac}$ of -9.2 ± 2.1 mV and a k_{ac} of -9.0 ± 0.4 (Figure 4-9 B, purple line, n=6).

The voltage-dependence of inactivation was assessed by giving 8s pre-pulses to voltages between -107 and +53mV followed by a test pulse to +43mV (Figure 4-10 A). The current measured 40ms after the onset of the test pulse (to avoid the A-current) was

normalised to the maximal current and plotted against pre-pulse potential (Figure 4-10 B, green triangles). A Boltzmann distribution was then fit to the normalised data which gave a $V_{1/2in}$ of $-35.9 \pm 1.5\text{mV}$ and a k_{in} of 10.8 ± 0.8 (Figure 4-10 B, Blue line, $n=7$).

Note that in obtaining the inactivation parameters it is valid to argue that the current completely inactivated, given the following points: The GHK current equation (Equation 2-9) clearly fits the current that remains at the end of the 8s pre-pulse (Figure 4-10 A, green square) as plotted against the pre-pulse voltage in Figure 4-10 C. Hence, the remaining current is mediated by a non voltage-gated K^+ leak. To further support this conclusion the difference between the fit and the real data is also plotted (Figure 4-10 C, blue squares), which is well fit by a linear regression and reverses close to 0mV.

The linear nature of the difference current and the fact that it reverses close to 0mV indicates that it is due to the seal leak. The slope of the seal current is $0.0008 \text{ nA mV}^{-1}$ which corresponds to a seal resistance of $1.25 \text{ G}\Omega$. Conventional leak subtraction (including P/N) subtracts a linear leak which is estimated at negative potentials and extrapolated (exampled in Figure 4-10 C, dashed red line); this method clearly fails to isolate voltage-gated K^+ channels from leak current as K^+ mediated leak is non-linear. Obviously a considerable amount of K^+ leak would remain at $+43\text{mV}$ ($\sim 0.8\text{nA}$), which would lead to the misinterpretation that the remaining leak was actually a non-inactivating component of the Kv channel.

The Boltzmann distributions fitted to the activation and inactivation data show that this conductance has little steady-state inactivation at resting membrane potentials, and is a high voltage-activated conductance, only beginning to turn on more positive than -35mV .

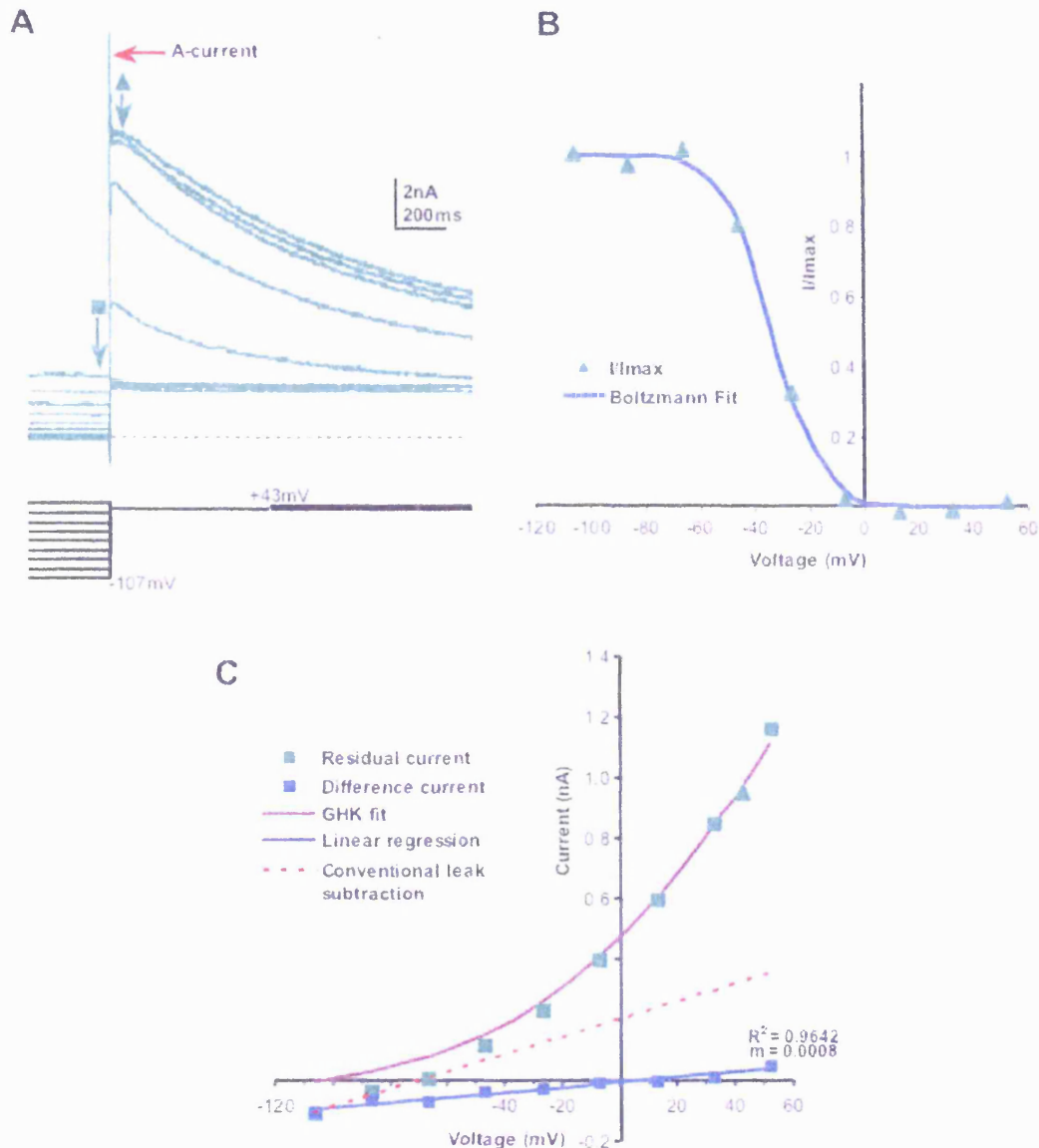


Figure 4-10 Assessing the voltage-dependence of inactivation for the slow conductance: A) A test step to +43mV was preceded by 8s pre-pulses to voltages between -107 and +53mV. Dashed line is the zero current level. **B)** The peak current was measured 20ms after the onset of the test step (to avoid the A-current), normalised to the maximum and plotted against voltage (green triangles), a Boltzmann function fit the data giving a $V_{1/2in}$ of -35.9 ± 1.5 mV and a k_{in} of 10.8 ± 0.8 . **C)** Plot of the residual current at the end of the pre-pulse in A (green squares) is fit by the GHK current equation, demonstrating that only leak remains. Blue squares represent the difference from the fit, which is linear and reverses at zero (consistent with “seal leak”). Red dashed line indicates what leak subtraction would subtract (see text). N.B. All data recorded in the presence of 3mM TEA and 10nM DTx-I.

As already mentioned it is clear that this current activates slowly. The activation rate over a range of voltages was assessed using the protocol shown in Figure 4-11 A. A -97mV pre-pulse removed any steady-state inactivation and then a brief 20ms pre-pulse to -37mV induced inactivation of the A-current (red arrow Figure 4-11 A), leaving the sustained current in isolation for the 200ms test steps. The voltage-dependence of activation is shown with single exponential fits to the rising phase of the current, with the averaged data plotted in Figure 4-11 B. The activation rate is extremely slow at negative voltages $\tau=39.6 \pm 5.2\text{ms}$ at -27mV (n=6) and accelerates e-fold with 17.7mV of depolarisation.

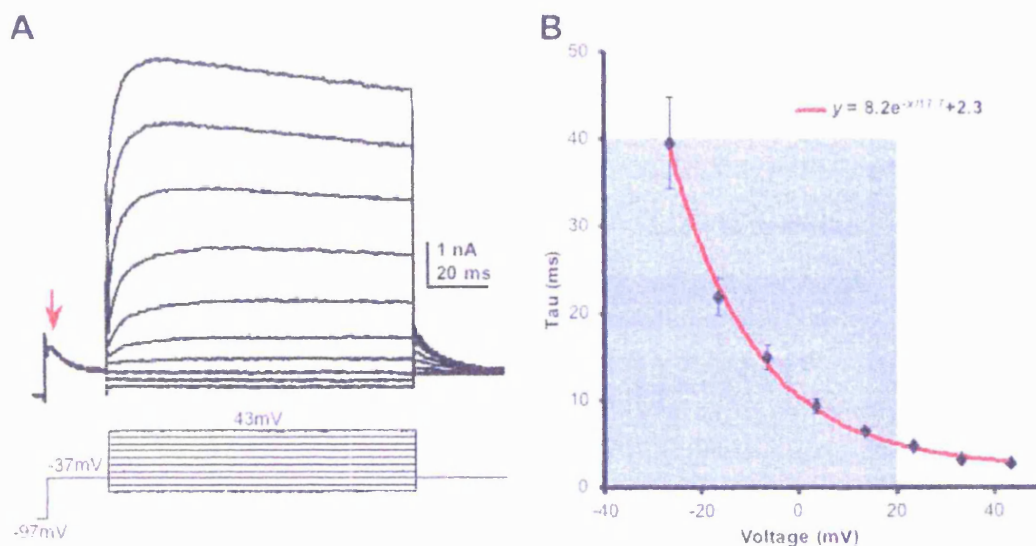


Figure 4-11 Voltage-dependence of activation rate for the slow conductance: A) Any steady state inactivation was removed by a -97mV pre-pulse, then inactivation of the A-current was induced by a 20ms pulse to -37mV (red arrow) leaving just the sustained current in the test pulses which were stepped between -57 and +43mV. **B)** Single exponentials fit the rising phase of the current response in A, the mean time constants of the exponentials from 6 cells are plotted against voltage. The activation rate as a function of voltage was approximated by an exponential function (red line), showing that the rate accelerates e-fold with 17.7mV of depolarisation. The blue box highlights the physiological range. N.B. All data recorded in the presence of 3mM TEA and 10nM DTx-I.

The blue box in Figure 4-11 B highlights the physiologically relevant voltages, emphasizing that this channel turns on extremely slowly requiring ~10ms at 0mV to activate by 67%.

This slow activating conductance also deactivates slowly in a voltage dependent manner. To assess its deactivation rate the channel was maximally activated by stepping to +63mV for 15ms (>5 activation taus) and then stepped back to test potentials (Figure 4-12 A). The current decay during the test potential was fit by single exponentials and the time constants are plotted against voltage in Figure 4-12 B. The values between -70 to -85mV were omitted due to the small size of the current at these voltages, close to the reversal potential. The deactivation rate is also slow being 10.6 ±0.7ms at -37mV accelerating e-fold with 30.6mV hyperpolarisation.

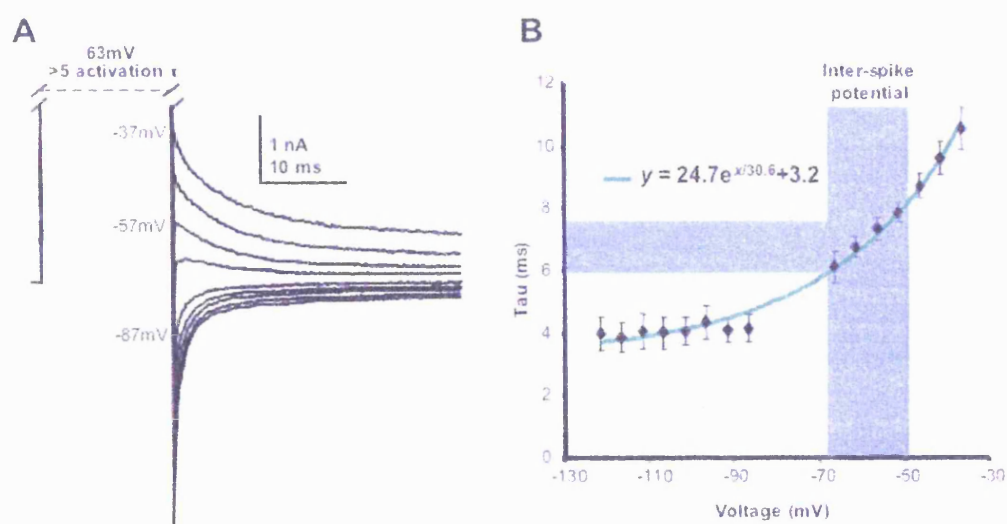


Figure 4-12 Deactivation rate of the slow conductance: A) The slow conductance was maximally activated by stepping to +63mV for 15ms (>5 τ_{ac}), then test steps were given to voltages between -37mV and -122mV. **B)** Single exponentials fit the current decay in the test steps in A, the mean time constants from 6 cells are plotted against voltage. The deactivation rate as a function of voltage was approximated by an exponential function (green line), showing that deactivation accelerated e-fold with 30.6mV of hyperpolarisation. The blue bars represent the physiological voltage ranges which will be examined later. N.B. All data recorded in the presence of 3mM TEA and 10nM DTx-I.

The inactivation of this slow conductance was examined by giving 8s test pulses to voltages between -107 and +53mV (preceded by a 20ms pre-pulse to -37mV to inactivate the A-current, Figure 4-13, red arrow). As can be seen in Figure 4-13 the inactivation rate is extremely slow occurring over 5-10 seconds. Neither a single nor a double exponential function would fit the decay over a range of voltages. The inability to reliably fit the inactivation is due to a number of factors, the most obvious being a change in voltage error. Which results from the large current passing across the series resistance, giving a change in the voltage error throughout the sweep. To give an estimate of the inactivation rate, the time to half-inactivation at -7mV was measured in 5 cells as 669 ± 32 ms.

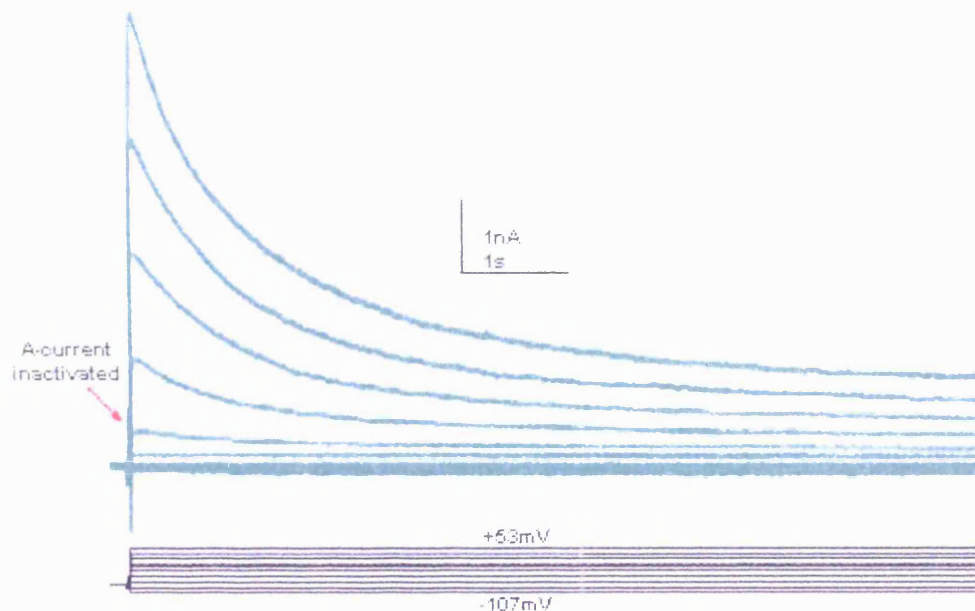


Figure 4-13 Inactivation rate of the slow conductance: Inactivation of the A-current was induced by a 20ms -37mV pre-pulse (red arrow) prior to stepping to test voltages between -107 and +53mV, which evoked large outward currents that inactivated extremely slowly with a time to 1/2 inactivation of 669 ± 32 ms ($n=5$).

The effect of long duration pulses on E_K

One further confounding problem when using long positive pulses is illustrated in Figure 4-14. I found that longer duration pulses resulted in a shift in the reversal potential.

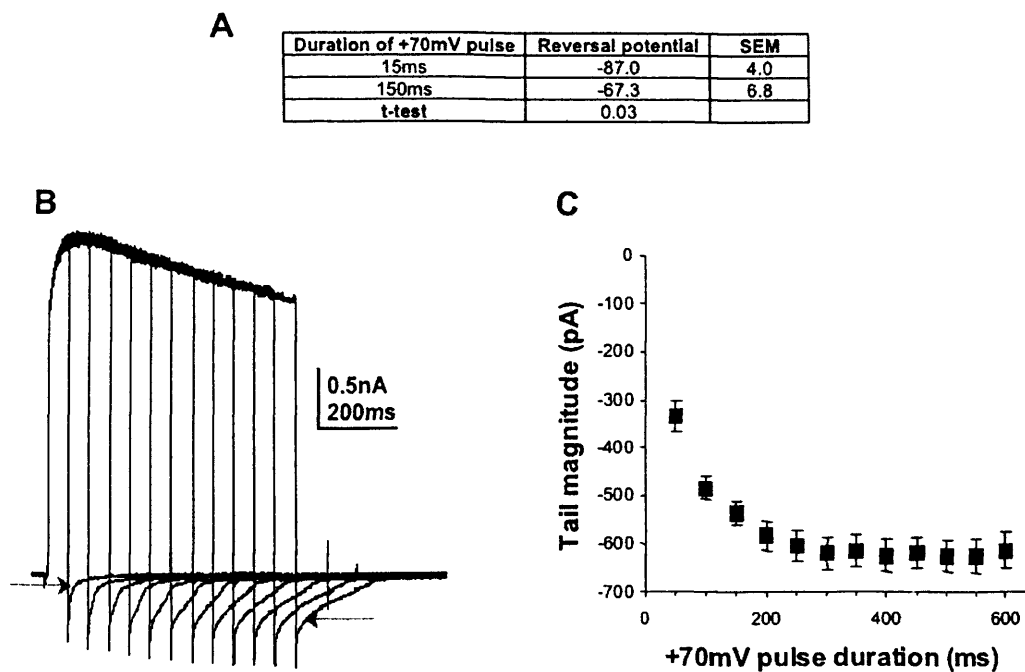


Figure 4-14 Long duration pulses results in a shift of the K^+ reversal potential: A) Table showing that the K^+ reversal potential becomes more positive for increasing durations of pulses to +63mV, all cells are paired ($n=3$). **B)** Example traces showing the tail current magnitude (grey arrows) increasing with duration of pulse to +63mV. **C)** Averaged data for the experiment in B shows that the shift in reversal potential saturates when the pulse duration is 250ms or longer ($n=5$). N.B. all data recorded in the presence of 10nM DTx-I and 3mM TEA.

Pulses of 15ms to activate the voltage gated current gave a reversal potential of -87.0 ± 4.0 mV, when the duration of the activating pulse was increased to 150ms the reversal potential shifted to -67.3 ± 6.8 mV (Figure 4-14 A, $n=3$, $P=0.03$). The shift in reversal potential seemed to saturate with pulses of around 250ms or greater, as the magnitude of the tail current increased up to 250ms but did not increase further (Figure 4-14 B & C). This change in reversal potential likely reflects an accumulation in external K^+ in the unstirred space (which is likely a small volume so a small amount of extra K^+ will have a large affect on the concentration).

Kv2.2 contributes to the slow conductance

The properties of the slowly activating and inactivating conductance are similar to those reported for recombinant Kv2 conductances (Schmalz *et al.*, 1998; Malin & Nerbonne, 2002). To assess whether a Kv2 subunit could contribute to the slow conductance we performed real time QrtPCR on pooled MNTB nuclei from 8 mice. Primers were designed to have similar efficiencies (~100%) to allow comparison of relative transcript abundance (see methods). β -actin was used as an internal standard, and we included both Kv2 members (2.1 & 2.2). In addition, we included Kv3.1 (known to be present, see Figure 3-6, and Wang *et al.*, 1998b) which we used as a standard for normalisation of the relative transcript abundance (see methods for table of primers).

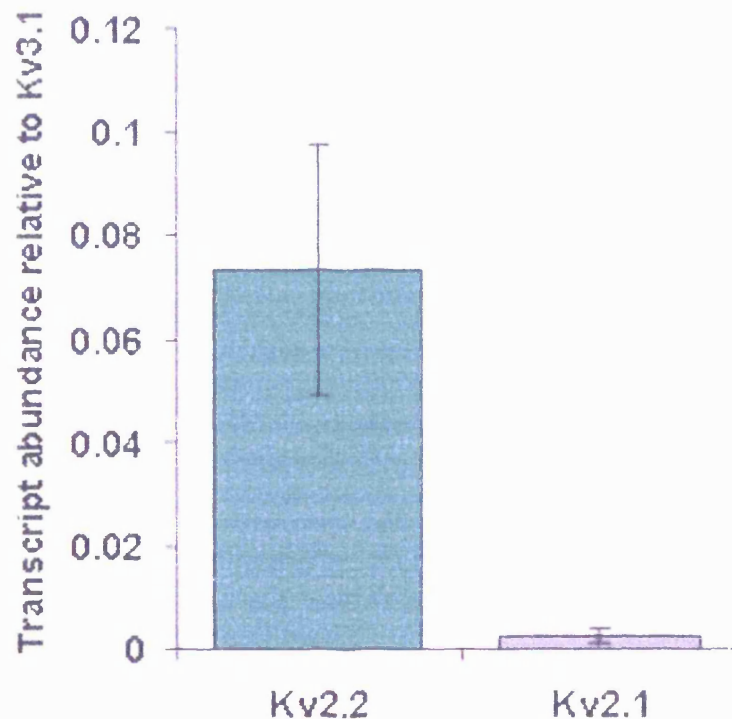


Figure 4-15 Kv2.2 mRNA is present whereas Kv2.1 is absent: Kv2.1, Kv2.2 mRNA transcripts expressed relative to Kv3.1. Each value is the mean of 3 separate reactions (and each reaction was performed as triplicates) normalised to β -actin and Kv3.1 transcripts, PCR method was performed by A. Skrzypiec.

Kv2.2 transcripts were $7.3 \pm 0.24\%$ as abundant as Kv3.1 transcripts, whereas Kv2.1 transcripts were only $0.25 \pm 0.12\%$ as abundant as Kv3.1 mRNA (Figure 4-15). The fact

that Kv2.1 was extremely low compared to Kv2.2, being ~30 times lower, is consistent with the absence of Kv2.1 immunostaining in the mouse MNTB (data which REW Fyffe kindly shared with us). As Kv2.2 transcripts were considerably higher than Kv2.1 it may be that Kv2.2 channels are responsible for the slow current.

One caveat to this hypothesis is that the PCR was performed on the whole MNTB nucleus; therefore we may be detecting Kv2.2 mRNA from non-principal cells e.g. glial cells.

To determine if Kv2.2 protein is indeed present in MNTB principal neurons we used an anti-Kv2.2 antibody (Alomone, Israel). We first validated the antibody's specificity by performing a western blot on whole brain homogenates. The anti-Kv2.2 antibody recognised a single band with a molecular weight of ~110 kDa (Figure 4-16) which is close to the predicted weight of mouse Kv2.2 protein (accession number XP_984002) of 102.2 kDa. Additionally pre-absorption with the blocking peptide resulted in no staining. The slight difference in molecular weights is likely explained by glycosylation and/or phosphorylation of the channel. The Western blotting was performed by A. Skrzypiec.

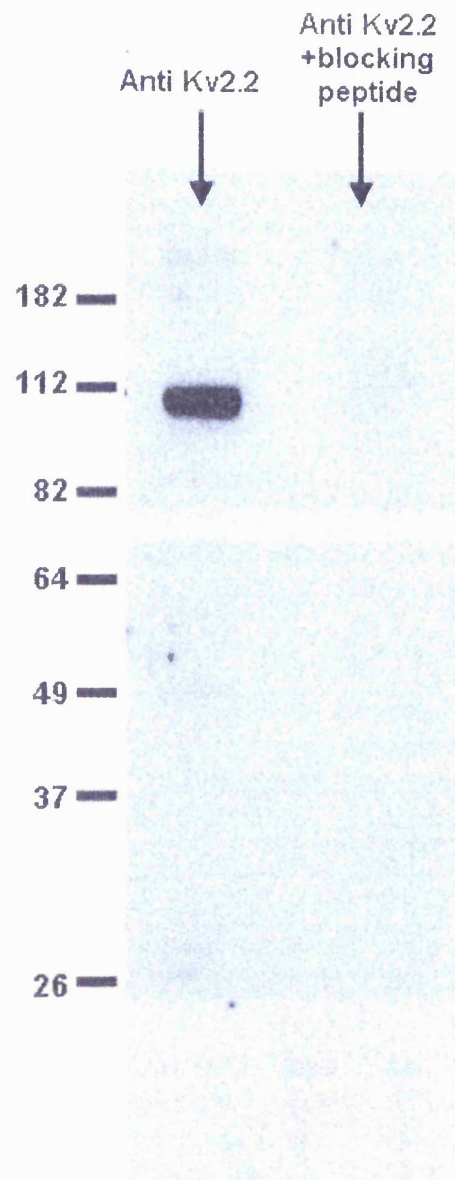


Figure 4-16 Anti-Kv2.2 stains a single band at the predicted molecular weight of Kv2.2: Western blot of whole brain homogenate with anti-Kv2.2 (1:1000), which recognises a single band of the predicted molecular weight of Kv2.2 (left lane). Pre-absorption with the blocking peptide results in no staining with anti-Kv2.2 (Right lane). Western blot performed by A. Skrzypiec.

For immunohistochemistry the antibody was used at the recommended dilution (1:1000). As the inset in Figure 4-17 A shows anti-kv2.2 stains the cell bodies of Purkinje cells and granule cells of the cerebellum consistent with previous reports (Hwang *et al.*, 1993).

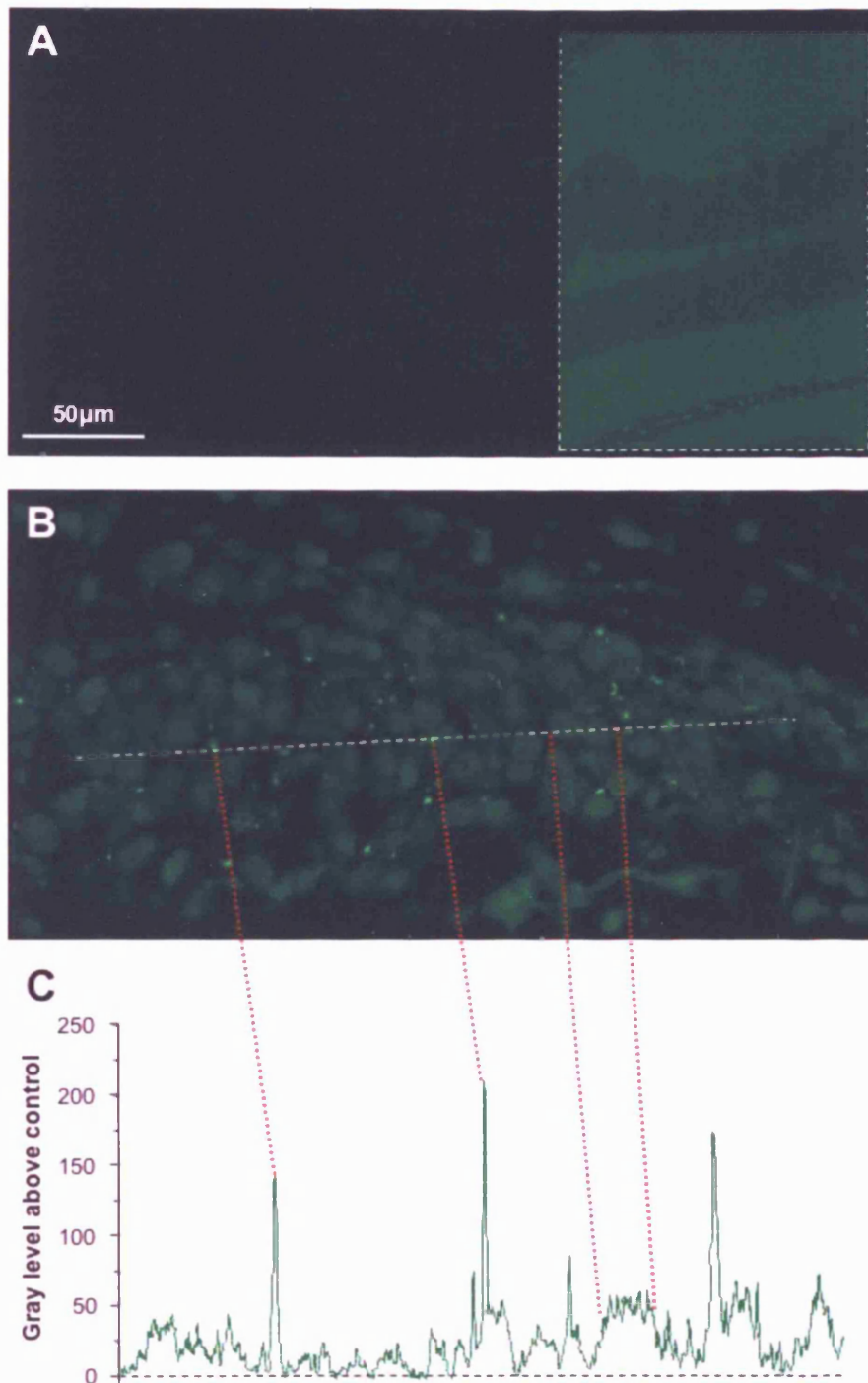


Figure 4-17 Kv2.2 is present in principal neurons of the MNTB: A) Pre-absorption with blocking peptide control, inset shows anti-Kv2.2 staining in the cerebellum. Scale bar applies to A & B. **B)** Principal neurons in the MNTB show robust staining with anti-Kv2.2 at 1:1000 (shown as signal above the control in A). **C)** Gray level above control for line in B, shows the different intensities of the specs compared to cell somas. Analysed with image-J (NIH). Similar results were seen in at least 3 animals.

The control used for examination of the MNTB was pre-incubation with the blocking peptide (Figure 4-17 A), the same settings on the camera and microscope were then used to capture the anti-Kv2.2 image shown in Figure 4-17 B. Note that the MNTB principal neurons are labelled and that there are also intense focal labelling in the MNTB nucleus. Figure 4-17 C shows the gray level profile of the line shown in Figure 4-17 B, which highlights the intensity of the specs (dashed red lines, up to 200 gray levels), also note the two adjacent cells which have a gray level of ~50.

The intense bright specs were intriguing as they were observed in all experiments, were absent the blocking peptide control and only appeared to be in the MNTB nucleus. To ascertain the locations of these intense specs, we examined the sections with a confocal microscope. Figure 4-18 B shows a single optical section through an MNTB stained with anti-Kv2.2 (green) and DAPI to visualise cell nuclei. As can be seen there is cytoplasmic staining (common for many ion channels, see chapter 3 and Dodson *et al.*, 2002; Elezgarai *et al.*, 2003), but the strongest signal is in the initial segment of the axon.

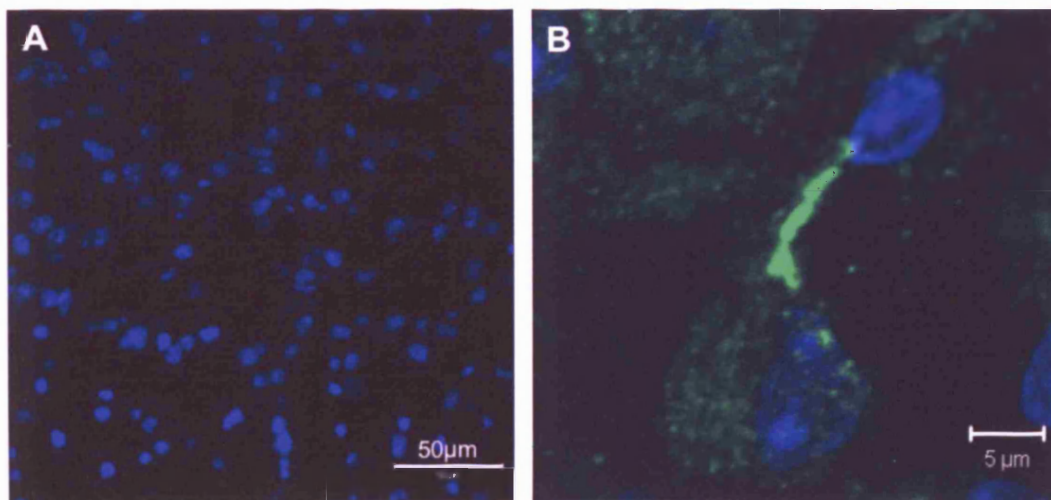


Figure 4-18 Kv2.2 is located in the initial segment of the axon: A) Pre-absorption with blocking peptide, shows no staining of anti-Kv2.2. **B)** Single confocal section through an MNTB neuron stained with anti-Kv2.2 (1:1000, green) and DAPI (blue) reveals cytoplasmic staining and intense staining in the initial segment of the axon. Also note the characteristic

large eccentric nucleus. Staining performed by A. Skrzypiec, and Dr. C. Guerin assisted with image collection.

Therefore it appears that the intense specs observed with light microscopy are due to intense labelling of the initial segments of axons (it is unlikely to be presynaptic since the heminode is much larger than the post synaptic axon, Leao *et al.*, 2005a), and possibly of regions along the axons. The fact that every cell in Figure 4-17 B does not have an intensely stained initial segment is due to the cryostat sections being only 12 μ m thick, whereas MNTB principal neuron somas are ~20 μ m.

Pharmacology of the slow conductance

To corroborate the molecular evidence for the presence of Kv2.2 we used a pharmacological approach. We know that the slow activating current is resistant to Kv3 and Kv1 channel antagonists as it is not blocked by 3mM TEA or 100nM DTx-I and CP-339 818 respectively.

Figure 4-19 A & B shows that the sustained current is completely blocked by application of 100 μ M Quinine (n=5), the residual current is mediated by a K⁺ selective leak as it is fit by the GHK current equation (Figure 4-19 A, blue line). Also note that the A-current is unaffected by quinine (Figure 4-19 B). The complete block by quinine is consistent with the conductance being mediated by Kv2.2 channels (Schmalz *et al.*, 1998). However, quinine is a rather "dirty" drug as it blocks a number of other K⁺ channels such as Kv1.3, Kv1.4, Kv1.5, EAG (Kv10) and K_{Na} at higher concentrations (1mM, Bhattacharjee *et al.*, 2005). However, we have already ruled out Kv1.3 and Kv1.4 channel using CP-339, 818 (Figure 3-9). Even worse quinine also blocks sodium channels (data not shown), which renders it useless for physiological studies in current-clamp.

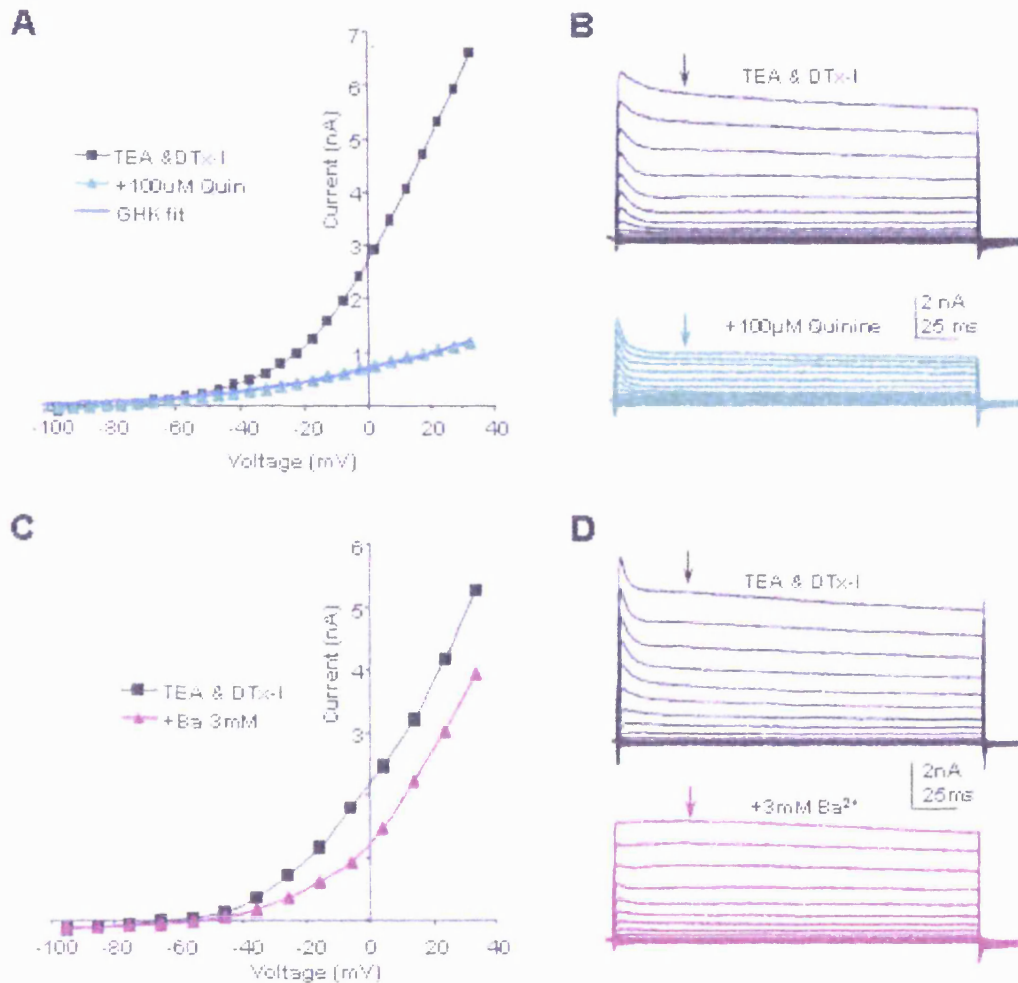


Figure 4-19 The slow conductance is blocked by quinine and partially blocked by Ba^{2+} :
A) I/V plot of the currents measured at the arrow from B, showing that 100 μ M Quinine blocks all the sustained current, a GHK fit the remaining current shows that only leak remains (n=5).
B) Example current traces for the cell in A. **C)** I/V plot of the currents measured at the arrow from D, Showing that 3mM Ba^{2+} only partially blocks the sustained current (n=4). **D)** Example current traces for the cell in C.

Application of 3mM Ba^{2+} only caused a partial block of the current resulting in a decrease of 1.34 ± 0.28 nA in the current measured 40ms into a +12mV pulse (Figure 4-19 C & D, n=4, P=0.017). As mentioned earlier 3mM Ba^{2+} also reduces the size of the A-current (Figure 4-6 A & B), however here the A-current is not contributing to the measurements as it will be completely inactivated by 40ms.

Other relevant pharmacological information is the resistance to 1 μ M E4031 (a selective blocker of EAG and ERG channels, Gessner & Heinemann, 2003) being

included in the patch solution ($n > 10$), even after repeated positive pulses. This rules out mediation by EAG and ERG channels. Furthermore the only partial sensitivity to 3mM Ba^{2+} rules out mediation by ELK channels, which are completely blocked by 1mM Ba^{2+} (Engeland *et al.*, 1998; Shi *et al.*, 1998; Zou *et al.*, 2003).

The presence of 50 μ M linopirdine (a supra-maximal dose for Kv7 channels, Coetzee *et al.*, 1999) also left the current unblocked ($n=2$). Which rules out mediation by a Kv7 (KCNQ) channel, which is consistent with the lack of expression of Kv7 mRNA in the MNTB (Kharkovets *et al.*, 2000; Saganich *et al.*, 2001).

Mediation by K_{Na} subunits (Slick & Slack) is also unlikely as this current inactivates whereas K_{Na} subunits do not (Bhattacharjee & Kaczmarek, 2005; Bhattacharjee *et al.*, 2005). Additionally all patch solutions contained 0 $[Na]_i$ which is required for activity (Bhattacharjee & Kaczmarek, 2005). Furthermore when 2mM Mg-ATP was included in the patch pipette, the current remained unaffected (data not shown).

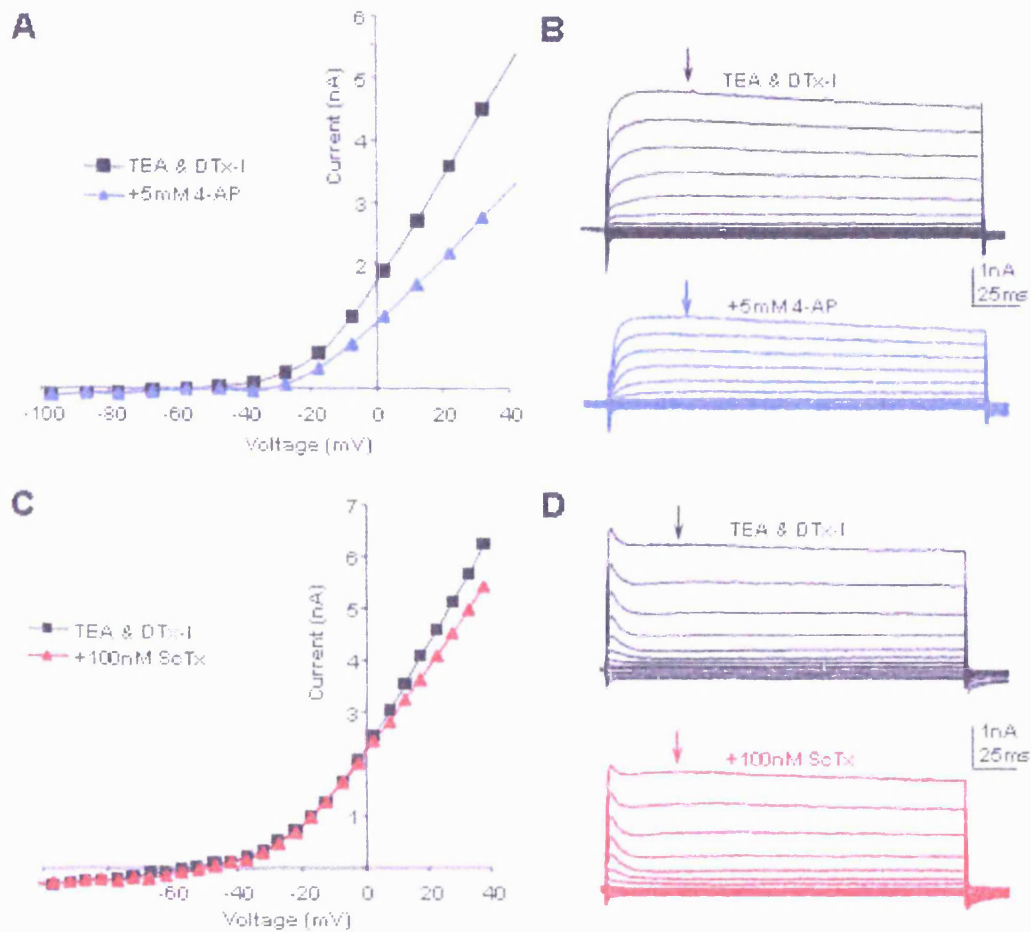


Figure 4-20 The slow conductance is partially blocked by 4-AP and unaffected by rScTx: **A)** I/V plot of the currents measured at the arrow from B, showing that 5mM 4-AP only causes a partial block of the sustained current ($n=4$). **B)** Example current traces for the cell in A, with the A-current inactivated with a 20ms -37mV pre-pulse. **C)** I/V plot of the currents measured at the arrow from D, showing that application of 100nM rScTx has no effect on the sustained current ($n=5$). **D)** Example current traces for the cell in C.

Application of 4-AP at 5-10mM only reduced the TEA & DTx-I insensitive sustained current by 1.67 ± 0.62 nA (Figure 4-20, A & B, $n=4$). This relative insensitivity to millimolar 4-AP rules out all the Kv1 subunits (Coetzee *et al.*, 1999), which was unlikely due to this conductance being relatively high voltage activated.

This still leaves the possibility that it may be mediated by a Kv2 subunit. The current appears largely insensitive to 3mM TEA consistent with the IC_{50} for Kv2.2 being 8mM (Coetzee *et al.*, 1999).

There are two pharmacological properties that are not wholly consistent with mediation by homomeric Kv2.2 channels. 4-AP has been reported to block recombinant homomeric Kv2.2 channels with an IC_{50} of 1.5mM (Schmalz *et al.*, 1998). A recombinant stromatoxin-1, of which the native toxin is reported to be selective for the Kv2 family (Escoubas *et al.*, 2002) also had no effect on the current (Figure 4-20 C & D, 100nM-5 μ M, n=5, three lots). These minor discrepancies could easily be explained by the conductance being mediated by heteromeric channels formed from Kv2.2 subunits and an electrically silent subunit (Kv5, 6, 8 & 9s). These modulatory μ subunits are able to form functional channels as heteromers with Kv2 members, under these circumstances they decrease the channel's sensitivity to pharmacological agents e.g. TEA (Post *et al.*, 1996; Robertson, 1997). Also as the silent subunits contribute to the pore they are likely to affect drugs that bind in or near the pore, such as 4-AP, TEA and toxins that occlude the pore. The native channel's insensitivity to rScTx may be due to the toxin being recombinant, as it is likely that the folding of the peptidergic toxin is important, or it may be the channel's stoichiometry.

A physiological role for Kv2.2 containing channels

We therefore know of no selective antagonists for this putative Kv2.2 containing conductance, so unravelling a physiological role is difficult. This Kv2.2 conductance has slow gating kinetics and a high-voltage activation range (Figure 4-9 & Figure 4-11). It therefore differs from the known Kv1 and Kv3 conductances which activate and deactivate rapidly (Brew & Forsythe, 1995). Hence, in the MNTB where physiological action potentials typically have half-widths of ≤ 0.5 ms, this Kv2.2 conductance will hardly be activated by a single action potential. Kv2.2 will therefore make little contribution to the action potential waveform which is dominated by the rapid Kv3 and Kv1 conductances (Klug & Trussell, 2006). However Kv2.2 also deactivates slowly (Figure 4-12), so once active it remains open for longer, suggesting that its activity may accumulate with trains of action potentials.

To describe this rationale: Only a fraction of the Kv2 current will activate with 1 action potential, and the deactivation rate of this will be determined by the inter-spike potential (V_{is}). V_{is} varies between ~ -50 to -70 mV (see Figure 4-21 B & C) which approximates to a deactivation time constant of ~ 7 ms (see Figure 4-12 B, blue bars). So to take an example, for a 50Hz train of action potentials, having an inter-spike interval of 20ms, we can predict that $\sim 6\%$ (see Equation 4-1, $t=20$, $\tau=7$) of the current activated by the 1st action potential will still be active by the 2nd.

$$\% \dots \textit{remaining} = e^{-t/\tau}$$

Equation 4-1 %...remaining is amount of Kv2.2 able to sum with that from the next action potential, t is inter-spike interval, τ is deactivation time constant.

However, for a 200Hz train ($t=5$ ms) $\sim 50\%$ would remain active for subsequent action potentials. Therefore one would expect to see a greater affect of the Kv2.2 conductance in a 200Hz train compared to a 50Hz train, as it should accumulate to a greater extent.

So how do we examine the predicted affect of Kv2.2? We know that the other Kv conductances are rapid (Brew & Forsythe, 1995) and are known to follow the action potential waveform (Klug & Trussell, 2006). Therefore in the after-depolarisation Kv2.2 should dominate, as Kv3 and Kv1 will have deactivated. The A-current is also unlikely to contribute here as it gates rapidly and will inactivate.

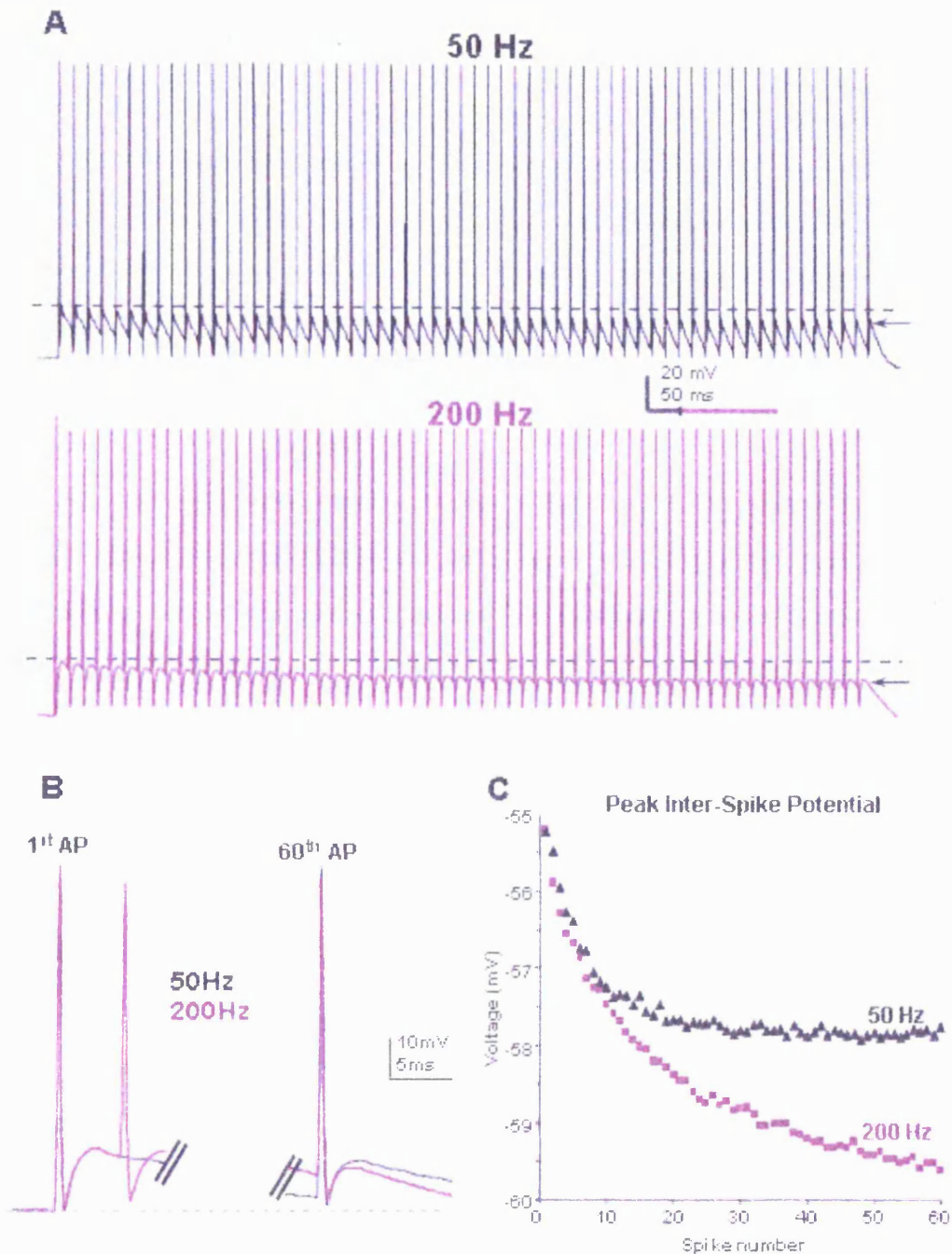


Figure 4-21 Action potential frequency determines amount of inter-spike hyperpolarisation, consistent with accumulation of Kv2.2: **A)** Example action potentials (averages of at least 10 sweeps) for a train of 60 stimuli at 50Hz (black) and 200Hz (purple). **B)** Shows the 1st and last action potentials from the two frequencies overlain, note that only the level of after depolarisation differs. **C)** Plot of the peak inter-spike potentials against action potential number shows that the inter-spike potential hyperpolarises with action potential number and frequency, consistent with build up of Kv2.2. Single example representing an n of 4 for 200Hz and 7 for 50Hz.

With this information, we decided to measure the peak of the after-depolarisation to assess whether our predictions were feasible. However as we were expecting only a small affect, we used the simulated synaptic current waveform that I developed earlier (Figure 3-2). However as the EPSC at the Calyx of Held depresses through out trains of stimuli the eighth response from a train was used to generate the synaptic current waveform. This scaled down version was used to represent the synaptic input in its depressed state. This method was preferable to using orthodromic stimulation as it avoids synaptic variability and depression.

I found that V_{is} hyperpolarised throughout 50Hz and 200Hz trains (Figure 4-21), which is consistent with activation of a K^+ current (since it is the only ion with an E_{rev} more negative than rest). Additionally, as predicted, the hyperpolarisation was greater with a higher frequency: at 50Hz V_{is} decreased by $1.9 \pm 0.5mV$ ($n=7$, $P=0.014$) whereas at 200Hz V_{is} hyperpolarised by $4.7 \pm 0.7mV$ ($n=4$, $P=0.0075$, similar results were seen in 2 further cells but were excluded from analysis due to double spiking at the 1st stimulus, commonly observed in mice (Brew & Forsythe, 1995)). Also note in the data that the fast after-hyperpolarisation remains fairly constant, consistent with mediation by the fast Kv3 channels, which follow the action potential waveform (Figure 4-21 A).

Since the membrane potential does not return to rest between spikes (Figure 4-21 A & B), one would expect summation of the inter-spike potential in the absence of this Kv2.2 conductance. But as Kv2.2 activates more with higher frequencies, it will oppose summation and lower input resistance. However it must be noted that the hyperpolarisation of V_{is} is relatively modest, being only $\sim 4.7mV$ by the 60th action potential, therefore it might be argued that this small hyperpolarisation has little physiological significance.

The sodium current is exquisitely sensitive to inter-spike voltages

An obvious target for small changes in inter-spike voltage is the voltage-gated sodium current (I_{Na}). However the study of native neuronal I_{Na} is notoriously difficult (due to space clamp and the reiterative problems with voltage error) so I used CsCl based pipettes (see methods) with TEA and 4-AP to block any K^+ channels permeable to Cs. Due to the MNTB's lack of processes (and hence ease of voltage-clamp) it has been shown by Leao *et al.*, 2005a that space clamp and voltage error only induced minor inaccuracy in studying inactivation with whole-cell recordings from MNTB slices.

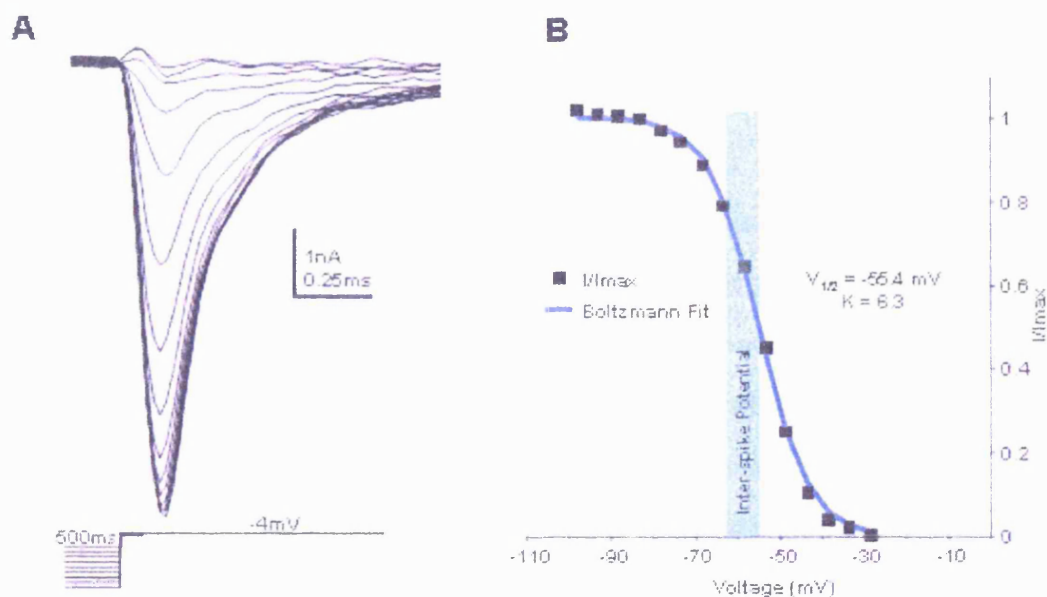


Figure 4-22 Voltage-dependence of inactivation of the sodium current: A) A test step to -4mV was preceded by 500ms pre-pulses between -107 and -27mV. p/n leak subtraction was used to eliminate capacitive transients. **B)** The peak I_{Na} in A was normalised to the maximum and plotted against pre-pulse potential. This was then fit with a Boltzmann distribution giving a $V_{1/2in}$ of -55.4 ± 1.7 mV and a k_{in} of 6.3 ± 0.1 ($n=5$). N.B all data recorded in the presence of $20\mu\text{M}$ DNQX, $10\mu\text{M}$ bicuculline, $1\mu\text{M}$ strychnine, $100\mu\text{M}$ CdCl₂, 3mM TEA, 1mM CsCl and 5nM TTx.

These errors were further reduced here by including 5nM TTx ($\sim IC_{50}$ for the reported Nav subunits in the MNTB) to partially block the current, thus further reducing voltage error. Additionally the test steps used to measure I_{Na} (being -4mV) were past the peak of its activation. Therefore any voltage error would not activate additional current.

To assess whether I_{Na} is sensitive to small hyperpolarisations, I measured the sodium current's voltage-dependence of inactivation by giving test steps to -4mV preceded by 500ms pre-pulses to voltages between -107 and -27mV (Figure 4-22 A). The peak sodium current was measured, normalised and plotted against the pre-pulse voltage (Figure 4-22 B, black squares). This was then fit with a Boltzmann distribution giving a $V_{1/2in}$ of -55.4 ± 1.7 mV and a k_{in} of 6.3 ± 0.1 (Figure 4-22 B, blue line, $n=5$). This shows that the I_{Na} has little steady-state inactivation at rest, however the inter-spike potential falls on the steepest part of the inactivation curve (Figure 4-22 B, green bar). This confirms that the sodium current is highly sensitive to the inter-spike voltages, and therefore to Kv2.2 activation.

Leao *et al.*, 2005a also examined the rate of recovery of I_{Na} mainly at the presynaptic terminal, but also looked at postsynaptic MNTB Nav channels. Here they found that the recovery of I_{Na} was fit by a double exponential, possessing a fast component with a tau ~ 2 ms and a much slower component having a tau ~ 80 -90ms. Although we know that the I_{Na} will be affected by the inter-spike voltage (Figure 4-22), it could potentially have a much larger affect than one would first estimate due to the slow component of recovery. Therefore to further understand what would happen to the sodium current in a 200Hz train with the absence of the Kv2.2 conductance, I designed the voltage-clamp protocol shown in Figure 4-23.

A 5ms test pulse (V_{Test}) to -4mV maximally activated and inactivated I_{Na} , each V_{Test} was followed by a 5ms period reproducing the actual inter-spike interval for a 200Hz AP train (see the protocol in Figure 4-23 with an AP overlaid in red). This period consisted of a 1ms step to -67mV (V_{AHP} , Figure 4-23), which mimicked the AHP mediated by the fast Kv3 current, and a 4ms step to varying voltages (V_{is} , Figure 4-23) mimicking the inter-spike potential. This protocol allowed me to test the affect of varying inter-spike potential (V_{is}) on the sodium current.

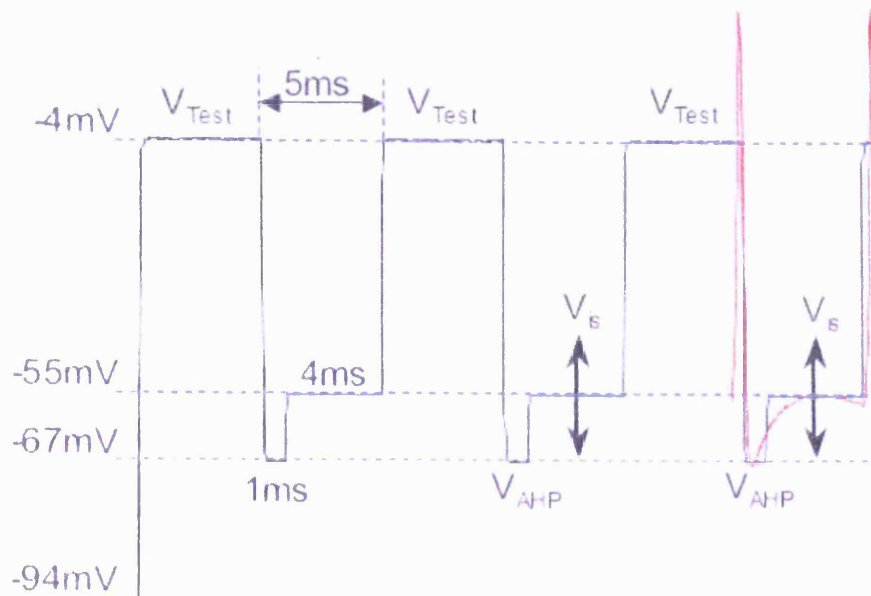


Figure 4-23 Protocol to assess the affect of V_{is} on I_{Na} : Protocol consists of a -94mV 500ms pre-pulse to remove any steady state inactivation, then 60 V_{Test} steps; V_{Test} = 5ms test steps to -4mV were used to evoke I_{Na} ; V_{AHP} = 1ms step to -67mV reproduced the Kv3 mediated fast AHP; V_{is} = 4ms step to variable voltages mimicked the inter-spike voltage. **Red trace** = Action potentials from a 200Hz train overlain to the same scale.

The first two V_{Test} steps were identical in each of the three paradigms used (Figure 4-24) with $59.5 \pm 5.8\%$ recovery of the sodium current between the first and second V_{Test} ($n=7$, $P < 0.001$). Further measurements were normalised to this value.

In the first paradigm (Figure 4-24 A) I set V_{is} to simulate mild summation of inter-spike potentials (depolarising 4.5mV over 60spikes, which may occur in the absence of the Kv2.2 conductance, as discussed earlier) and observed a $49.9 \pm 4.0\%$ decrease in I_{Na} by the 60th repetition (Figure 4-24 A & D green, $n=5$, $P=0.007$). The asterisks indicate the onset of statistically significant difference (assessed with an ANOVA). This shows that with mild summation of the inter-spike potential, there is a striking decline in I_{Na} availability, which would eventually lead to action potential failures.

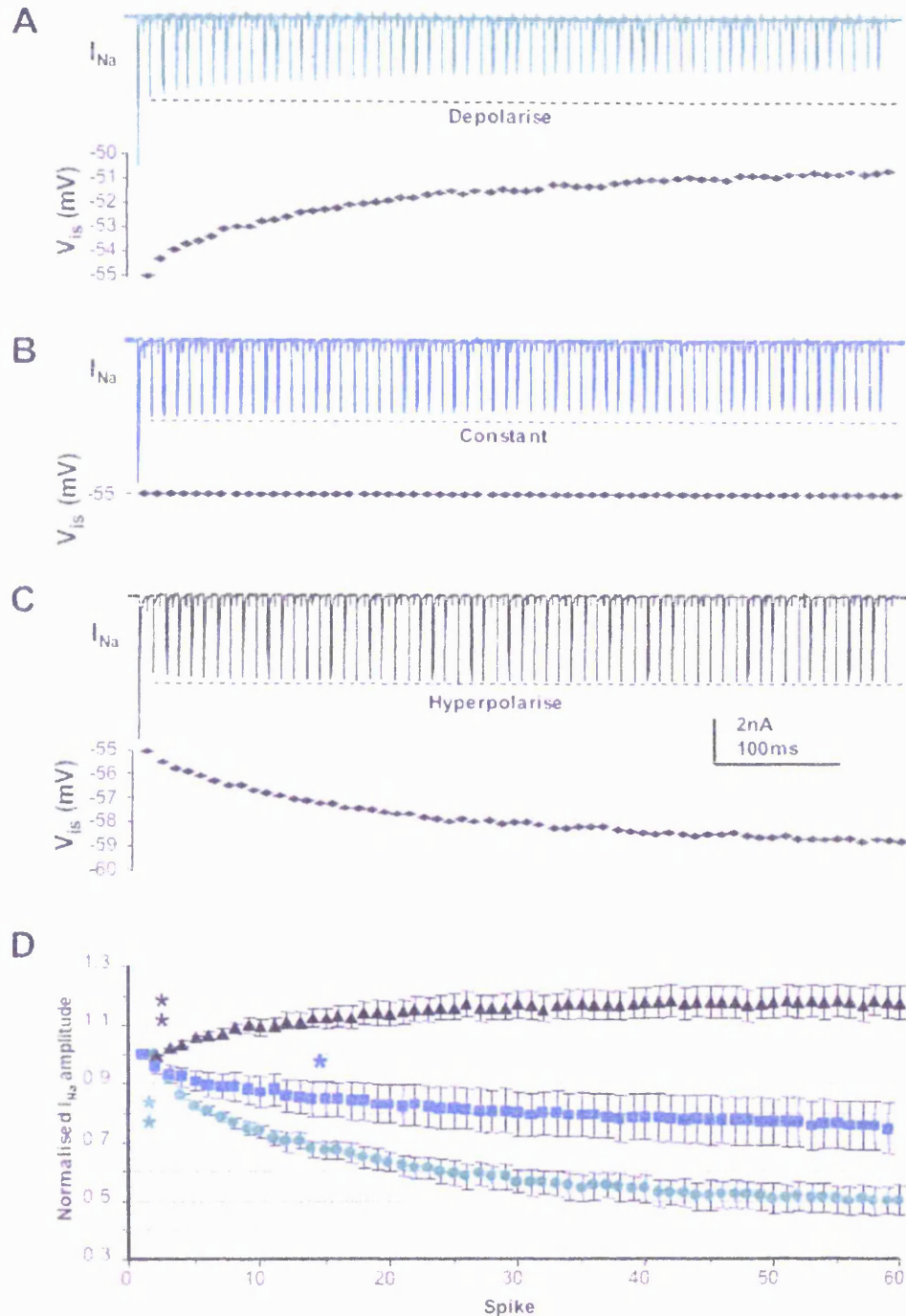


Figure 4-24 I_{Na} is exquisitely sensitive to the inter-spike voltage: The protocol in Figure 4-23 has been used to test the affect of the inter-spike voltage (V_{is}). V_{is} is plotted underneath the appropriate sodium spike in each paradigm **A)** Example current trace for V_{is} depolarising to simulate mild summation. **B)** Example current trace for V_{is} remaining constant. **C)** Example current trace for V_{is} mimicking physiological values of V_{is} . **D)** Averaged data for A, B and C ($n=5, 8$ and 7 respectively). Asterisks indicate onset of significance, data in A-C from the same cell.

The second paradigm was similar (Figure 4-24 B) but V_{is} remained constant throughout the 60 pulses. Under these conditions I_{Na} decreased by $25.1 \pm 8.6\%$ and was still declining by the 60th spike (Figure 4-24 B & D, blue, $n=8$, $P=0.02$). This continued decline indicates that I_{Na} can accumulate in its inactivated state during the inter-spike interval of a 200Hz train, consistent with a slow component of recovery from inactivation (Leao *et al.*, 2005a).

In the third paradigm V_{is} was adjusted to mimic the observed physiological voltages for V_{is} (Figure 4-24 C). I observed an increase of $17 \pm 14.4\%$ in the Nav current, which reached a plateau by the 30th repetition (Figure 4-24 C & D, black, $n=7$, $P=0.004$).

This demonstrates the remarkable sensitivity of the sodium current to the inter-spike voltage, and that the modest hyperpolarisation caused by accumulation of the Kv2.2 conductance is sufficient to sustain the sodium current for prolonged periods of high frequency firing.

Developmental and tonotopic gradients

Kv2.2 current magnitude increase with development

All the data presented here is from P10-14 CBA mice. To assess whether there are developmental changes in the amount of Kv2.2 current, the current measured 40ms into a +13mV test step in the presence of 10nM DTx-I and 3mM TEA was recorded (as at this voltage the channel should be maximally activated Figure 4-9). I plotted the peak currents at +13mV against animal age. An ANOVA with a post hoc test for a linear trend between means showed that there was an extremely significant increase ($P < 0.0001$) with development. Figure 4-25 shows this trend with data from P18-19 animals included (collected by Dr. S. J. Griffin). When the older animals were included the trend was still as significant $P < 0.0001$. Additionally when the peak tail currents (Figure 4-9 A) from data pooled from the P18-19 animals ($n=5$) were compared with that from the P10-14 animals

(n=6) there was an increase from $0.80 \pm 1.2\text{nA}$ to $1.9 \pm 0.13\text{nA}$. This 2.41 fold increase was also highly significant ($P < 0.0001$).

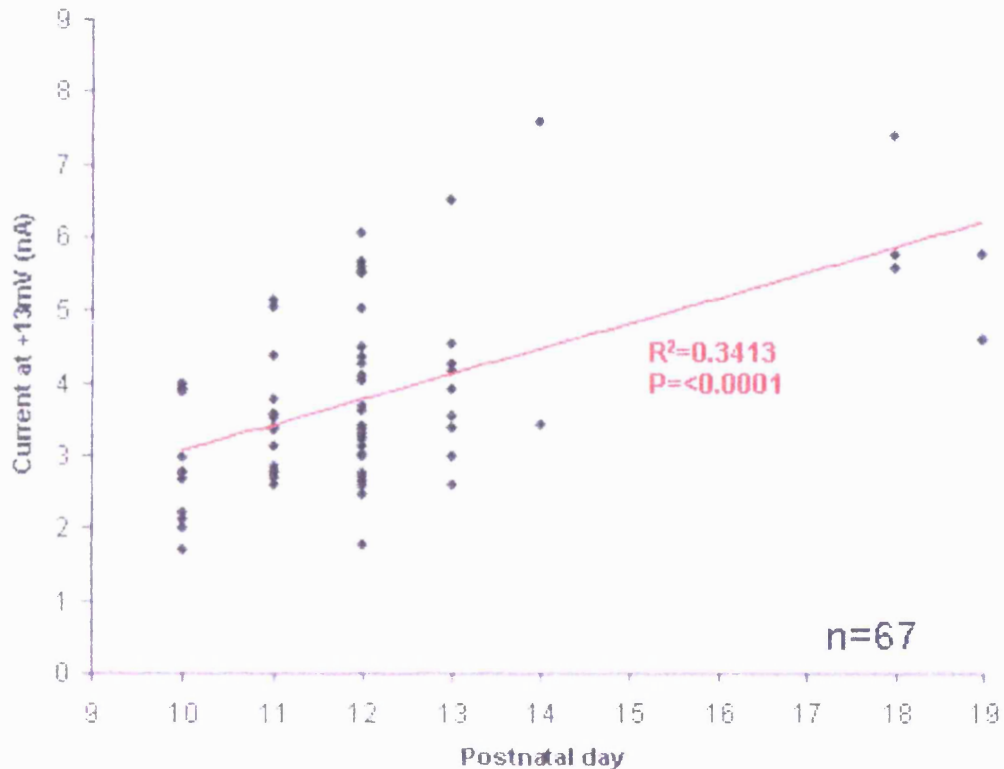


Figure 4-25 The Kv2.2 conductance increases with development: The current measured 40ms into a +13mV pulse is plotted against age. N.B. All data recorded in the presence of 3mM TEA and 10nM DTx-I.

The whole cell capacitance was estimated from the whole-cell capacitance dial on the amplifier (a rather crude method). For the tail current data there was an increase in capacitance from 13pF (n=6) in the P10-14 animals to 13pF (n=5) in the P18-19 animals, which was not significant ($P=0.68$). When the peak tail currents were normalised for capacitance, the current densities were $63.2 \pm 10.8\text{pA pF}^{-1}$ for P10-14 and $148.9 \pm 20.3\text{pA pF}^{-1}$ for the P18-19, which still gave an increase of 2.36 fold ($P=0.003$). The difference in current density may be slightly less with more accurate measurements of capacitance (e.g. fits from an uncompensated 5mV step). Unfortunately, these are the only estimates that were recorded.

Kv2.2 is tonotopically distributed

The MNTB is known to have a medio-lateral tonotopic gradient, with medial neurons receiving inputs from high frequency hair cells and lateral neurons receiving inputs from low frequency hair cells. Both Kv1, Kv3 and I_h have been shown to have a tonotopic distribution in the MNTB (Brew & Forsythe, 2005; Leao *et al.*, 2006b). The location of the cells in the MNTB nucleus was recorded by taking a photograph of the slice under 4x magnification. To assess whether the Kv2.2 conductance has a tonotopic gradient a stencil was used to divide the recordings into medial, intermediate or lateral (Figure 4-26 A). The data measured 40ms into a +13mV test pulse was taken from just the P12 animals (to eliminate the age gradient) and plotted against location (Figure 4-26 B). An ANOVA with a post hoc test for a linear trend between means was used to assess any tonotopic gradient. I found that there was a significant gradient of current amplitude across the MNTB, being larger in the lateral neurons and smaller in the medial neurons ($P=0.035$).

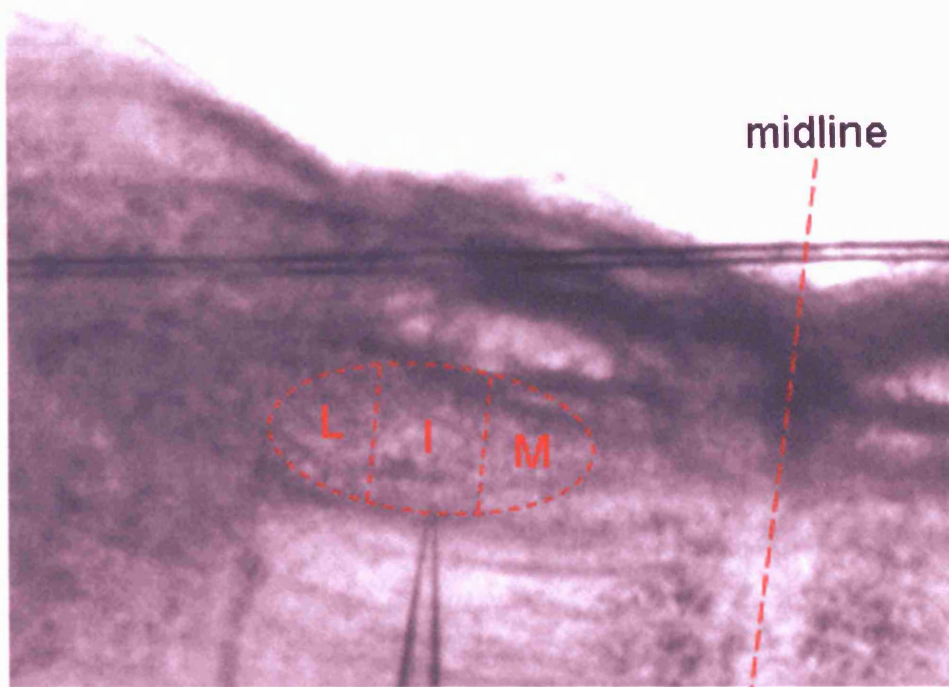
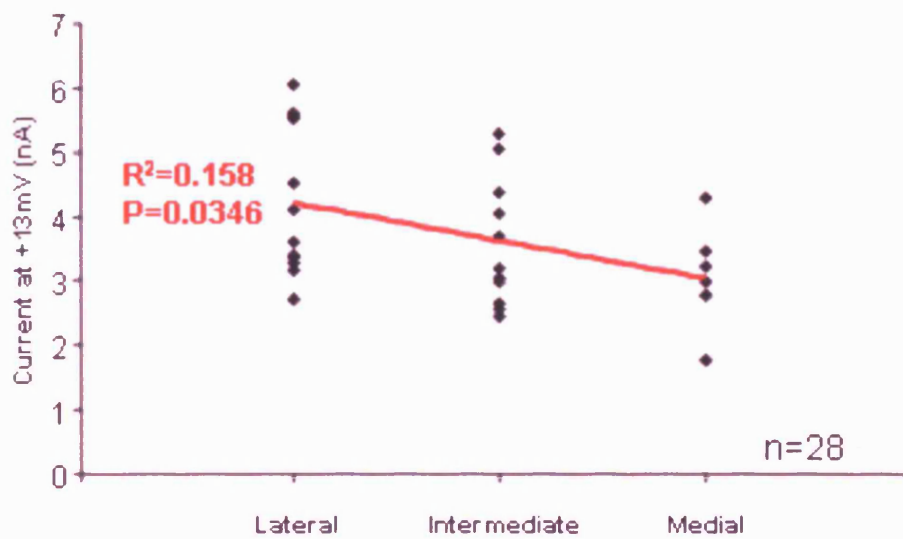
A**B**

Figure 4-26 Tonotopic distribution of Kv2.2 current in the MNTB at P12: **A)** Example photograph showing the MNTB nucleus, patch pipette still on cell and the stencil overlain. **B)** Plot of the current measured 40ms into a +13mV test step against cell location. N.B. All data recorded from P12 animals in the presence of 3mM TEA and 10nM DTx-I.

This gradient of current amplitudes is consistent with (Brew & Forsythe, 2005) who reported a similar gradient for an unidentified (i.e. not Kv1 or Kv3) slowly deactivating current in the rat, which is likely to be mediated by a similar conductance to the Kv2.2 reported here.

Discussion

In this chapter I have demonstrated that in addition to Kv1 and Kv3 the mouse MNTB possess two further Kv currents: A small rapidly inactivating A-current is present, which could contribute to the first action potential of a train, but makes only a minor contribution to the resting conductance due to high levels of steady-state inactivation.

A large magnitude slowly activating Kv2.2 current makes a major contribution to outward currents under voltage clamp, though its physiological affect is rather subtle. This Kv2.2 current accumulates throughout high frequency trains, hyperpolarising the inter-spike voltage, which is required for sustained periods of firing. The properties and physiological roles of these two currents will be discussed in turn.

The A-current

Molecular identity of the A-current

The small A-type conductance characterised here is insensitive to TEA and DTx-I but blocked by 4-AP (see Figure 4-3 & Figure 4-6) consistent with previous reports (Brew *et al.*, 2003). I also report sensitivity to external 3mM Ba²⁺ (Figure 4-6) and insensitivity to 100µM quinine (Figure 4-19 B).

The molecular identity of this conductance is as yet uncertain. However, we can exclude some of the inactivating subtypes based on the current's pharmacology. Both Kv3.3 and Kv3.4 can form rapidly inactivating currents; however they are both blocked by sub-millimolar concentrations of TEA (Coetzee *et al.*, 1999; Rudy & McBain, 2001).

Kv1.1 channels when associated with Kvβ1.1 mediate rapidly inactivating currents (Jow *et al.*, 2004), but these would still be sensitive DTx-I as the β-subunit associates with the intracellular C-termini (Yellen, 2002) and DTx binds externally to the pore region (Tytgat *et al.*, 1995). The DTx-I insensitive subunits Kv1.3 and Kv1.4 also produce inactivating currents but these can both be excluded since their antagonist CP 339 818 (Nguyen *et al.*, 1996; Jager *et al.*, 1998) had no effect (Figure 3-9).

In light of this the most likely candidate is a member of the Kv4 family, all of which mediate classical A-currents i.e. rapid activation and inactivation and a large amount of steady-state inactivation (Figure 4-3, Tkatch *et al.*, 2000). Additionally Kv4 channels are insensitive to TEA but blocked by millimolar concentrations of 4-AP (Coetzee *et al.*, 1999; Birnbaum *et al.*, 2004).

Kv4.1 seems to be absent from both the cerebellum and auditory brainstem, only being expressed in the hippocampus and olfactory bulb (Serodio & Rudy, 1998; Fitzakerley *et al.*, 2000). Kv4.2 is strongly expressed in the AVCN (The location of the globular bushy cells (GBC), which give rise to the calyx of Held, Fitzakerley *et al.*, 2000). Kv4.3 increases with development but is at low levels compared to Kv4.2 (Serodio & Rudy, 1998; Fitzakerley *et al.*, 2000). Interestingly the GBC soma in rat has an A-type current likely mediated by Kv4.2, yet the calyx of Held does not have any transient currents (Dodson *et al.*, 2003) nor does the mouse calyx (data not shown). At present there is no data on Kv4 expression in the MNTB, but it seems likely that Kv4.2 and or Kv4.3 will contribute. Indeed the Immunostaining shown in Figure 4-7 is consistent with Kv4.3 mediating the A-current.

The MNTB's A-current has an inactivation $V_{1/2}$ of -76mV, which is more negative than rest (RMP being ~ -70mV, Forsythe & Barnes-Davies, 1993). Therefore under my recording conditions at rest the A-current is greater than half-inactivated. This large amount of steady state inactivation is seen in Kv4 mediated A-currents in the basal forebrain (Tkatch *et al.*, 2000), CA1 hippocampal neurons (Chen & Johnston, 2004) and for those in expression systems (Birnbaum *et al.*, 2004).

The A-current begins to activate positive to -60mV, and at positive voltages inward rectification develops (Figure 4-4 C). This inward rectification at positive potentials is strongly reminiscent of voltage-dependent block by internal Mg^{2+} observed in A-currents (Forsythe *et al.*, 1992) and ShkB channels (Slesinger *et al.*, 1993), and it is possible that this is the case for the MNTB's A-current (as 1mM Mg^{2+} is included in the patch solution).

The A-current is a relatively low voltage-activated channel having a $V_{1/2ac}$ -35.6mV, assuming it has reached maximal activation by -7mV. Therefore it starts to turn on at potentials below action potential threshold, consistent with reports for A-currents mediated by Kv4 members (Serodio *et al.*, 1994).

One factor that does not quite fit with previous reports of Kv4 channels is the rapidity of the inactivation. The inactivation rate is fit by a single exponential function having a time constant of 4.75ms at -17mV (Figure 4-2 B). This inactivation rate is considerably faster than that reported for other inactivating currents, however by P18-19 the inactivation rate has slowed to 7.7ms at -17mV (n=5 P=0.001, data not shown, collected by Dr. S. J. Griffin). The A-current amplitude remains unchanged with development.

It should be noted that more direct correlations of the A-current's properties (i.e. $V_{1/2}$ etc) with those of Kv4 channels are difficult as Kv4 channels have a plethora of accessory subunits that fine tune their gating (Birnbbaum *et al.*, 2004), a fact that may contribute to the rapid inactivation rate observed here.

The Physiological role of the A-current

The observation that the 1st AP was 0.03 ± 0.005 ms (n=4, p=0.01) quicker than the 2nd or subsequent in a 200Hz train (Figure 4-8 A) is consistent with a small contribution from the A-current to repolarisation of the first AP. Even though it activates rapidly and at negative potentials it will only have a limited effect on the action potential peak due to development of a negative slope conductance at positive voltages (Figure 4-4 C).

By P25 an extremely robust ~200nS glycinergic input has formed on the MNTB (Awatramani *et al.*, 2004). This inhibition will lower the membrane potential, where the A-current will rapidly recover from inactivation (Figure 4-5), permitting it to contribute more current upon subsequent depolarisation. Figure 4-8 B, where an inhibitory input has been simulated, hints that under these circumstances the A-current will alter the time to peak of the action potential. The A-current's rapid activation and the fact that its activation curve

straddles the action potential threshold fit with this hypothesis. One can imagine this may be a strategy used to fine tune the timing information that the MNTB is transmitting.

The fact that the A-current has a large amount of steady-state inactivation strongly implies that it is performing some form of integration, otherwise what is the purpose of the "extra current" in its inactivated state? As the A-current activates just negative to action potential threshold, it is possible that it integrates the sub-threshold events such as those reported by Hamann *et al.*, 2003.

The A-current is present in the MNTB of at least two strains of mice (CBA, reported here & C3HeB/FeJ, Brew *et al.*, 2003), yet there is no evidence for an A-current in the rat (Brew & Forsythe, 1995; Dodson *et al.*, 2002 and J. Johnston & I. D. Forsythe unpublished observations). Also, as discussed earlier, the rat has nearly twice the Kv1 current that mouse has. Therefore it is tempting to postulate that this mouse A-current is contributing to the role of Kv1 channels, however as (Figure 3-12) shows it clearly is not sufficient to prevent multiple spiking.

A plausible explanation would be that mouse Kv1 currents have a slower activation rate, and require this A-current to provide a rapid current component at sub-action potential voltages. Consistent with this idea, is the fact that the A-current becomes readily apparent when the Kv1 channels are blocked by DTx-I (Figure 3-15), and also when Kv1 and Kv3s are blocked (Figure 4-1), however it is not easily seen when only Kv3s are blocked (Figure 3-4).

As this discussion has highlighted, it is difficult to pin down the physiological role of the A-current. This is, perhaps, due to its relatively small amplitude, furthermore its significance is undermined by the fact that the rat can manage without it. The sub-cellular localisation which could be determined by immunohistochemistry will help in understanding this channel. The specific toxins mentioned earlier are gating modifiers (Mackinnon *et al.*, 1997), shifting the $V_{1/2ac}$ rather than blocking the pore and therefore may prove unhelpful in elucidating the physiological role.

The slowly-gating high threshold Kv2.2 current

Kv2.2 containing channels mediate the slowly gating sustained current

The antagonist-insensitive (TEA & DTX) sustained current is slowly gating, and as Table 4-1 highlights we have considered all possibilities as to what can mediate this conductance.

Kv1 channels have been ruled out due to insensitivity to dendrotoxins, CP-339, 818 and relative insensitivity to 4-AP (Nguyen *et al.*, 1996; Hopkins, 1998; Coetzee *et al.*, 1999).

Kv3 channels activate too quickly to mediate this current and are ruled out due to insensitivity to low concentrations of TEA (Coetzee *et al.*, 1999).

Kv4 members all mediate A-currents which activate rapidly (Birnbaum *et al.*, 2004), and probably mediate the small A-current discussed earlier.

	Pharmacology		Kinetics		Possibility
 Kv1	DTx-I CP-339,818	X	Delayed rectifiers	~	X
 Kv2	Quinine Block	~	Delayed rectifiers	~	✓
 Kv3	Low [TEA]	X	Too slow	X	X
 Kv4	4-AP	X	Not A-type	X	X
 Kv7	Linopridine	X	Too Fast	X	X
 eag	E4031 Relative Ba ²⁺ insensitive	X	Too fast	X	X
 BK _{Ca}	Low [TEA]	X	Delayed rectifier	~	X
 K _{H3a}	No [Na ⁺] _i , [ATP] _i	X	Inactivates	X	X

Table 4-1 Summary of argument for Kv2

Kv7 members (KCNQ channels) all activate slowly and are sensitive to linopirdine (Robbins, 2001), and their encoding mRNA is not detected (Kharkovets *et al.*, 2000) in the MNTB.

EAG nor ERG mediate the current as it is unaffected by the presence of E4031 (Gessner & Heinemann, 2003).

ELK channels are also unlikely contributors as they are generally open at rest (Gutman *et al.*, 2003), completely blocked by 1mM Ba²⁺ (Engeland *et al.*, 1998; Shi *et al.*,

1998; Zou *et al.*, 2003), and they are not expressed in the superior olivary complex (Kharkovets *et al.*, 2000).

BKCa channels are very sensitive to TEA (Gutman *et al.*, 2003) and calcium-activated currents were minimised by recording in low extracellular calcium with 5 mM internal EGTA and on occasions 100 μ M extracellular Cd²⁺. Additionally they have previously been reported to be absent (Brew & Forsythe, 1995).

Sodium-dependent K⁺ channel (KNa, Slick/Slack) subunit immunolabelling has been reported in the MNTB nucleus (Bhattacharjee *et al.*, 2002; Bhattacharjee *et al.*, 2005). Additionally a recent review has quoted their presence in principal neurons (Kaczmarek *et al.*, 2005). However, on inspection of the data Slick appears to be in small non-principal cells and Slack is clearly absent from the principal neurons and expressed in glial cells. Nevertheless the fact that both are activated by raised [Na]_i and inhibited by [ATP]_i rules these currents out: Our conditions exclude activation since no [Na⁺]_i was present and 2mM [ATP]_i did not block the current (n=3, data not shown). Additionally both Slick and Slack inactivate (Bhattacharjee & Kaczmarek, 2005).

After taking into account this pharmacological and basic biophysical information when we examine Table 4-1 the only remaining possibility is a Kv2 channel. The block by quinine (although reasonably non-specific) also fits with this conclusion (Schmalz *et al.*, 1998). Therefore even without further evidence it is difficult to conceive of anything other than a voltage-gated Kv2 conductance mediating this current.

Consistent with the concept that a Kv2 channel mediates this current, Kv2.2 mRNA was detected at ~30 times higher levels than Kv2.1 (Figure 4-15). The absence of Kv2.1 is consistent with immunohistochemical data that REW Fyffe kindly shared with us. Further to Kv2.2 mRNA being transcribed we also find that Kv2.2 protein is strongly detected with a new anti-Kv2.2 antibody (Figure 4-16 & Figure 4-17) which we have verified. Considering the evidence presented I am confident that a Kv2.2 subunit mediates the slow gating Kv1-Kv3 antagonist-insensitive sustained current.

Kv2 channels

The two members of the Kv2 family (Kv2.1 & Kv2.2) display a high degree of sequence homology (87%) in the first 521 amino acids, but only 24% homology in the rest of their C-termini (Mohapatra & Trimmer, 2006). Both Kv2.1 and Kv2.2 are ubiquitously expressed in the brain (Hwang *et al.*, 1993). Although Kv2 subunits have been identified as major components of delayed rectifier current in several neurons (Baranauskas *et al.*, 1999; Murakoshi & Trimmer, 1999), the physiological roles of Kv2 channels in the brain are still poorly understood when compared to the other Kv subfamilies. Though Kv2 channels are involved in action potential repolarisation in SCG neurons (Malin & Nerbonne, 2002), where action potentials are of much longer in duration than in the MNTB.

Subunit composition

Interestingly Kv2 α -subunits don't appear to form heteromers with each other. (Hwang *et al.*, 1993) reports the expression of both Kv2 subunits in the same cell but notes that they have different subcellular distributions. (Malin & Nerbonne, 2002) also show, with the use of dominant negative subunits, that the Kv2 subunits form distinct currents in native cells and when expressed within the same cell. Our findings in the MNTB indicate that Kv2.2 is present, whilst Kv2.1 is absent, is consistent with their inability to form heteromers.

It is well established that Kv2 subunits form functional channels with members of the electrically silent families (i.e. Kv5, 6, 8 & 9) of which there are a total of 10 genes (Post *et al.*, 1996; Robertson, 1997; Salinas *et al.*, 1997a; Salinas *et al.*, 1997b; Kramer *et al.*, 1998; Kerschensteiner & Stocker, 1999; Ottschytsch *et al.*, 2002; Sano *et al.*, 2002; Ottschytsch *et al.*, 2005). These silent subunits cannot form functional channels by themselves; they require a Kv2 α -subunit in order to form a conducting channel. It has not yet been established whether more than one silent subunit can contribute to a Kv2 heteromer.

The kinetics of the Kv2 containing channels are altered by the inclusion of a silent subunit. The effect not only depends on the identity of the silent subunit but also on the Kv2 subunit e.g. Kv9.1 slows deactivation of Kv2.1 but speeds up Kv2.2's deactivation rate (Salinas *et al.*, 1997b).

Kv9.1 and 9.2 are highly expressed in the same neurons as Kv2 subunits e.g. cerebellar granule and Purkinje neurons (Salinas *et al.*, 1997b). Kv8.1 is also expressed in the cerebellum. However the distribution of the silent subunits in the brain is still poorly understood. There is some evidence that Kv6.1 may be expressed in the MNTB (see figure 4 of, Drewe *et al.*, 1992).

The silent subunits modulate gating properties and pharmacological sensitivity, e.g. Kv2.1/Kv6.1 has a lower sensitivity to TEA compared to a Kv2.1 homomer. Although there is no conclusive evidence for heteromeric Kv2.2 channels in the MNTB, this would explain the channel's lower sensitivity to 4-AP than that reported for homomeric Kv2.2 in *Xenopus* oocytes (Schmalz *et al.*, 1998). It may also explain the channel's insensitivity to recombinant Stromatoxin-1 (reported to be selective for Kv2 subunits, Escoubas *et al.*, 2002), although this may also be explained by the toxin being recombinant.

Subcellular location

Kv2.1 staining shows punctuate labelling first reported by (Hwang *et al.*, 1993), and has been investigated to some depth by several groups (Misonou *et al.*, 2004; Muennich & Fyffe, 2004; O'Connell *et al.*, 2006). It appears that Kv2.1 is inserted into fluid microdomains (i.e. they are restricted to a certain area but can move within it), and when dephosphorylated they can spread out in the membrane (O'Connell *et al.*, 2006).

Kv2.2 is much less studied than Kv2.1, probably because it lacks the interesting punctuate localisation, rather Kv2.2 is dispersed in the membrane (Mohapatra & Trimmer, 2006).

Kv2.2 is found in neuronal processes (including axons) of inhibitory neurons in both the hippocampus and cortex as found by (Hwang *et al.*, 1993) using an antibody they produced. The observation that Kv2.2 is in axons of inhibitory neurons is intriguing, as in

the MNTB (an inhibitory neuron) there is intense labelling of Kv2.2 in the initial segment of the axon (Figure 4-17 & Figure 4-18) and possibly in segments along the axon. This commonality of location suggests that Kv2.2 may serve a similar function in other inhibitory neurons (which are also typically fast spiking). It is also interesting that Kv2.2 is located in the same region as the Nav channels (Leao *et al.*, 2005a), on which they seem to exert their affect.

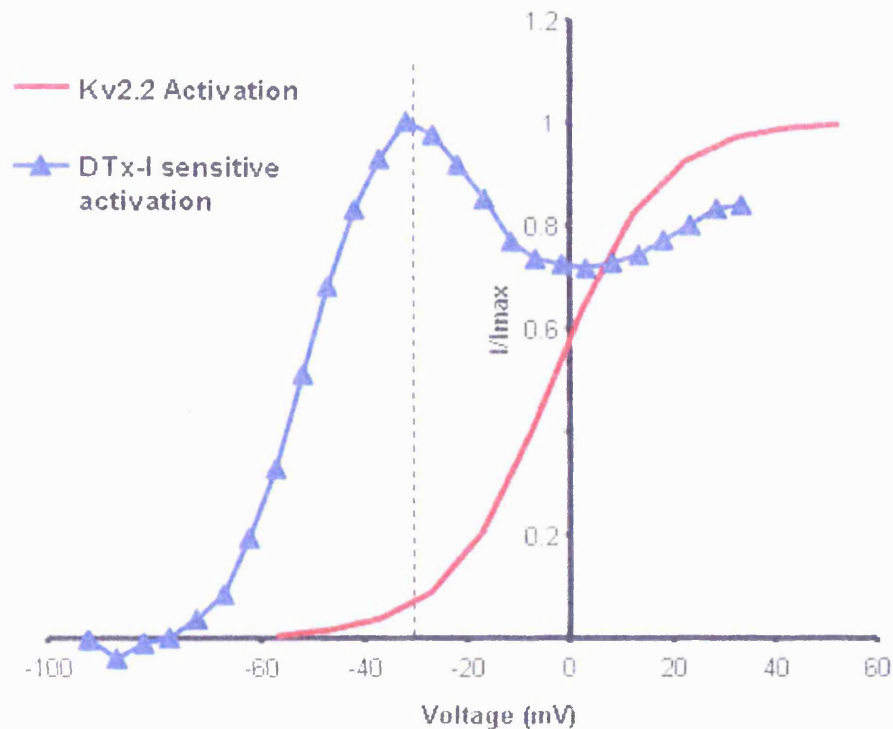


Figure 4-27 The subcellular location of Kv2.2 influences the apparent activation of Kv1: Plot of the GHK normalised Kv1 activation from Figure 3-11 (blue) along with kv2.2's activation (Figure 4-9 B) shows that the kink in the DTx-I sensitive activation corresponds to Kv2.2 activating (dashed line).

The localisation of Kv2.2 to the initial segment of the axon was predicted (see discussion of chapter 3). The Kv1 channels known to be in the same location (Dodson *et al.*, 2002), has a kink in its activation curve (obtained by subtraction of the DTx sensitive current, Figure 3-11), and it was predicted that this was due to the "other" (i.e. Kv2.2) current

being in the same location. Figure 4-27 shows that the activation of Kv2.2 does indeed correspond to the development of the kink in the Kv1 curve (dashed line).

A physiological role of Kv2.2 channels in the MNTB

The rate and range of activation of the Kv2.2-mediated current in MNTB neurons implies that it makes little contribution to single action potentials. Studies of Kv2 in other native neurons do indicate a role in AP repolarisation (Blaine & Ribera, 2001; Malin & Nerbonne, 2002). However it is important to appreciate that action potential durations in MNTB neurons, with half-widths of <0.5ms, are several fold faster than those in the above studies (which have half-widths of 2.5-3.5ms). Such long action potentials would permit greater activation of Kv2 channels, hence contributing more to repolarisation.

The large Kv2.2 current measured under voltage-clamp in MNTB neurons belies its small functional contribution and subtle physiological effects. The slow deactivation rate allows for cumulative activation and I show that the inter-spike potential exhibits a frequency-dependent hyperpolarisation, which is only explained by a cumulative increase in a potassium conductance. This hyperpolarisation cannot be mediated by the Kv3 or Kv1 channels as they both deactivate rapidly (Brew & Forsythe, 1995) and Kv3 activity follows the AP waveform, whereas Kv1s reach steady-state after the second stimulus (but may contribute at very high frequencies i.e. 600 Hz, Klug & Trussell, 2006). Also any electrogenic contributions from Na/K ATPase were avoided due to the exclusion of ATP from the patch pipettes.

This frequency or activity-dependent role for Kv2 in the MNTB is consistent with evidence for the physiological role of *Shab* (Kv2 equivalent) currents at the *Drosophila* neuromuscular junction where *Shab* activity becomes apparent only with high frequency stimulation and not with single stimulations (Ueda & Wu, 2006).

The affect of the Kv2.2 mediated cumulative hyperpolarisation

The cumulative activation of this Kv2.2 containing conductance will decrease the input resistance after each spike; in itself this will lower the amount of depolarisation subsequent EPSCs will cause. Even though the MNTB has extremely brief EPSCs, the resultant EPSPs would still be expected to summate at high frequencies (Magee, 2000). This does not occur, and can only be explained by a parallel increase in a K⁺ conductance throughout higher frequency trains, since any other ion would add to the depolarisation.

In addition to countering summation, the Kv2.2 conductance actually causes a small hyperpolarisation of the inter-spike potential. These small changes in the voltage of the inter-spike have a large effect on the available Nav current, since they fall on the steepest part of the Nav inactivation curve (Figure 4-22 B). I demonstrate that in a 200Hz train INa is able to increase by ~17% and crucially reaches steady state, when the inter-spike potential follows the cumulative hyperpolarisation observed in physiology (Figure 4-24 C & D, black).

Furthermore I observed a severe decline in INa when mild summation of the inter-spike potential was simulated (4.5mV by the 60th spike), a condition which is likely to occur in the absence of Kv2.2 (Figure 4-24 A & D, green).

A significant decline in INa still occurred when the inter-spike potential was maintained constant (Figure 4-24 B & D, blue) demonstrating that accumulation of Nav inactivation would occur. These data are consistent with a slow component of recovery from INa inactivation as found by (Leao *et al.*, 2005a). A cumulative decline in INa will lead to eventual spike failure, as has been observed in pyramidal neurons in the hippocampus (Jung *et al.*, 1997). Therefore in MNTB neurons the Kv2.2-mediated hyperpolarisation sustains action potential firing by preventing such cumulative inactivation during high frequencies. This hyperpolarisation is required, since if the Kv2.2 conductance was

“tuned” to merely balance synaptic summation, then Nav channels would still accumulate in their inactivated state. It is also worth noting that the Kv2.2 channels are largely localised to the initial segment of the axon (Figure 4-18), close to the Nav channels (Leao *et al.*, 2005a) upon which they are exerting an affect.

Developmental changes

I show that in P10-14 animals Kv2.2 is already a major component of the outward K⁺ current, but the current magnitude further increases with development. By P18-19 the current magnitude has more than doubled. The MNTB neuron's ability to fire at higher frequencies also increases with development (Taschenberger & von Gersdorff, 2000). This happens through a number of mechanisms, many of which are presynaptic, although the postsynaptic EPSC also speeds up (Taschenberger & von Gersdorff, 2000). It is not too surprising that Kv2.2 also increases in parallel with these other changes, as part of a broader adaptation to prolonged high frequency firing.

It would be interesting to examine whether this Kv2.2 current is present in more immature neurons i.e. P5 which are unable to follow high frequency trains (Taschenberger & von Gersdorff, 2000).

Tonotopic gradient

Previous studies of tail currents in MNTB neurons of rat have suggested the presence of a third conductance in addition to Kv1 and Kv3 (Brew & Forsythe, 1995). Along with the description of the tonotopic gradients of Kv1 and Kv3 currents (Brew & Forsythe, 2005) also finds a medio-lateral gradient for the third conductance, with greater current magnitudes in the lateral versus the medial end. This gradient is identical to that reported here for the Kv2.2 conductance (Figure 4-26).

The data of Figure 4-26 was not normalised for cell capacitance as the only recorded estimate of capacitance was that from the dial of the amplifier. A more accurate method would be to record a -5mV uncompensated step, which would allow fitting of the capacitance transients and a more accurate estimate. (Brew & Forsythe, 2005) used this method and found no significant gradient across the MNTB in the capacitance associated with the cell soma. Therefore, I felt justified in not normalising the data for cell capacitance.

The observed lateral to medial gradient is puzzling, as it is the neurons in the medial end that fire at higher frequencies (owing to them encoding higher frequency sounds). One would expect that they would also require higher levels of Kv2 to maintain high firing rates.

One plausible explanation is that the high frequency neurons of the medial end which tend to project to the LSO (encoding level differences) only need to encode brief bursts of action potentials. Conversely the lateral neurons, which tend to project to the MSO (encoding timing differences), need to maintain accurate following of the lower frequency sound, in order to compare phase differences. This may then require prolonged levels of high firing rates, and thus more Kv2.2.

Chapter 5 – Results 3

The non voltage-gated K⁺ “leak” currents of the MNTB

The previous chapters characterised the voltage-gated K⁺ channels present in the mouse MNTB. In certain parts of the previous chapter it was alluded that there was an additional K⁺ mediated “leak” current (see Figure 4-13 & Figure 4-19). The leak current is the focus of this chapter.

This chapter contains a detailed discussion on how to study non-voltage gated “leak” channels, then goes on to examine the leak present in the MNTB and examines its physiological role, finally it has a preliminary look at what channels might mediate this current.

Methods

The methods used in this chapter are similar to those described in chapter 2, except for the following modifications.

1. For major ionic changes an agar bridge was used in place of the bath earth. The Agar bridge was constructed by heating agar containing 1M KCl to a liquid. U shaped glass capillaries were dropped into the liquid agar. The heat evacuated the air from the glass replacing it with agar. The capillaries were allowed to cool and set. For recording, an agar filled glass filament was placed so that one end was in the bath and the other in a sealed pot of 1M KCl which contained the bath earth.
2. For the ion substitutions, Na^+ was replaced with K^+ and gluconate was used as a substitute for Cl^- .
3. Immediately prior to use, volatile anaesthetics were dissolved in the appropriate aCSF, by vortexing in a glass container. The resultant solution was then injected (using a glass syringe) directly into the bath via short Teflon tubing. During injection the inlet of the peristaltic pump was turned off and the level of the bath was kept constant. 5mls of the anaesthetic containing aCSF was injected which is greater than twice the bath volume.
4. For pH changes the NaHCO_3 buffer was replaced with 10mM HEPES, adjusted to the desired pH by titration with NaOH and made up to ~310 mOsM with sucrose. This aCSF was constantly bubbled with O_2 instead of carbogen.

How to study leak

With patch-clamp recording the aim is to measure the current flowing through the membrane ion channels. In order to do this a glass pipette is “sealed” against the membrane and the membrane underneath the electrode is ruptured to obtain electrical access to the cell. The seal between the glass and the pipette is ideally of high resistance ($\sim 10\text{ G}\Omega$). However in brain slice recordings, seal resistances of this level are difficult to achieve due to cellular debris and the membrane being “dirty”. So some of the current flowing through the pipette is not membrane current, rather it is due to current flowing through the space between the glass and the pipette i.e. seal leak (Figure 5-1). This seal leak is linear and reverses close to 0 mV, since it is non-specific (i.e. carried by all ions) and the pipette was “zeroed” prior to sealing.

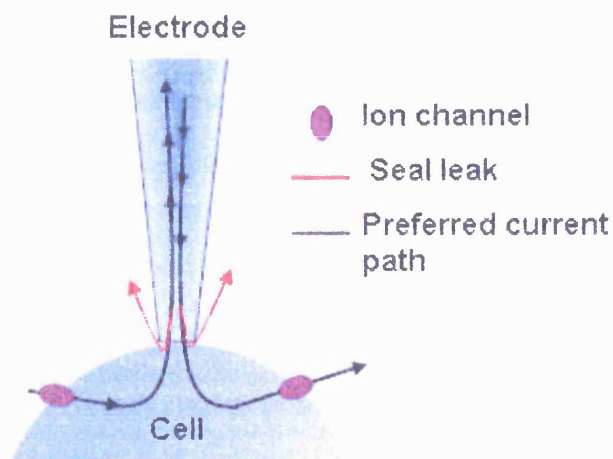


Figure 5-1 The problem with seal leak: Schematic representing the current paths in patch clamp recording.

In general this seal leak is not problematic as the current flowing through it is usually negligible compared to that flowing through the membrane. However, it will become problematic when the aim is the study of small amplitude currents. It therefore requires careful consideration.

On stepping to new voltages it has long been appreciated that there is an instantaneous current component, which must be attributable to a channel that is already open at rest. This current component has also been termed leak, or background conductance. When studying voltage gated channels attempts are usually made to eliminate this passive "leak" conductance. Since I wanted to study the ionic membrane leak, which is generally of small amplitude, it was necessary to consider these subtraction methods, which are detailed below.

1. A linear portion of the current voltage relationship is chosen (usually between -100 and -70mV, if ZD7288 is included to block I_h) where there are few voltage-gated channels active; this linear portion is then extrapolated over the entire voltage range and subtracted from the data.

2. The more common P/N method used to subtract leak (often automatically), by giving small, scaled pulses (usually in the opposite polarity to the voltage waveform). Similar to method 1, it then extrapolates the passive conductance over the entire voltage range, subtracting it from the data.

Method 2 has the advantage over method 1 in that it also subtracts the capacitive transients, which do indeed scale linearly. However one danger when using pClamp is that method 2 adjusts the data online and only saves the modified data (not the raw data).

As already mentioned in chapter 4, a background current permeable to a single ion does not have a linear I/V if the permeable ion is asymmetrical across the membrane; rather it is described by the GHK current equation (Equation 2-9). However seal leak is linear because it is non-specific (i.e. carried by all ions). The impact of the leak subtraction methods is illustrated in Figure 5-2 A, where the black I/V is the raw data recorded from an MNTB neuron. When the traditional leak subtraction methods are employed it results in subtraction of the blue line (Figure 5-2 B) resulting in the blue I/V in Figure 5-2 A.

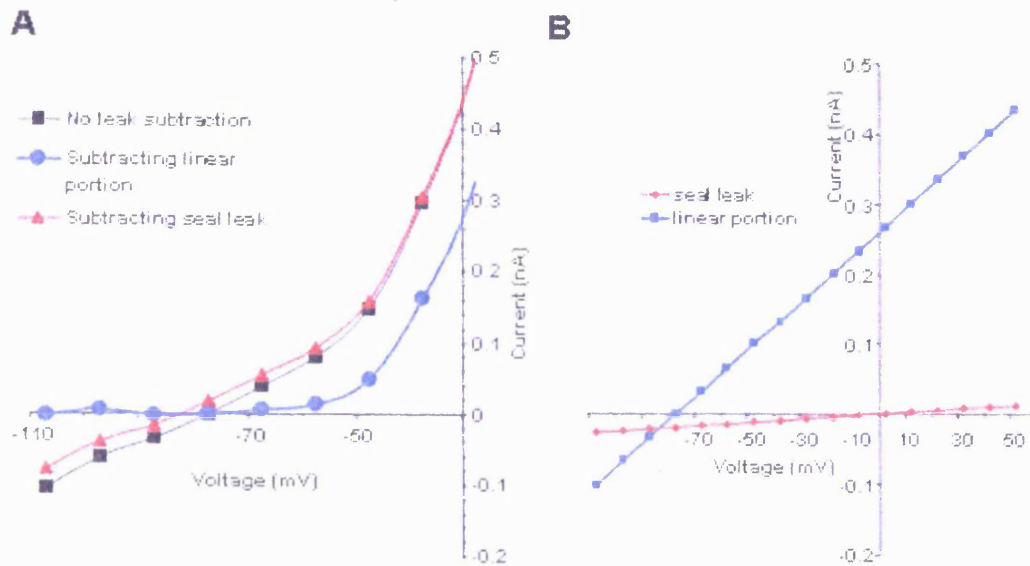


Figure 5-2 Leak subtraction methods: **A)** *Black*, example of a cell that had a 4GΩ seal resistance prior to going whole cell, without any leak subtraction performed. *Red*, the same cell with leak subtracted according to what would flow across the seal resistance of 4GΩ. *Blue*, the same cell with leak subtraction estimated from the linear portion of the I/V (i.e. -100 to -70mV), this method is equivalent to the commonly used P/N leak subtraction method. **B)** Plot of the leak that was subtracted in A. *Blue*, P/N subtracted leak. *Red*, subtraction of the calculated seal leak. N.B data recorded in the presence of 3mM TEA, 10nM DTx-I and 10μM ZD 7288.

The blue line is obviously removing more than just the seal leak (though it does not remove the entire membrane ionic leak, see Figure 4-10 C). This suggests that existing methods are unsatisfactory. A better method would be to subtract only the seal leak. The seal leak can be calculated from Equation 5-1. However, the seal resistance can only be accurately measured in the on cell mode, prior to going whole cell. If we assume that the seal resistance remains unchanged after going whole cell, the leak through the seal can be subtracted according to Equation 5-1, as shown in Figure 5-2 A & B (red).

$$I_m = I_p - \frac{V_p}{R_{seal}}$$

Equation 5-1 Where I_m is the membrane ionic current, I_p is the current measured by the pipette, V_p is the pipette voltage and R_{seal} is the seal resistance.

However it is unlikely that the seal resistance will remain constant since the act of going whole cell is purposefully disruptive; so it is possible that the seal resistance would differ from the initial on cell value.

Is it feasible to estimate the seal resistance after going whole cell? We can assume that the endogenous leak reverses at E_K and hence, at E_K the current flow through the membrane is zero. It is clear that the seal leak reverses at 0mV, so subtraction of a linear current that passes through 0mV and E_K will only remove the current through the seal and leave the membrane current intact.

If this method is going to be implemented there are several caveats to consider: 1. I_h must be blocked and 2. There must be minimal contribution from a Cl^- conductance i.e. K^+ is the major ion contributing to current flow.

I_h was routinely blocked by 10 μ M ZD 7288 so will not contribute at negative voltages. To check how much Cl^- contributed to the ionic current flow, to do this I shifted the Cl^- reversal potential from -35mV to +36mV (calculated from Equation 2-6). An agar bridge was used in place of the bath electrode to eliminate problems with junction potentials in the bath (Neher, 1992), and all voltages were adjusted for the appropriate junction potentials.

Perfusion of the low Cl^- solution would cause the development of an inward current at negative potentials, if a Cl^- mediated leak was present. Voltage-gated Cl^- channels (e.g. CLC-1) strongly outwardly rectify, which is based on E_d (Jow *et al.*, 2004; Jentsch *et al.*, 2005). Therefore, if a CLC conductance were present, washing on the low Cl^- solution would result in inhibition of the current positive to -35mV (the E_{Cl} in control).

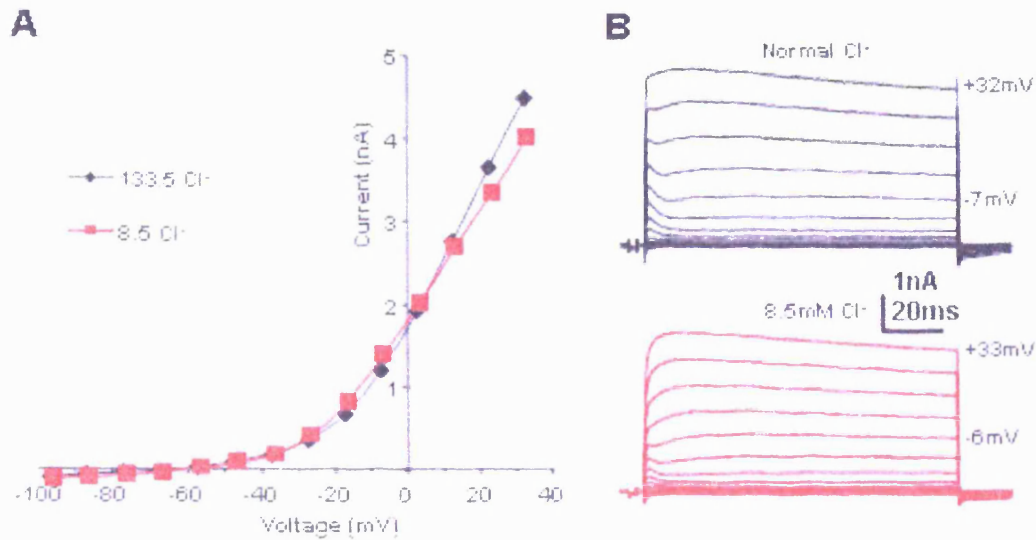


Figure 5-3 The MNTB lacks a Cl⁻ current: **A)** Current voltage relationship for a cell in normal chloride (black) and lowered extracellular chloride (8.5mM, red). This corresponds to a +73mV change in E_{Cl} . **B)** Example current traces from the I/V in A. single example representing an n of 3. N.B. all data recorded in the presence of 3mM TEA, 10nM DTx-I.

As Figure 5-3 A shows no noticeable effect was seen on changing the external Cl⁻ concentration (n=3). This absence of a Cl⁻ leak or a CLC channel is consistent with MNTB cell bodies having low internal Cl⁻ concentrations (Price & Trussell, 2006) as if they had a Cl⁻ leak it would result in depletion of this gradient.

In the conditions used, there is no I_h current and no Cl⁻ current at negative voltages, so at E_K the measured conductance must be the sum of the cell membrane conductance and the seal conductance. Hence, any displacement from zero at E_K must reflect current flow through the seal leak, thus giving a measure of the seal resistance which can then be subtracted according to Equation 5-1. Unless otherwise stated, the data in the rest of this chapter has been "seal leak" subtracted by this method.

The K⁺ leak in the MNTB

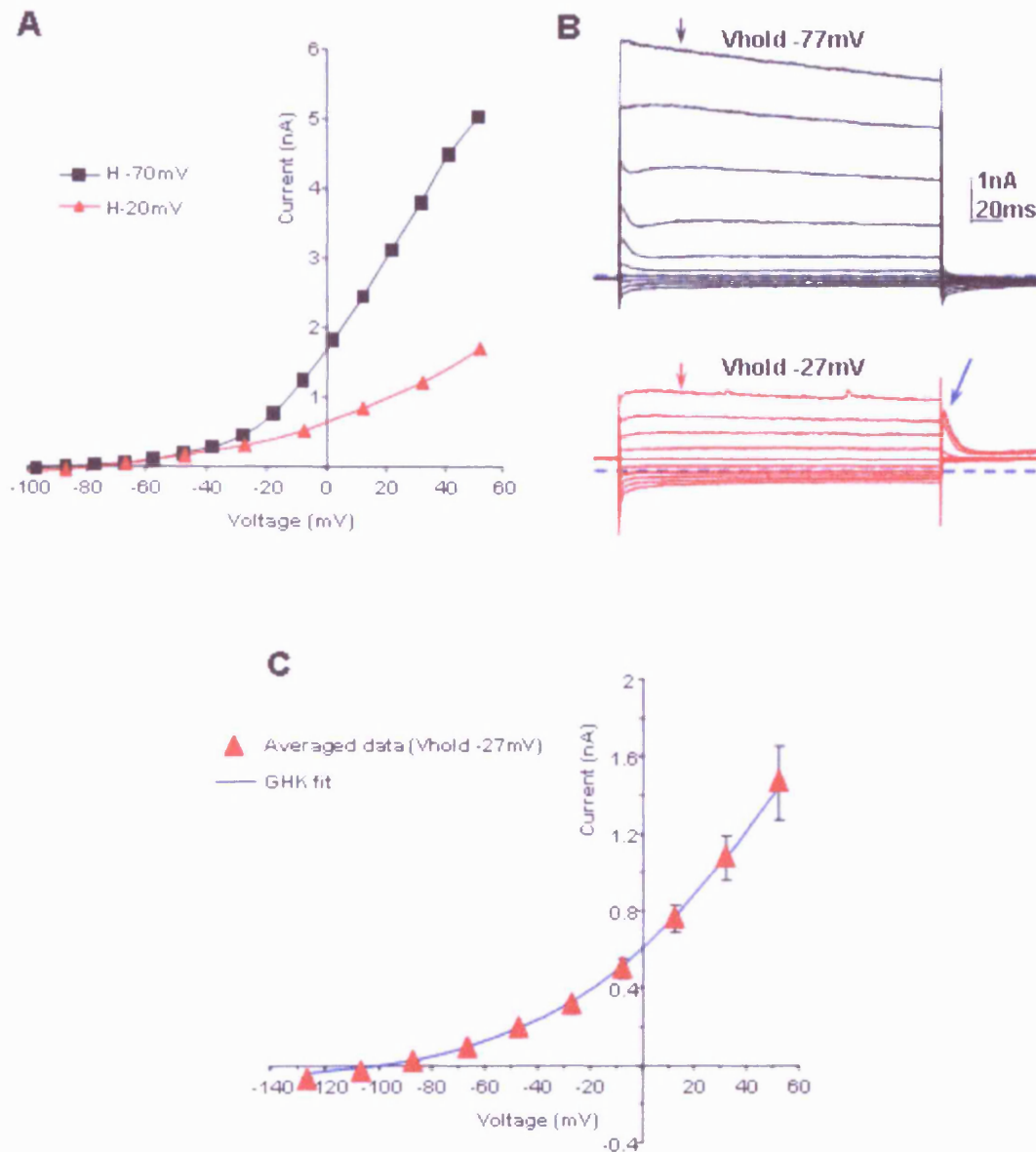


Figure 5-4 K⁺ mediated leak in the MNTB: **A)** I/V from a single cell in the presence of 3mM TEA & 10nM DTx-I from a holding potential of -77mV (black) and with the other currents inactivated by holding at -27mV (red). **B)** Current traces for the example cell in A, current in the I/V was plotted at the time point of the arrows. Note the recovery of the A-current with negative steps (blue arrow). **C)** Averaged I/V for 8 cells with Kv channels inactivated (red triangles), fit with the GHK current equation (blue line).

There are no known selective antagonists for any of the K_{2p} channels. Therefore to establish how much current is mediated by these channels in the MNTB I isolated the K⁺ leak by removing all the other K_v currents.

With K_v3 and K_v1 channels blocked by 3mM TEA & 10nM DTx-I the current measured 40 ms into a voltage step consists of the K_v2.2 current and the leak current Figure 5-4 A (black squares). To establish how much leak is in the MNTB I inactivated the K_v2 current by holding the membrane at -27mV for >10s prior to each voltage step. With the K_v2 current inactivated by holding at -27mV an instantaneous current is predominant (Figure 5-4 A & B). Averaged data from 8 MNTB cells with the K_v2 current inactivated is shown in Figure 5-4 C (red triangles), this data is well fit by the GHK current equation (blue line). The estimated seal resistances for the data in Figure 5-4 was 957 ±86 MΩ (n=8).

To determine whether this instantaneous current, active at negative voltages, has any voltage-dependence of activation, I changed the concentration of external K⁺ so that it was symmetrical across the membrane. An agar bridge was used in place of the bath earth for the [K⁺]_{out} changes. To limit interference caused from transmitter release from the surrounding presynaptic terminals and others cells, ligand gated ion channels were blocked with 40μM 6-cyano-7-nitroquinoxaline-2, 3-dione (CNQX), 10μM bicuculline and 1μM strychnine. 3mM TEA & 10nM DTx-I was also included to block K_v3 and K_v1 channels. Cells were held at -77mV under these pharmacological conditions. Of the eight cells tested in symmetrical potassium, all reversed at zero, indicating that K⁺ is the major ion carrying current in these conditions. In all eight cells a “kink” developed which was due to the K_v2 conductance (similar to the example shown in Figure 5-6 A). The current at negative voltages (i.e. -100 to -70mV) always became linear and would reverse at zero if extrapolated (n=8, data not shown).

Two cells were also held at -25mV to inactivate the K_v2 current, from this potential voltage ramps were given (positive to negative). Application of symmetrical K⁺ resulted in I/V becoming linear and reversing at 0mV (Figure 5-5 B). This indicates that the leak current is selective for K⁺ and is non voltage-gated. Since the I/V for a K_v

channel in symmetrical K^+ would display a distinct inward kink corresponding to the K_v channels opening, due to increasing the membrane conductance (see Figure 5-5 A).

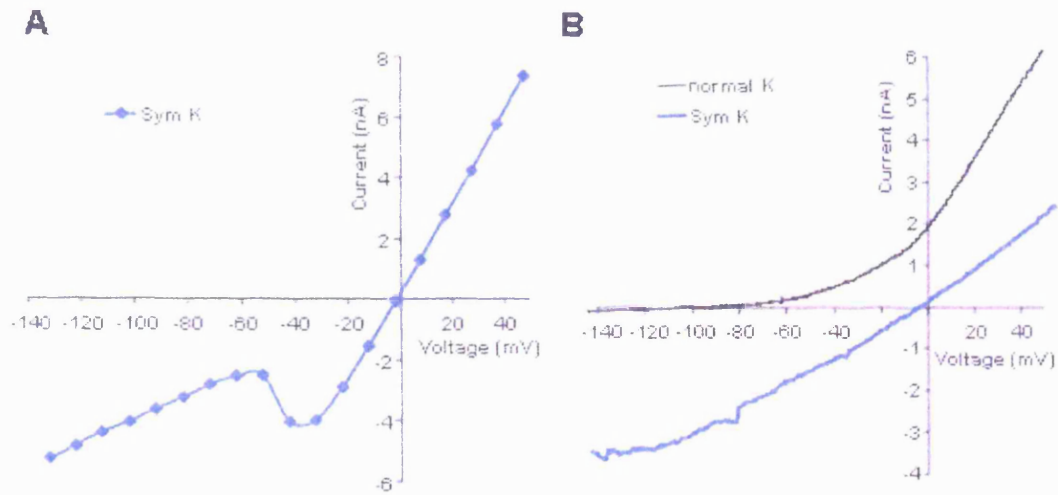


Figure 5-5 The K^+ leak is non voltage-gated: **A)** I/V for a different cell from a holding potential of -77mV without any K^+ channel antagonists, shows an expected kink as the K_v channels open. (N.B. all data recorded in the presence of $1\mu\text{M}$ TTx, $40\mu\text{M}$ CNQX, $10\mu\text{M}$ bicuculline, $1\mu\text{M}$ strychnine, $100\mu\text{M}$ CdCl). **B)** I/V constructed from a ramp for an MNTB neuron from a holding potential of -27mV in the presence of K_v1 and K_v3 antagonists (3mM TEA, 10nM DTx-I, black) and in the presence of symmetrical K^+ (blue) single example of a n of 2.

The fact that this current activates instantaneously (Figure 5-4 B, red), is fit with the GHK current equation (Figure 5-4 C) and is non voltage gated (and therefore is open at rest, Figure 5-5 A) strongly implies mediation by a K_{2p} channel.

At the $+13\text{mV}$ (around the peak of the action potential) there is $760 \pm 72\text{pA}$ ($n=8$) of K^+ leak. This implies that leak will contribute to action potential repolarisation. Additionally as the K_{2p} current is open at rest, it is likely to be involved in setting the resting membrane potential.

K2p channels set the resting membrane potential

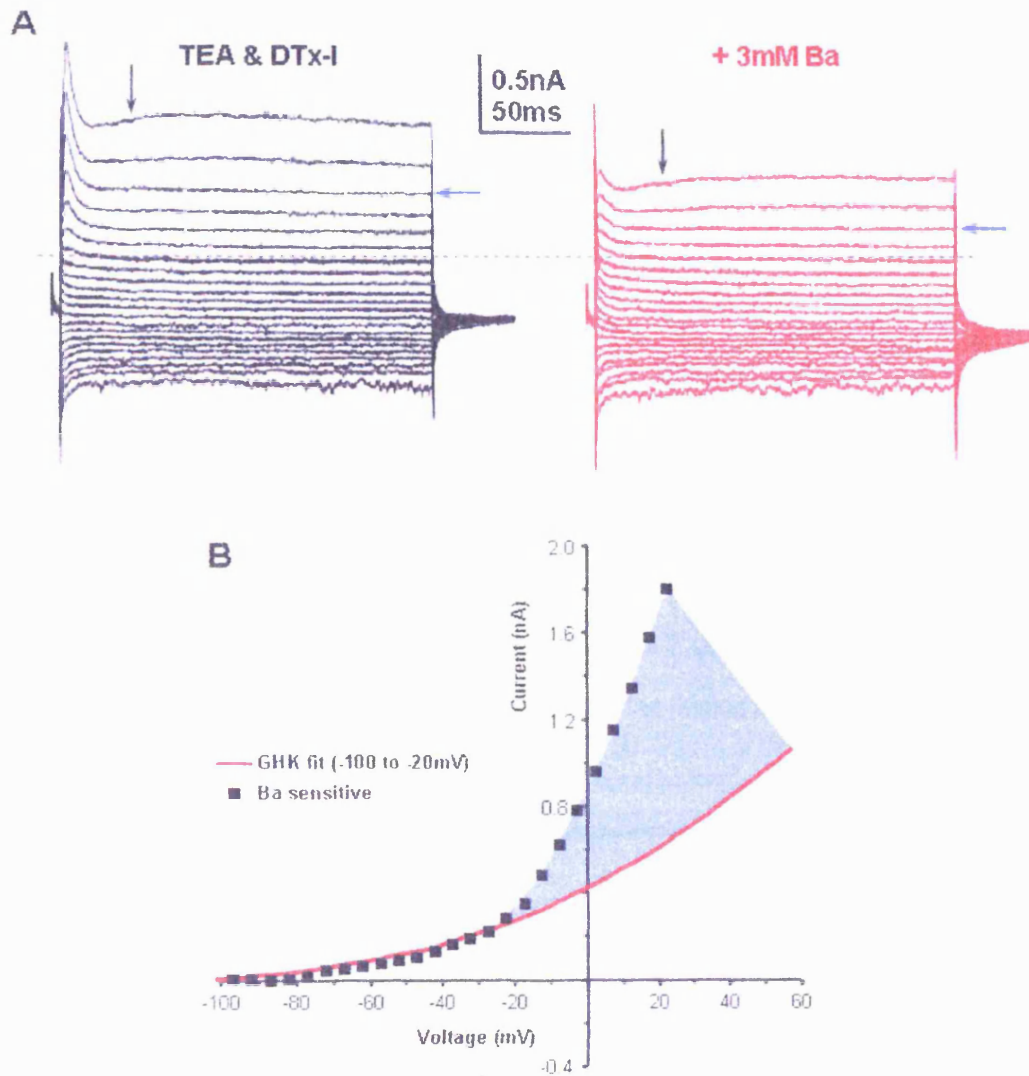


Figure 5-6 Ba^{2+} blocks a substantial portion of the K^+ leak: **A**) Example traces for the voltage range of -100mV to -7mV , in the presence of 3mM TEA, 10nM DTx-I, $100\mu\text{M}$ CdCl & 2mM CsCl (black) and with the addition of 3mM BaCl₂ (red). Dashed line represents zero current. Black arrows are time point of current measurement. Blue arrows indicate current at -20mV . **B**) The averaged Ba^{2+} sensitive current from four neurons (black squares), fit with the GHK current equation (red line) over the voltage range of -100mV to -20mV and extrapolated to the positive voltages. Shaded blue area represents activation of the Kv2.2 channel.

In the presence of 3mM TEA and 10nM DTx-I, application of 3mM Ba²⁺ resulted in a 48.3 ±3.6% reduction in the measured current 40ms into a -27mV step (n=4, P=0.04). This is likely due to block of the K2p current, as the majority of K2p channels are sensitive to mM concentrations of Ba²⁺ (O'Connell *et al.*, 2002; Goldstein *et al.*, 2005). The Ba²⁺ sensitive current from 4 neurons was averaged and is plotted in Figure 5-6 B (black squares). Note that the Kv2 current was not inactivated in these experiments. The Ba²⁺ sensitive current over the voltage range of -100mV to -20mV was well fit by the GHK current equation (red line, Figure 5-6 B). The GHK fit was then extrapolated to +60mV to give a clear idea of the Ba²⁺ sensitive leak current over the full voltage range. Note the Kv2 current is also blocked by 3mM Ba²⁺ (shaded blue area). Ba²⁺ appears to block a large proportion of the K⁺ mediated leak, compare Figure 5-4 C to Figure 5-6 B.

As the K2p channels in the MNTB appear to be largely blocked by 3mM Ba²⁺, this allowed me to examine the role they play in setting the resting membrane potential. This was done by recording in I=0 mode on the amplifier (as in this mode it does not draw or pass any current) to allow accurate measurements of the resting membrane potential.

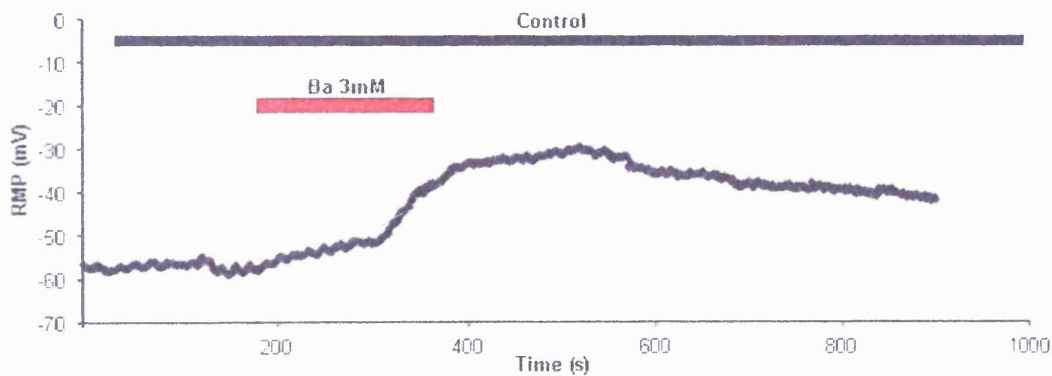


Figure 5-7 Block of the K⁺ leak depletes the membrane potential: Control conditions block Kv3, Kv1, I_h, Kir, Nav, Cav channels with 3mM TEA, 10nM DTx-I, 2mM CsCl, 100µM TTx & 100µM CdCl. Application of 3mM Ba²⁺ results in a 16.6 ±3.2mV depolarisation (n=4).

Cells were then perfused with 3mM TEA, 10nM DTx-I, 100µM CdCl, 1 µM TTx and 2mM CsCl. This cocktail of drugs will block Kv3, Kv1, Cav, Nav, I_h and any Kir channels present. Under these conditions the resting membrane potential was -64 ±6.8mV (n=4).

Subsequent perfusion of 3mM Ba²⁺ resulted in depolarisation of the membrane potential by 16.6 ± 3.2mV (Figure 5-7, n=4, P=0.01). The membrane potential failed to run down completely, which is likely explained by the Kv2 channels being partially unblocked and then activated as the membrane potential depolarises towards their activation range.

Which K2p channels mediate the K⁺ leak in the MNTB

To try to elucidate which K2p subunits underlie the K⁺ leak in the MNTB, I applied 1mM lidocaine, which resulted in partial block of the Kv2 current, but had no effect on the current more negative than -20mV (n=4, data not shown). On changing the external pH from pH7.4 to pH 8.5 followed by a change to pH 6.2 no effect was seen on the leak current (n=4, data not shown). This insensitivity to lidocaine rules out mediation by TASK-1 (Kindler *et al.*, 1999), TASK-2 (Reyes *et al.*, 1998) and TASK-3 (Kim *et al.*, 2000), which is consistent with the currents insensitivity to pH.

Several of the K2p channels are potentiated by volatile anaesthetics i.e. TREK 1 & 2, TRAAK and TASK 1-3, while some are inhibited i.e. THIK 1 & 2 (O'Connell *et al.*, 2002; Patel & Lazdunski, 2004). To assess the influence of volatile anaesthetics on the K⁺ mediated leak, 3mM TEA, 10nM DTx-I, and 100µM quinine was included in the aCSF to block Kv3, Kv1 and Kv2 channels respectively. Quinine was used here as these experiments were performed prior to understanding the ability to inactivate the Kv2 channel. A solution of 10mM halothane dissolved in aCSF was applied directly into the bath; such a high concentration was used as we were unsure how much would evaporate before reaching the slice. Perfusion of this halothane aCSF resulted in potentiation of the current evoked from 200ms voltage ramps from -100 to +50mV. The potentiation measured at 0mV was 71 ±18.3% (Figure 5-8 A, n=4, P=0.04). Chloroform dissolved in aCSF at 10mM also resulted in a similar 69.4 ±18.3% (n=3) potentiation of the current measured at 0mV (Figure 5-8 B).

Perfusion of aCSF had no effect on the current in the presence of 3mM TEA & 10nM DTx-I (Figure 5-8 B, n=2), showing that the method of delivery was not contaminating the result.

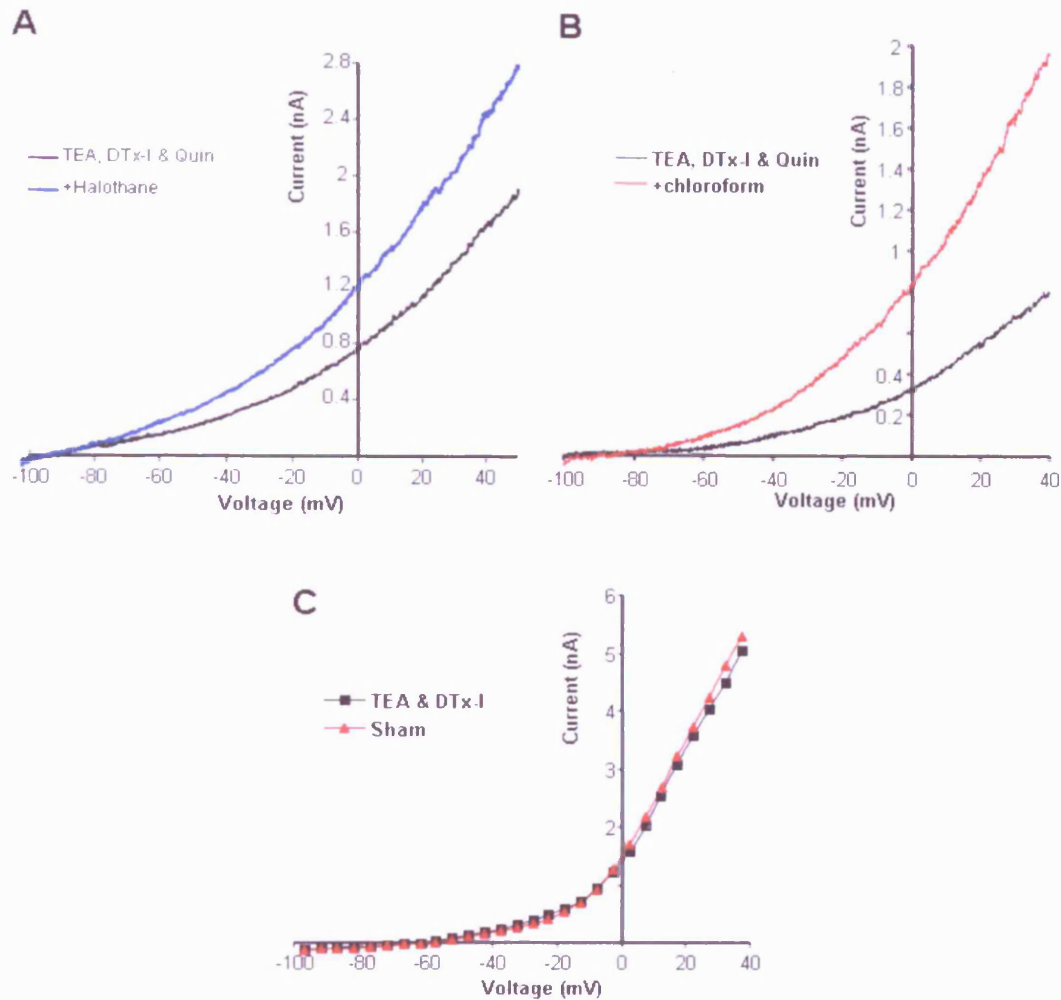


Figure 5-8 Volatile anaesthetics potentiate the quinine insensitive K^+ leak: **A)** ≤ 10 mM halothane delivered directly to the bath potentiates the quinine insensitive K^+ leak by $71 \pm 18.3\%$ at 0mV (n=4). **B)** ≤ 5 mM Chloroform delivered directly to the bath potentiates the quinine insensitive current by $69.4 \pm 18.3\%$ at 0mV (n=3). **C)** The delivery method has no effect on the measured currents (leak subtraction was not performed on the data in C).

The data shown in Figure 5-8 A & B has been leak subtracted as described previously. The % potentiation was measured at 0mV, as at this voltage the data remains unchanged with leak subtraction since this is the seal leak reversal potential (see Figure

5-2). In all anaesthetic applications the estimated seal resistance deteriorated from control conditions. In control the average R_{seal} was estimated to be $1380\text{M}\Omega$, whereas in the presence of anaesthetic this fell to $354\text{M}\Omega$. This deterioration in the seal is likely due to the effects on lipid fluidity caused by high concentrations of volatile anaesthetics (Reyes & Latorre, 1979) as used here. The deterioration is unlikely to contribute to the observed potentiation which was measured at 0mV , since non-selective leak will reverse at zero.

The potentiation by halothane rules out THIK channels mediating the K^+ leak (Rajan *et al.*, 2001). Therefore considering lidocaine had no effect and the current was potentiated by both chloroform and halothane, possible candidates include TREK-1 and TREK-2. TWIK is also a possibility, however little is known about its sensitivity to anaesthetics due to problems with expression, which have only recently been elucidated (Sindhu *et al.*, 2005). Interestingly high levels of TWIK have recently been reported in the auditory pathway (Chen & Davis, 2006; Holt *et al.*, 2006) including the MNTB (Kaczmarek *et al.*, 2005).

Discussion

This chapter has dealt with the non-voltage gated K^+ channels in the MNTB. These were the most difficult experiments to conduct and interpret, but the results do provide significant new insights into the leak conductance. To study the leak an appropriate method for subtracting the seal leak was developed. The magnitude of the leak current has been assessed and it has been shown that it sets the resting membrane potential. Attempts have been made to establish the channel responsible for mediating the leak.

K2p channels

A molecular correlate of the background conductance of neurons has only been identified in the last decade, the K2p family (Goldstein *et al.*, 1996). K2p channels mediate a K^+ selective "leak" in that they are active at rest (Goldstein *et al.*, 2001). Although K2p channels don't possess an intrinsic "gating domain" their open probability is modulated by many physiological and exogenous substances e.g. pH (Berg *et al.*, 2004), small ubiquitin modulating protein (SUMO, Sindhu *et al.*, 2005), mechanical stretch (Maingret *et al.*, 1999), volatile anaesthetics (O'Connell *et al.*, 2002), local anaesthetics (Kindler *et al.*, 1999) and by various metabotropic receptor pathways (Bushell *et al.*, 2002).

Although K2p channels were discovered over 10 years ago, their contribution to physiology is poorly understood, with the exception of contributing to the resting membrane potential (Larkman & Perkins, 2005; Meuth *et al.*, 2006).

The K2p current in the MNTB

As Figure 5-4 C shows there is a K^+ selective leak current in the MNTB. This current appears to activate instantaneously with voltage steps (Figure 5-4 B, red) and its reversal potential is determined by E_K (Figure 5-5 A). Previously the contribution from leak to

action potential repolarisation has been underestimated, as shown here at the peak of the action potential there is ~0.8nA of K⁺ current which is active instantly, in comparison to the 1.5nA of Kv1 current activated as shown by (Klug & Trussell, 2006). As the K2p channels are open at rest they also contribute to the resting membrane potential as shown in Figure 5-7. Activity seems to be important for the correct expression of K2p channels, as when peripheral deafness is induced the K2p channel expression falls off dramatically in the cochlear nucleus (Holt *et al.*, 2006). It remains to be determined whether this is also the case in the MNTB.

Subunit composition

TWIK-1 mRNA is highly expressed in the auditory pathway (Chen & Davis, 2006; Holt *et al.*, 2006) and the MNTB (Kaczmarek *et al.*, 2005), which implies that it is likely functionally expressed. Although TWIK-1 mRNA levels are the highest of the K2p channels that have been assessed, it does not mean they mediate the functional current. As was seen for Kv2.2, whose mRNA level is ~1/10 of Kv3.1 (Figure 4-15) Kv2.2 actually has a larger functional current. TWIK-1 can be silenced by sumoylation (Sindhu *et al.*, 2005). Small ubiquitin-like modifier (SUMO) the enzyme responsible for sumoylation has been reported to be highly expressed in the MNTB (H. Chen, 2005). The potentiation by volatile anaesthetics (Figure 5-8) is consistent with mediation by a TREK channel (Franks & Honore, 2004). However the data does not exclude TWIK as the affects of volatile anaesthetics on this channel are unknown.

Preliminary work using RT PCR on the twin pore subunits has been done but not included in this thesis. TWIK-1 shows the highest level of expression and TREK-2 is also detectable. Although only preliminary this data is consistent with previous reports and the possibility of the current being TWIK or TREK.

In other neurons a heterogenous population of K2p channels contribute to the K⁺ mediated leak e.g. in cerebellar granule neurons at least 4 distinct channels contribute

(Han *et al.*, 2002; Aller *et al.*, 2005). Therefore it is possible that in the MNTB the leak current is mediated by TWIK-1, TREK-1 and / or TREK-2.

Chapter 6 – Discussion

In this chapter I will summarise the K^+ channels present in the mouse MNTB and discuss their roles. The topics that were omitted from the discussions in the previous chapters will then be addressed. Then the findings of this thesis will be related to the physiological role of the MNTB. Finally future directions will be considered.

The K^+ channels of the MNTB

There are at least five distinct K^+ currents in the MNTB. Four of these are voltage gated; the other is a constitutively active leak current. Leak channels are the most fundamental of the K^+ channels in any neuron. Since they are constitutively open they are a major determinant of the resting membrane potential, and also contribute to action potential repolarisation. The unequal distribution of the permeant ion (i.e. K^+) across the membrane results in a curved “rectifying” I/V (described by the GHK equation). This results in less current passing through the leak channels at negative voltages compared to more positive voltages. Therefore the leak can be thought of as a rather loose elastic band; it starts to exert its greatest effect when it is most stretched and proportionally much less of an effect when it is closer to rest. All the other voltage-gated K^+ channels sit on top of the leak and due to their time and voltage dependence “add more tension” at the appropriate moment.

Kv channels of the MNTB

All four functional members of the classic Kv channels are represented in the MNTB. The largest contribution to outward current comes from the newly realised Kv2.2 conductance, closely followed by Kv3 (Kv2.2=3.8nA vs Kv3=3.2nA at +30mV). There is a considerable drop in the amount of outward current provided by the next largest contributor which is the putative Kv4 channel (1.25nA at -17mV) however; this is greater

than half-inactivated under physiological conditions. The Kv1 channels provide a similar level of current to the physiological amount of Kv4.

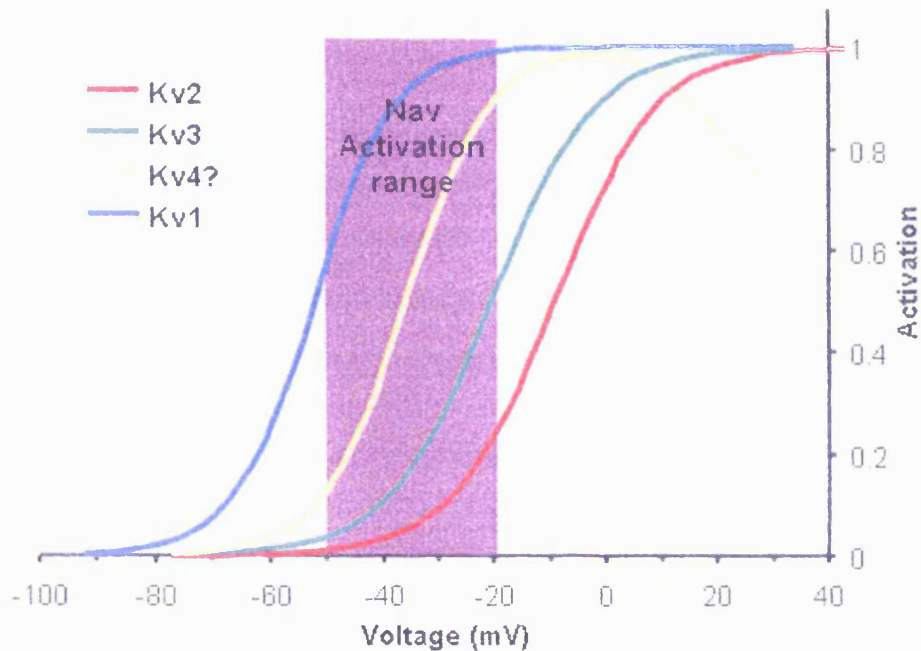


Figure 6-1 The activation ranges of the Kv channels in the MNTB: Kv2, Kv3 and Kv4 are Boltzmann distributions constructed with the averaged parameters from data in chapters 3 & 4. The activation curve for Kv1 was obtained by using the slope constant from (Brew & Forsythe, 1995) with the estimated $V_{1/2}$ from chapter 3. The activation range for the Nav channels was obtained from (Leao *et al.*, 2005a). N.B. The development of inward rectification for the Kv4 is represented schematically.

It is interesting to note that the Kv2.2 channels give the largest contribution to outward current in voltage clamp, yet under physiological conditions, they only contribute a minute amount of current; a result of their slow activation rate and high activation threshold. The activation ranges of these four different Kv channels in relation to the sodium current are summarised in Figure 6-1. At rest ~ -70 mV a small component of the Kv1 current will be open, and upon depolarisation a considerable proportion of the current can activate before the Nav channels begin to open (Figure 6-1, blue), which means that blocking them results in a lower threshold for action potential initiation (see Figure 3-12). The Kv4 channels activate over the same range as the sodium current

(Figure 6-1, yellow), which fits with their proposed role in delaying the time to peak (see Figure 4-8). The Kv3 channels have a more negative activation range than previous suggestions (Macica *et al.*, 2003), though they only begin to turn on after the Nav channels (Figure 6-1, green) consistent with their role in action potential repolarisation (Figure 3-7). Their lower range of activation is required for a sufficient amount to activate with each action potential (Baranauskas *et al.*, 2003). Finally the Kv2 channels turn on much later than the Nav channels (Figure 6-1, red) and are the only slow activating conductance, which restricts their physiological activation to high frequency trains of action potentials (Figure 4-21).

Other channels of the MNTB

The voltage-gated sodium current in the MNTB

Voltage-gated sodium currents of the MNTB have been partially characterised by Leao *et al.*, 2005a & Leao *et al.*, 2006a. Both authors find that Nav1.2 is absent in the MNTB. Nav1.6 channels were proposed to mediate the postsynaptic current in the rat by Leao *et al.*, 2005a, based on immunostaining. Though Leao *et al.*, 2006a found Nav1.6 staining to be at low levels in the mouse, with high Nav1.1 staining.

The voltage-dependence of inactivation for the sodium current reported here (i.e. $V_{1/2in} = -55.4\text{mV}$, $k = 6.3$) is close to that of Nav1.6 (Catterall *et al.*, 2003a) as is the slope constant (Raman *et al.*, 1997). Also the Nav channel has a non-inactivating component (Figure 3-3, and Leao *et al.*, 2005a; Leao *et al.*, 2006a) which is consistent with Nav1.6 having a non-inactivating component (Raman *et al.*, 1997). The $V_{1/2in}$ of Nav1.1 is -72mV (Catterall *et al.*, 2003a) which is very different to what is found here. Nav1.5, Nav1.8 and Nav1.9 can be excluded based on their insensitivity to TTx. At present it is unclear which Nav subunit mediates the sodium current in MNTB neurons, though my data fits with Nav1.6.

Previous reports find the presence of a slow component of recovery from inactivation of the postsynaptic Nav current (~80-90ms, Leao *et al.*, 2005a; Leao *et al.*, 2006a). It is this feature of the Nav current that will allow inactivation to accumulate throughout trains of action potentials (Jung *et al.*, 1997), which is demonstrated in (Figure 4-24, blue). In contrast, the presynaptic Nav current recovers rapidly from inactivation with a single exponential function having a time constant of ~2.4ms (Leao *et al.*, 2005a). It is puzzling that the postsynaptic cell does not implement a similar Nav channel to that located presynaptically. The potential for accumulation of inactivation of the postsynaptic current seems detrimental for high frequency firing. However it necessitates the presence of the Kv2.2 conductance which permits sustained high frequency firing. Kv2 channels are highly modulated in neurons (Park *et al.*, 2006), this may provide a mechanism for “tuning” cells to best follow their required frequencies. A fact that is hinted at by the Kv2.2 channels tonotopic gradient (Figure 4-26).

A role for K_{Na} subunits?

K_{Na} subunits (i.e. Slick and Slack) have been reported to be expressed in the MNTB nucleus (Bhattacharjee *et al.*, 2002; Bhattacharjee *et al.*, 2005). Although a recent review has stated their presence in the MNTB principal neurons, examination of the immunohistochemical data clearly shows the absence of Slack from principal neurons (see figure 4 B of Bhattacharjee *et al.*, 2002). Slick also appears to be in smaller non-principal cells (see figure 2 B of Bhattacharjee *et al.*, 2005). In the unlikely case that either of these subunits is present in the MNTB, it could be argued that it would result in the same frequency dependent hyperpolarisation observed for the Kv2.2 channel. However, this is unlikely when one considers their properties and the experimental conditions. Both Slick and Slack are activated by internal Na^+ , and Slick is inhibited by ATP (Bhattacharjee & Kaczmarek, 2005). No internal Na^+ was present in any of the recordings, and the inclusion of ATP had no effect on the Kv2.2 mediated current. The MNTB is packed with mitochondria (Satzler *et al.*, 2002; Elezgarai *et al.*, 2003; Leao *et*

al., 2005a), so if K_{Na} channels were present they are unlikely to play a role in normal physiology as they would be inhibited by ATP, it is likely that they afford a degree of protection from ischemic insult.

Summary of how the MNTB acts as a fast relay

In this thesis I have considered how ion channels, specifically K^+ channels, shape the physiological properties of the MNTB, allowing it to perform its role as a fast inverting relay. The MNTB receives a huge EPSC ($\sim 7nA$, Figure 3-1 B) directly on to its soma (Figure 3-1 A), which is ~ 30 times threshold. This huge current injection into the cell body provides the MNTB with an extremely short latency response (i.e. the postsynaptic cell fires extremely quickly after a presynaptic action potential).

To help “manage” this massive synaptic input $Kv1.1/Kv1.2$ heteromeric channels are present in the initial segment of the axon, where they prevent the MNTB from firing multiple action potentials in response to a single synaptic input (Figure 6-2, blue dots).

$Kv3$ channels located in the cell body help to keep the EPSP brief without attenuating its amplitude, and ensure rapid action potential repolarisation (Figure 6-2, green dots).

To maintain high firing rates the MNTB has $Kv2.2$ containing channels located in the initial segment, where they activate in response to high frequency trains, hyperpolarising the inter-spike potential, and thus preventing accumulation of inactivation of the Nav channels (Figure 6-2, red dots).

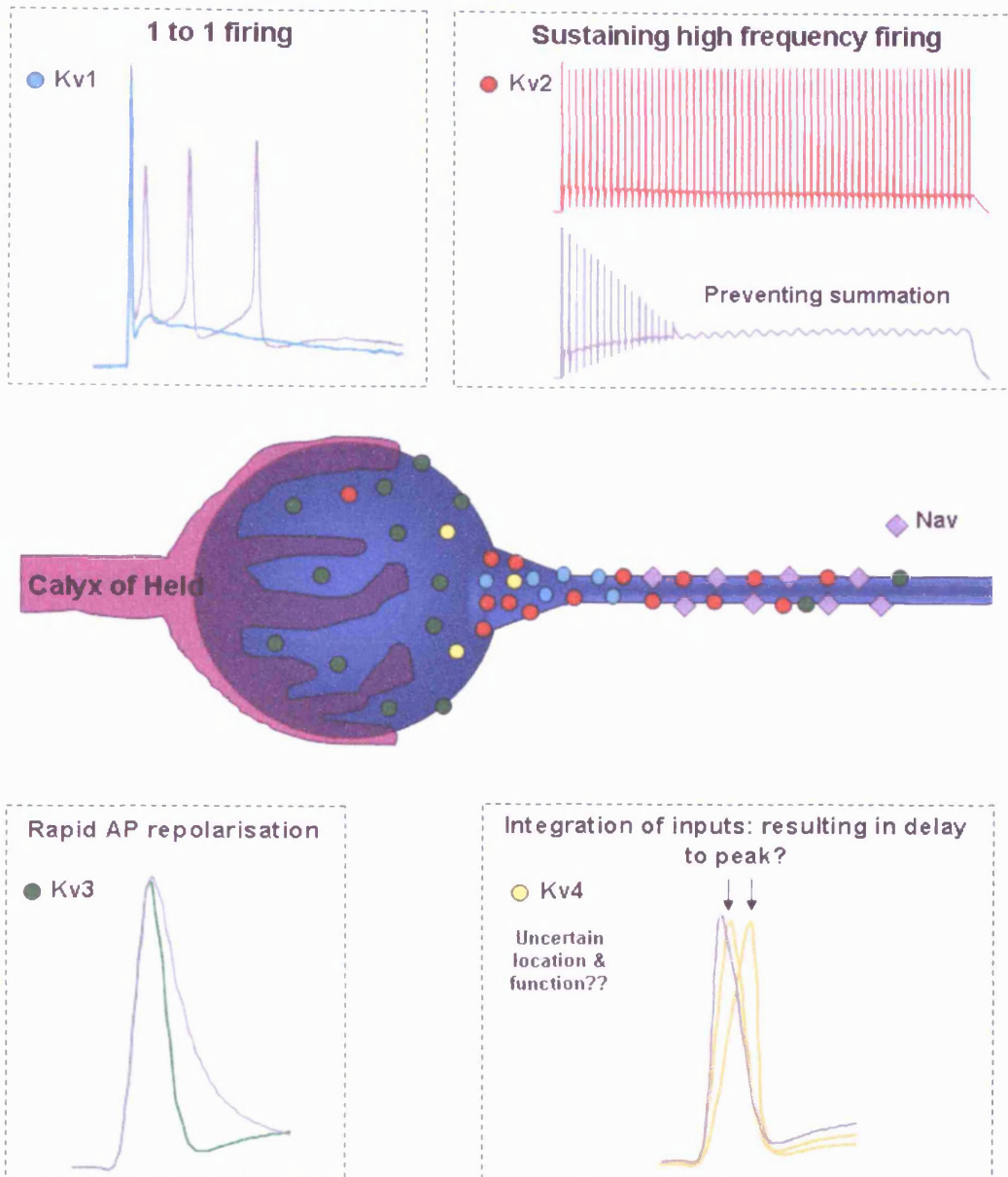


Figure 6-2 Summary of the composition, locations and roles of the MNTB's voltage gated channels: Grey trace represents the effect of the absence of the equivalent channel, location of Nav channels obtained from (Leao *et al.*, 2005a).

The mouse MNTB also possesses an A-type current probably mediated by the Kv4 family; it possibly acts by changing the time to peak of calyceal generated action potentials depending on the amount of previous inhibition (Figure 6-2, yellow dots). It may also be involved in integrating non-calyceal inputs or may just complement the existing low threshold Kv1 current. A definitive function remains to be established.

A considerable K^+ leak current, probably mediated by TWIK and / or TREK channels sets the resting membrane potential of the MNTB as well as contributing to action potential repolarisation.

Future directions

To try to elucidate the Kv3 subunit composition RT Qrt-PCR could be performed on Kv3.3 and Kv3.1 with primers designed to recognise all splice variants (i.e. PAN). Then primers to recognise the individual variants could be used to obtain the mRNA expression ratios. The resulting expression ratios could then be used in a cell line allowing comparison with the native channels.

More work could be performed on the kinetics of the Kv2.2 channels, as a single open closed model is not adequate to fit the kinetics of the native current. RT-PCR could be used to test the presence of electrically silent subunits in the MNTB. Co-expression of this finding with Kv2.2 channels may give a current with more complex kinetics similar to that observed of the native channel.

References

- AGGARWAL, S. K. & MACKINNON, R. (1996). Contribution of the S4 segment to gating charge in the Shaker K⁺ channel. *Neuron* **16**, 1169-1177.
- ALLER, M. I., VEALE, E. L., LINDEN, A.-M., SANDU, C., SCHWANINGER, M., EVANS, L. J., KORPI, E. R., MATHIE, A., WIDEN, W. & BRICKLEY, S. G. (2005). Modifying the Subunit Composition of TASK Channels Alters the Modulation of a Leak Conductance in Cerebellar Granule Neurons. *J. Neurosci.* **25**, 11455-11467.
- ARMSTRONG, C. M. (1974). Ionic pores, gates, and gating currents. *Q Rev Biophys* **7**, 179-210.
- ARMSTRONG, C. M. & BEZANILLA, F. (1973). Currents related to movement of the gating particles of the sodium channels. *Nature* **242**, 459-461.
- ATTALI, B., WANG, N., KOLOT, A., SOBKO, A., CHEREPANOV, V. & SOLIVEN, B. (1997). Characterization of delayed rectifier Kv channels in oligodendrocytes and progenitor cells. *J Neurosci* **17**, 8234-8245.
- AWATRAMANI, G. B., TURECEK, R. & TRUSSELL, L. O. (2004). Inhibitory Control at a Synaptic Relay. *J. Neurosci.* **24**, 2643-2647.
- BANKS, M. I., PEARCE, R. A. & SMITH, P. H. (1993). Hyperpolarization-activated cation current (I_h) in neurons of the medial nucleus of the trapezoid body: voltage-clamp analysis and enhancement by norepinephrine and cAMP suggest a modulatory mechanism in the auditory brain stem. *J Neurophysiol* **70**, 1420-1432.
- BANKS, M. I. & SMITH, P. H. (1992). Intracellular recordings from neurobiotin-labeled cells in brain slices of the rat medial nucleus of the trapezoid body. *J Neurosci* **12**, 2819-2837.
- BARANAUSKAS, G., TKATCH, T., NAGATA, K., YEH, J. Z. & SURMEIER, D. J. (2003). Kv3.4 subunits enhance the repolarizing efficiency of Kv3.1 channels in fast-spiking neurons. *Nat Neurosci* **6**, 258-266.
- BARANAUSKAS, G., TKATCH, T. & SURMEIER, D. J. (1999). Delayed rectifier currents in rat globus pallidus neurons are attributable to Kv2.1 and Kv3.1/3.2 K(+) channels. *J Neurosci* **19**, 6394-6404.
- BARRY, P. H. (1994). JPCalc, a software package for calculating liquid junction potential corrections in patch-clamp, intracellular, epithelial and bilayer measurements and for correcting junction potential measurements. *J Neurosci Methods* **51**, 107-116.
- BAUER, C. K. & SCHWARZ, J. R. (2001). Physiology of EAG K⁺ Channels. *Journal of Membrane Biology* **182**, 1-15.
- BAUKROWITZ, T. & YELLEN, G. (1995). Modulation of K⁺ current by frequency and external [K⁺]: a tale of two inactivation mechanisms. *Neuron* **15**, 951-960.
- BERG, A. P., TALLEY, E. M., MANGER, J. P. & BAYLISS, D. A. (2004). Motoneurons Express Heteromeric TWIK-Related Acid-Sensitive K⁺ (TASK) Channels Containing TASK-1 (KCNK3) and TASK-3 (KCNK9) Subunits. *J. Neurosci.* **24**, 6693-6702.

- BHATTACHARJEE, A., GAN, L. & KACZMAREK, L. K. (2002). Localization of the Slack potassium channel in the rat central nervous system. *J Comp Neurol* **454**, 241-254.
- BHATTACHARJEE, A. & KACZMAREK, L. K. (2005). For K⁺ channels, Na⁺ is the new Ca²⁺. *Trends Neurosci* **28**, 422-428.
- BHATTACHARJEE, A., VON HEHN, C. A., MEI, X. & KACZMAREK, L. K. (2005). Localization of the Na⁺-activated K⁺ channel Slick in the rat central nervous system. *J Comp Neurol* **484**, 80-92.
- BIRNBAUM, S. G., VARGA, A. W., YUAN, L.-L., ANDERSON, A. E., SWEATT, J. D. & SCHRADER, L. A. (2004). Structure and Function of Kv4-Family Transient Potassium Channels. *Physiol. Rev.* **84**, 803-833.
- BLAINE, J. T. & RIBERA, A. B. (2001). Kv2 channels form delayed-rectifier potassium channels in situ. *J Neurosci* **21**, 1473-1480.
- BRAND, A., BEHREND, O., MARQUARDT, T., MCALPINE, D. & GROTHE, B. (2002). Precise inhibition is essential for microsecond interaural time difference coding. *Nature* **417**, 543-547.
- BREW, H. & FORSYTHE, I. (1995). Two voltage-dependent K⁺ conductances with complementary functions in postsynaptic integration at a central auditory synapse. *J. Neurosci.* **15**, 8011-8022.
- BREW, H. M. & FORSYTHE, I. D. (2005). Systematic variation of potassium current amplitudes across the tonotopic axis of the rat medial nucleus of the trapezoid body. *Hear Res* **206**, 116-132.
- BREW, H. M., HALLOWS, J. L. & TEMPEL, B. L. (2003). Hyperexcitability and reduced low threshold potassium currents in auditory neurons of mice lacking the channel subunit Kv1.1. *J Physiol (Lond)* **548**, 1-20.
- BUSHELL, T., CLARKE, C., MATHIE, A. & ROBERTSON, B. (2002). Pharmacological characterization of a non-inactivating outward current observed in mouse cerebellar Purkinje neurones. *Br J Pharmacol* **135**, 705-712.
- CAMM, A. J., JANSE, M. J., RODEN, D. M., ROSEN, M. R., CINCA, J. & COBBE, S. M. (2000). Congenital and acquired long QT syndrome. *Eur Heart J* **21**, 1232-1237.
- CARR, C. E. & KONISHI, M. (1988). Axonal delay lines for time measurement in the owl's brainstem. *Proc Natl Acad Sci U S A* **85**, 8311-8315.
- CARR, C. E. & KONISHI, M. (1990). A circuit for detection of interaural time differences in the brain stem of the barn owl. *J Neurosci* **10**, 3227-3246.
- CATTERALL, W. A., GOLDIN, A. L. & WAXMAN, S. G. (2003a). International Union of Pharmacology. XXXIX. Compendium of voltage-gated ion channels: sodium channels. *Pharmacol Rev* **55**, 575-578.
- CATTERALL, W. A., STRIESSNIG, J., SNUTCH, T. P. & PEREZ-REYES, E. (2003b). International Union of Pharmacology. XL. Compendium of voltage-gated ion channels: calcium channels. *Pharmacol Rev* **55**, 579-581.

- CHEN, W. C. & DAVIS, R. L. (2006). Voltage-gated and two-pore-domain potassium channels in murine spiral ganglion neurons. *Hear Res* **222**, 89-99.
- CHEN, X. & JOHNSTON, D. (2004). Properties of single voltage-dependent K⁺ channels in dendrites of CA1 pyramidal neurones of rat hippocampus. *J Physiol (Lond)* **559**, 187-203.
- CHITTAJALLU, R., CHEN, Y., WANG, H., YUAN, X., GHIANI, C. A., HECKMAN, T., MCBAIN, C. J. & GALLO, V. (2002). Regulation of Kv1 subunit expression in oligodendrocyte progenitor cells and their role in G1/S phase progression of the cell cycle. *Proc Natl Acad Sci U S A* **99**, 2350-2355.
- CLAY, J. R. (2000). Determining K⁺ channel activation curves from K⁺ channel currents. *European Biophysics Journal* **29**, 555-557.
- COETZEE, W. A., AMARILLO, Y., CHIU, J., CHOW, A., LAU, D., MCCORMACK, T., MORENO, H., NADAL, M. S., OZAITA, A., POUNTNEY, D., SAGANICH, M., VEGA-SAENZ DE MIERA, E. & RUDY, B. (1999). Molecular diversity of K⁺ channels. *Ann N Y Acad Sci* **868**, 233-285.
- COX, D. H., CUI, J. & ALDRICH, R. W. (1997). Allosteric gating of a large conductance Ca-activated K⁺ channel. *J Gen Physiol* **110**, 257-281.
- CUTTLE, M. F., RUSZNAK, Z., WONG, A. Y., OWENS, S. & FORSYTHE, I. D. (2001). Modulation of a presynaptic hyperpolarization-activated cationic current (I_h) at an excitatory synaptic terminal in the rat auditory brainstem. *J Physiol* **534**, 733-744.
- DODSON, P. D. (2003). The role of voltage-gated potassium channels in regulating excitability at a central synapse. *Doctoral Thesis*.
- DODSON, P. D., BARKER, M. C. & FORSYTHE, I. D. (2002). Two Heteromeric Kv1 Potassium Channels Differentially Regulate Action Potential Firing. *J. Neurosci.* **22**, 6953-6961.
- DODSON, P. D., BILLUPS, B., RUSZNAK, Z., SZUCS, G., BARKER, M. C. & FORSYTHE, I. D. (2003). Presynaptic rat Kv1.2 channels suppress synaptic terminal hyperexcitability following action potential invasion. *J Physiol (Lond)* **550**, 27-33.
- DODSON, P. D. & FORSYTHE, I. D. (2004). Presynaptic K⁺ channels: electrifying regulators of synaptic terminal excitability. *Trends in Neurosciences* **27**, 210-217.
- DOUGHTY, J. M., BARNES-DAVIES, M., RUSZNAK, Z., HARASZTOSI, C. & FORSYTHE, I. D. (1998). Contrasting Ca²⁺ channel subtypes at cell bodies and synaptic terminals of rat anteroventral cochlear bushy neurones. *J Physiol* **512 (Pt 2)**, 365-376.
- DOYLE, D. A., MORAIS CABRAL, J., PFUETZNER, R. A., KUO, A., GULBIS, J. M., COHEN, S. L., CHAIT, B. T. & MACKINNON, R. (1998). The structure of the potassium channel: molecular basis of K⁺ conduction and selectivity. *Science* **280**, 69-77.
- DREWE, J. A., VERMA, S., FRECH, G. & JOHO, R. H. (1992). Distinct spatial and temporal expression patterns of K⁺ channel mRNAs from different subfamilies. *J Neurosci* **12**, 538-548.
- ELEZGARAI, I., DIEZ, J., PUENTE, N., AZKUE, J. J., BENITEZ, R., BILBAO, A., KNOPFEL, T., DONATE-OLIVER, F. & GRANDES, P. (2003). Subcellular localization of the voltage-

- dependent potassium channel Kv3.1b in postnatal and adult rat medial nucleus of the trapezoid body. *Neuroscience* **118**, 889-898.
- ENGELAND, B., NEU, A., LUDWIG, J., ROEPER, J. & PONGS, O. (1998). Cloning and functional expression of rat ether-a-go-go-like K⁺ channel genes. *J Physiol* **513** (Pt 3), 647-654.
- ESCOUBAS, P., DIOCHOT, S., CELERIER, M.-L., NAKAJIMA, T. & LAZDUNSKI, M. (2002). Novel Tarantula Toxins for Subtypes of Voltage-Dependent Potassium Channels in the Kv2 and Kv4 Subfamilies. *Mol Pharmacol* **62**, 48-57.
- FERNANDEZ, F. R., MORALES, E., RASHID, A. J., DUNN, R. J. & TURNER, R. W. (2003). Inactivation of Kv3.3 Potassium Channels in Heterologous Expression Systems. *J. Biol. Chem.* **278**, 40890-40898.
- FETTIPLACE, R. & HACKNEY, C. M. (2006). The sensory and motor roles of auditory hair cells. *Nat Rev Neurosci* **7**, 19-29.
- FINK, M., DUPRAT, F., LESAGE, F., HEURTEAUX, C., ROMEY, G., BARHANIN, J. & LAZDUNSKI, M. (1996). A New K⁺ Channel beta Subunit to Specifically Enhance Kv2.2 (CDRK) Expression
10.1074/jbc.271.42.26341. *J. Biol. Chem.* **271**, 26341-26348.
- FITZAKERLEY, J. L., STAR, K. V., RINN, J. L. & ELMQUIST, B. J. (2000). Expression of Shal potassium channel subunits in the adult and developing cochlear nucleus of the mouse. *Hearing Research* **147**, 31-45.
- FORSYTHE, I., LINDELL, P. & STANFIELD, P. (1992). Unitary A-currents of rat locus coeruleus neurones grown in cell culture: rectification caused by internal Mg²⁺ and Na⁺. *J Physiol.* **451**, 553-583.
- FORSYTHE, I. D. (1994). Direct patch recording from identified presynaptic terminals mediating glutamatergic EPSCs in the rat CNS, in vitro. *J Physiol* **479** (Pt 3), 381-387.
- FORSYTHE, I. D. (2002). Auditory Processing. *Encyclopaedia Of Life Sciences*, 1-16.
- FORSYTHE, I. D. & BARNES-DAVIES, M. (1993). The binaural auditory pathway: membrane currents limiting multiple action potential generation in the rat medial nucleus of the trapezoid body. *Proc Biol Sci* **251**, 143-150.
- FRANKS, N. P. & HONORE, E. (2004). The TREK K2P channels and their role in general anaesthesia and neuroprotection. *Trends in Pharmacological Sciences* **25**, 601-608.
- GAZULA, V. & KACZMAREK, L. K. (2006). Localization of Kv1.3 potassium channel immunoreactivity in nervous system of wild-type and Kv1.3^{-/-} mice. *Society for Neuroscience Abstract* **544.5/S3**.
- GEIGER, J. R., MELCHER, T., KOH, D. S., SAKMANN, B., SEEBURG, P. H., JONAS, P. & MONYER, H. (1995). Relative abundance of subunit mRNAs determines gating and Ca²⁺ permeability of AMPA receptors in principal neurons and interneurons in rat CNS. *Neuron* **15**, 193-204.
- GESSNER, G. & HEINEMANN, S. H. (2003). Inhibition of hEAG1 and hERG1 potassium channels by clofilium and its tertiary analogue LY97241. *Br J Pharmacol* **138**, 161-171.

- GITTELMAN, J. X. & TEMPEL, B. L. (2006). Kv1.1 Containing Channels are Critical for Temporal Precision during Spike Initiation. *J Neurophysiol*.
- GOLDSTEIN, S. A., BAYLISS, D. A., KIM, D., LESAGE, F., PLANT, L. D. & RAJAN, S. (2005). International Union of Pharmacology. LV. Nomenclature and molecular relationships of two-P potassium channels. *Pharmacol Rev* **57**, 527-540.
- GOLDSTEIN, S. A., PRICE, L. A., ROSENTHAL, D. N. & PAUSCH, M. H. (1996). ORK1, a potassium-selective leak channel with two pore domains cloned from *Drosophila melanogaster* by expression in *Saccharomyces cerevisiae*. *Proc Natl Acad Sci U S A* **93**, 13256-13261.
- GOLDSTEIN, S. A. N., BOCKENHAUER, D., O'KELLY, I. & ZILBERBERG, N. (2001). POTASSIUM LEAK CHANNELS AND THE KCNK FAMILY OF TWO-P-DOMAIN SUBUNITS. *Nature Reviews Neuroscience* **2**, 175-184.
- GRIGG, J. J., BREW, H. M. & TEMPEL, B. L. (2000). Differential expression of voltage-gated potassium channel genes in auditory nuclei of the mouse brainstem. *Hearing Research* **140**, 77-90.
- GUINAN, J. J., NORRIS, B. & GUINAN, S. (1972). Single auditory units in the superior olivary complex. II: Location of unit categories and tonotopic organisation. *Intl. J. Neurosci* **4**, 147-166.
- GULBIS, J. M., ZHOU, M., MANN, S. & MACKINNON, R. (2000). Structure of the cytoplasmic beta subunit-T1 assembly of voltage-dependent K⁺ channels. *Science* **289**, 123-127.
- GUTMAN, G. A., CHANDY, K. G., ADELMAN, J. P., AIYAR, J., BAYLISS, D. A., CLAPHAM, D. E., COVARRIUBIAS, M., DESIR, G. V., FURUICHI, K., GANETZKY, B., GARCIA, M. L., GRISSMER, S., JAN, L. Y., KARSCHIN, A., KIM, D., KUPERSCHMIDT, S., KURACHI, Y., LAZDUNSKI, M., LESAGE, F., LESTER, H. A., MCKINNON, D., NICHOLS, C. G., O'KELLY, I., ROBBINS, J., ROBERTSON, G. A., RUDY, B., SANGUINETTI, M., SEINO, S., STUEHMER, W., TAMKUN, M. M., VANDENBERG, C. A., WEI, A., WULFF, H. & WYMORE, R. S. (2003). International Union of Pharmacology. XLI. Compendium of voltage-gated ion channels: potassium channels. *Pharmacol Rev* **55**, 583-586.
- H. CHEN, V. G., J. STRUMBOS, Y. ZHANG, L.K. KACZMAREK. (2005). Biochemical regulation of K2p1 channels in auditory neurons. *Society for Neuroscience Abstract*, Program No. 609.608.
- HAMANN, M., BILLUPS, B. & FORSYTHE, I. D. (2003). Non-calyceal excitatory inputs mediate low fidelity synaptic transmission in rat auditory brainstem slices. *European Journal of Neuroscience* **18**, 2899-2902.
- HAN, J., TRUETT, J., GNATENCO, C. & KIM, D. (2002). Characterization of four types of background potassium channels in rat cerebellar granule neurons. *J Physiol (Lond)* **542**, 431-444.
- HARVEY, A. L. (2001). Twenty years of dendrotoxins. *Toxicon* **39**, 15-26.
- HEGINBOTHAM, L., LU, Z., ABRAMSON, T. & MACKINNON, R. (1994). Mutations in the K⁺ channel signature sequence. *Biophys J* **66**, 1061-1067.

- HEINEMANN, S. H., RETTIG, J., GRAACK, H. R. & PONGS, O. (1996). Functional characterization of Kv channel beta-subunits from rat brain. *J Physiol* **493** (Pt 3), 625-633.
- HELD, H. (1893). Die centrale Gehorleitung. *Arch Anat Physiol Anat Abt*, 201-248.
- HILLE, B. (2001). Ion Channels of Excitable Membranes. *Sinauer Associates Incorporated*, 730 pages.
- HODGKIN, A. L. & HUXLEY, A. F. (1952). A quantitative description of membrane current and its application to conduction and excitation in nerve. *J Physiol* **117**, 500-544.
- HODGKIN, A. L., HUXLEY, A. F. & KATZ, B. (1952). Measurement of current-voltage relations in the membrane of the giant axon of Loligo. *J Physiol* **116**, 424-448.
- HOLT, A. G., ASAKO, M., KEITH DUNCAN, R., LOMAX, C. A., JUIZ, J. M. & ALTSCHULER, R. A. (2006). Deafness associated changes in expression of two-pore domain potassium channels in the rat cochlear nucleus. *Hear Res* **216-217**, 146-153.
- HOPKINS, W. F. (1998). Toxin and Subunit Specificity of Blocking Affinity of Three Peptide Toxins for Heteromultimeric, Voltage-Gated Potassium Channels Expressed in *Xenopus* Oocytes. *J Pharmacol Exp Ther* **285**, 1051-1060.
- HWANG, P., FOTUHI, M., BREDT, D., CUNNINGHAM, A. & SNYDER, S. (1993). Contrasting immunohistochemical localizations in rat brain of two novel K⁺ channels of the Shab subfamily. *J. Neurosci.* **13**, 1569-1576.
- INDA, M. C., DEFELIPE, J. & MUNOZ, A. (2006). Voltage-gated ion channels in the axon initial segment of human cortical pyramidal cells and their relationship with chandelier cells. *Proc Natl Acad Sci U S A* **103**, 2920-2925.
- ISHIKAWA, T., NAKAMURA, Y., SAITOH, N., LI, W.-B., IWASAKI, S. & TAKAHASHI, T. (2003). Distinct Roles of Kv1 and Kv3 Potassium Channels at the Calyx of Held Presynaptic Terminal. *J. Neurosci.* **23**, 10445-10453.
- IWASAKI, S., MOMIYAMA, A., UCHITEL, O. D. & TAKAHASHI, T. (2000). Developmental changes in calcium channel types mediating central synaptic transmission. *J Neurosci* **20**, 59-65.
- JAGER, H., RAUER, H., NGUYEN, A. N., AIYAR, J., CHANDY, K. G. & GRISSMER, S. (1998). Regulation of mammalian Shaker-related K⁺ channels: evidence for non-conducting closed and non-conducting inactivated states. *J Physiol (Lond)* **506**, 291-301.
- JEFFRESS, L. A. (1948). A place theory for sound localisation. *Journal of Comp Physiol & Psychol* **41**, 35-39.
- JENTSCH, T. J. (2000). NEURONAL KCNQ POTASSIUM CHANNELS: PHYSIOLOGY AND ROLE IN DISEASE. *Nature Reviews Neuroscience* **1**, 21-30.
- JENTSCH, T. J., NEAGOE, I. & SCHEEL, O. (2005). CLC chloride channels and transporters. *Curr Opin Neurobiol* **15**, 319-325.
- JIANG, Y., LEE, A., CHEN, J., CADENE, M., CHAIT, B. T. & MACKINNON, R. (2002). Crystal structure and mechanism of a calcium-gated potassium channel. *Nature* **417**, 515-522.

- JIANG, Y., LEE, A., CHEN, J., RUTA, V., CADENE, M., CHAIT, B. T. & MACKINNON, R. (2003). X-ray structure of a voltage-dependent K⁺ channel. *Nature* **423**, 33-41.
- JORIS, P. X., CARNEY, L. H., SMITH, P. H. & YIN, T. C. (1994). Enhancement of neural synchronization in the anteroventral cochlear nucleus. I. Responses to tones at the characteristic frequency. *J Neurophysiol* **71**, 1022-1036.
- JORIS, P. X., SMITH, P. H. & YIN, T. C. T. (1998). Coincidence detection in the auditory system: 50 years after Jeffress. *Neuron* **21**, 1235-1238.
- JOW, F., ZHANG, Z., KOPSCO, D., CARROLL, K. & WANG, K. (2004). Functional coupling of intracellular calcium and inactivation of voltage-gated Kv1.1/Kv β 1.1 A-type K⁺ channels., -.
- JUNG, H. Y., MICKUS, T. & SPRUSTON, N. (1997). Prolonged sodium channel inactivation contributes to dendritic action potential attenuation in hippocampal pyramidal neurons. *J Neurosci* **17**, 6639-6646.
- KACZMAREK, L. K., BHATTACHARJEE, A., DESAI, R., GAN, L., SONG, P., VON HEHN, C. A., WHIM, M. D. & YANG, B. (2005). Regulation of the timing of MNTB neurons by short-term and long-term modulation of potassium channels. *Hear Res* **206**, 133-145.
- KALMAN, K., NGUYEN, A., TSENG-CRANK, J., DUKES, I. D., CHANDY, G., HUSTAD, C. M., COPELAND, N. G., JENKINS, N. A., MOHRENWEISER, H., BRANDRIFF, B., CAHALAN, M., GUTMAN, G. A. & CHANDY, K. G. (1998). Genomic organization, chromosomal localization, tissue distribution, and biophysical characterization of a novel mammalian Shaker-related voltage-gated potassium channel, Kv1.7. *J Biol Chem* **273**, 5851-5857.
- KANDEL, E. R., SCHWARTZ, J. H. & JESSELL, T. M. (2000). Principles of Neural Science. **Fourth edition.**
- KANE, G. C., LIU, X. K., YAMADA, S., OLSON, T. M. & TERZIC, A. (2005). Cardiac KATP channels in health and disease. *J Mol Cell Cardiol* **38**, 937-943.
- KASHUBA, V. I., KVASHA, S. M., PROTOPOPOV, A. I., GIZATULLIN, R. Z., RYNDITCH, A. V., WAHLESTEDT, C., WASSERMAN, W. W. & ZABAROVSKY, E. R. (2001). Initial isolation and analysis of the human Kv1.7 (KCNA7) gene, a member of the voltage-gated potassium channel gene family. *Gene* **268**, 115-122.
- KERSCHENSTEINER, D. & STOCKER, M. (1999). Heteromeric Assembly of Kv2.1 with Kv9.3: Effect on the State Dependence of Inactivation. *Biophys. J.* **77**, 248-257.
- KETCHUM, K. A., JOINER, W. J., SELLERS, A. J., KACZMAREK, L. K. & GOLDSTEIN, S. A. (1995). A new family of outwardly rectifying potassium channel proteins with two pore domains in tandem. *Nature* **376**, 690-695.
- KHARKOVETS, T., HARDELIN, J.-P., SAFIEDDINE, S., SCHWEIZER, M., EL-AMRAOUI, A., PETIT, C. & JENTSCH, T. J. (2000). From the Cover: KCNQ4, a K⁺ channel mutated in a form of dominant deafness, is expressed in the inner ear and the central auditory pathway. *PNAS* **97**, 4333-4338.
- KIM, Y., BANG, H. & KIM, D. (2000). TASK-3, a new member of the tandem pore K(+) channel family. *J Biol Chem* **275**, 9340-9347.

- KINDLER, C. H., YOST, C. S. & GRAY, A. T. (1999). Local anesthetic inhibition of baseline potassium channels with two pore domains in tandem. *Anesthesiology* **90**, 1092-1102.
- KITA, H. & KITAI, S. T. (1991). Intracellular study of rat globus pallidus neurons: membrane properties and responses to neostriatal, subthalamic and nigral stimulation. *Brain Res* **564**, 296-305.
- KLUG, A. & TRUSSELL, L. O. (2006). Activation and deactivation of voltage-dependent K⁺ channels during synaptically driven action potentials in the MNTB. *J Neurophysiol* **96**, 1547-1555.
- KOCH, U., BRAUN, M., KAPFER, C. & GROTHE, B. (2004). Distribution of HCN1 and HCN2 in rat auditory brainstem nuclei. *Eur J Neurosci* **20**, 79-91.
- KOPP-SCHEINPFLUG, C., LIPPE, W. R., DORRSCHIEDT, G. J. & RUBSAMEN, R. (2003). The medial nucleus of the trapezoid body in the gerbil is more than a relay: comparison of pre- and postsynaptic activity. *J Assoc Res Otolaryngol* **4**, 1-23.
- KOTAK, V. C., KORADA, S., SCHWARTZ, I. R. & SANES, D. H. (1998). A developmental shift from GABAergic to glycinergic transmission in the central auditory system. *J Neurosci* **18**, 4646-4655.
- KRAMER, J. W., POST, M. A., BROWN, A. M. & KIRSCH, G. E. (1998). Modulation of potassium channel gating by coexpression of Kv2.1 with regulatory Kv5.1 or Kv6.1 alpha-subunits. *Am J Physiol Cell Physiol* **274**, C1501-1510.
- KUNER, T., SEEBURG, P. H. & GUY, H. R. (2003). A common architecture for K⁺ channels and ionotropic glutamate receptors? *Trends Neurosci* **26**, 27-32.
- KUWABARA, N. & ZOOK, J. M. (1991). Classification of the principal cells of the medial nucleus of the trapezoid body. *J Comp Neurol* **314**, 707-720.
- LARKMAN, P. M. & PERKINS, E. M. (2005). A TASK-like pH- and amine-sensitive 'leak' K⁺ conductance regulates neonatal rat facial motoneuron excitability in vitro. *Eur J Neurosci* **21**, 679-691.
- LARSSON, H. P., BAKER, O. S., DHILLON, D. S. & ISACOFF, E. Y. (1996). Transmembrane movement of the shaker K⁺ channel S4. *Neuron* **16**, 387-397.
- LEAO, R. M., KUSHMERICK, C., PINAUD, R., RENDEN, R., LI, G.-L., TASCHENBERGER, H., SPIROU, G., LEVINSON, S. R. & VON GERSDORFF, H. (2005a). Presynaptic Na⁺ Channels: Locus, Development, and Recovery from Inactivation at a High-Fidelity Synapse. *J. Neurosci.* **25**, 3724-3738.
- LEAO, R. N., NAVES, M. M., LEAO, K. E. & WALMSLEY, B. (2006a). Altered sodium currents in auditory neurons of congenitally deaf mice. *Eur J Neurosci* **24**, 1137-1146.
- LEAO, R. N., SUN, H., SVAHN, K., BERNTSON, A., YOUSSEFIAN, M., PAOLINI, A. G., FYFFE, R. E. W. & WALMSLEY, B. (2006b). Topographic organization in the auditory brainstem of juvenile mice is disrupted in congenital deafness 10.1113/jphysiol.2005.098780. *J Physiol (Lond)* **571**, 563-578.
- LEAO, R. N., SVAHN, K., BERNTSON, A. & WALMSLEY, B. (2005b). Hyperpolarization-activated (I_h) currents in auditory brainstem neurons of normal and congenitally deaf mice. *European Journal of Neuroscience* **22**, 147-157.

- LI, W., KACZMAREK, L. K. & PERNEY, T. M. (2001). Localization of two high-threshold potassium channel subunits in the rat central auditory system. *J Comp Neurol* **437**, 196-218.
- LIBERMAN, M. C. & OLIVER, M. E. (1984). Morphometry of intracellularly labeled neurons of the auditory nerve: correlations with functional properties. *J Comp Neurol* **223**, 163-176.
- LINDSEY, B. G. (1975). Fine structure and distribution of axon terminals from the cochlear nucleus on neurons in the medial superior olivary nucleus of the cat. *J Comp Neurol* **160**, 81-103.
- LIU, S. J. & KACZMAREK, L. K. (1998). The expression of two splice variants of the Kv3.1 potassium channel gene is regulated by different signaling pathways. *J Neurosci* **18**, 2881-2890.
- LONG, S. B., CAMPBELL, E. B. & MACKINNON, R. (2005a). Crystal Structure of a Mammalian Voltage-Dependent Shaker Family K⁺ Channel. *Science* **309**, 897-903.
- LONG, S. B., CAMPBELL, E. B. & MACKINNON, R. (2005b). Voltage Sensor of Kv1.2: Structural Basis of Electromechanical Coupling. *Science* **309**, 903-908.
- LU, Z., KLEM, A. M. & RAMU, Y. (2002). Coupling between voltage sensors and activation gate in voltage-gated K⁺ channels. *J Gen Physiol* **120**, 663-676.
- LUDWIG, A., ZONG, X., JEGLITSCH, M., HOFMANN, F. & BIEL, M. (1998). A family of hyperpolarization-activated mammalian cation channels. *Nature* **393**, 587-591.
- MACICA, C. M., VON HEHN, C. A. A., WANG, L.-Y., HO, C.-S., YOKOYAMA, S., JOHO, R. H. & KACZMAREK, L. K. (2003). Modulation of the Kv3.1b Potassium Channel Isoform Adjusts the Fidelity of the Firing Pattern of Auditory Neurons. *J. Neurosci.* **23**, 1133-1141.
- MAGEE, J. C. (1999). Dendritic I_h normalizes temporal summation in hippocampal CA1 neurons. *Nat Neurosci* **2**, 848.
- MAGEE, J. C. (2000). DENDRITIC INTEGRATION OF EXCITATORY SYNAPTIC INPUT. *NATURE REVIEWS NEUROSCIENCE* **1**, 181-190.
- MAGISTRETTI, J., MANTEGAZZA, M., GUATTEO, E. & WANKE, E. (1996). Action potentials recorded with patch-clamp amplifiers: are they genuine? *Trends Neurosci* **19**, 530-534.
- MAINGRET, F., PATEL, A. J., LESAGE, F., LAZDUNSKI, M. & HONORE, E. (1999). Mechano- or acid stimulation, two interactive modes of activation of the TREK-1 potassium channel. *J Biol Chem* **274**, 26691-26696.
- MALIN, S. A. & NERBONNE, J. M. (2002). Delayed Rectifier K⁺ Currents, I_K, Are Encoded by Kv2 alpha -Subunits and Regulate Tonic Firing in Mammalian Sympathetic Neurons. *J. Neurosci.* **22**, 10094-10105.
- MARTINA, M., SCHULTZ, J. H., EHMKE, H., MONYER, H. & JONAS, P. (1998). Functional and molecular differences between voltage-gated K⁺ channels of fast-spiking interneurons and pyramidal neurons of rat hippocampus. *J Neurosci* **18**, 8111-8125.

- MCALPINE, D. (2005). Creating a sense of auditory space. *J Physiol (Lond)* **566**, 21-28.
- MCALPINE, D. & GROTHE, B. (2003). Sound localization and delay lines--do mammals fit the model? *Trends Neurosci* **26**, 347-350.
- MCALPINE, D., JIANG, D. & PALMER, A. R. (2001). A neural code for low-frequency sound localization in mammals. *Nat Neurosci* **4**, 396-401.
- MCCORMACK, K., MCCORMACK, T., TANOUYE, M., RUDY, B. & STUHMER, W. (1995). Alternative splicing of the human Shaker K⁺ channel beta 1 gene and functional expression of the beta 2 gene product. *FEBS Lett* **370**, 32-36.
- MCCORMICK, D. A. (2003). Membrane properties and neurotransmitter actions. *In The Synaptic Organisation of the Brain Fifth Edition*, 41-43.
- MELLOR, J., NICOLL, R. A. & SCHMITZ, D. (2002). Mediation of hippocampal mossy fiber long-term potentiation by presynaptic Ih channels. *Science* **295**, 143-147.
- MEUTH, S. G., KANYSHKOVA, T., MEUTH, P., LANDGRAF, P., MUNSCH, T., LUDWIG, A., HOFMANN, F., PAPE, H.-C. & BUDDE, T. (2006). The membrane resting potential of thalamocortical relay neurons is shaped by the interaction among TASK3 and HCN2 channels
10.1152/jn.01212.2005. *J Neurophysiol*, 01212.02005.
- MISONOU, H., MOHAPATRA, D. P., PARK, E. W., LEUNG, V., ZHEN, D., MISONOU, K., ANDERSON, A. E. & TRIMMER, J. S. (2004). Regulation of ion channel localization and phosphorylation by neuronal activity. *Nature Neuroscience* **7**, 711-718.
- MOHAPATRA, D. P. & TRIMMER, J. S. (2006). The Kv2.1 C Terminus Can Autonomously Transfer Kv2.1-Like Phosphorylation-Dependent Localization, Voltage-Dependent Gating, and Muscarinic Modulation to Diverse Kv Channels
10.1523/JNEUROSCI.4620-05.2006. *J. Neurosci.* **26**, 685-695.
- MORAIS-CABRAL, J. H., ZHOU, Y. & MACKINNON, R. (2001). Energetic optimization of ion conduction rate by the K⁺ selectivity filter. *Nature* **414**, 37-42.
- MUENNICH, E. A. & FYFFE, R. E. (2004). Focal aggregation of voltage-gated, Kv2.1 subunit-containing, potassium channels at synaptic sites in rat spinal motoneurons. *J Physiol* **554**, 673-685.
- MURAKOSHI, H. & TRIMMER, J. S. (1999). Identification of the Kv2.1 K⁺ channel as a major component of the delayed rectifier K⁺ current in rat hippocampal neurons. *J Neurosci* **19**, 1728-1735.
- NEHER, E. (1992). Correction for liquid junction potentials in patch clamp experiments. *Methods Enzymol* **207**, 123-131.
- NEISES, G. R., MATTOX, D. E. & GULLEY, R. L. (1982). The maturation of the end bulb of Held in the rat anteroventral cochlear nucleus. *Anat Rec* **204**, 271-279.
- NGUYEN, A., KATH, J., HANSON, D., BIGGERS, M., CANNIFF, P., DONOVAN, C., MATHER, R., BRUNS, M., RAUER, H., AIYAR, J., LEPPLE-WIENHUES, A., GUTMAN, G., GRISSMER, S., CAHALAN, M. & CHANDY, K. (1996). Novel nonpeptide agents potently block the C-type inactivated conformation of Kv1.3 and suppress T cell activation. *Mol Pharmacol* **50**, 1672-1679.

- NISHIDA, M. & MACKINNON, R. (2002). Structural basis of inward rectification: cytoplasmic pore of the G protein-gated inward rectifier GIRK1 at 1.8 Å resolution. *Cell* **111**, 957-965.
- O'CONNELL, A. D., MORTON, M. J. & HUNTER, M. (2002). Two-pore domain K⁺ channels--molecular sensors. *Biochimica et Biophysica Acta (BBA) - Biomembranes* **1566**, 152-161.
- O'CONNELL, K. M., ROLIG, A. S., WHITESSELL, J. D. & TAMKUN, M. M. (2006). Kv2.1 potassium channels are retained within dynamic cell surface microdomains that are defined by a perimeter fence. *J Neurosci* **26**, 9609-9618.
- OERTEL, D. (1983). Synaptic responses and electrical properties of cells in brain slices of the mouse anteroventral cochlear nucleus. *J Neurosci* **3**, 2043-2053.
- OTTSCHYTSCH, N., RAES, A., VAN HOORICK, D. & SNYDERS, D. J. (2002). Obligatory heterotetramerization of three previously uncharacterized Kv channel alpha - subunits identified in the human genome 10.1073/pnas.122617999. *PNAS* **99**, 7986-7991.
- OTTSCHYTSCH, N., RAES, A. L., TIMMERMANS, J.-P. & SNYDERS, D. J. (2005). Domain analysis of Kv6.3, an electrically silent channel. *J Physiol (Lond)* **568**, 737-747.
- PAL, B., POR, A., POCSAI, K., SZUCS, G. & RUSZNAK, Z. (2005). Voltage-gated and background K⁺ channel subunits expressed by the bushy cells of the rat cochlear nucleus. *Hear Res* **199**, 57-70.
- PARK, K. S., MOHAPATRA, D. P., MISONOU, H. & TRIMMER, J. S. (2006). Graded regulation of the Kv2.1 potassium channel by variable phosphorylation. *Science* **313**, 976-979.
- PATEL, A. J. & LAZDUNSKI, M. (2004). The 2P-domain K⁺ channels: role in apoptosis and tumorigenesis. *Pflugers Arch* **448**, 261-273.
- POST, M. A., KIRSCH, G. E. & BROWN, A. M. (1996). Kv2.1 and electrically silent Kv6.1 potassium channel subunits combine and express a novel current. *FEBS Letters* **399**, 177-182.
- PRICE, G. D. & TRUSSELL, L. O. (2006). Estimate of the chloride concentration in a central glutamatergic terminal: a gramicidin perforated-patch study on the calyx of Held. *J Neurosci* **26**, 11432-11436.
- PROKS, P. & LIPPIAT, J. D. (2006). Membrane ion channels and diabetes. *Curr Pharm Des* **12**, 485-501.
- RAJAN, S., WISCHMEYER, E., KARSCHIN, C., PREISIG-MULLER, R., GRZESCHIK, K.-H., DAUT, J., KARSCHIN, A. & DERST, C. (2001). THIK-1 and THIK-2, a Novel Subfamily of Tandem Pore Domain K⁺ Channels. *J. Biol. Chem.* **276**, 7302-7311.
- RAMAN, I. M., SPRUNGER, L. K., MEISLER, M. H. & BEAN, B. P. (1997). Altered subthreshold sodium currents and disrupted firing patterns in Purkinje neurons of Scn8a mutant mice. *Neuron* **19**, 881-891.
- RAMAN, I. M., ZHANG, S. & TRUSSELL, L. O. (1994). Pathway-specific variants of AMPA receptors and their contribution to neuronal signaling. *J Neurosci* **14**, 4998-5010.

- RASHID, A. J., DUNN, R. J. & TURNER, R. W. (2001). A prominent soma-dendritic distribution of Kv3.3 K⁺ channels in electrosensory and cerebellar neurons. *J Comp Neurol* **441**, 234-247.
- REYES, J. & LATORRE, R. (1979). Effect of the anesthetics benzyl alcohol and chloroform on bilayers made from monolayers. *Biophys J* **28**, 259-279.
- REYES, R., DUPRAT, F., LESAGE, F., FINK, M., SALINAS, M., FARMAN, N. & LAZDUNSKI, M. (1998). Cloning and expression of a novel pH-sensitive two pore domain K⁺ channel from human kidney. *J Biol Chem* **273**, 30863-30869.
- ROBBINS, J. (2001). KCNQ potassium channels: physiology, pathophysiology, and pharmacology. *Pharmacology & Therapeutics* **90**, 1-19.
- ROBERTSON, B. (1997). The real life of voltage-gated K⁺ channels: more than model behaviour. *Trends in Pharmacological Sciences* **18**, 474-483.
- ROBERTSON, B., OWEN, D., STOW, J., BUTLER, C. & NEWLAND, C. (1996). Novel effects of dendrotoxin homologues on subtypes of mammalian Kv1 potassium channels expressed in *Xenopus* oocytes. *FEBS Letters* **383**, 26-30.
- ROEPER, J., SEWING, S., ZHANG, Y., SOMMER, T., WANNER, S. G. & PONGS, O. (1998). NIP domain prevents N-type inactivation in voltage-gated potassium channels. *Nature* **391**, 390-393.
- RUDY, B., CHOW, A., LAU, D., AMARILLO, Y., OZAITA, A., SAGANICH, M., MORENO, H., NADAL, M. S., HERNANDEZ-PINEDA, R., HERNANDEZ-CRUZ, A., ERISIR, A., LEONARD, C. & VEGA-SAENZ DE MIERA, E. (1999). Contributions of Kv3 channels to neuronal excitability. *Ann N Y Acad Sci* **868**, 304-343.
- RUDY, B. & MCBAIN, C. J. (2001). Kv3 channels: voltage-gated K⁺ channels designed for high-frequency repetitive firing. *Trends in Neurosciences* **24**, 517-526.
- SAGANICH, M. J., MACHADO, E. & RUDY, B. (2001). Differential Expression of Genes Encoding Subthreshold-Operating Voltage-Gated K⁺ Channels in Brain. *J. Neurosci.* **21**, 4609-4624.
- SALINAS, M., DE WEILLE, J., GUILLEMARE, E., LAZDUNSKI, M. & HUGNOT, J.-P. (1997a). Modes of Regulation of Shab K⁺ Channel Activity by the Kv8.1 Subunit 10.1074/jbc.272.13.8774. *J. Biol. Chem.* **272**, 8774-8780.
- SALINAS, M., DUPRAT, F., HEURTEAUX, C., HUGNOT, J.-P. & LAZDUNSKI, M. (1997b). New Modulatory alpha Subunits for Mammalian Shab K⁺ Channels. *J. Biol. Chem.* **272**, 24371-24379.
- SANGUINETTI, M. C., JOHNSON, J. H., HAMMERLAND, L. G., KELBAUGH, P. R., VOLKMANN, R. A., SACCOMANO, N. A. & MUELLER, A. L. (1997). Heteropodatoxins: peptides isolated from spider venom that block Kv4.2 potassium channels. *Mol Pharmacol* **51**, 491-498.
- SANO, Y., MOCHIZUKI, S., MIYAKE, A., KITADA, C., INAMURA, K., YOKOI, H., NOZAWA, K., MATSUSHIME, H. & FURUICHI, K. (2002). Molecular cloning and characterization of Kv6.3, a novel modulatory subunit for voltage-gated K⁺ channel Kv2.1. *FEBS Letters* **512**, 230-234.

- SANTORO, B., LIU, D. T., YAO, H., BARTSCH, D., KANDEL, E. R., SIEGELBAUM, S. A. & TIBBS, G. R. (1998). Identification of a gene encoding a hyperpolarization-activated pacemaker channel of brain. *Cell* **93**, 717-729.
- SATZLER, K., SOHL, L. F., BOLLMANN, J. H., BORST, J. G. G., FROTSCHER, M., SAKMANN, B. & LUBKE, J. H. R. (2002). Three-Dimensional Reconstruction of a Calyx of Held and Its Postsynaptic Principal Neuron in the Medial Nucleus of the Trapezoid Body. *J. Neurosci.* **22**, 10567-10579.
- SCHMALZ, F., KINSELLA, J., KOH, S. D., VOGALIS, F., SCHNEIDER, A., FLYNN, E. R. M., KENYON, J. L. & HOROWITZ, B. (1998). Molecular identification of a component of delayed rectifier current in gastrointestinal smooth muscles. *Am J Physiol Gastrointest Liver Physiol* **274**, G901-911.
- SCHNEIDER, M. F. & CHANDLER, W. K. (1973). Voltage dependent charge movement of skeletal muscle: a possible step in excitation-contraction coupling. *Nature* **242**, 244-246.
- SCHREIBER, M., WEI, A., YUAN, A., GAUT, J., SAITO, M. & SALKOFF, L. (1998). Slo3, a novel pH-sensitive K⁺ channel from mammalian spermatocytes. *J Biol Chem* **273**, 3509-3516.
- SCHWARZ, J. R., GLASSMEIER, G., COOPER, E. C., KAO, T. C., NODERA, H., TABUENA, D., KAJI, R. & BOSTOCK, H. (2006). KCNQ channels mediate IKs, a slow K⁺ current regulating excitability in the rat node of Ranvier. *J Physiol* **573**, 17-34.
- SEOH, S. A., SIGG, D., PAPAIZIAN, D. M. & BEZANILLA, F. (1996). Voltage-sensing residues in the S2 and S4 segments of the Shaker K⁺ channel. *Neuron* **16**, 1159-1167.
- SERODIO, P., KENTROS, C. & RUDY, B. (1994). Identification of molecular components of A-type channels activating at subthreshold potentials. *J Neurophysiol* **72**, 1516-1529.
- SERODIO, P. & RUDY, B. (1998). Differential expression of Kv4 K⁺ channel subunits mediating subthreshold transient K⁺ (A-type) currents in rat brain. *J Neurophysiol* **79**, 1081-1091.
- SHEN, W., HERNANDEZ-LOPEZ, S., TKATCH, T., HELD, J. E. & SURMEIER, D. J. (2003). Kv1.2-Containing K⁺ Channels Regulate Sub-Threshold Excitability of Striatal Medium Spiny Neurons. *J Neurophysiol*, 00414.02003.
- SHENG, M., TSAUR, M. L., JAN, Y. N. & JAN, L. Y. (1994). Contrasting subcellular localization of the Kv1.2 K⁺ channel subunit in different neurons of rat brain. *J Neurosci* **14**, 2408-2417.
- SHI, W., WANG, H. S., PAN, Z., WYMORE, R. S., COHEN, I. S., MCKINNON, D. & DIXON, J. E. (1998). Cloning of a mammalian elk potassium channel gene and EAG mRNA distribution in rat sympathetic ganglia. *J Physiol* **511 (Pt 3)**, 675-682.
- SINDHU, R., D., P. L., L., R. M., H., B. M. & A.N., G. S. (2005). Sumoylation Silences the Plasma Membrane Leak K⁺ Channel K2P1. *Cell* **121**, 37-47.
- SLESINGER, P. A., JAN, Y. N. & JAN, L. Y. (1993). The S4-S5 loop contributes to the ion-selective pore of potassium channels. *Neuron* **11**, 739-749.

- SMITH, A. J., OWENS, S. & FORSYTHE, I. D. (2000). Characterisation of inhibitory and excitatory postsynaptic currents of the rat medial superior olive. *J Physiol* **529 Pt 3**, 681-698.
- SMITH, P. H. (1995). Structural and functional differences distinguish principal from nonprincipal cells in the guinea pig MSO slice. *J Neurophysiol* **73**, 1653-1667.
- SMITH, P. H., JORIS, P. X. & YIN, T. C. (1998). Anatomy and physiology of principal cells of the medial nucleus of the trapezoid body (MNTB) of the cat. *J Neurophysiol* **79**, 3127-3142.
- SONG, P. & KACZMAREK, L. K. (2006). Modulation of Kv3.1b potassium channel phosphorylation in auditory neurons by conventional and novel protein kinase C isozymes. *J Biol Chem* **281**, 15582-15591.
- SONG, P., YANG, Y., BARNES-DAVIES, M., BHATTACHARJEE, A., HAMANN, M., FORSYTHE, I. D., OLIVER, D. L. & KACZMAREK, L. K. (2005). Acoustic environment determines phosphorylation state of the Kv3.1 potassium channel in auditory neurons. *Nat Neurosci* **8**, 1335-1342.
- SOUTHAN, A. P. & ROBERTSON, B. (2000). Electrophysiological Characterization of Voltage-Gated K⁺ Currents in Cerebellar Basket and Purkinje Cells: Kv1 and Kv3 Channel Subfamilies Are Present in Basket Cell Nerve Terminals. *J. Neurosci.* **20**, 114-122.
- STANLEY, E. F. (1992). The calyx-type synapse of the chick ciliary ganglion as a model of fast cholinergic transmission. *Can J Physiol Pharmacol* **70 Suppl**, S73-77.
- STOCKER, M. (2004). Ca²⁺-activated K⁺ channels: molecular determinants and function of the SK family. *Nat Rev Neurosci* **5**, 758-770.
- STRUTT, J. W. (1877). Acoustical Observations. *Phil. Mag* **3**, 456-464.
- STRUTT, J. W. L. R. (1907). On our perception of sound direction. *Phil. Mag.* **13**, 214-232.
- SULLIVAN, W. E. & KONISHI, M. (1986). Neural map of interaural phase difference in the owl's brainstem. *Proc Natl Acad Sci U S A* **83**, 8400-8404.
- TASCHENBERGER, H. & VON GERSDORFF, H. (2000). Fine-tuning an auditory synapse for speed and fidelity: developmental changes in presynaptic waveform, EPSC kinetics, and synaptic plasticity. *J Neurosci* **20**, 9162-9173.
- THOMAS, M. V. (2000). *Optopatch Manual: Cairn Research Limited*.
- TKATCH, T., BARANAUSKAS, G. & SURMEIER, D. J. (2000). Kv4.2 mRNA Abundance and A-Type K⁺ Current Amplitude Are Linearly Related in Basal Ganglia and Basal Forebrain Neurons. *J. Neurosci.* **20**, 579-588.
- TOLLIN, D. J. (2003). The lateral superior olive: a functional role in sound source localization. *Neuroscientist* **9**, 127-143.
- TRISTANI-FIROUZI, M. & SANGUINETTI, M. C. (2003). Structural determinants and biophysical properties of HERG and KCNQ1 channel gating. *J Mol Cell Cardiol* **35**, 27-35.
- TYTGAT, J., DEBONT, T., CARMELIET, E. & DAENENS, P. (1995). The alpha-Dendrotoxin Footprint on a Mammalian Potassium Channel. *J. Biol. Chem.* **270**, 24776-24781.

- UEDA, A. & WU, C.-F. (2006). Distinct Frequency-Dependent Regulation of Nerve Terminal Excitability and Synaptic Transmission by IA and IK Potassium Channels Revealed by *Drosophila* Shaker and Shab Mutations. *J. Neurosci.* **26**, 6238-6248.
- VERVAEKE, K., GU, N., AGDESTAIN, C., HU, H. & STORM, J. F. (2006). Kv7/KCNQ/M channels in glutamatergic hippocampal axons and their role in regulation of excitability and transmitter release. *J Physiol.*
- VON HEHN, C. A., BHATTACHARJEE, A. & KACZMAREK, L. K. (2004). Loss of Kv3.1 tonotopicity and alterations in cAMP response element-binding protein signaling in central auditory neurons of hearing impaired mice. *J Neurosci* **24**, 1936-1940.
- WANG, H., KUNKEL, D. D., MARTIN, T. M., SCHWARTZKROIN, P. A. & TEMPEL, B. L. (1993). Heteromultimeric K⁺ channels in terminal and juxtaparanodal regions of neurons. *Nature* **365**, 75-79.
- WANG, H., KUNKEL, D. D., SCHWARTZKROIN, P. A. & TEMPEL, B. L. (1994). Localization of Kv1.1 and Kv1.2, two K channel proteins, to synaptic terminals, somata, and dendrites in the mouse brain. *J Neurosci* **14**, 4588-4599.
- WANG, H. S., PAN, Z., SHI, W., BROWN, B. S., WYMORE, R. S., COHEN, I. S., DIXON, J. E. & MCKINNON, D. (1998a). KCNQ2 and KCNQ3 potassium channel subunits: molecular correlates of the M-channel. *Science* **282**, 1890-1893.
- WANG, L.-Y., GAN, L., FORSYTHE, I. D. & KACZMAREK, L. K. (1998b). Contribution of the Kv3.1 potassium channel to high-frequency firing in mouse auditory neurones. *J Physiol (Lond)* **509**, 183-194.
- WANG, L.-Y. & KACZMAREK, L. K. (1998). High-frequency firing helps replenish the readily releasable pool of synaptic vesicles. *Nature* **394**, 384-388.
- WATKINS, C. S. & MATHIE, A. (1996). A non-inactivating K⁺ current sensitive to muscarinic receptor activation in rat cultured cerebellar granule neurons. *J Physiol* **491** (Pt 2), 401-412.
- WEISER, M., VEGA-SAENZ DE MIERA, E., KENTROS, C., MORENO, H., FRANZEN, L., HILLMAN, D., BAKER, H. & RUDY, B. (1994). Differential expression of Shaw-related K⁺ channels in the rat central nervous system. *J Neurosci* **14**, 949-972.
- WIGMORE, M. A. & LACEY, M. G. (2000). A Kv3-like persistent, outwardly rectifying, Cs⁺-permeable, K⁺ current in rat subthalamic nucleus neurones. *J Physiol* **527** Pt 3, 493-506.
- WU, S. H. & KELLY, J. B. (1991). Physiological properties of neurons in the mouse superior olive: membrane characteristics and postsynaptic responses studied in vitro. *J Neurophysiol* **65**, 230-246.
- XIA, X. M., FAKLER, B., RIVARD, A., WAYMAN, G., JOHNSON-PAIS, T., KEEN, J. E., ISHII, T., HIRSCHBERG, B., BOND, C. T., LUTSENKO, S., MAYLIE, J. & ADELMAN, J. P. (1998). Mechanism of calcium gating in small-conductance calcium-activated potassium channels. *Nature* **395**, 503-507.
- XU, J., YU, W., WRIGHT, J. M., RAAB, R. W. & LI, M. (1998). Distinct functional stoichiometry of potassium channel beta subunits. *Proc Natl Acad Sci U S A* **95**, 1846-1851.

- YELLEN, G. (2002). The voltage-gated potassium channels and their relatives. *Nature* **419**, 35-42.
- YEUNG, S. Y. M., THOMPSON, D., WANG, Z., FEDIDA, D. & ROBERTSON, B. (2005). Modulation of Kv3 Subfamily Potassium Currents by the Sea Anemone Toxin BDS: Significance for CNS and Biophysical Studies
10.1523/JNEUROSCI.2119-05.2005. *J. Neurosci.* **25**, 8735-8745.
- YI, B. A. & JAN, L. Y. (2000). Taking apart the gating of voltage-gated K⁺ channels. *Neuron* **27**, 423-425.
- YUSAF, S. P., WRAY, D. & SIVAPRASADARAO, A. (1996). Measurement of the movement of the S4 segment during the activation of a voltage-gated potassium channel. *Pflugers Arch* **433**, 91-97.
- ZHOU, Y., MORAIS-CABRAL, J. H., KAUFMAN, A. & MACKINNON, R. (2001). Chemistry of ion coordination and hydration revealed by a K⁺ channel-Fab complex at 2.0 Å resolution. *Nature* **414**, 43-48.
- ZOU, A., LIN, Z., HUMBLE, M., CREECH, C. D., WAGONER, P. K., KRAFTE, D., JEGLA, T. J. & WICKENDEN, A. D. (2003). Distribution and functional properties of human KCNH8 (Elk1) potassium channels. *Am J Physiol Cell Physiol* **285**, C1356-1366.